Dipl.-Ing. Harald Kolk, B. Sc.

Prospective effectiveness assessment of autonomous emergency braking systems by a combination of traffic flow simulation and crash simulation

Doctoral Thesis

to achieve the university degree of

Doctor of Technical Sciences

submitted to

Graz University of Technology

Vehicle Safety Institute, Graz University of Technology
Head: Univ.-Prof. Dipl.-Ing. Dr. techn. Hermann Steffan

Supervisor:
Assoc. Prof. Dipl.-Ing. Dr. techn. Wolfgang Sinz

First reviewer:
Univ.-Prof. Dipl.-Ing. Dr. techn. Arno Eichberger

Second reviewer:
Prof. Dr. rer. nat. Hermann Winner

Graz, April 2021

Statutory Declaration

I declare that I have authored this thesis independently, that I have not used other than the declared sources/resources, and that I have explicitly indicated all material which has been quoted either literally or by content from the sources used. The text document uploaded to TUGRAZonline is identical to the present doctoral thesis.

Graz, _____ _____

Date Signature

Acknowledgments

First of all, I sincerely thank anyone who provided valuable feedback on any of the topics related to this thesis, regardless of whether the feedback came in the form of lengthy discussions, simple questions, or concrete suggestions for improvements. In this regard, I particularly mention my supervisor and Assoc. Prof. Dipl.-Ing. Dr.techn. Wolfgang Sinz of the Vehicle Safety Institute (VSI), Graz University of Technology. Furthermore, I thank my reviewers Prof. Dr. rer. nat. Hermann Winner of the Institute of Automotive Engineering (FZD), Technical University of Darmstadt, and Assoc. Prof. Dipl.-Ing. Dr. techn. Arno Eichberger of the Institute of Automotive Engineering (FTG), Graz University of Technology, for agreeing to review my thesis and for providing their valuable feedback in a timely manner. In addition, I warmly thank my project partners from the project IMPROVE, i.e., the members Univ.-Prof. Dr.-Ing. Martin Fellendorf and Dipl.-Ing. Michael Haberl, B. Sc. of the Institute of Highway Engineering and Transport Planning (ISV), Graz University of Technology, and Dipl.-Ing. Dr. techn. Andreas Moser of the Dr. Steffan Datentechnik Ges.m.b.H. (DSD). The basic methodology presented in this thesis was created as part of the FFG-funded project IMPROVE. I repeatedly received new perspectives through the discussions with the members of the P.E.A.R.S. initiative, who greatly helped me compare my own methods with those of others. More than once, I cited someone in my publications and, later on, had a chance to meet them at one of the P.E.A.R.S. meetings.

I thank all my colleagues, who provided me with a positive work environment. This really helped keeping me positive and motivated.

Furthermore, I warmly thank my family and friends, who often helped me by providing the (sometimes much needed) distraction from work.

Finally, I thank my fiancée Sarah for her support and encouragement and for accompanying me on my journey to finish this thesis. She still thinks she is an impatient person, but I think she showed a lot of patience when I had to invest more extra hours than I ever thought I would need.

Kurzfassung

Um der Vision Zero, und damit dem Ziel von Mobilität ohne Verkehrstoten näher zu kommen, werden Fahrerassistenzsysteme entwickelt, wie die autonomen Bremsassistenten, die im Fall der gegenwärtigen Arbeit untersucht wurden. Damit eine gezielte Entwicklung zur größtmöglichen Reduktion der Verkehrstoten oder der Verletzungsschwere stattfinden kann, ist es wichtig, den Sicherheitsgewinn dieser Systeme objektiv bestimmen zu können. Ein möglicher Ansatz sind numerische Methoden, die prospektiv die Systemeffektivität evaluieren.

Bei den bisher bestehenden Methoden ist jedoch offen, wie der Verkehr, der möglicherweise Unfälle und Verkehrskonflikte umgibt, in der Simulation mitberücksichtigt werden kann, oder wie kritische Szenarien erzeugt werden können, die nicht notwendigerweise Kollisionen enthalten. Dafür wurde in dieser Dissertation ein validiertes mikroskopisches Verkehrsflusssimulationsmodell verwendet, um stochastisch Verkehr für eine gewählte innerstädtische Verkehrsstelle inklusive Lichtsignalanlagen zu erzeugen. Aus dem so erzeugten Verkehr wurden über Kenngrößen wie der Time-to-Collision diejenigen kritischen Situationen als Konflikte identifiziert, die beim Ausbleiben einer Geschwindigkeits- oder Fahrtrichtungsänderung zu Unfällen führen können. Um auch die Fahrdynamik und Kollisionsmechanik miteinbeziehen zu können, wurden die gefundenen Szenarien dann in höherem Detailgrad in nanoskopischer Unfallsimulation betrachtet, wo auch die autonomen Bremsassistenten berücksichtigt werden konnten.

Im Zuge eines Baseline-to-Treatment Vergleichs wurden zwei unterschiedlich konfigurierte Systeme untersucht, und deren möglicher Sicherheitsgewinn über Effektivitätsmetriken objektiv beschrieben. Unter anderem wurde ermittelt, dass ein System, welches basierend auf der Enhanced Time-to-Collision unter Berücksichtigung der longitudinalen Fahrzeugbeschleunigung auslöst, nur zur etwa halben Anzahl an Falschauslösungen führt wie ein System, welches basierend auf der Time-to-Collision auslöst. In einigen Fällen kann ein Systemeingriff sogar zu einer zusätzlichen Kollision mit Fahrzeugen aus dem Umgebungsverkehr führen, falls die anderen Fahrer unaufmerksam sind.

Des weiteren stellte sich heraus, dass durch die Kopplung Kollisionen entstehen können, die in der Verkehrsflusssimulation nicht vorkommen. In einer Sensitivitätsanalyse wurde ermittelt, dass diese Kollisionen maßgeblich vom verwendeten kinetischen Pfadfolgemodell beeinflusst werden, während auch ein längeres simuliertes Zeitfenster zu mehr Kollisionen führte. In der Analyse der Methodik zur Auswahl von Szenarien stellte sich heraus,

dass die Effektivitätsmetriken so definiert werden sollten, dass sie möglichst unabhängig gegenüber dem Hinzufügen einer großen Anzahl an minderkritischen Szenarien sind. Dahingegen spielte eine Erhöhung der Verkehrsstärke um 50 % eine eher untergeordnete Rolle. Sichtabschattungen wirkten sich nicht auf die Effektivitätsmetriken aus.

Die vorgestellte Methode stellt einen vielversprechenden Ansatz dar, um die Qualität der Entscheidungsalgorithmen von Assistenzsystemen zu bewerten und um Auswirkungen von Systemauslösungen auf den unmittelbaren Umgebungsverkehr zu untersuchen. Es sollten jedoch speziell das Fahrerverhalten, die Anzahl von Konflikten und deren Verteilung genauestens auf den Realverkehr abgestimmt werden.

Abstract

To support the Vision Zero and thereby reach the goal of mobility without traffic fatalities, advanced driver assistance systems are being developed, such as the autonomous inner-city emergency brake assists that were investigated in this thesis work. For this reason, it is important to objectively evaluate the safety benefits associated with active safety strategies, to reduce traffic casualties and injuries as much as possible. The development of prospective numerical methods offers a possible solution.

When evaluating the current state-of-the-art methods, several open questions remain. These include how the traffic that surrounds accidents and conflict situations can be included in the assessment, and how to generate critical scenarios that do not necessarily contain collisions. To address these questions, a validated microscopic traffic flow simulation model was used in this thesis work to generate traffic stochastically for an inner-urban road site, including traffic signals. Using safety surrogate measures such as the Time-to-Collision, critical situations could be identified as conflicts. These have the potential to lead to accidents if the movement direction and velocity are not changed. Once identified, these conflicts were used to define a scenario catalog. To additionally consider driving dynamics and collision mechanics in the assessment, the chosen scenarios were simulated in more detail in nanoscopic accident simulations, where the active safety systems were considered.

Two different safety system configurations were investigated in a baseline-to-treatment comparison. Their potential safety benefits were described objectively based on effectiveness metrics. Among other results, this led to the conclusion, that using a system that is triggered based on the Enhanced Time-to-Collision, and considering the longitudinal vehicle acceleration, leads to half as many false positive system activations as when the system is triggered based on the Time-to-Collision. Furthermore, it was found that in some cases, a system intervention led to a new collision with vehicles in the surrounding traffic, if it is assumed that other drivers are inattentive.

In addition, it was found that by applying the coupling approach, collisions occurred in the nanoscopic simulation which did not occur in the traffic flow simulation. These collisions were significantly influenced by the parameterization of the kinetic path driver model. Increasing the length of the simulated time frame chosen for each conflict led to additional collisions. In the sensitivity study of the scenario selection method, it was found that the effectiveness metrics should be defined as independent as possible from adding further scenarios of minor criticality. In contrast, a 50 % increase in the traffic density had a lower

influence on the results, while sight obstructions posed by surrounding traffic and static objects were identified as not relevant to the effectiveness metrics.

The described method represents a promising approach that can be taken to evaluate the quality of safety system activation algorithms and to investigate the consequences of emergency maneuvers on the immediately surrounding traffic. However, in future studies, particular attention should be paid to further validating driver model behavior, the number of conflicts and the distribution of their severity, with respect to real traffic conditions.

Contents

List of candidate's publications

H. Kolk, E. Tomasch, et al. (2018). "Active safety effectiveness assessment by combination of traffic flow simulation and crash-simulation." In: *8th International Conference on ESAR "Expert Symposium on Accident Research"*. Ed. by ESAR

- Contribution: conceptualization, simulation, data curation, formal analysis, methodology, software, validation, visualization, writing: original draft and editing
- Relevance to this thesis: preliminary study that presents the approach used in thesis that combines microscopic traffic flow simulation and crash simulation.
- Peer-reviewed: No

H. Kolk, S. K. Kirschbichler, et al. (2016). "Prospective evaluation of the collision severity of L7e vehicles considering a Collision Mitigation System." In: *Transportation Research Procedia*. Elsevier

- Contribution: conceptualization, simulation, data curation, formal analysis, methodology, software, validation, visualization, writing: original draft and editing
- Relevance to this thesis: development of a prospective effectiveness assessment methodology to predict the safety benefit of autonomous braking for L7e vehicles.
- Peer-reviewed: Yes

H. Kolk, W. Sinz, et al. (2016). "Evaluation of a momentum based impact model and application in an effectivity study considering junction accidents." In: *7th International Conference on ESAR "Expert Symposium on Accident Research"*. Ed. by ESAR

- Contribution: conceptualization, simulation, data curation, formal analysis, methodology, software, validation, visualization, writing: original draft and editing
- Relevance to this thesis: the impact model used in this thesis to calculate the collision severity is investigated regarding its sensitivity to specific configuration parameters, by comparison with reconstructed real accidents.
- Peer-reviewed: No

P. Wimmer, M. Düring, et al. (2019). "Toward harmonizing prospective effectiveness assessment for road safety: Comparing tools in standard test case simulations." In: *Traffic Injury Prevention* 20.sup1, S139–S145. ISSN: 1538-957X. DOI: 10.1080/15389588.2019.1616086

- Contribution: conceptualization, simulation, formal analysis, methodology, software, writing (original draft and review)
- Relevance to this thesis: this study represents a further step in the verification process of the simulation results generated by X-RATE, the main software used in this thesis to simulate active safety systems, by defining a detailed test scenario catalog and comparing simulation results to the results generated by comparable software products.
- Peer-reviewed: Yes

S. Smit et al. (2019). "Evaluation of a momentum based impact model in frontal car collisions for the prospective assessment of ADAS." In: *European Transport Research Review* 11.1, p. 75. ISSN: 1867-0717. DOI: 10.1186/s12544-018-0343-3

- Contribution: simulation, software, writing (review)
- Relevance to this thesis: the impact model used in this thesis to calculate the collision severity is investigated regarding its sensitivity to specific configuration parameters by comparison with reconstructed real accidents.
- Peer-reviewed: Yes

M. Gruber, H. Kolk, et al. (2019). "The effect of P-AEB system parameters on the effectiveness for real world pedestrian accidents." In: *The 26th ESV Conference Proceedings*. Ed. by NHTSA. ESV Conference Proceedings. NHTSA

- Contribution: formal analysis, methodology, software, visualization, writing (review)
- Relevance to this thesis: application of X-RATE and effectiveness assessment methodology to pedestrian accident scenarios.
- Peer-reviewed: Yes

M. Haberl et al. (2018). "Simulation Assisted Safety Impact Analyses for Signalized Urban Intersections." In: *Transport Research Arena*

- Contribution: simulation, software, visualization, writing (review)
- Relevance to this thesis: this study presents approaches for the validation of microscopic traffic flow simulation regarding safety aspects, by combining microscopic traffic flow simulation with crash simulation.
- Peer-reviewed: Yes

M. Gruber, C. Matt, et al. (2018). "Effectiveness assessment of a generic collision mitigation system for motorcycles at junctions." In: *8th International Conference on ESAR*

- Contribution: formal analysis, methodology, software, visualization, writing (review)
- Relevance to this thesis: application of X-RATE and a prospective effectiveness assessment methodology to motorcycle accident scenarios.
- Peer-reviewed: No

E. Tomasch, H. Kolk, et al. (2015). "Prospektive Bewertung der Kollisionsschwere von L6e Fahrzeugen unter Berücksichtigung eines Kollisionsminderungssystems." In: *10. VDI-Tagung Fahrzeugsicherheit - Sicherheit 2.0*. Vol. 2265. VDI-Berichte. Düsseldorf: VDI-Verlag, pp. 407–418. ISBN: 978-3-18-092265-2

- Contribution: simulation, software, writing (review)
- Relevance to this thesis: development of a prospective effectiveness assessment methodology to predict the safety benefits of autonomous emergency braking systems for L6e vehicles.
- Peer-reviewed: No

E. Tomasch, W. Sinz, et al. (2015). "Bewertungsmethodik von integralen Sicherheitssystemen durch Kombination von Test und Simulation am Beispiel von Fußgängerunfällen." In: *10. VDI-Tagung Fahrzeugsicherheit - Sicherheit 2.0*. Vol. 2265. VDI-Berichte. Düsseldorf: VDI-Verlag, pp. 157–169. ISBN: 978-3-18-092265-2

- Contribution: simulation, software, writing (review)

- Relevance to this thesis: development of a prospective effectiveness assessment methodology to predict the safety benefits of autonomous emergency braking systems in pedestrian accident scenarios.
- Peer-reviewed: No

Acronyms

ABS	Anti-lock Braking System
ACC	Adaptive Cruise Control
ADAS	Advanced Driver Assistance System
AEB	Autonomous Emergency Brake
ASIL	Automotive Safety Integrity Level
BrIC	Brain Injury Criterion
BTN	Brake Threat Number
CEDATU	Central Database for In-Depth Accident Study
eCall	Automatic Emergency Call
ESC	Electronic Stability Control
ETTC	Enhanced Time-to-Collision
FCW	Forward Collision Warning
FEA	Finite Element Analysis
FOT	Field Operational Test
GIDAS	German In-Depth Accident Study
HBM	Human Body Model
HIC	Head Injury Criterion
MAIS	Maximum Abbreviated Injury Scale Level
MTFS	Microscopic Traffic Flow Simulation
NCAP	New Car Assessment Programme
NDS	Naturalistic Driving Study

PET Post-Encroachment-Time

SSAM Safety Surrogate Assessment Model

SSM Safety Surrogate Measure

TET Time Exposed Time-to-Collision

TIT Time Integrated Time-to-Collision

TTC Time-to-Collision

Glossary

Active safety: Safety systems that are capable of intervening in the pre-crash phase in the vehicle guidance or by warning the driver, to avoid collisions or to mitigate the consequences of collisions.

Baseline: Original, unaltered concrete scenarios, in which the safety system under investigation is not installed.

Baseline-to-treatment: The baseline-to-treatment comparison approach compares the results of the scenario representation of concrete baseline and treatment scenarios with each other, to determine the relative safety effect of the active safety system under investigation.

Changed collision: If a collision occurs both in the concrete baseline scenario and the concrete treatment scenario, but between different traffic participants, then the collision is denoted as changed collision.

Concrete scenario: Definition as presented in Menzel et al., 2018: "Concrete scenarios distinctly depict operating scenarios on a state space level. Concrete scenarios represent entities and the relations of those entities with the help of concrete values for each parameter in the state space." This extends the definition of *scenario* in Ulbrich et al., 2015 by distinguishing different levels of abstraction. Example for a concrete scenario: "vehicle A drives with a velocity of 36 km/h exactly in the middle of the furthest right hand lane of road R, starting at position P, with angular orientation O and continuing to drive south to north in the middle of its lane and in parallel to the lane markings".

Conflict: A conflict is defined as a scene, where one or several specified Safety Surrogate Measures fall below their respective thresholds.

Conflict participants: The two traffic participants that are involved in a conflict with each other, are defined as the conflict participants. In this thesis work, since only conflicts between passenger cars and vans are investigated, both are vehicles. In the treatment simulations, both conflict participants (vehicles) are equipped with the same safety system under investigation.

Crash phase: Once the first contact occurs between a traffic participant and its collision partner, they enter the crash phase. The beginning of this phase is, in general, when most passive safety systems trigger appropriate measures to mitigate the consequences of the crash. The main goal in this phase is to prevent injuries during the crash.

Critical scenario: In this thesis, a critical scenario is defined as a scenario that contains at least one critical scene.

Critical scene: In this thesis, a critical scene is defined as a scene in which a collision course exists between two traffic participants. A collision course exists if the movement direction and velocity of at least one involved traffic participant must be changed to avoid a collision (Gettman and Head, 2003).

Effectiveness: The effectiveness of a safety system expresses the how well a system can increase the level of safety when a vehicle equipped with that system is driven, i.e., the effectiveness describes the system's safety effect. The effectiveness can be expressed by several effectiveness metrics.

Effectiveness function: An effectiveness function is defined as a function that objectively quantifies a specific safety-related aspect for a specific concrete scenario. It is applied to individual concrete scenarios, and the results are aggregated by effectiveness metrics.

Effectiveness metric: An effectiveness metric is defined as a method that quantifies a specific safety-related aspect for each concrete scenario in the scenario catalog and aggregates the results to express the effectiveness as a single value. This is done for example, by computing an average value of an effectiveness function for each concrete scenario in the scenario catalog.

Environment: The term environment refers to environmental conditions, such as the weather, air humidity, temperature or lighting conditions.

Evaluation objective: The evaluation objective is a precise formulation of the questions that are to be answered during the effectiveness assessment procedure.

Injury risk function: Injury risk functions describe a probabilistic relationship between a kinematic quantity related to collisions and a risk that injuries of a specific degree of severity are incurred to a person.

In-the-loop: In-the-loop methods couple hardware and software components, to a varying degree of virtualization.

Logical scenario: Definition as presented in Menzel et al., 2018: "Logical scenarios include operating scenarios on a state space level. Logical scenarios represent the entities and the relations of those entities with the help of parameter ranges in the state space. The parameter ranges can optionally be specified with probability distributions. Additionally, the relations of the parameter ranges can optionally be specified with the help of correlations or numeric conditions. A logical scenario includes a formal notation of the scenario." This extends the definition of *scenario* in Ulbrich et al., 2015 by distinguishing different levels of abstraction. A simple example of a logical scenario description would be: "vehicle A drives from south to north on road R, within a speed range from 30 km/h to 70 km/h under all weather conditions.".

Microscopic traffic flow simulation: In microscopic traffic flow simulation, traffic at a selected road site is simulated. The simulation resolves individual traffic participants and their actions. The driving dynamics consider fewer details than nanoscopic simulation (e.g., no sliding is possible).

Nanoscopic simulation: Nanoscopic simulation methods are applied to consider only few traffic participants (in this thesis: two to 30 participants at most) and simulate the

driving process in detail. Physical effects that are considered include sliding in curves or suspension characteristics. Nanoscopic simulations are also used to consider active safety systems.

New collision: If a collision occurs in the concrete treatment scenario, but not in the concrete baseline scenario, then the collision in the treatment is denoted as new collision.

Penetration depth: The duration for which traffic participants continue their movement after initial contact in collisions.

Post-crash phase: In this phase, the collision partners have separated, and they have reached their final rest positions. Possible measures are of life sustaining character. Contributing factors in this phase are, for example, the first-aid skills of persons present at the accident site, access to medics, or ease of access to persons involved in the accident, including the transportation to hospitals and treatment therein. Furthermore, Automatic Emergency Call (eCall) systems help reduce the time between the collision and notification of first responders.

Pre-crash phase: Crash prevention and reduction of risk exposure is possible in this phase. Based on the current state of driving, a traffic participant enters a course of movement that would lead to a collision with other traffic participants, objects, or a single vehicle accident if no preventive action is taken. In this phase, active safety systems contribute, by issuing warnings to the driver and intervening at some point if the critical driving state is not changed, or by intervening directly without warning.

Prospective effectiveness assessment: Assessment of the effectiveness of a given safety system, carried out to forecast the potential of the system, based on current accident data or other scenario sources.

Rating: In this step of the effectiveness assessment process, outputs of the scenario representation step are collected and used to quantify the effectiveness of the investigated system.

Retrospective effectiveness assessment: Statistical data are used to infer on the effect of a safety system. Since it uses data collected in the past, this assessment method is only possible after a significant amount of time (e.g., years), after market introduction or when a sufficient amount of historic data has been collected.

Safety zone: Forms a virtual zone around traffic participants that should not be intruded. Used for example by the TTC calculation. The box-shaped geometry of the traffic participants is virtually enlarged in normal direction by the safety zone.

Scenario: Definition as presented in Ulbrich et al., 2015: ”A scenario describes the temporal development between several scenes in a sequence of scenes. Every scenario starts with an initial scene. Actions and events as well as goals and values may be specified to characterize this temporal development in a scenario. Other than a scene, a scenario spans a certain amount of time.” This definition is extended in Menzel et al., 2018 to define the terms *logical scenario*, *functional scenario* and *concrete scenario* to distinguish further levels of abstraction. The term *traffic scenario* is used synomyously in this thesis.

Scenario catalog: The scenario catalog is a set of concrete scenarios that should be consid-

ered in the scenario representation step.

Scenario cloud: All possible concrete traffic scenarios, needs input from different sources, such as traffic flow simulation, real accident scenarios from databases, expert opinions, or other scenario collection or generation methods.

Scenario representation: Starting with the initial conditions defined in the concrete scenario, a scenario representation method is a way to execute the temporal evolution of the concrete scenario.

Scenario sub-cloud: It is not possible to provide descriptions of all concrete scenarios. The output from each scenario source is, therefore, a subset of the scenario cloud, i.e., a scenario sub-cloud.

Scene: Definition as presented in Ulbrich et al., 2015: ”A scene describes a snapshot of the environment including the scenery and dynamic elements, as well as all actors’ and observers’ self-representations, and the relationships among those entities. Only a scene representation in a simulated world can be all-encompassing (objective scene, ground truth). In the real world it is incomplete, incorrect, uncertain, and from one or several observers’ points of view (subjective scene)”.

Scenery: Definition as presented in Ulbrich et al., 2015: ”The scenery subsumes all geo-spatially stationary aspects of the scene. This entails metric, semantic and topological information about roads and all their components like lanes, lane markings, road surfaces, or the roads’ domain types. Moreover, this subsumes information about conflict areas between lanes as well as information about their interconnections, e.g., at intersections. Apart from the before mentioned environment conditions, the scenery also includes stationary elements like houses, fences, curbs, trees, traffic lights, or traffic signs”.

Treatment: Concrete scenarios in which one or more vehicles have the safety system under investigation installed.

Unchanged collision: If a collision occurs between the same traffic participants both in the concrete baseline scenario and the concrete treatment scenario, then this collision is denoted as an unchanged collision.

What-if-approach: Synonymous to baseline-to-treatment comparison approach.

Mathematical notation

Symbol	Description
a	Symbol used for scalar quantities that describe an acceleration
$a^{\min}$	Minimum possible acceleration that can be used for braking, limited by friction conditions
a_{L}	Longitudinal acceleration of the lead vehicle
a_{F}	Longitudinal acceleration of the follow vehicle
a_{rel}	Longitudinal relative acceleration, i.e., $a_{\mathrm{rel}} = a_{\mathrm{L}} - a_{\mathrm{F}}$
∇a	Brake gradient, describes the amount by which the acceleration is decreased per time interval
A_X, $B_{X\,add}$, $B_{X\,mult}$	Parameters used to describe vehicle follow behavior in the Wiedemann 74 model
$\delta_{\mathrm{steer}}^{\max}$	Maximum steering angle
$\dot{\delta}_{\mathrm{steer}}^{\max}$	Maximum change of the steering angle per time interval
d	Symbol used for quantities that describe a distance
d_{rel}, x_{rel}	Relative distance between a lead and a follow vehicle
$d^{\min}$	Minimum distance reached during a concrete scenario
d_{SZ}	Safety zone. Vehicle geometries are virtually enlarged by this distance for collision detection
Δt_p	Penetration depth
Δv	Collision induced velocity change
Δt	Time step size
δ	Steering angle of the outer front wheel
δ_{unif}	Unified steering angle of the outer front wheel to compare the steering angles for vehicles with a different wheelbase
E	Symbol used for effectiveness metrics
E_{conf}	Ratio of the number of conflicts with and without safety system
E_{new}	Ratio between the number of concrete scenarios in the treatment with new collisions and the total number of collisions in the treatment
E_{av}	Ratio between avoided collisions in the baseline and total number of collisions in the baseline
E_{ch}	Ratio between the number of concrete scenarios in the treatment with changed collisions and the total number of collisions in the baseline
E_{unch}	Ratio between the number of concrete scenarios in the treatment with unchanged collisions and the total number of collisions in the baseline
$E_{\Delta v}^{\mathrm{BL,\,mean}}$, $E_{\Delta v}^{\mathrm{BL,\,50\,\%}}$	Average and median Δv, for concrete scenarios in the baseline where a collision occurs
$E_{\Delta v}^{\mathrm{TR,\,mean}}$, $E_{\Delta v}^{\mathrm{TR,\,50\,\%}}$	Average and median Δv, for concrete scenarios in the treatment where a collision occurs

Symbol	Description
$E_{\Delta v}^{\text{new, 50 \%}}$	Median Δv, counting only new collisions in the treatment
$E_{\Delta v}^{\text{ch, 50 \%}}$	Median Δv, counting only changed collisions in the treatment
$E_{\Delta v}^{\text{unch, 50 \%}}$	Median Δv, counting only unchanged collisions in the treatment
$E_{\Delta v}^{\text{mean}}$, $E_{\text{IRF}}^{\text{mean}}$, $E_{v_c}^{\text{mean}}$	Average change of Δv, an injury probability or v_c, counting only concrete scenarios where a collision occurs both in the baseline and concrete treatment scenario
$E_{\Delta v}^{0,\text{mean}}$, $E_{\text{IRF}}^{0,\text{mean}}$, $E_{v_c}^{0,\text{mean}}$	Average change of Δv, an injury probability or v_c. If no collision occurs in concrete scenario $TR(s)$, $\Delta v(s)$, the injury probability or $v_c(s)$ are assumed to be 0
$E_{\text{Rel, }\Delta v}^{\text{mean}}$, $E_{\text{Rel, IRF}}^{\text{mean}}$, $E_{\text{Rel, }v_c}^{\text{mean}}$	Average relative change of Δv, an injury probability or v_c, counting only concrete scenarios where a collision occurs both in the baseline and concrete treatment scenario
$E_{\text{Rel, }\Delta v}^{0,\text{mean}}$, $E_{\text{Rel, IRF}}^{0,\text{mean}}$, $E_{\text{Rel, }v_c}^{0,\text{mean}}$	Average relative change of Δv, an injury probability or v_c. If no collision occurs in concrete scenario $TR(s)$, $\Delta v(s)$, the injury probability or $v_c(s)$ are assumed to be 0
E_{corr}	Proportion of correct decisions in the total number of conflicts
$E_{\text{MCC}}^{\text{norm}}$	Matthews's correlation coefficient, transformed to the interval $[0, 1]$
E_{sens}	Sensitivity: describes a system's ability to treat dangerous situations correctly by triggering an emergency maneuver
E_{spec}	Specificity: describes a system's ability to treat non-dangerous situations correctly by not reacting
ϵ	Coefficient of restitution, used by the collision model
τ_{ETTC}	Enhanced Time-to-Collision
$\tau_{\text{ETTC,X}}$	Enhanced Time-to-Collision calculated by X-RATE
$\tau_{\text{ETTC}}^{\text{Trig}}$	The τ_{ETTC} threshold at which the active safety system triggers
f_{eff}	Symbol used for effectiveness functions
$\vec{F}$	Position vector of the center of the vehicle front
g	Standard acceleration of free fall ($9.806\,65\,\text{m/s}^2$)
H	Event horizon, used for spatial filtering of traffic participants
I	Time interval in MTFS data that is used to extract a concrete scenario for nanoscopic simulation
κ	Curvature of the trajectory of a vehicle's outer front wheel
κ^{max}	Curvature (i.e., the inverse of the radius) of a vehicle's turning circle
l, w, h	Length, width and height of the box-shaped traffic participant model
μ	Friction coefficient for the contact between the road and the tires
N_{new}	Number of concrete scenarios in S^{TR} with new collisions
N_{av}	Number of collisions in the baseline that were avoided
N_{ch}	Number of concrete scenarios in S^{TR} with changed collisions
N_{unch}	Number of concrete scenarios in S^{TR} with unchanged collisions
N^{act}	Number of concrete scenarios in S^{TR} in which a safety system has triggered an emergency maneuver
N_{rays}^{h}	Number of rays that cover the horizontal opening angle to describe a sensor's field of view
$\vec{\omega}_S^V$	Sensor orientation. Defined relative to the vehicle coordinate system. The vector $\vec{\omega}_S^V = (0, 0, 0)$ represents a forward facing sensor
P	Set of all traffic participants that are present at a given time

Symbol	Description
P_{crit}	Set of critical traffic participants
P_{close}	Set of all close traffic participants
τ_{PET}	Post-Encroachment-Time
$Q^{50\,\%}_{S_{\text{dang}}}(f_{\text{eff}}(s))$	The 50 %-quartile, also known as the median, computed for the values $f_{\text{eff}}(s)$ with $s \in S_{\text{dang}}$.
$\vec{R}$	Position vector of the center of the vehicle rear
R	Sensor range. Describes how far each "vision ray" extends at most from the sensor origin
s	Symbol used for individual concrete scenarios
S	Scenario catalog
S_C	The set of all baseline concrete scenarios $s \in S$ where a collision occurs
S^{TR}	The set of all concrete treatment scenarios $TR(s)$ with $s \in S$
S_C^{TR}	The set of all concrete treatment scenarios $TR(s)$ with $s \in S$ where a collision occurs
S_{DX}, S_{DV}, C_{LDV}, O_{PDV}	Additional parameters used to describe vehicle follow behavior in the Wiedemann 74 model
t_{acq}	Acquisition time. Minimum time delay from first detection until classification can be reached
t_{srt}	System response time, i.e., the time needed from fulfillment of the trigger condition until the brakes start building up brake force
t_{sim}	Time that is simulated in nanoscopic simulation before and after $t_{\tau^{\min}_{\text{TTC}}}$, i.e., $I = \left[t_{\tau^{\min}_{\text{TTC}}} - t_{\text{sim}},\ t_{\tau^{\min}_{\text{TTC}}} + t_{\text{sim}}\right]$
t_{imp}	Time in nanoscopic simulation when the first collision occurred
t_{LA}, d_{LA}	Look ahead time and look ahead distance (kinetic path driver model parameters)
$t_{\tau^{\min}_{\text{TTC}}}$	The time during a concrete scenario when $\tau^{\min}_{\text{TTC,S}}$ is reached
$TR(s)$	Treatment representation of a concrete scenario s
τ_{TTC}	Time-to-Collision
$\tau_{\text{TTC,S}}$	Time-to-Collision calculated by SSAM
$\tau^{\min}_{\text{TTC}}$	Minimum τ_{TTC} reached during a concrete scenario (any calculation method)
$\tau_{\text{TTC,X}}$	Time-to-Collision calculated by X-RATE
$\tau^{\min}_{\text{TTC,X}}$	Minimum τ_{TTC} reached during a concrete scenario, as calculated by X-RATE
$\tau^{\min}_{\text{TTC,S}}$	Minimum τ_{TTC} reached during a concrete scenario, as calculated by SSAM
$\tau^{\text{Trig}}_{\text{TTC}}$	The τ_{TTC} threshold at which the active safety system triggers
$\tau^{\text{Filt}}_{\text{TTC}}$	The τ_{TTC} threshold used for filtering conflicts
$\tau^{\text{Crit}}_{\text{TTC}}$	The τ_{TTC} threshold used to filter traffic participants for the definition of P_{crit}
θ_{conf}	Relative heading angle in conflicts
$\theta^{\max}$	Horizontal opening angle. Describes the extent of the sensor field of view, which extends by $\theta_{\max}/2$ to the left and right of the central ray
v	Symbol used for scalar quantities that describe a velocity
$v^{\max}$	Maximum velocity reached during a conflict
v_{rel}	Relative velocity between a lead and a follow vehicle

Symbol	Description
$\vec{v}$	Notation used for vectorial velocity direction
v_c	Collision velocity
$\|x\|$	Number of elements in a set x
$xMinPET$, $yMinPET$	The x- and y- coordinates where the minimum Post-Encroachment-Time was reached during the conflict
X^x	x-coordinate of a vector $\vec{X}$. The y- and z-coordinates are defined analogously
$\vec{X}$	Denotes a position vector $\vec{X}$
$\vec{X}_{\text{COG}}$	Position vector of the center of gravity of a traffic participant
$\vec{X}_S^V$	Sensor position on the vehicle. Specified in the vehicle coordinate system

1. Introduction

1.1. Motivation

According to the global status report on road safety prepared by the World Health Organization (World Health Organization, 2018), 1.35 million people died on roads in 2016, while most of the deaths occurred in low- and middle-income countries. Death numbers relative to the global population size remained stable at around 18 road deaths per 100 000 persons, see Figure 1.1. While the problem of road fatalities has not significantly worsened over the

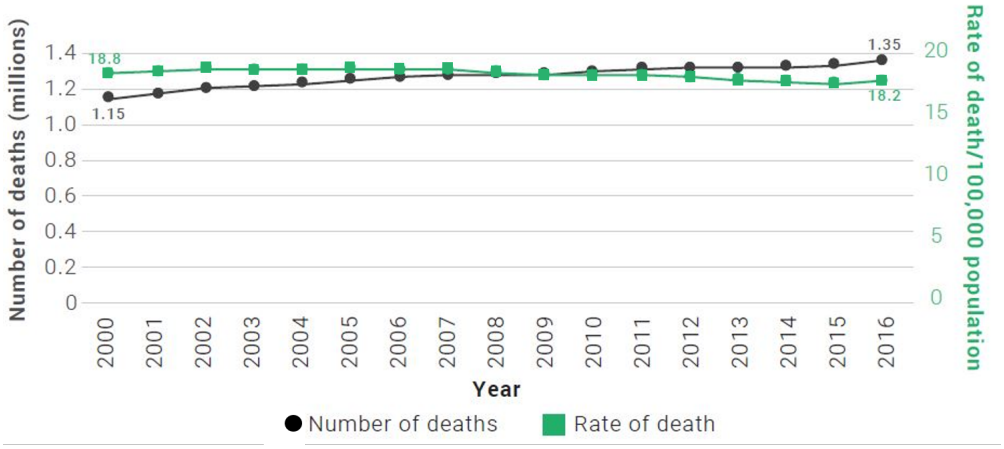

Figure 1.1.: Global number of road fatalities and rate of death per 100 000 persons in the years 2000 to 2016 (World Health Organization, 2018).

past two decades, society is still far from reaching the sustainable development goal #3.6, i.e. to halve the total number of worldwide road deaths by 2020 (World Health Organization, 2018). Road deaths are not acceptable in any way, and measures must be taken to reduce their number as far as possible. The goal is to not only achieve a stagnation of road deaths in relation to population size, but also to decrease this number and ideally reduce it to zero deaths at some point in the future. This means that new approaches must be taken to achieve this goal. Researchers around the world are questioning why the situation is not improving and what can be done to improve it.

Approaches to reduce road fatalities include regulation changes, better new driver education, vehicle structure changes, road infrastructure changes, and many more. An important measure is the installation of safety systems in vehicles. Safety systems can become active in various crash phases. Braess, 1996 (see also in the glossary) categorized crash phases as: the

pre-crash phase (the phase where collisions or hazardous consequences are imminent), the *crash phase* (the phase after first contact between the collision partners) and the *post-crash phase* (the phase after the collision partners have reached their rest positions). This phase categorization also allows the categorization of safety features installed in vehicles in terms of active, passive, and integral safety, see Figure 1.2. Safety functions that can contribute before crashes, i.e., in the pre-crash phase (Braess, 1996), are known as active safety features. Unlike active safety features, safety functions that act in the crash phase are assigned to the area of passive safety. Integral safety, meanwhile, combines aspects of both accident avoidance and the mitigation of accident consequences. Such integral systems may be used, for example, to adjust passive safety measures on the basis of information on the driving state and conflict situation, which are gathered in the pre-crash phase.

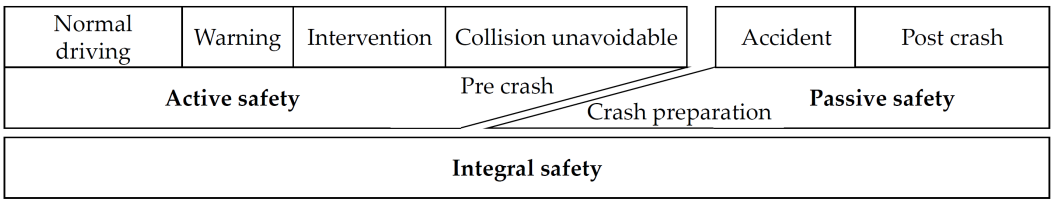

Figure 1.2.: Accident phases, following Helmer, 2014 and Braess, 1996.

The earliest safety systems in vehicles were passive safety systems. Such passive systems include for example the seat belt. A study by the NHTSA (Kahane, 2000) cited that use of the seat belt reduced fatalities by around 45 %, based on data collected from 1986 to 1999 (before the sustainable development goal of halving the total number of worldwide road deaths was formulated). Today, active safety systems such as Autonomous Emergency Brake systems are installed with increasing frequency in modern vehicles (Global Market Insights, 2019). Advances in a wide array of fields such as telematics (e.g., sensor technology, Winner et al., 2015, chapter IV, or inter-vehicle communication, Fuchs et al., 2015), computer science (e.g., real-time capable image processing algorithms, Stiller et al., 2015), vehicle safety, and many more offer many options to design active and integral safety features.

Scientists have studied the mechanisms of how passive systems increase the safety of passengers for many years, and these mechanisms are already well-understood. However, researchers require additional methodologies to develop active and integral safety systems and estimate their safety benefits. After all, active or integral safety system can provide real benefits in several ways. One way is that they can react more quickly than humans when responding to a dangerous traffic situation. To decrease the time before preventive or consequence mitigating measures are applied, active or integral safety systems must automate specific driving tasks. This automation may be installed to varying degrees, extending up to full automation, which is also called autonomous driving. Gasser et al., 2015 presented a categorization system, which can be used to distinguish among the following categories of automation for Advanced Driver Assistance Systems (ADAS) (which include active safety systems):

A) Informing and warning functions: Acts exclusively in an indirect way through the driver on vehicle guidance. Examples: Traffic Sign Assist (warns if a speed limit is detected) and Lane Departure Warning (warns when the vehicle leaves its driving lane)

B) Continuously automating functions: Functions that ensure comfort and which directly influence vehicle guidance. Can be overruled by the driver. Examples: Adaptive Cruise Control (adapts the current speed up to the speed limit or follows other vehicles at a safe distance) and Lane Keep Assist (continuously interferes in the steering process to keep the vehicle in the lane)

C) Intervening emergency functions: Functions related to safety which directly influence the vehicle guidance in situations that might lead to accidents, e.g., situations that cannot be controlled by the driver. Examples: Autonomous Emergency Brake (AEB) (initiates a brake maneuver if a collision is imminent) and Autonomous Emergency Steering (initiates emergency steering maneuvers)

While the systems in category B can contribute to the safety of the driver and occupants through prophylactic measures, the systems in category C intervene at highly specific moments, such as when a collision is imminent. To increase the practicability of automating functions and achieve the intended effect, several aspects have to be considered in the development of ADAS (Abendroth and Bruder, 2015):

- The performance limits of humans in vehicle guidance
- Driver behavior
- Boundary conditions of the development (e.g., legal or regulatory boundaries)
- Traffic safety, i.e., the potential of active and integral safety systems to increase the safety of occupants and other road users
- Behavioral aspects of the human-vehicle interaction
- Functional safety, i.e., ensuring the correct and safe functionality of a product

Regarding the aspects to be considered, the two most central questions are the ones that justify the overall purpose of active or integral safety systems: how much can the investigated active or integral safety system reduce the accident risk? How much can the system reduce the severity of accident consequences, for the vehicle that is equipped with the system and its occupants, as well as for other traffic participants?

1.2. Problem statement

This thesis work was carried out to answer these central questions, targeting active safety systems of type C (intervening emergency functions, see Gasser et al., 2015).

The process that can be carried out to objectively quantify the extent to which an active safety system can increase the safety of vehicle occupants and other road users is commonly called an *effectiveness assessment* (Fildes et al., 2015 or Wimmer, Rieser, et al., 2012), *safety*

assessment Wang et al., 2017 or Helmer, 2014) or, when it is used in a broader safety-related context, the testing of *automated driving functions* (Stellet et al., 2015). In this thesis, the term *effectiveness assessment* is used.

One way to categorize effectiveness assessment methods is to distinguish between *retrospective effectiveness assessment* and *prospective effectiveness assessment* methods (Kühn and Hannawald, 2015). The discerning characteristic is the time of evaluation in relation to the development process or life cycle of the safety system in question. Retrospective effectiveness assessments are carried out to estimate safety benefits using historic data after market introduction (for a more detailed description and an analysis of advantages and disadvantages of retrospective assessment, see Appendix A).

1.2.1. Prospective effectiveness assessment

The prospective approach is favored during the development of new active safety functions, where the safety effect should be be estimated before market introduction. prospective effectiveness assessment methods offer certain advantages (Helmer, 2014):

- The possibility to consider different variations in safety systems (e.g., as was done in J. M. Scanlon et al., 2017, Stefan Schramm, 2011 or Kolk, Kirschbichler, et al., 2016).
- Their early applicability during the development cycle (Hannawald, 2008).
- Only one data set is used (i.e., all available scenarios are used to form the baseline), which eliminates some of the above-mentioned limitations (Hannawald, 2008).

Due to the advantages offered by this approach, prospective effectiveness assessment methods were used in this thesis work.

In the majority of prospective effectiveness assessment methods, a selection of traffic scenarios is considered to form the *baseline*, whereby the safety system to be investigated is not present. Adopting the nomenclature in Ulbrich et al., 2015, the term *traffic scenario*, or synonymously in this thesis simply *scenario*, is defined as the temporal development of several scenes, including an initial scene as the initial condition, see glossary entry "scenario". Thereby, a *scene* is defined as a snapshot in traffic that describes the *environment* (environmental conditions such as weather or lighting conditions), *scenery* (all static elements), dynamic elements, all actors' and observers' self-representations and the relationships among those entities (see glossary entry "scene"). The term *concrete scenario* is based on Menzel et al., 2018 and is defined as a concrete expression of a scenario, where start conditions, parameters and other influencing factors are fixed, such as fixed velocity at the beginning. To define a *treatment* that allows a comparison with the baseline, one or more vehicles in each baseline scenario is/are equipped with the active safety system to be investigated. The scenarios in the baseline can then be compared to scenarios in the treatment to identify differences in the outcome. Within this thesis, this approach is called the *baseline-to-treatment comparison*

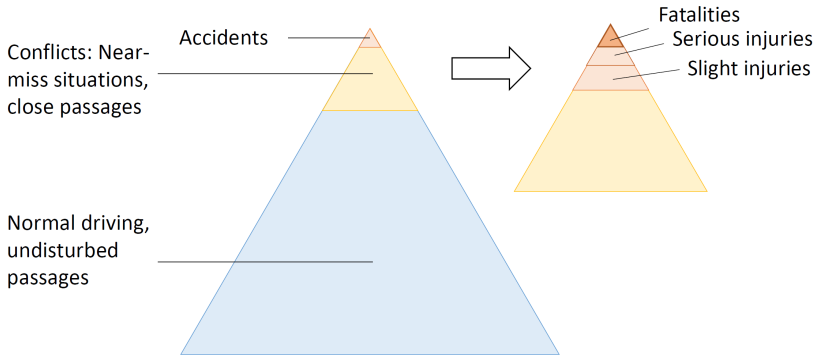

Figure 1.3.: Accidents and scenarios with critical scenes comprise only a small part of all possible scenarios that occur in the flow of traffic (figure based on Hydén et al., 1987).

approach. In the literature, the term *what-if-approach* is also sometimes used, e.g., in Kühn and Hannawald, 2015.

The scenarios that are used to define the baseline represent an important aspect of the effectiveness assessment. Normal driving conditions constitute by far the largest proportion of all traffic scenarios, with the majority of movements being undisturbed passages and the rarest type of traffic events being accidents. Hydén et al., 1987 suggested that a relation exists between the frequency of a certain type of traffic scenario and the severity of the consequences of that traffic scenario. This assumption implies that the most severe events are the least common, i.e., accidents with fatal injuries. A pyramid is often used to depict this relation, see Figure 1.3. When assessing the functionality of active safety systems, however, normal driving events, slight accidents, or near-miss scenarios (i.e., close encounters) can also be of interest. Therefore, one reason for conducting this thesis work was to develop a method that could be used to assesses the effectiveness of both scenarios contained in the upper-most part (accidents) of the pyramid but also of critical scenarios. In this thesis, a critical scenario is defined as a scenario that contains at least one critical scene, i.e., a scene in which a collision course exists between two traffic participants. A collision course exists if the movement direction and velocity of at least one involved traffic participant must be changed to avoid a collision (Gettman and Head, 2003).

1.2.2. A generalized process for prospective effectiveness assessment

To categorize the individual methods that are described later in this thesis, it is necessary to present a generalized process for prospective effectiveness assessment. Page et al., 2015 introduced a method to categorize the steps involved in a prospective effectiveness assessment. Figure 1.4 shows a generalized version of this categorization, which also allows the use of various methods to represent traffic scenarios and introduces an additional intermediate step, i.e., the filtering step.

Figure 1.4 shows the following four main steps:

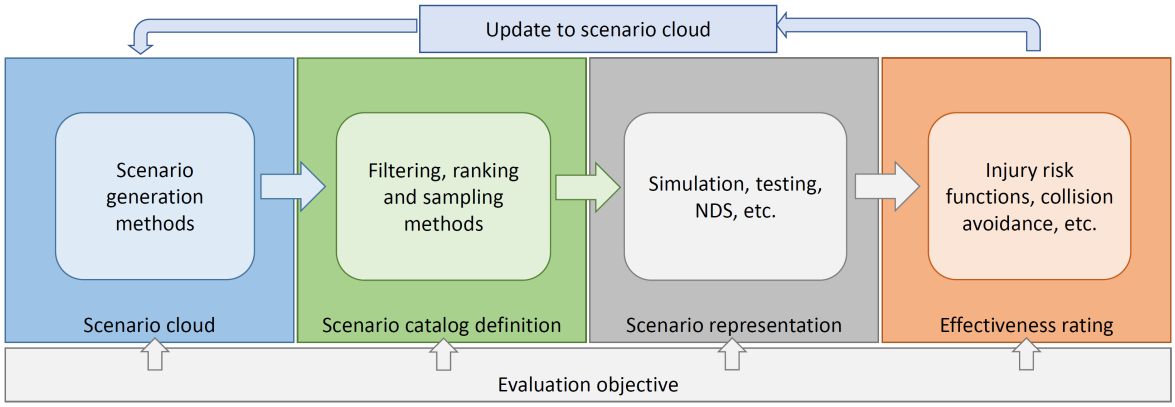

Figure 1.4.: The active safety assessment process, based on the process presented by Page et al., 2015. This process consists of the scenario creation step (*scenario cloud*), the scenario selection (*scenario catalog definition*), the *scenario representation*, and the final *rating* step. Each step is influenced by the evaluation objective. Results may be used to update the scenario cloud.

Scenario cloud: The scenario cloud comprises all possible concrete traffic scenarios, needs input from different sources such as traffic flow simulation, real accident scenarios from databases, expert opinions or other scenario collection or generation methods.

Scenario catalog: The output of the second step is the so-called scenario catalog, which is a set of concrete scenarios that should be considered in the third assessment step. Often, this step is conducted by applying several filters. A filter could be applied, for example, to select only scenarios of a specific type, such as rear-end or lane-change scenarios. The scenario selection algorithm can also employ some type of ranking, e.g., by selecting only the 100 most relevant concrete scenarios for representation, based on a previously defined relevance criterion.

Scenario representation: This is an execution step carried out for the concrete scenarios, which represents the course of actions in traffic. Various options for scenario representation exist: simulation, real physical testing, Naturalistic Driving Studies (NDSs), and more.

Rating: In this step, outputs of the scenario representation step are collected and used to quantify the safety effect, i.e., the effectiveness, of the investigated safety system. A possible output, could be for example the proportion of accidents in the baseline that were avoided in the treatment.

Furthermore, the evaluation objective influences each of the above-mentioned steps. The effectiveness assessment procedure, is carried out to answer questions, formulated precisely in the evaluation objective, such as: who is asking and for what purpose? What type of safety technology will be evaluated?

Finally, the scenarios in the treatment can be used to update the scenario cloud, since the interventions of active safety systems change the course of actions in traffic and might produce new scenarios that would otherwise not occur.

1.2.3. Solution requirements

In this thesis work, the following requirements were defined; based on these, state-of-the-art effectiveness assessment methods were analyzed:

Baseline-to-Treatment comparison approach: The method should allow application of the baseline-to-treatment comparison approach, where each concrete scenario is first considered without a safety system and then with the system under consideration. The representation of the concrete baseline scenario should be repeatable exactly, i.e., when the same concrete scenario is considered twice in the scenario representation step, the results should show no differences. Outcomes can be compared, and the influence of the safety system can be directly evaluated, thus allowing one to reach direct and causal conclusions regarding the safety effects of the investigated systems. Variations in the results due to different safety system configurations and their consequences can be quantified. This requirement is investigated for methods in the scenario representation step and in the rating step.

Critical scenarios: The chosen method should allow the user to assess the effectiveness of active safety systems, not only in accident scenarios but also in critical scenarios, i.e., provide a way to generate this type of traffic scenario and measure the effectiveness of the system in these scenarios. The attempt to avoid a collision in a critical scenario may create new critical scenes that involve additional traffic participants. This requirement is investigated for methods in the scenario generation and in the rating step.

High number of concrete scenarios: The method should allow the user to consider a high number of concrete traffic scenarios, such that the effectiveness results become more robust, i.e., they are not affected significantly when additional new concrete traffic scenarios are considered with the effectiveness assessment. This criterion is understood to be fulfilled when at least 1 000 concrete scenarios can be considered with a reasonable investment of effort. The number 1 000 is chosen to include more concrete scenarios as were included in other well known prospective effectiveness assessment studies, e.g. Sander and Lubbe, 2018 (around 800 concrete scenarios) or Bareiss et al., 2019; J. M. Scanlon et al., 2017 (450 to 500 concrete scenarios). This requirement is investigated for methods in the scenario generation, representation and in the rating step.

Surrounding traffic: In many traffic scenarios, additional participants can be present who are not on a direct collision course with one another. When one or more traffic participants enter a kinematic relationship with each other that might lead to an accident, the non-conflicting (surrounding) traffic can be relevant in that it may obstruct sensors. These participants can also become collision partners if emergency maneuvers are conducted. Therefore, to be able to make a more comprehensive statement about the effectiveness of the system, the surrounding traffic should be considered. This requirement is investigated for methods in the scenario generation and representation step.

Scenery: It should be possible to consider the scenery (the term scenery refers to the road, static objects outside of the road, e.g., buildings, as well as to weather and lighting conditions, see glossary). The scenery can affect the effectiveness assessment, since sensor perception might be limited by visibility obstructions (e.g., trees) or difficult weather conditions (e.g., fog). This requirement is investigated for methods in the scenario generation and representation step.

Resolves the safety technology: Bours and Tideman, 2010 recommended that the following items are considered in particular in prospective active safety assessment methods: sensing technology (e.g., sensor type, resolution, range, field of view), vehicle dynamics (e.g., braking, steering, suspension characteristics), and control algorithms (e.g., sensor data interpretation, decision-making, vehicle dynamics control). To consider these items, the individual respective technological components of active safety systems must be resolved. This requirement is only investigated for methods in the scenario representation step.

1.2.4. Scope definition

The methods were developed with the goal in mind to be extensible to a broad range of scenario types and safety systems, but for the purpose of demonstration in this thesis, the following restrictions were made:

- Only prospective effectiveness assessment methods are considered.
- Only active safety functions of category C (intervening emergency functions, see Section 1.1) are considered.
- Only active safety functions that do not need interaction with the driver are considered (this excludes for example the consideration of Human-Machine-Interface functionalities).
- Only scenarios that contain a critical scene between a passenger car and another passenger car or a passenger car and a van are considered, i.e., this excludes conflicts between passenger cars (or vans) and vulnerable road users (e.g., cyclists or pedestrians).
- No lateral evasion is considered as emergency maneuver.
- Safety benefits of active safety systems are the primary concern, i.e., no cost analysis for safety systems or sensor setups is done. Effects on user acceptance are also not considered.
- Various effects of different market penetration rates are not considered. It is assumed that both conflicting vehicles are equipped with a safety system.
- Traffic participants are represented as moving boxes, i.e., the geometrical shape of each participant consists of six quadrangular faces with right angles.
- No overall rating of safety systems or vehicles is established. Instead, individual safety-related aspects are evaluated.

- No collisions between traffic participants and static objects are considered. Static objects are only considered as possible visibility obstructions.
- No projection of results is applied.
- No variation of driver model parameters in the scenario generation step was conducted.
- The influence of conflict type, collision type (e.g., rear-end, lane-change or crossing) or collision partner type on the effectiveness metrics was not investigated.
- Only two very similar microscopic traffic flow simulation models, representing the same urban traffic site, were investigated for scenario generation.

2. State of the art

In the following four sections, methods are described which are applicable to the four steps (”Scenario cloud”, ”Scenario calaog definition”, ”Scenario representation” and ”Effectiveness rating”) included in the generalized effectiveness assessment process presented in Section 1.2.2. Each section includes a description of the state-of-the-art methods used to take the respective effectiveness assessment steps. At the end of each of the four sections, the presented methods are summarized and reflected in light of the solution requirements established in Section 1.2.3. This allows to define a list for each step in the effectiveness assessment process of current state-of-the-art methods that fulfill the most requirements.

2.1. Scenario cloud

The scenario cloud is defined as the set of all possible concrete traffic scenarios. Since many factors contribute to individual concrete scenarios, it is not possible to provide descriptions of all concrete scenarios. Therefore, the output of each scenario source (e.g., accident databases) is a subset of the scenario cloud, i.e., a scenario sub-cloud.

In general, three different types of scenario generation methods can be distinguished (Alvarez et al., 2017):

1. Establishing a scenario sub-cloud with *original concrete scenarios* of real-world traffic scenarios (e.g., reconstructed real accidents from databases without modification. Zauner et al., 2014 is an exemplary study using this type of scenario cloud).
2. Establishing a scenario sub-cloud with *modified concrete scenarios* of real-world traffic scenarios (e.g., replacing the original vehicle in a reconstructed real accident with another vehicle model, as shown in Kolk, Kirschbichler, et al., 2016)
3. Establishing a scenario sub-cloud with *synthetic concrete scenarios* based on relevant characteristics of real-world traffic scenarios. This method requires an understanding of the contributing factors involved in the targeted traffic scenarios. It uses random distributions of selected parameters to generate indefinite numbers of unique scenarios (e.g., Helmer, 2014).

In the following sub-section, the existing approaches are described for various sources. They are grouped according to the three above-mentioned categories.

2.1.1. Original concrete scenarios

2.1.1.1. In-depth accident databases

Many countries maintain some type of tracking system that is used to record information on traffic accidents. Accident databases contain information with varying amounts of detail. Thomas et al., 2003 distinguished three different types of accident databases:

- Base level: often maintained to prepare national statistics, e.g., useful for the examination of trends, evaluation of effects of legislation, or assessment of accident situations (intended to answer who-, where-, when-, and what-questions about the accident). Input source examples: traffic police reports and national road transport statistics.
- Intermediate level: e.g., useful for the identification of dangerous road locations (intended to additionally answer how-questions about the accident), reconstruction of accidents and determination of appropriate countermeasures. Input source examples: traffic police reports, traffic site observation, evidence from witnesses, and judicial reports.
- In-depth level: e.g., useful for the assessment of accident causation mechanisms, investigation of accident and injury prevention mechanisms, research on vehicle safety and injury mechanisms, and effectiveness of legislative measures. Input source examples: traffic police reports, traffic site observation, evidence from police officers or witnesses, and interviews with involved road users.

The distinction between individual levels is not completely unambiguous. Therefore, for simplicity, the intermediate level is not described further. While national statistics (base level) are available in nearly all countries worldwide, in- depth accident databases are not available for many countries. For national statistics purposes, often all accident are recorded (high case number and low information depth). In the example of the database maintained by Statistik Austria, 2020, all reported accidents that occur in public traffic in Austria are entered into the database (data entries are based on police reports), where at least one moving vehicle and at least one injured person is involved. Since all accidents with fatalities have to be reported, an exact number of fatal accidents can be derived. The IRTRAD road safety database (OECD, 2019) is an example of an international platform (base level) in which accident data can be entered by individual member states, making comparisons between countries possible. Accident databases at the base level are not suitable for use in studies on the accident causes, since this information may simply not be tracked. Furthermore, they are not usable as scenario sources.

In-depth databases such as GIDAS (Seeck et al., 2009) or CEDATU (Tomasch and Steffan, 2006, Tomasch, Steffan, and Darok, 2008) lie at the other end of the spectrum of information depth. These databases contain a rich amount of information on individual accidents, e.g., detailed information on human factors, vehicle factors and installed safety systems,

infrastructure, weather and lighting conditions (see Tomasch and Steffan, 2006). Table 2.1 lists several examples of in-depth databases available all over the world.

Name	Country	Number of parameters	Pre-crash time series data available	Start year	Number of analyzed accidents (p.a.: per annum)	Reference
GIDAS	Germany	ca. 2000	yes	1999	ca. 2000 p.a.	Seeck et al., 2009
CEDATU	Austria	ca. 2000	yes	2007	Up to 200 cases p.a.	Tomasch and Steffan, 2006
CIDAS	China	ca. 2000	yes	2011	ca. 550 p.a.	China Automotive Technology and Research, 2013
ETAC	Europe	ca. 3000	no	2004	624	European Commission, 2008
IGLAD	World	ca. 110	not all cases	2007	ca. 800-1000 p.a.	Ockel et al., 2012
ITARDA's J-TAD	Japan	ca. 70	no	1993	ca. 300 p.a.	ITARDA, 1994
NASS-CDS (SCI)	USA	ca. 250	no	2004	ca. 130 p.a.	NHTSA, 2013
CCIS / OTS / RAIDS	UK	ca. 200	no	2000	more than 3000	Mansfield et al., 2008
RASSI	India	ca. 700	yes	2011	ca. 2000	RASSI, 2014
Insurance in-depth databases	Different company specific databases are available that focus on material damage claims					Gwehenberger and Borrack, 2015

Table 2.1.: Examples of in-depth databases, extracted from a report by the P.E.A.R.S. initiative, 2016.

In some cases, in-depth databases include reconstructions made with the time series data from the pre-crash phase (see column "Pre-crash time series data available" in Table 2.1), making such in-depth databases possible direct scenario sources for original concrete scenarios. The suitability of in-depth databases as scenario sources depends on how they are maintained, with the main criterion being whether pre-crash data are available. There can be other fundamental differences between these databases, as can be seen in Table 2.1, for example, in terms of the number of cases, accident types represented, number of new cases per year, number of parameters, age of data and other factors. Reconstructed real accidents from in-depth databases have been used in several studies as sources for scenarios:

- Simulation by Busch, 2005 or in the PreEffect-iFGS method in Stefan Schramm, 2011. These authors reconstructed the real accidents based on a parameterization of the accidents in the GIDAS database and used the reconstructions as concrete scenarios to form the baseline.
- In the rateEffect method, time series data for the pre-crash phase of accidents in the GIDAS database are used as input for the simulation (Döring et al., 2012 and Schubert et al., 2012).
- Reconstructed real accidents from the CEDATU that include time series data for the pre-crash phase in the form of PC-Crash simulations (Moser, 2020) were used in the following studies: Billicsich, Tomasch, Markovic, et al., 2016; Billicsich, Tomasch, Sinz, et al., 2015; Eichberger, Tomasch, Rohm, and Hirschberg, 2009; Eichberger, Tomasch, Rohm, Hirschberg, and Steffan, 2011; Kolk, Kirschbichler, et al., 2016; Smit et al., 2019;

Zauner et al., 2014.

Compared to databases maintained at the base level, where less detail is contained in the data entries, the case numbers in in-depth databases are often lower due to the higher effort required for data entry. One consequence is that certain accident configurations may be over- or underrepresented, which skews the results of the evaluation of an active system if they are well or badly suited for an over- or underrepresented accident configuration. Imbalances in the sample size can be discovered by comparing the number of accidents for specific accident types in the in-depth database with the appropriate number in national statistics (base level). Such imbalances can be accounted for by carrying out a projection of results using data from databases at the base level, see for example Hautzinger et al., 2006.

One general disadvantage of accident databases when serving as a scenario source of a prospective effectiveness assessment is that they only contain accidents; only some databases (not all) focus purely on fatal accidents, thus comprising the upper-most level of Hyden's pyramid, as shown in Figure 1.3.

2.1.1.2. Naturalistic Driving Study and Field Operational Test data as scenario source

Naturalistic Driving Study (NDS) and Field Operational Test (FOT) are study methods that are primarily conducted to investigate driver behavior, by observing how humans perform the driving task under real traffic conditions (further information about NDSs and FOTs and examples can be found in Appendix B). They are also used to study the interaction between drivers and active safety systems (Faber et al., 2011). In FOTs and NDSs, data are continuously recorded for detailed analysis. These data may include GPS positions, kinematic quantities (e.g., speed, longitudinal and lateral acceleration), video recordings, and more (Fitch and Hanowski, 2012, Russell et al., 2018). The recorded data may contain a high variety of detailed information about the observed vehicles. However, even if the experimental vehicles have several cameras installed, it is extremely difficult to gather the same variety of information on other nearby traffic participants that do not participate in the study. Nevertheless, researchers can record simple kinematic quantities in relation to other traffic participants, such as the temporal distance (time headway) to the vehicle in front or the estimated time to collision (if the experiment vehicle enters on a collision course with another vehicle, Faber et al., 2011). Analysts manually identify relevant crash- or near-crash-scenarios (events where a collision would occur if no evasive measure were executed) or by applying appropriate sampling techniques to automatically extract the scenarios (see Section 2.2.2.1).

Like databases, this scenario source serves as a direct source in methods that use *original concrete scenarios*, and may provide important insights that allow researchers to generate *synthetic concrete scenarios* by supplying necessary information for the development of driver models (as is done, for example, in Bärgman, 2016).

2.1.1.3. Stationary traffic surveillance

Researchers can apply traffic surveillance techniques with stationary cameras or other equipment to produce valuable information and generate a scenario sub-cloud. Based on the level of sophistication of the surveillance equipment and methodology, they can extract time series data, such as the velocities or trajectories of vehicles. C. Erbsmehl et al., 2016 present an example of such a tracking technique. Al-Smadi et al., 2016 reviewed current vehicle detection and tracking methods, Arinaldi et al., 2018 noted that some surveillance techniques use modern machine learning methodology. The extracted time series data can either be used directly as *original concrete scenarios* or to find the necessary parameter distributions (e.g., average velocities, distances, vehicle following behavior) to generate *synthetic concrete scenarios*, such as those generated by traffic flow simulation models (see Section 2.1.3.1).

2.1.2. Modified real concrete scenarios

Modified scenarios are scenarios that are created by changing existing concrete scenarios taken from real traffic, e.g., reconstructed real accidents from in-depth accident databases, scenarios taken from NDS / FOT, or traffic surveillance. The change can be applied to several aspects and parameters of the scenarios: vehicle models, scenery conditions, and more. This can be done either by varying the aspects and parameters stochastically, or by modifying the scenarios in a pre-defined way. Exemplary applications are given in Kolk, Kirschbichler, et al., 2016, in which the original vehicles were replaced by smaller and less heavy L7e, respectively, L6e vehicles, or in Bostrom, 2014, in which the vehicle path leading to an accident was varied such that the vehicles drive in trajectories that are slightly altered as compared to the original trajectories. In Schramm and Roth, 2009, reconstructed real accidents in the GIDAS database were re-simulated while varying the start time when certain maneuvers, such as emergency braking, occurred.

These new scenarios can, in turn, be seen as an update to the scenario cloud (see Figure 1.4), because they represent scenarios that might be equally as plausible as the original reconstruction or might be possible in the future.

2.1.3. Synthetic concrete scenarios

2.1.3.1. Traffic flow simulation

Traffic streams in the real world exhibit a high degree of complexity, and researchers must often overcome high barriers to perform experiments with real world traffic (e.g., regulatory barriers), making traffic flow simulation an essential tool in traffic engineering. The physical propagation of traffic flow can be described by using computational models. Such models are classified as *macroscopic*, *mesoscopic*, *microscopic*, or *nanoscopic* models, depending on

the level of detail (e.g., see Detering, 2011 or Langenberg, 2015). A list of traffic simulation software, along with the level of model detail, is given in Table 2.2.

Macroscopic models place a focus on statistical measures of traffic flow such as vehicles per hour. Every vehicle is handled in the same way, and single vehicles are combined into a group or into a traffic stream (Passos et al., 2011). One of the theoretical backgrounds is based on principles of fluid mechanics, allowing the use of the continuity equation.

Microscopic models are used to resolve the flow on a vehicle-by-vehicle basis, including positions and velocities over time. As an example, Fellendorf and Vortisch, 2010 described the microscopic traffic simulator VISSIM as four connected modules: the first module describes the physical properties of road and railway infrastructure; the second module, the vehicles and drivers together with their route planning; the third module, all elements necessary to control the traffic such as priority rules, traffic signals and more; and the fourth module, simulation control. The first three modules are constantly active during the simulation, while the last module is responsible for the collection of simulation results. In a microscopic traffic flow simulation, it is possible, to model individual road lanes, the behavior of individual traffic participants and their interactions with each other and with traffic light-signal systems.

Mesoscopic models fall into a category between microscopic and macroscopic in terms of the level of detail that can be attained, see Daganzo, 1995. They offer users the possibility to investigate individual vehicles and examine macroscopic traffic performance indicators such as velocity-density indicators. Interactions between vehicles are not considered.

Nanoscopic simulation: Detering, 2011 and Langenberg, 2015 also distinguished a fourth type of simulation, the nanoscopic traffic simulation. Users not only use nanoscopic simulation to consider the interactions between vehicles, their drivers, and traffic in great detail, but also to consider further physical effects. This means that users can obtain detailed information about driving dynamics such as the engine, suspension characteristics, Anti-lock Braking System (ABS), Electronic Stability Control (ESC), or skidding in curves. However, nanoscopic simulation requires a higher amount of computational effort than the other model scales to simulate the same number of vehicles (Detering, 2011).

Except for the macroscopic method, traffic flow simulation can be used as a source of concrete scenarios. Unlike an accident database that only contains accidents, traffic flow simulation also serves as a source of critical scenarios and normal driving scenarios, thus also yielding scenarios in the middle and lower part of the traffic pyramid, as described by Hyden, Figure 1.3. Accident databases rarely contain detailed information about the surrounding traffic (except the two colliding traffic participants), which might have been present during the accidents. Kolk, Tomasch, et al., 2018 used microscopic traffic flow simulation as a scenario source, to show that this surrounding traffic can play a role due to visibility obstruction. Microscopic and nanoscopic traffic flow simulation provide

Traffic-simulation tool	Macroscopic	Mesoscopic	Microscopic	Nanoscopic
AIMSUN	yes	yes	yes	no
MITSIMLab	yes	no	no	no
PARAMICS	yes	no	no	no
PELOPS	yes	no	no	yes
SUMO	yes	no	no	no
VISSIM	no	no	yes	no
VISSUM	yes	no	no	no

Table 2.2.: Examples of traffic flow simulation software, based on Detering, 2011 and a report by the P.E.A.R.S. initiative, 2016.

such information on the surrounding traffic in the form of detailed time series data. The interference of an active safety system can influence the further flow of traffic, and this effect can be seen when using this scenario source, as has been done in Jeong and Oh, 2017. A disadvantage of using traffic flow simulation as a scenario source is that the resulting scenarios are restricted to the simulated traffic site. Users can obtain a more comprehensive view of traffic when simulation models for larger areas are applied, e.g., city districts. Traffic flow simulation itself does not yield information about the scenery. Such data have to be entered manually or by automated processes. Furthermore, traffic flow simulation models must be calibrated and validated to produce realistic concrete scenarios.

2.1.3.2. Stochastic variation in logical scenarios

Stochastic variation is a tool to produce an indefinite number of new *synthetic concrete scenarios* to be used in assessment methods that involve simulation. Instead of variation in original concrete scenarios which leads to modified concrete scenarios (see Section 2.1.2), stochastic variation can also be applied to logical scenarios to generate synthetic concrete scenarios. Logical scenarios are scenarios which are for example derived based on the definition of accident types, e.g., accidents between vehicles and pedestrians who cross the street, see glossary entry "logical scenario" or Menzel et al., 2018. After definition of the logical scenario, new concrete scenarios are then created stochastically based on knowledge on distributions and characteristics of relevant parameters and scenario influencing factors. After all, most of the influencing factors active during scenarios in the real world are not fully deterministic but rather follow a distribution. The stochastic concept can be applied to various aspects of the scenario, for example:

- Driver models. Many variables describing the behavior of drivers follow distributions, e.g., reaction times, the desired speed traffic participants choose in urban areas or the maximum chosen acceleration.
- Environmental variables, e.g., road friction, lightning conditions or weather conditions.

- Variation in kinematic initial conditions, e.g., by changing start position or start velocity of vehicles. Schmidt et al., 2018 developed a simulation framework that stochastically places vehicles on a motorway with their initial speed following a normal distribution, thereby generating concrete motorway scenarios.

Ebner et al., 2011 is an example for an approach that first analyses reconstructed pedestrian accidents in the GIDAS database to acquire distributions for accident relevant parameters. These distributions are the used to define new scenarios based on logical scenarios. Similarly, Roesener, Fahrenkrog, et al., 2016; Roesener, Sauerbier, et al., 2017 present a generally applicable approach that first uses Kernel Density Estimation to find distributions for relevant parameters based on FOT data and then generates concrete scenarios stochastically.

A fundamental difficulty when using stochastic approaches is to find the right distributions for the parameters under variation. Depending on the parameter type, some of these distributions can be found by analyzing sources such as databases, NDS or FOT data (Alvarez et al., 2017). Other parameter distributions may be more difficult to find, for example driver reaction times in the case of certain events. Often, they have to be researched through specifically designed studies such as driving simulator studies.

2.1.3.3. Test protocols

Test protocols define a fixed set of concrete scenarios for physical testing, which are relevant to specific safety features. Test protocols are published by several institutions such as New Car Assessment Programmes (NCAPs) (consumer protection agencies), insurances or governments. Examples can be found in Table 2.3.

Name	Region	Initiator	Driver assistance
ANCAP	Australia	ANCAP, Canberra	Emergency brake systems vehicle vs. vehicle
ASEAN NCAP	Southeast Asia		None
C-NCAP	China		None
Euro NCAP	EU-28	Euro NCAP, Brussels	Emergency brake systems (vehicle vs. vehicle and vehicle vs. pedestrian), lane departure warnings, speed limiters
US NCAP	USA	NTHSA, Washington	Collision warning, lane departure warning
IIHS	USA	Insurance Institute for Highway Safety, Arlington	Emergency brake systems vehicle vs. vehicle

Table 2.3.: Examples of NCAP and insurance test protocols and organizations that publish them, based on Seiniger and A. Weitzel, 2015

Test protocols are testing procedures which are usually very clearly defined to increase reproducibility. Their description includes the relevant contributing factors such as initial

speeds and positions of objects and vehicles or how to prepare the vehicles for the tests. Usually a range of values for relevant parameters (e.g., a speed range of 20 km/h to 60 km/h, in steps of 5 km/h) is defined to be tested and a few variations of the test setup are prescribed (e.g., pedestrian crossing the street from the left and crossing from the right). The variation parameters and their values are chosen based on knowledge sources such as accident databases. Test protocols aim to define concrete scenarios that represent the most common accident scenarios (e.g., based on accident databases at the base level). Concrete scenarios from test protocols are an abstraction of real accidents and fall under the category *synthetic concrete scenarios* with a variation in several parameters.

2.1.4. Summary and discussion of the solution requirements

	Critical scenarios	High number of concrete scenarios	Surrounding traffic	Environment
In-depth accident databases	–	d	–	∼
NDS / FOT as scenario source	+	d	∼	∼
Traffic surveillance	+	–	+	∼
Modified scenarios	+	d	d	∼
Microscopic traffic flow simulation	+	+	+	∼
Nanoscopic traffic flow simulation	+	∼	+	∼
Test protocols	–	–	+	+
Stochastic variation of logical scenarios	+	+	+	∼

Table 2.4.: Methods for scenario generation. Distinction of suitability to fit the defined solution requirements: well suited (+), insufficiently suited (–), neutral (∼) and depends on the chosen method (d).

This section discusses the valuation of each scenario cloud method individually paragraph by paragraph, according to the solution requirements established in Section 1.2.3. For scenario generation, the applicable solution requirements are ”critical scenarios”, ”high number of concrete scenarios”, ”surrounding traffic” and ”scenery”. Each method is rated according to each requirement in the categories well suited, neutral, insufficiently suited or depends (i.e., suitability depends on the specific implementation). The results are summarized in Table 2.4.

Critical scenarios: Except in-depth accident databases, which contain only accidents by definition (insufficiently suited), and test protocols, which usually only describe scenarios that lead to accidents (insufficiently suited), every method can come up with critical scenarios (well suited). When using the modified scenario approach, even

when using accident databases as primary source, critical scenarios might occur (well suited), see Alvarez et al., 2017 (e.g., due to changed vehicle geometries).

High number of concrete scenarios: Regarding a high number of concrete scenarios (more than 1000 concrete scenarios), for in-depth databases, it depends on the database to be used. Not all databases contain a sufficient number of cases, see Table 2.1. Similarly, NDS and FOT also need to be conducted for a sufficient amount of time with sufficiently many vehicles. One of the largest of such studies, the SHRP2 NDS, aggregated data for 52 million driven kilometers, during which around 700 crashes and 7000 safety critical events (violent evasive maneuvers involved) occurred (Campbell et al., 2013). However, some of the smaller studies aggregate below 1000 such events. For example, only 5 minor crashes and 66 critical scenarios were registered in the L2 NDS, where around 350 000 km were driven, see Russell et al., 2018 (depends). No direct crash numbers can be found in the literature for traffic surveillance. However, accident data published by the Statistik Austria, 2020 can be considered to put traffic surveillance as scenario source into perspective. For example, on Austria's motorways, around 2000 accidents with injured occupants occur per year. Austria has around 1750 km of motorways, i.e., 1.14 accidents occur per km per year. Even if a traffic surveillance installation covers 1 km of motorway, and assuming a ten-fold number of critical scenarios (the same factor as can be observed for SHRP2 or L2 NDS), it would take roughly 80 years to record 1000 accidents and critical concrete scenarios. Therefore, at least for motorway scenarios in Austria, traffic surveillance as scenario source would not fulfill the requirement of a high number of concrete scenarios (insufficiently suited). For modified concrete scenarios, it depends on the primary scenario source (depends). Stochastic methods (including traffic flow simulation) can generate as many individual concrete scenarios as required (well suited). However, as noted by Detering, 2011, the nanoscopic variant (neutral) requires significantly more computation time than the microscopic traffic flow simulation method. Test protocols typically only define a limited number of concrete scenarios, since they are designed for real physical testing, where 1000 or more test runs is near impossible to obtain (insufficiently suited).

Surrounding traffic is most of the time not included in real accident reconstructions from in-depth databases, since vehicles that are potentially present, but not part of the accident, are in most cases not reported (insufficiently suited). For NDS or FOT, only basic kinematic relationships to other traffic participants are recorded, see Section 2.1.1.2. However, advanced object recognition might be applicable in the future to generate time series data within a limited radius around the test vehicle from video recordings in a post-processing step (neutral). Traffic surveillance also offers information on the full traffic within the investigation region. For modified scenarios, it depends on the underlying scenario source (well suited). Traffic flow simulation offers the full traffic that is present in the simulated time frame (well suited). For most test protocols, additional traffic is defined in the case that it is relevant for a specific scenario (well

suited). Stochastic variation in logical scenarios does not restrict the consideration of additional surrounding traffic if required (well suited).

Scenery: For any method except test protocols, scenery descriptions are not a vital part and have to be added if needed, resulting in additional effort (neutral). In test protocols, such as the Euro NCAP AEB VRU systems protocol (Euro NCAP, 2019), the environment is defined where it is relevant to the system under test or at least in the form of road friction or lighting conditions. In some cases, sight obstructions are defined, e.g., in the Car-to-Pedestrian Nearside Child scenario (Euro NCAP, 2019) (well suited).

Considering the results in Table 2.4 and in the summary in this section, it can be seen that microscopic traffic flow simulation and stochastic variation in logical scenarios match the solution requirements from Section 1.2.3 with the least restrictions. Logical scenarios are defined without correspondence to real traffic sites. In contrast, traffic flow simulation models are created to reflect traffic on real traffic sites, i.e., they can be validated using traffic and driver behavior data recorded for specifically that traffic site. Between microscopic and nanoscopic traffic flow simulation, there is the difference that microscopic simulation requires less computation time and can therefore span a larger road network, i.e., it can be used to produce a larger variety of concrete scenarios (Detering, 2011).

2.2. Scenario catalog

The first step in the effectiveness assessment process sketched in Section 1.2.2 yields a sub-set of the scenario cloud, i.e., a scenario sub-cloud. Not all concrete scenarios in the scenario sub-cloud will be relevant for the effectiveness assessment of a specific safety system. Furthermore, out of the concrete scenarios in the scenario sub-cloud, not all concrete scenarios are *addressable* by the safety system. A concrete scenario is considered *addressable*, when the safety system is designed to influence the course of actions in this type of scenario. A clear description of which type of scenario is addressable should be given in the evaluation objective, see Section 1.2.2. Based on the addressable concrete scenarios which are contained in the scenario sub-cloud, a *scenario catalog* is formed through appropriate scenario selection methods. In addition, it is possible that not all addressable concrete scenarios are produced by a specific scenario generation method. For example, if an emergency braking system designed to avoid intersection accidents should be investigated, and an in-depth database is used as scenario source, it is not possible that the database contains all possible intersection accidents. The relationships between the related sets scenario cloud, scenario sub-cloud and scenario catalog are shown in Figure 2.1.

When selecting concrete scenarios, there can be two different situations: the source is finite, i.e the scenario catalog has to be defined by selecting concrete scenarios from a countable number of addressable concrete scenarios in the sub-cloud, or the source is infinite, i.e., when parameter distributions are defined for stochastic variation in logical scenarios as the

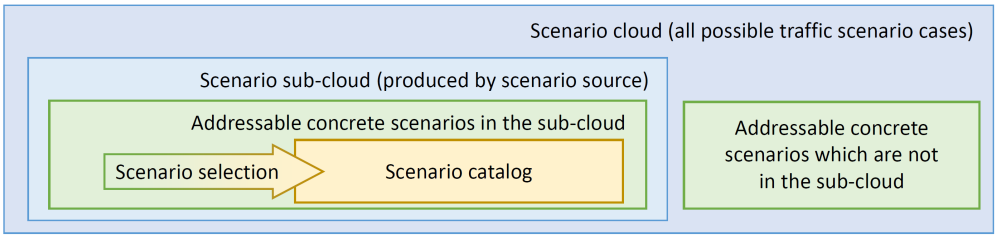

Figure 2.1.: Quantitative relationships of the sets *scenario cloud*, *scenario sub-cloud*, *addressable concrete scenarios* and *scenario catalog*.

scenario source. Using parameter distributions for stochastic variation, an infinite number of concrete scenarios can be generated and appropriate methods for the determination of specific values from random distributions need to be applied.

For the selection from finite sources, Lagares and Puerto, 2001 and Krapp and Nebel, 2011 distinguish the following two methods:

Random selection: Every element of the scenario sub-cloud has the same probability to be selected.

Non-random selection: Certain scenarios of the scenario sub-cloud are never being drawn, not drawn with equal probability, do not have computable selection probability or when the selection chance is related to a feature of the elements.

Since random selection from finite sources is rarely necessary in the context of active safety effectiveness assessment, it is not explained in more detail. Among other methods, Bourier, 2013 lists the following methods applicable for non-random selection:

Selection of typical elements: Only elements that are representative of a group within the scenario sub-cloud are selected. An example is the selection only of those accidents of a specific type.

Concentration principle: If the sum of some feature is concentrated on few elements, those elements are chosen and the others left out. An example in the context of effectiveness assessment would be to choose scenarios based on a criticality criterion, i.e., scenarios that have a higher inclination to lead to an accident. With this approach, concrete scenarios of lower criticality (e.g., scenarios that are categorized as normal driving, see Hyden's pyramid in Figure 1.3) would be neglected.

It is also possible that the mentioned selection methods are applied iteratively, i.e., a sub-selection is defined based on a previous selection.

In the following, scenario selection methods are grouped in three categories depending on whether they use the concentration principle, selection of typical elements or parameter distributions as an infinite source.

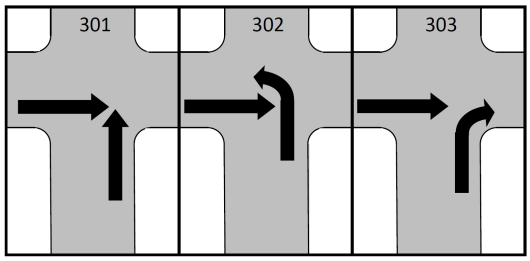

Figure 2.2.: Examples of scenario types in the category "conflict vehicle coming from the right ignores priority rights": collision when conflict vehicle drives straight (301), turns left (302) or turns right (303) (Statistik Austria, 2000).

2.2.1. Selection of typical elements: scenario type

With this selection method, only traffic scenarios of specific types are chosen. This represents a non-random selection of typical elements. It is often the first selection step before other selection methods are applied and can be a way to find the addressable scenarios.

There are several ways to categorize traffic scenarios into types. A common categorization for accident scenarios are accident type catalogs, such as the one by the GDV (Unfallforschung der Versicherer, 2016) or Statistik Austria, 2000. Accident type descriptions usually define the driving mode before the accident (e.g., one car follows the other before the crash). Thus, the various possible driving modes before collision can be deduced from the accident types and can thus be used to categorize conflict-free driving or critical scenarios without accidents. Examples of some intersection accident types are given in Figure 2.2.

The distinction in the mentioned accident type catalogs is of fine granularity. Also a more coarse categorization is possible: select all scenarios that involve car-following on a single road lane, or all scenarios that involve lane-changes on motorways. For example, a preliminary selection step could involve considering only traffic scenarios that fall under the category "rear-end collision", as well as all driving modes that can directly lead to a rear-end conflict.

Examples of studies that conduct selection by accident type (using in-depth databases as scenario source) are Kolk, Kirschbichler, et al., 2016 or Sander and Lubbe, 2018, where intersection Autonomous Emergency Brakes (AEBs) were investigated for intersection accidents.

2.2.2. Concentration principle

2.2.2.1. Identification of critical scenarios through Safety Surrogate Measures

With this selection method, a measure of safety is applied to individual concrete scenarios or continuous traffic data (e.g., from traffic flow simulation or traffic surveillance), which

then allows to focus on those concrete scenarios which are considered the least safe by the measure. In this regard, this type of selection method applies the concentration principle.

For the purpose of defining the criticality of a traffic scene, a criterion that correlates with the risk of a given scene to lead to an accident is required. Such criteria are termed *Safety Surrogate Measures (SSMs)* in the literature (Gettman, Pu, et al., 2008), while scenes where the measures lie below a defined threshold are termed *conflicts*. An investigation on which criteria might be suitable was for example done by Minderhoud and Bovy, 2001, with two examples being *Time-to-Collision (TTC)* and *Post-Encroachment-Time (PET)*. TTC is defined as the time needed from the current moment in time to first contact between two traffic participants under the assumption that they continue on their current path of motion without change of longitudinal vehicle control by the driver (accelerating or braking). If two traffic participants are not on a collision course, the TTC is not defined, i.e., it is possible that two traffic participants miss each other by mere centimeters and TTC does not detect this situation as conflict. A criterion that does not have that disadvantage is the PET criterion (initially proposed in Allen et al., 1978), which is defined as the time from when a traffic participant leaves a conflict zone until another traffic participant enters that zone. This criterion exists if two traffic participants occupy the same space during their course of motion, but not necessarily at the same time. However, PET has the disadvantage that it is only useful in the case of crossing trajectories (Mahmud et al., 2017). For a visual explanation of PET and TTC, see Figure 2.3.

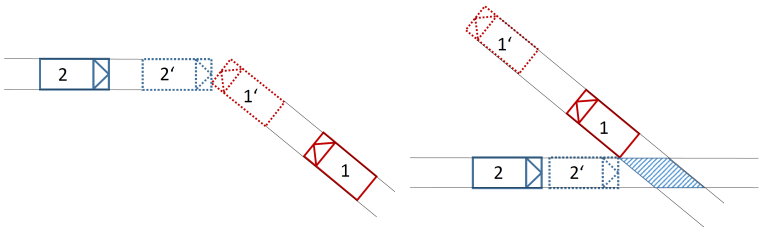

Figure 2.3.: Left picture: TTC is defined as the time needed to travel from the current position 1 and 2 to positions 1′ and 2′, the positions at first contact. Right picture: If the paths of two traffic participants intersect (shaded area), they have a mutual conflict zone. PET is the time from when the first vehicle leaves the zone (positions 1 and 2) to the time when the other enters it (Positions 1′ and 2′).

TTC and PET are two time based SSMs. Mahmud et al., 2017 present an extensive summary of safety surrogate measures that not only covers temporal indicators (e.g., TTC), but also distance based (e.g., *Proportion of Stopping Distance*, Allen et al., 1978) and deceleration based surrogate measures (e.g., *Deceleration Rate to avoid a crash*, Almqvist et al., 1991). Hillenbrand, 2011 describes the composite measure Time-to-React (TTR), which is defined as the maximum of the Time-to-Brake (TTB, the time until the latest possible initiation of a collision avoiding brake maneuver), the Time-to-Kickdown (TTK, the time until the latest possible initiation of a collision avoiding brake maneuver), and the Time-to-Steer (TTS, the time until the latest possible initiation of a collision avoiding steering maneuver). While most distance based measures are often easy to calculate in comparison to the other measure

types, they are often only applicable in specific conflict types. Many deceleration based measures acknowledge the severity of the required braking maneuver to avoid a potential collision, which is often not considered in time based measures.

To identify a conflict based on TTC, the minimum TTC can be used (denoted by the variable $\tau_{\text{TTC}}^{\text{min}}$). For intervals during which the TTC exists, i.e., during which a collision course exists, the minimum value of TTC is calculated. The point in time when $\tau_{\text{TTC}}^{\text{min}}$ is reached is denoted by $t_{\tau_{\text{TTC}}^{\text{min}}}$. If $\tau_{\text{TTC}}^{\text{min}}$ falls below a defined threshold, the scene at $t_{\tau_{\text{TTC}}^{\text{min}}}$ is considered to be a conflict. By including a time span before and after $t_{\tau_{\text{TTC}}^{\text{min}}}$, a scenario can be defined around the conflict. This principle is for example applied in Kolk, Tomasch, et al., 2018, where a scenario is identified in microscopic traffic flow simulation results based on a conflict defined using TTC. Another example where this principle is applied for effectiveness assessment of Adaptive Cruise Control (ACC) and Forward Collision Warning (FCW) systems is Faber et al., 2011. They identified conflicts in FOT data using measures such as TTC to investigate the frequency of occurrence of conflicts in regard to safety system presence.

2.2.2.2. Ranking by relevance

Another non-random sampling method that falls under the category of the concentration principle is ranking by relevance. The relevance is thereby composed as the scalar product of several factors. In the simplest form, the relevance of a concrete scenario can be expressed by

$$Rel = Exp \cdot Sev \cdot (1 - Cont), \tag{2.1}$$

using the following quantities:

Exposure Exp**:** Represents the probability of occurrence of the specific scenario type and is composed of several other factors, with values ranging 0 to 1, where 0 means that the scenario type never occurs and 1 means that only this scenario type occurs.

Severity Sev**:** Describes the consequences of a collision. Values range from 0 to 1. The value 0 can mean, for example, that there is a 0 probability that an injury of a specific type is suffered, and can 1 mean that an injury of that type is always the consequence.

Controllability $Cont$**:** A measure of how controllable a scenario is for the investigated safety system, or how controllable the scenario is if the safety system does not act appropriately (e.g., in the case of a false positive system response). The values range 0 to 1, where 0 can mean, for example, that the human does not have the chance to react properly, and 1 means that a collision can always be avoided.

The method was created on the basis of the ISO-norm 26262 (see Wilhelm et al., 2015 or Hillenbrand, 2011) and uses aspects of functional safety management with the Automotive Safety Integrity Level (ASIL) as key element (Kafka, 2012). Ranking can be used to find the concrete scenarios that are most relevant to the effectiveness of a system and can be implemented as a two-step process, e.g., by preliminary simulation to determine the

controllability and severity and subsequent simulation or physical testing of only the most relevant scenarios. Equation 2.1 leads to the effect that an easily controllable scenario with severe consequences (e.g., severe injuries) would lead to a similar relevance as a barely controllable scenario with negligible consequences.

D. A. Weitzel, 2013 investigates an approach based on the aspects mentioned above to determine to which extent safety system interventions that are not appropriate for a given scenario can be controlled by human drivers. He divides scenario influence factors (e.g., precipitation or driver drowsiness) into classes, defines concrete scenarios for these classes and applies objective criteria (e.g., time to break) to estimate the controllability through simulation. This further allows estimation of the relevance of individual parameter expressions in influence factor classes through multiplication of Exp and $Cont$. The most relevant parameter combinations can then be selected for real tests.

In Mikschofsky, 2017, a ranking method using Equation 2.1 was developed and applied for effectiveness rating of an autonomous emergency brake system for pedestrians (AEB-P). Mikschofsky defines the severity as the probability to suffer a specific injury through injury risk curves, the exposure based on the relative occurrence of a specific pedestrian accident type in an accident database and the controllability based on the extent to which the initial velocity can be reduced by the AEB-P in simulation. The most relevant concrete scenarios are selected for real testing.

A similar approach to identify the worst-case concrete scenarios through simulation to test them on test tracks is presented by Chelbi et al., 2018. For each concrete scenario s, they first identify the baseline impact speed $v_c(s)$ and then the impact speed reduced by safety systems $v_c(TR(s))$ (with $TR(s)$ being the concrete treatment scenario) and compute a risk score between 0 and 1 based on the product $v_c(s)v_c(TR(s))$. After an additional weighting, scenarios with risk higher than 0.9 are suggested for physical testing.

An advantage of relevance based ranking is that it is a way to reduce the number of concrete scenarios, if they could otherwise not be represented due to their high number. A disadvantage is that the relevance measure is chosen with respect to a specific effectiveness metric that is applied in the final rating step (Section 2.4), i.e., if a scenario is not relevant based on the employed relevance and related effectiveness metric and is therefore omitted, the omission might still influence other effectiveness metrics.

2.2.3. Selecting from random distributions for stochastic variation

For stochastic variation in logical scenarios, the definition of appropriate random distributions and their parameterization can be interpreted as the scenario generation step (Section 2.1). In that sense, generating individual values from the defined distributions can be seen as scenario selection. For that purpose, a random *sampling method* is required. Sampling methods to generate random numbers from commonly occurring distributions

such as the Gaussian normal distribution (Kroese et al., 2011) are implemented in almost all modern programming packages. In some cases, advanced algorithms have to applied, such as the Metropolis-Hastings algorithm used in Chelbi et al., 2018 that generates values from parameter distributions for relative distance, relative velocity and weather conditions. The distributions used by Chelbi were extracted from a FOT study through kernel density estimation (see for example Rosenblatt, 1956).

When a scenario's parameters are varied randomly to generate several concrete scenarios, it is possible that many concrete scenarios are produced that do not lead to a critical situation according to a previously defined criticality criterion, and might even fall under the category of normal driving (see Hyden's pyramid, Figure 1.3). This can be a desirable effect for example in effectiveness studies where false positive activations of safety systems are investigated. However, the resulting number of concrete scenarios can be huge. A remedy if computational resources are limited is to use a guided algorithm, where the output of previous simulation runs is used to setup the scenario in the next simulation run with the expectation that it is more critical. Such an approach was followed by Puch et al., 2013 or Hu, 2005.

2.2.4. Summary and discussion of the solution requirements

For the scenario selection step, none of the requirements mentioned in Section 1.2.3 is applicable to the scenario selection step, except that the scenario selection method must be compatible to the remaining method. This requirement is discussed in the solution approach (Chapter 4.

2.3. Scenario representation

Starting with the initial conditions defined in the concrete scenarios to be investigated, a scenario representation method is a way to execute the temporal evolution of the concrete scenarios. Hakuli and Krug, 2015 distinguish available scenario representation methods based on the degree of involved virtualization. They denote methods where at least one component (e.g., controller hardware or the vehicle) is virtualized as in-the-loop methods and use the following categories (Hakuli and Krug, 2015). In addition, driving simulators (Driver-in-the-loop) are added as further category to this list:

Model-in-the-loop (MiL): All components are simulated. This serves as an early opportunity to identify necessary system specifications and is often the first step in the development of the final system (Hakuli and Krug, 2015).

Software-in-the-loop (SiL): Tries to recreate the hardware conditions as closely as possible in simulation, including real-time behavior, performance and resolution of real

hardware components, without actually integrating real hardware (Hakuli and Krug, 2015).

Driver-in-the-loop (DiL): Real driving conditions (i.e., the driving process, the road, other traffic participants and the scenery) are simulated in software and exposed to human drivers in driving simulators through haptic, kinesthetic, auditory and visual interfaces of varying complexity and sophistication to investigate the behavior of the drivers (Schöner and Morys, 2015).

Hardware-in-the-loop (HiL): Replaces single components step-wise (e.g., controller hardware or sensor) that were previously represented by mathematical models by physical prototypes. This verifies the functioning of the components in combination with each other.

Vehicle-in-the-loop (ViL): The full vehicle is placed in a framework that involves virtualized components, e.g., other traffic participants. This may involve placing the vehicle on a roller dynamometer or a proving ground.

The basic idea is to couple real hardware (or drivers) with software and simulation models over clearly defined interfaces. That requires a modular concept of the simulation frameworks in use, but allows a step-by-step process in the development and effectiveness assessment from purely virtual simulation to physical testing of a final system, which is fully integrated in the real vehicle as real hardware, e.g., on proving grounds (Schäuffele, 2010). Real testing (i.e., no virtualized components) is considered as additional category to structure the methods in the following section. An overview of the categories and the components that are virtualized within each category is given in Table 2.5.

	MiL	SiL	DiL	HiL	ViL	Real testing
Functional code	V	R	R	R	R	R
Controller hardware	V	V	V	R	R	R
Assistance system	V	V	V	V/R	R	R
Vehicle	V	V	V/R	V	R	R
Driver	V	V	R	V	V/R	R
Driving dynamics	V	V	V	V	R	R
Road surface	V	V	V	V	R	R
Traffic/Scenery	V	V	V	V	V	R

Table 2.5.: Degree of virtualization for various in-the-loop implementations, based on Hakuli and Krug, 2015. ”V” refers to virtual, ”R” to real.

2.3.1. Model-in-the-loop

The main idea behind using simulation is to virtually recreate real driving only through the use of appropriate physical and mathematical models. No prototypes need to be available.

Instead, this necessity is replaced by a necessity for validated simulation models.

Model-in-the-loop methods do not aim to simulate the exact behavior of the final hardware. The MiL methods in this section are grouped by the way how they solve the driving dynamics. In many cases, the individual methods are coupled with other simulation methods in additional software packages or software extensions, e.g., to add active safety functionality.

2.3.1.1. Kinematic driving simulation

To model vehicle movement, two common approaches are *kinematic* and *kinetic simulation*. They are both implemented for example in PC-Crash (Moser, 2020).

In kinematic simulation, a forward acceleration a is defined using the vertical force for each tire (calculated from the static tire force due to the vehicle weight and its weight distribution, depending on the location of the center of gravity) and the brake or acceleration force at each tire (see technical manual for PC-Crash (Moser, 2020). The velocity is then calculated by numeric integration of the acceleration a. Lateral slip due to loss of adhesion between road and tires in curved driving cannot be considered with the kinematic model. Furthermore, no three dimensional effects in driving can be considered (e.g., no vehicle pitching). Simulation of active safety functionality has to be added through a coupling with additional software or software extensions. The motion of vehicles in microscopic traffic flow simulation is represented through kinematic driving simulation (Detering, 2011).

In the PreEffect-iFGS method (Stefan Schramm, 2011), PC-Crash is used. However, in his thesis on prospective effectiveness assessment of a pedestrian AEB, Stefan Schramm, 2011 does not document whether the kinematic or kinetic module is used.

One of the advantages of kinematic simulation is its simplicity, leading to very fast calculations and easy comprehensibility. For some applications and simple scenarios such as rear-end collisions, it might be sufficient. However, the model meets its limitations when curved driving is involved, since no effects such as skidding can be considered. Furthermore, suspension characteristics and other physical effects involved in driving dynamics are not considered.

2.3.1.2. Kinetic driving dynamics simulation

A more sophisticated model is the kinetic model, which considers dynamic vehicle forces. The following rules are implemented in PC-Crash (see technical manual for DSD, 2020) to calculate each individual time step:

- The tire forces are calculated according to the following rules:
  - Similar to the kinematic simulation, the vertical tire force F_z is calculated from the static tire force due to the vehicle weight and the mass distribution.

  - Lateral and longitudinal tire forces are calculated from F_z, the lateral slip angle, brake or acceleration forces and the coefficient of friction μ by means of a tire model.
  - The tire force tangential to the road surface must not exceed μF_z.
- The acceleration of the center of gravity and the rotational accelerations are calculated based on the external forces, including tire forces under consideration of a tire model and suspension characteristics, air resistance and wind, gravity, trailer hitch forces and moments and contact forces with other traffic participants.
- Numeric integration of equations of motion for a fixed time step. This leads to the updated positions, velocities and angular orientation and angular velocities of the centers of gravity of the vehicles.

The kinetic model considers more physical effects that are involved in the driving process than the kinematic model, including full consideration of three dimensions. Other examples of software packages that implement a similar model are *CarMaker* by IPG or *CarSim* by Mechanical Simulation Corporation. The kinetic model in PC-Crash is used for prospective effectiveness assessment by the rateEffect method (Döring et al., 2012) in a coupling with external software for simulation control and to simulate active safety systems. In the VUFO Simulation method (C. T. Erbsmehl, 2009), CarSim is coupled with *MATLAB*. For simulation by various authors from TU Graz (Billicsich, Tomasch, Markovic, et al., 2016; Billicsich, Tomasch, Sinz, et al., 2015; Eichberger, Rohm, et al., 2011; Eichberger, Tomasch, Rohm, and Hirschberg, 2009; Eichberger, Tomasch, Rohm, Hirschberg, and Steffan, 2011; Eichberger, Tomasch, Rohm, Steffan, et al., 2010; Kolk, Kirschbichler, et al., 2016; Zauner et al., 2014), PC-Crash with kinetic simulation is used in a coupling with *MATLAB*. In such studies, MiL provided a benefit since this made it possible to evaluate the potential of a generic exemplary system that does not (yet) exist as real hardware.

Depending on the evaluation objective, using kinetic simulation instead of kinematic simulation can be a necessity. Consideration of three dimensions allows to investigate a multitude of effects, e.g., in sensor simulation when a car's pitching motion due to braking causes the sensor field of view to be directed to the ground instead of in front of the vehicle. The computation times for kinetic driving dynamics simulation in PC-Crash are not significantly longer compared to kinematic simulation.

2.3.2. Software-in-the-loop

The goal of software-in-the-loop (SiL) methods is to replicate the behavior of the final system as closely as possible in simulation and match it in terms of computational performance, real time behavior or computational resolution without the requirement to use real hardware (Martinus et al., 2013). The SiL method is a way to verify the specifications of individual system components (Hakuli and Krug, 2015). This method requires more effort in the validation of simulation models but also provides more realism in the representation of

the individual components. However, when it comes to the effectiveness assessment of generic or exemplary safety systems or when the objective of an assessment is a preliminary estimation of the safety potential of a specific safety strategy, a MiL approach is in general sufficient.

2.3.3. Driver-in-the-loop

According to Schöner and Morys, 2015, driving simulators are used for a multitude of purposes, e.g., functional demonstration, investigation of driver reactions, training of personnel or testing of active safety systems. The main focus and reason to use a driving simulator is to include the human driver and his or her interaction with the vehicle.

A simulator consists in the simplest form of the typical elements needed to drive a car. Visual sensory inputs are represented through screens, auditory inputs through the imitation of sounds and kinesthetic inputs through actuators. A simple setup of a driving simulator may incorporate a car seat, gear shift, a screen and a pedal and steering wheel combination (also called fixed base and fixed screen simulators, see Slob, 2008), while more sophisticated ones offer immersive surround view screens, a replication of a vehicle's interior and actuators to imitate vehicle accelerations and rotations. An example for a highly immersive dynamic driving simulator would be Daimler's full-scale simulator in Sindelfingen, see Zeeb, 2010.

Winter et al., 2012 list controllability, reproducibility, standardization, ease of data collection, the possibility to represent hazardous driving conditions without physical harm and the opportunity for feedback and instructions as the main advantages in using driving simulators. As disadvantages, they list limited fidelity regarding physics, perception and behavior. Furthermore, it is not clear to which extent human driving performances in driving simulators can be transferred to real conditions. In addition, there is the problem of simulator sickness (see Winter et al., 2012).

The advantage to study driver behavior in critical situations without physical risk was for example used by Unselt et al., 2004 for effectiveness assessment to investigate in which cases a brake assist (a system that immediately decreases the brake acceleration as soon as a driver intention for emergency braking is detected) would provide the necessary benefit to avoid pedestrian accidents. Since the brake assist responds sensitively to driver input to detect the intentions, having the driver in the loop provided a benefit. However, the need for test drivers limits the number of cases that can be tested in active safety studies with driving simulators as compared to MiL, SiL or HiL methods.

2.3.4. Hardware-in-the-loop

HiL methods are the first step to integrate real hardware in the testing of automotive systems. The method involves step by step replacement of models in the SiL framework by real

hardware components, such that they can be tested whether they fulfill their specifications and the integration with each other. The involved simulation methods require real-time capability, i.e., they should be able to operate at the same signal frequencies as the hardware components (Hakuli and Krug, 2015).

Tumasov et al., 2019 employed a HiL test bench for the functional verification of Electronic Stability Control (ESC) system. They coupled the full brake system hardware with a simulation model of the remaining hardware components over the CAN bus. With this setup, they were able to verify the operational adequacy of the ESC control unit. In their thesis, Björklund and Karlström, 2017 evaluated the possibility to test a lateral active safety system using HiL. They coupled a forward facing camera, the active safety controller and the vehicle master controller as real hardware with a simulation model for the scenario, the vehicle and particularly the steering system. In both cases, the primary safety benefit of the active safety systems was not the primary concern.

As is the case with above mentioned studies, the main purpose of HiL is to test hardware components and their communication with each other, while the safety benefit is of subordinate importance. The real-time requirements are an additional complication, while the method does not provide enough benefits for safety effectiveness assessment.

2.3.5. Vehicle-in-the-loop

Before testing on proving grounds with real vehicles or in traffic is conducted, vehicle-in-the-loop (ViL) methods can be used. The vehicle is placed in a virtual framework, which is generated artificially in the form of simulated sensor input or by directly replacing the sensors, i.e., by generating the sensor output (Hakuli and Krug, 2015). The vehicle then responds to events in the virtual framework. The prototype can then be tested in a relatively safe test setup, which also allows testing of evasive maneuvers in a low-risk framework. With this method, even driver reactions can be considered by using virtual reality or augmented reality approaches to project the virtual environment to the perception of the test driver (T. Bock, 2008). This method addresses the need for the high effort that comes with real testing of active safety systems and is an important step towards functional validation (Hakuli and Krug, 2015).

In the following, two examples for ViL test facilities are described. However, such test facilities exist in many variations.

The first example is the VEHIL test facility developed by TNO (Verburg et al., 2003 and Gietelink et al., 2007): first, a virtual framework is defined, together with a concrete traffic scenario from a scenario database. Then, a full-scale physical vehicle is placed on the roller dynamometer which recreates the loads necessary to replicate real driving conditions for the vehicle under test. The dynamometer is connected to the simulation models. Furthermore, one or more surrounding virtual traffic participants is replaced by a real artifact, which in

this setup is a moving base that is able to represent the relative movements of the traffic participants. Gietelink et al., 2007 describe how the VEHIL test framework can be used to assess the effectiveness of a forward collision warning system (FCW) and adaptive cruise control system (ACC). They argue that the VEHIL offers advantages for "sensor verification, rapid control prototyping, model validation, function level validation, fine-tuning of control algorithms, production sign-off test or preparation of test drives". Tests can be executed quicker than with real tests on proving grounds, the reproducibility is high and the risk for hardware or personal injury is low. However, since the vehicle is placed on a roller dynamometer, the representation of driving dynamics is not possible.

Another example represents the VIL by T. Bock, 2008: the VIL couples a traffic simulation with a real vehicle which is equipped with an inertial measurement unit and DGPS to accurately track its location and orientation. The vehicle is driven by a human driver on a test track. The test track is replicated in the traffic simulation using the position and orientation measurements of the real vehicle. Virtual vehicles from the traffic simulation are then visualized to the driver through augmented reality. The safety system controller logic receives information on the traffic through appropriate sensor simulation models. Compared to the VEHIL test setup, the VIL is better suited to investigate driver behavior in interaction with active safety systems, according to Berg and Färber, 2015.

2.3.6. Real testing

2.3.6.1. Testing on proving grounds

According to Seiniger and Seiniger and A. Weitzel, 2015, testing of vehicles is conducted for various purposes and stakeholders. These purposes include vehicle and component development, while the stakeholders include organizations such as companies, universities, rulemaking authorities or consumer protection organizations.

In testing on proving grounds, a fully physical vehicle is tested without the involvement of virtualized components. Possible other traffic participants, including vulnerable road users, can be represented either by real physical vehicles or dummies that have the same geometrical shape and optical properties, see for example Figures 2.4a and 2.4b. Another example for a dummy vehicle is the EVITA (Experimental Vehicle for Unexpected Target Approach), see Fecher et al., 2015, which offers the rear chassis of an Opel Adam, installed on a trailer that is towed by another vehicle. The EVITA target allows effectiveness assessment of collision avoidance systems in longitudinal traffic, without endangering the test persons that are driving and steering the vehicles under test.

Testing on proving grounds allows full experimental control, i.e., also parameters regarding the road surface can be controlled (see Lietz et al., 2011). The repeatability of experiments is particularly high when driving robots are used. For example, in their article, Schöner, Hurich, et al., 2011 describe how one of the test setups at Daimler's proving grounds can

(a) Testing of rear-end collision mitigation systems, Seiniger and A. Weitzel, 2015.

(b) An overrunable test platform allowing free control of pedestrian motion, Seiniger and A. Weitzel, 2015.

Figure 2.4.: Testing of active safety systems on proving grounds.

achieve a reproducible accuracy of 3 cm for the stopping point in goal braking. The lateral accuracy for staying on track in curved driving is around 10 cm. In several hours of driving in a defined pattern, a temporal accuracy of 20 ms for reaching control points can be achieved. Furthermore, the full real vehicle and its dynamics are represented under real conditions (Breuer, 2009, T. Bock, 2008), but the scenery can often be represented only under high effort. Fach and Ockel, 2009 compared testing on test proving ground to other testing methods and concluded that "it is not realistic that [...] overall functionality and performance [can] be evaluated on basis of a limited number of tests" and that "A full forecast of their potential is only possible with respect to the complete relation of driver-vehicle-system-scenery".

The primary purpose of real testing on proving grounds is the functional verification of the full system at a late stage of the development rather than for the estimation of the potential of safety systems.

2.3.6.2. Natural driving studies and field operational tests

In NDSs and FOTs, in the context of the assessment process presented in Section 1.2.2, scenarios are generated and represented at the same time as they occur naturally in real traffic. Each scenario is a unique combination of the driver, vehicle, traffic and environmental conditions which are very difficult, if not impossible, to reproduce. This makes it equally difficult to repeat the occurring situations to test the alternative in terms of a direct baseline-to-treatment comparison. In Faber et al., 2011, the effectiveness of safety systems such as ACC or FCW was assessed by comparing the relative frequency of occurrence (relative risk) of safety-critical scenes that are relevant to the respective systems for the baseline (no system installed) versus frequency of occurrence of such scenes in the treatment (system installed). The baseline-to-treatment comparison cannot be done for individual concrete scenarios.

2.3.7. Summary and discussion of the solution requirements

Paragraph by paragraph, the individual solution requirements established in Section 1.2.3 are discussed in this section for each of the mentioned scenario representation methods. For scenario representation, the applied solution requirements, which explained in detail in Section 1.2.3, are ”baseline-to-treatment comparison approach”, ”critical scenarios”, ”high number of concrete scenarios”, ”surrounding traffic”, ”scenery” and ”resolves the safety technology”. Each method is rated according to the categories well suited, neutral, insufficiently suited or depends (i.e., suitability depends on the specific implementation). A summary can be seen in Table 2.6.

	Baseline-to-treatment comparison approach	High number of concrete scenarios	Surrounding traffic	Environment	Resolves the safety technology
Kinematic simulation	+	+	+	+	–
Kinetic simulation	+	+	+	+	+
Software-in-the-loop	+	+	+	+	+
Driver-in-the-loop	∼	∼	+	+	+
Hardware-in-the-loop	∼	+	+	+	+
Vehicle-in-the-loop	∼	d	d	d	+
Testing on proving grounds	∼	–	–	–	+
NDS / FOT	–	d	+	+	+

Table 2.6.: Scenario representation methods. Distinction of suitability to fit the defined solution requirements: well suited (+), insufficiently suited (–), neutral (∼) and depends on the chosen method (d).

Baseline-to-treatment comparison approach: Both the MiL and SiL methods only involve virtual components, meaning that all investigated scenario representations are exactly repeatable, i.e., they fulfill the requirement baseline-to-treatment comparison approach (well suited). The HiL, DiL and ViL approaches as well as testing on proving grounds involve highly controlled test setups or simulation environments that are not subject to uncontrollable factors such as the real traffic in NDS or FOTs. However, the repeatability is not as ”perfect” as with pure simulation (neutral). Within NDS or FOTs, every scene is a unique combination of the driver, vehicle, traffic and environmental conditions, thus making the baseline-to-treatment comparison approach very difficult, or even impossible (insufficiently suited).

High number of concrete scenarios: Both the MiL and SiL methods allow consideration of a high number of concrete scenarios. E.g., Sander and Lubbe, 2018 investigated an intersection AEB in more than 500 concrete scenarios for several system configurations. Counting each system configurations as individual concrete scenario, it can thereby be seen that MiL and SiL can result in more than 1000 concrete scenarios (well suited).

Using driving simulators, the representation of relevant concrete scenarios requires the involvement of human test persons who are willing to participate in the study. While possible, it is certainly not as easy as with simulation to reach 1000 concrete scenarios (neutral). Since HiL methods can be fully automated without human intervention, 1000 concrete scenarios are possible (well suited). The ViL test setup by T. Bock, 2008 involves human test subjects (neutral), limiting the number of tests, while the VEHIL allows automatic setup of concrete scenarios (well suited). Real testing on proving grounds requires high effort to be setup and is therefore not suited to represent a high number of concrete scenarios (insufficiently suited). NDSs and FOTs require a high number of test vehicles or a long time frame of the study to reach a high number of concrete scenarios. The number of concrete scenarios therefore depends on the size of the study, see Section 2.1.4 (depends).

Surrounding traffic and scenery: In principle, no method poses a restriction to which degree surrounding traffic or the scenery can be considered. In Mil, SiL, DiL and HiL, the scenery and other traffic participants can be created artificially in simulation (well suited). In the ViL test setup by T. Bock, 2008, static objects can be integrated virtually in the same way as other traffic participants. VEHIL recreates other traffic participants as moving bases - it is not clear how static objects are represented (depends). Testing on proving ground requires manual setup of static objects (insufficiently suited), other traffic participants need to be synchronized. In NDSs or FOTs, the scenery and surrounding traffic is naturally represented (well suited).

Resolves the safety technology: Except for kinematic simulation (insufficiently suited), where driving dynamics are not resolved in detail, every other method is capable to fulfill the requirement resolves the safety technology (well suited).

The methods that fulfill all solution requirements are kinetic simulation and SiL (see Table 2.6). However, according to the scope defined in Section 1.2.4, it is sufficient to consider exemplary safety systems. Hence, the kinetic simulation method is preferred for this thesis.

2.4. Effectiveness rating

After representing the concrete scenarios from the scenario catalog, the results need to be evaluated. For this purpose, *effectiveness functions* and *effectiveness metrics* are used. An effectiveness function, is defined in this thesis as a function that objectively quantifies a specific safety-related aspect for a specific concrete scenario. An effectiveness metric is defined as a method that first quantifies a specific safety-related aspect for each concrete scenario in the scenario catalog and then aggregates the results to express the effectiveness as a single value. Often, this is conducted by aggregating the results of a specific effectiveness function applied to each concrete scenario defined in the scenario catalog. The term *effectiveness metric* is based on Alvarez et al., 2017, where simply the term *metric* is used. Both variants are used synonymously in this thesis.

No unified notation to describe the various effectiveness metrics and functions can be found in the literature, hence, a new notation is introduced for the context of this thesis. Let $S := \{\text{concrete traffic scenarios } s \text{ to be considered}\}$ be the scenario catalog, where s refers to individual traffic concrete scenarios. Furthermore, the set of concrete scenarios $s \in S$, such that a collision occurs in s, is denoted by S_C. The concrete treatment scenario, i.e., the concrete scenario s under consideration of one or more safety systems in one or more vehicles, is denoted by $TR(s)$. Additionally, let $S^{TR} := \{TR(s) \text{ for } s \in S\}$ and $S_C^{TR} := \{TR(s) \text{ for } s \in S, \text{ such that a collision occurs in } TR(s)\}$. The notation $|x|$ is used to denote the number of elements (i.e., concrete scenarios) in a set x.

The letter E is used to denote an effectiveness metric, while the term f_{eff} is used to denote an effectiveness function.

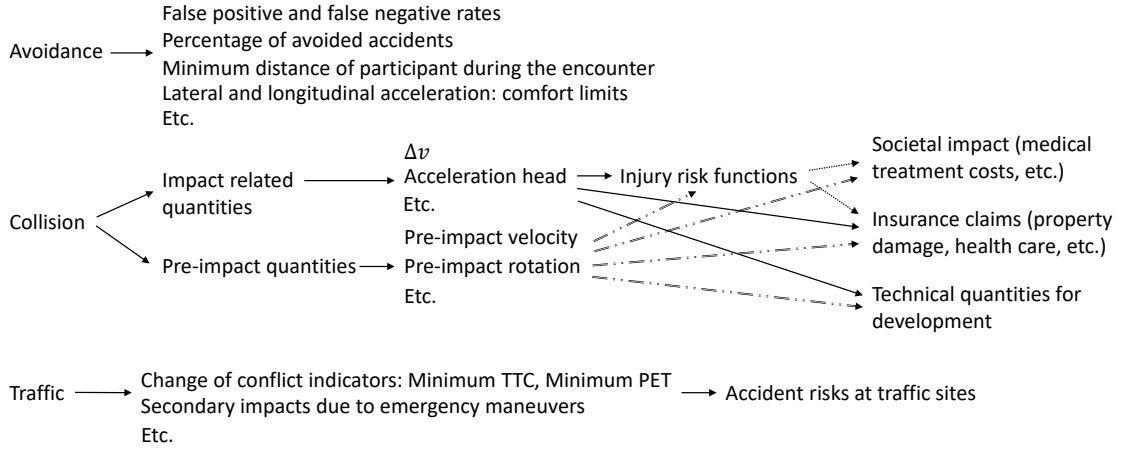

Figure 2.5.: Categorization of effectiveness metrics and functions. Either the quantities from intermediary steps can be used to rate the effectiveness (e.g., Δv), or higher level results (e.g., injury risk), depending on what is required in the evaluation objective.

As the general structure for the following sections, the following three categories are used to group effectiveness metrics and functions in the literature, see Figure 2.5:

Avoidance-related quantities: dealing with scenarios in which an accident was avoided
Collision-related quantities: quantification of accident consequences
Traffic-related quantities: dealing with the impact of a safety system on the traffic system as a whole

In some evaluations, further processing of the results such as projection to different evaluation regions is needed as an additional step in the assessment process to consider the results in a generally broader and more comprehensive context. However, due to the restrictions in the thesis scope (Section 1.2.4), projection of effectiveness results is not discussed further.

2.4.1. Avoidance-related effectiveness metrics

A simple effectiveness metric applicable in baseline-to-treatment comparisons is the proportion of concrete scenarios where the accident in the baseline concrete scenario was avoided in the treatment concrete scenario, i.e.,

$$E_{\text{av}} := \frac{\text{number of collisions in the baseline that were avoided}}{|S_C|}.$$

This metric was listed in Alvarez et al., 2017 as one of the most commonly applied metrics, based on an expert inquiry involving more than 30 participants. Examples where the metric was applied to investigate an AEB in intersection accidents include the study by Kolk, Kirschbichler, et al., 2016, where E_{av} was found to be between 45 % and 66 %, or the study by J. Scanlon et al., 2017, where E_{av} was found to be between 14 % and 71 % (also for intersection accidents). The metric E_{av} was also used in Eichberger, Tomasch, Rohm, Hirschberg, and Steffan, 2011, to estimate the safety benefit of various types of assistance systems, for several types of fatal accidents.

An avoidance-related metric which is specific to application in NDS or FOT studies is presented in the study by McLaughlin et al., 2008. Based on crash- and near-crash-events extracted from recorded data and using kinematic relationships, they determine the time span which would be needed by human drivers for reactions to avoid the events. Under the assumption of a specific driver reaction time distribution, they present a method to compute the percentage of the population that is able to react to a specific Forward Collision Warning (FCW) strategy as an effectiveness metric.

2.4.2. Effectiveness metrics related to the collision severity

This type of effectiveness functions and effectiveness metrics is applied to quantify the severity of collisions. The computation of collision-related effectiveness functions can involve kinematic quantities from the moment directly before impact or more sophisticated collision models such as finite element models to represent the occupants, restraints systems and more in the crash phase.

2.4.2.1. Kinematic collision-related quantities

Depending on the scenario representation method, different quantities can be used to describe the severity of collisions. Examples are the velocity v_c at the time of impact or the crash-related velocity change Δv. In the approach presented in Kolk, Sinz, et al., 2016, the quantity Δv is calculated using information on the pre-impact velocity, the collision configuration (i.e., heading and velocity angles at the moment of first contact, orientation of vehicles in space, etc.) and vehicle material properties (estimated stiffness, friction between vehicles, etc.), see Appendix E. When using the notation defined at the beginning at this

section (in this case $f_{\text{eff}} = \Delta v$), the effectiveness metric used in Kolk, Sinz, et al., 2016 to calculate the average change of Δv between the baseline and the treatment can be expressed in the following way:

$$E_{\Delta v}^{0,\,\text{mean}} := \frac{1}{2|S_C|} \sum_{s \in S_C} \left[\Delta v_{p_1}(s) - \Delta v_{p_1}(TR(s))\right] + \left[\Delta v_{p_2}(s) - \Delta v_{p_2}(TR(s))\right] \tag{2.2}$$

where $\Delta v_{p_1}(s)$ and $\Delta v_{p_2}(s)$ denote the values for Δv that are experienced by the collision partners p_1 and p_2, respectively, in a concrete scenario s. The superscript 0 in $E_{\Delta v}^{0,\,\text{mean}}$ refers to the definition $\Delta v(TR(s)) := 0$ for concrete scenarios s in which no collision occurs in $TR(s)$. This definition of $E_{\Delta v}^{0,\,\text{mean}}$ is only valid if the collision partners remain the same, both in s and $TR(s)$ for each concrete scenario s. It describes the average change in Δv for all traffic concrete scenarios s in the scenario catalog S_C. Furthermore, the average relative reduction of Δv between the treatment and baseline situation can be investigated for concrete scenarios $s \in S_C$:

$$E_{\text{Rel},\,\Delta v}^{0,\,\text{mean}} := 1 - \frac{1}{2|S_C|} \sum_{s \in S_C} \left[\frac{\Delta v_{p_1}(TR(s))}{\Delta v_{p_1}(s)} + \frac{\Delta v_{p_2}(TR(s))}{\Delta v_{p_2}(s)}\right] \tag{2.3}$$

where the superscript 0 again refers to the definition $\Delta v(TR(s)) := 0$ if there is no collision in $TR(s)$. A variant of $E_{\Delta v}^{0,\,\text{mean}}$ is the metric $E_{\Delta v}^{\text{mean}}$, where only concrete scenarios s are considered such that a collision occurs both in s and $TR(s)$. In Gruber, Kolk, et al., 2019, the form of Equation 2.2 was used, but Δv was replaced for an investigation on vehicle to pedestrian accidents by v_c (collision velocity), thus calculating the average change in the collision velocity $E_{v_c}^{0,\,\text{mean}}$. They investigated both variants $E_{v_c}^{\text{mean}}$ (analogous to $E_{\Delta v}^{\text{mean}}$) and $E_{v_c}^{0,\,\text{mean}}$. The metric $E_{v_c}^{0,\,\text{mean}}$ was also applied in Wimmer, Düring, et al., 2019 to compare the effectiveness results by different effectiveness assessment simulation toolboxes, by investigating car to cyclist accident scenarios. Analogously, v_c can also be replaced in $E_{\text{Rel},\,\Delta v}^{\text{mean}}$ to define $E_{\text{Rel},\,v_c}^{0,\,\text{mean}}$.

2.4.2.2. Injury risk functions based on basic kinematic quantities

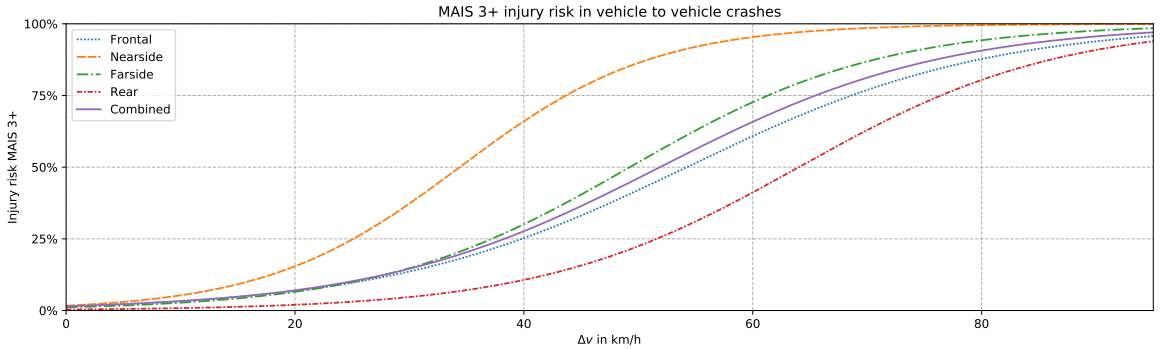

Figure 2.6.: Risk to suffer MAIS +3 injuries in frontal, nearside, farside or rear-end collisions. The solid purple line marks the combined risk for all accident configurations. Based on the findings by Augenstein et al., 2003.

Without further processing, Δv or the impact velocity v_c are rather technical quantities. A common procedure (e.g., used in Tomasch, Kolk, et al., 2015, Bareiss, 2019 or Bahouth et al., 2012) therefore is to use injury risk functions which correlate such technical quantities to injury risks. Injury risk functions are established through logistic regression models that are fitted to express the probability to suffer an injury of a specific severity grade, based on accident data. In Rosén and Sander, 2009, impact velocity is related to pedestrian fatality risk in vehicle-versus-pedestrian collisions. In Augenstein et al., 2003, Δv is used as indicator to estimate the risk to suffer an injury of category MAIS 3+ (Maximum Abbreviated Injury Scale Level, see "Abbreviated Injury Scale 2005 Update 2008" by Association for the Advancement of Automotive Medicine, 2008) in frontal, side or rear accidents, for vehicle-to-vehicle impacts, based on data for approximately 9 000 crashes between 1994 to 2002 in the United State (see Figure 2.6). Analogous to the definitions of $E_{\Delta v}^{0,\,\mathrm{mean}}$, $E_{\Delta v}^{\mathrm{mean}}$, $E_{\mathrm{Rel},\,\Delta v}^{0,\,\mathrm{mean}}$ or $E_{\mathrm{Rel},\,\Delta v}^{\mathrm{mean}}$ in the previous subsection, the metrics $E_{\mathrm{IRF}}^{0,\,\mathrm{mean}}$, $E_{\mathrm{IRF}}^{\mathrm{mean}}$, $E_{\mathrm{Rel,\,IRF}}^{0,\,\mathrm{mean}}$ and $E_{\mathrm{Rel,\,IRF}}^{\mathrm{mean}}$ can be defined by replacing Δv with an injury risk function to express the average absolute or relative change in injury risks.

2.4.2.3. Advanced injury criteria based on Finite Element Analysis and multibody simulation

Finite Element Analysis (FEA) and Multibody Simulation (MBS) provide a possibility to analyze the in-crash phase in high detail and can be used to assess the severity of collisions. In general, the simulation for a MBS model can be calculated faster than for a FEA model. MBS and FEA methods allow calculation of accelerations of individual body parts, angular velocities and more. These quantities can be used to calculate injury criteria as effectiveness functions such as the ones employed in crash testing, i.e., Head Injury Criterion (HIC), Brain Injury Criterion (BrIC) and others, see for example Cichos et al., 2015. These injury criteria values can in turn be related to the risk to suffer injuries of a specific degree on a given body part. In Wimmer, Benedikt, et al., 2015 for example, a FEA model of a head impactor and vehicle geometry was used to calculate the HIC (see Cichos et al., 2015) for several collision configurations and a fast calculating statistical model was then applied to estimate injury risks for the effectiveness assessment of a pedestrian AEB.

Based on FEA or MBS simulation, also Human Body Models (HBMs) are available, which are specifically designed to represent the human body and to allow investigation of crash-induced damage to vital organs such as the human brain, the spinal chord or more. Two commonly used examples of HBM based on FEA are the Total Human Model for Safety (THUMS) (for an overview of THUMS versions see Fressmann, 2016) and Global Human Body Model (GHBMC) (see for example Combest, 2016). They can be used for occupant load simulations, vehicle to pedestrian or bicyclist accidents and more. Relevant output quantities of HBM simulations, such as acceleration of occipital condyle for brain injuries, are evaluated and can be further used within injury risk functions. E.g., in Klug et al., 2015,

11 injury criteria related to head injuries, derived from output of a HBM simulation, were analyzed.

For the evaluation of active and integral safety functionality, Active Human Body Models (A-HBM) are often used. They differ in the fact that individual muscles can be stiffened to simulate muscle tension. When a pre-crash braking maneuver is applied, e.g., by an automated emergency brake system, occupant position is changed from a relaxed position to a forward position closer to the steering wheel. This motion is influenced by muscle activation. In Prüggler, 2015, a controller to influence model kinematics to simulate muscle activity in the THUMS was developed, such that human kinematics in the pre-crash phase can be studied. Östmann and Jakobsson, 2016 and Saito et al., 2016 applied an A-HBM (Active Human Body Model) to investigate and improve collision mitigation system performance with respect to occupant protection. Using FEA simulations with a combination of THUMS versions 4 and 5, Yamada et al., 2016 showed that an AEB not only reduces injuries by reducing the collision velocity, but also by changing the occupant posture due to the deceleration. In Bastien, 2013, an A-HBM based on multibody simulation was used that can be used to assess the severity of collisions under consideration of occupant forward movement that results from emergency braking maneuvers.

An advantage of injury criteria based on FE or MBS simulation is the high level of detail with which the injury mechanisms can be represented. However, this advantage comes with the disadvantage that higher computation times are involved when using such models as compared to using injury risk functions based on kinematic collision-related quantities.

2.4.3. Traffic-related effectiveness metrics

Functions such as safety surrogate measures (SSM) can be used to quantify the criticality of a scene. An investigation on which criteria might be suitable was done by Minderhoud and Bovy, 2001, with examples being minimum Time-to-Collision (TTC), minimum Post-Encroachment-Time (PET), minimum distance between participants during the encounter and more. While safety surrogate measures may serve as a selection method to extract critical scenes from a large base population of traffic scenarios (see Section 2.2.2.1), one can also use them to define the effectiveness metric, e.g., as the percentage by how much the number of traffic conflicts was reduced after introduction of a safety system:

$$E_{\text{conf}} := 1 - \frac{\text{number of conflicts with safety system}}{\text{number of conflicts without safety system}}. \tag{2.4}$$

Jeong and Oh, 2017 used Equation 2.4 in a MTFS based approach to assess the influence of a longitudinal and lateral vehicle control system for motorways on the number of rear-end and lane-change conflicts. Thus, they were able to identify the system configuration with highest reduction of conflicts (between 10 % and 80 % reduction). Further effectiveness metrics could involve statistical metrics such as mean values, standard deviation or more of the safety surrogates measures.

A possible effectiveness metric that relates to traffic in general could be whether an emergency maneuver triggered by an active safety system introduces problems in traffic flow such as traffic jams or even a collision with vehicles other than the conflicting vehicle that was primarily avoided. Ideally, a safety system would have to check whether other traffic participants are endangered before triggering maneuvers to avoid an imminent collision.

When NDS or FOT are used to assess the effectiveness of active safety systems, the technique Events Based Analysis (EBA) can be used (Faber et al., 2011). The basic principle is to identify events that are related to crash involvement (e.g., moments when the distance in time or space to other traffic participants becomes small) and to investigate whether NDS or FOT vehicles equipped with the active system under investigation experienced less such events than vehicles without the active system. These events described in Faber et al., 2011 are analogous to the conflicts mentioned above. In addition to EBA, Aggregation Based Analysis (ABA) can be used (Faber et al., 2011). ABA investigates factors such as average following distance or travel speed decrease in the presence of an active system.

For studies that investigate real traffic such as NDSs or FOTs, scenarios cannot be repeated exactly. Thus, a direct comparison of the scenario with and without the safety system is not possible. For that purpose, different assessment methods must be applied than in baseline-to-treatment comparisons.

2.4.4. Summary and discussion of the solution requirements

	Baseline-to-treatment comparison approach	Critical scenarios	High number of concrete scenarios
Avoidance share	+	–	+
Kinematic avoidance for NDSs and FOTs	–	+	+
Kinematic collision-related quantities	+	–	+
Injury risk functions	+	–	+
FEA and MBS	+	+	d
Reduction of traffic conflicts based on SSM	+	+	+
EBA and ABA for NDSs and FOTs	–	+	+

Table 2.7.: Effectiveness rating methods. Distinction of suitability to fit the defined solution requirements: Well suited (+), Insufficiently suited (–), Neutral (∼) and depends on the chosen method (d).

In the following paragraphs, respective solution requirements established in Section 1.2.3 are discussed individually for each of the mentioned scenario representation methods. For the rating step, the applied solution requirements are ”baseline-to-treatment comparison approach”, ”critical scenarios” and ”high number of concrete scenarios”. Each method is rated according to the categories well suited, neutral, insufficiently suited or depends (i.e., suitability depends on the specific implementation). A summary can be seen in Table 2.7.

Baseline-to-treatment comparison approach: Since an exact repetition of concrete scenarios is not possible for NDSs and FOTs, the requirement baseline-to-treatment comparison approach cannot be fulfilled by the assessment method by McLaughlin et al., 2008 (see Section 2.4.1), the EBA or the ABA method mentioned in Section 2.4.3 (insufficiently suited). The other methods pose no restriction (well suited).

Critical scenarios: The avoidance share as it is described in Section 2.4.1 is not suited to consider all possible collision configurations that can arise when critical or uncritical (no collision course) scenarios are used in the baseline (insufficiently suited). For example, it does not specifically distinguish the situation that an emergency maneuver that was triggered to avoid a potential collision might cause another collision with a traffic participant that was not involved in the baseline concrete scenario. Collision-related quantities as well as injury risk functions are by definition not applicable to non-collision scenarios (insufficiently suited). The advanced injury criteria that can be evaluated using FEA or MBS simulations can also be evaluated in critical scenarios (well suited), e.g., to investigate the consequences of high deceleration emergency maneuvers. Traffic conflicts based on Safety Surrogate Measures (SSM) and the values of the SSM are suited for critical scenarios. The assessment method by McLaughlin et al., 2008 (see Section 2.4.1) and the EBA method mentioned in Section 2.4.3 also consider critical scenarios (well suited). The ABA method is not applicable to this criterion as it considers a quantity aggregated from continuous traffic flow.

High number of concrete scenarios: All of the methods require a low computational effort (well suited), except FEA, HBM or multi-body simulations. For FEA, or MBS simulation, it depends on how detailed the models are. Some HBM simulations using FEA can take hours or days for a single simulation, depending on the available computational resources. Schwartz et al., 2015 mention that 2.2 million elements are calculated in GHBMC 50th percentile male seated occupant model v4.3 (M50-O), which results in 8.4 min/ms normalized run time (Decker et al., 2017). Assuming a duration of the crash-phase in a frontal crash of 150 ms (e.g., see Burg and Moser, 2017), this would result in 21 hours of simulation time for one concrete scenario and might therefore only be of interest in the future when the computational power is increased significantly. However, simulation models can always be simplified as long as they fit the requirements of the evaluation objective (depends).

As can be seen in Table 2.7, only reduction of traffic conflicts based on SSM fulfills all of the solution requirements. However, the application of one effectiveness metric does not exclude the application of one of the other metrics, as long as they are compatible to the previous steps in the effectiveness assessment.

3. Objective

This thesis work was carried out to develop a method for the **prospective effectiveness assessment** of active safety systems.

Current discussions in the field reveal that few of the state-of-the-art methods for scenario generation fulfill the requirements to produce a higher number of critical concrete scenarios, also including all surrounding traffic. Microscopic Traffic Flow Simulation (MTFS) and stochastic variation of logical scenarios can be used as available options to fulfill these requirements. MTFS offers an advantage in that it enables the user to validate the model to a real traffic site. However, MTFS only features kinematic driving simulation, which means that skidding in curves, suspension characteristics and other important effects are not considered. Such effects can be relevant to the effectiveness assessment of active safety systems, for example, when considering emergency braking in curves or evasion maneuvers together with the Electronic Stability Control (ESC) functionality. In addition, when MTFS is used, traffic participants can only follow pre-defined paths; this limits the assessment method such that arbitrary lateral evasion maneuvers cannot be considered. Therefore, a scenario representation approach that allows the consideration of all driving dynamics is needed.

When representing scenarios, many methods that involve non-virtual components display the disadvantage that baseline-to-treatment comparisons can never be repeated as exactly as when pure simulation methods are used. This requirement for accurate repetition becomes important, for example, when researchers investigate the influence of individual system configuration parameters on the effectiveness. In addition, simulation offers more opportunities for the full automation of the effectiveness assessment process, enabling researchers to consider more concrete scenarios than they can if they use methods that involve non-virtual components.

Through the analysis of the state-of-the-art in Chapter 2, these considerations led to the identification of coupling MTFS and driving dynamics simulation as an approach that was previously unexplored for effectiveness assessment of active safety systems and to combine the advantages of both methods. Corresponding research questions were formulated as follows:

Q1 How can the prospective effectiveness assessment of active safety systems be conducted when using concrete traffic scenarios that are generated through microscopic traffic flow simulation, while considering the driving dynamics and including traffic that surrounds the conflicting traffic participants?

Question Q1 is further specified by formulating the following sub-research questions:

Q1.1 As a source of stochastically generated concrete scenarios, how can traffic flow simulation be coupled with nanoscopic simulation of driving dynamics and active safety systems?

Q1.2 How can the safety benefit of active safety systems be measured, and which metrics allow the evaluation of the effectiveness in critical scenarios and the system's interactions with the surrounding traffic?

Q1.3 How sensitive are the results of the effectiveness assessment method developed to answer research questions Q1.1 and Q1.2, with regard to changes in the involved components, models and parameters?

4. Solution approach

Like the generalized effectiveness assessment process described in Section 1.2.2, the solution approach depicted in Figure 4.1 was chosen in this thesis work to implement the following individual assessment steps:

1. Scenario generation: an urban arterial road in Graz (Austria) with four signalized intersections of varying complexity was chosen to be represented in a validated microscopic traffic flow simulation model using the software VISSIM (see Fellendorf and Vortisch, 2010). The modeled segment was about 900 m long. As in many other European mid-sized cities, the traffic in the urban arterial consists of passenger cars, truck traffic, buses and trams. Those vehicles were prioritized at the traffic lights, and pedestrians and cyclists moved along separate sidewalks and bike paths, respectively. All side roads were modeled as well, such that the simulated vehicle queues, delays and speeds corresponded to traffic counts and observations for the morning peak hour (7:15–8:15 a.m.). All vehicle movements were recorded as vehicle trajectories. To capture the stochastic effect of traffic flow and driver behavior, 50 simulation runs were generated with different random seeds. For each of the 50 model runs, different random numbers that describe the placement and generation of traffic participants as well as their behavior were generated by VISSIM. The number 50 for the number of model runs was chosen such that the solution requirement "High number of concrete scenarios" can easily be satisfied and to investigate the convergence of effectiveness metrics. Another 50 simulation runs were generated for a model variant in which the traffic density was artificially increased by 50 % for a specific road section, thereby

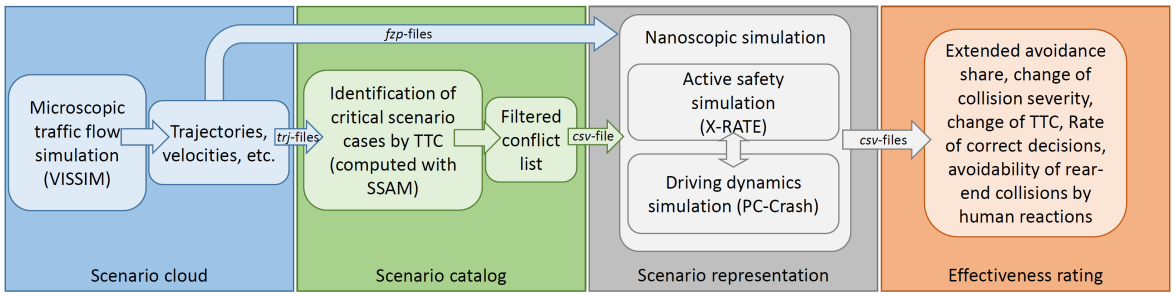

Figure 4.1.: Solution approach: after their generation, MTFS results are transferred to a safety surrogate assessment tool. Based on this analysis and the application of appropriate conflict selection criteria, conflicts are transferred to the nanoscopic simulation step, where they are simulated individually. In a final step, the benefits of the safety systems is assessed through effectiveness metrics.

violating the validation, to conduct a sensitivity analysis of the effectiveness assessment results.

The results of the scenario generation were continuous traffic flow data, in the form of time series for each simulated traffic participant. The output is created as files in the *trj*-format (PTV Planung Transport Verkehr AG, 2017), one for each simulated model run, which specify the positions, velocities, orientations and more of each simulated traffic participant at each simulated time step. The *trj*-files containing binary data were converted to the *fzp*-format (PTV Planung Transport Verkehr AG, 2017) for further processing. The MTFS models were primarily developed by the Institute of Highway Engineering and Transport Planning (ISV) of Graz University of Technology (TU Graz) in the FFG-funded project IMPROVE (FFG, 2020). This project was carried out in the form of a close collaboration between the ISV and the Vehicle Safety Institute (VSI) at TU Graz.

2. Scenario catalog: for each generated model run, representing one hour of traffic each, about 5 000 trajectories of all vehicles and pedestrians were exported for further analysis. To identify critical concrete scenarios within this large amount of continuous traffic flow output from VISSIM, the software SSAM (Safety Surrogate Assessment Model, see Gettman, Pu, et al., 2008) was applied to the generated *trj*-files to compute the TTC (under the assumption of constant velocity). The TTC and a corresponding threshold (which is varied in a sensitivity analysis to identify its influence) were chosen as criterion to define a conflict as concrete scenario for the scenario catalog. TTC was chosen because TTC can be applied to continuous traffic flow data, and since the existence of the TTC is analogous to the definition of the term *critical scenario* (the TTC exists if a collision course exists), and because TTC is a Safety Surrogate Measure widely accepted for conflict analysis. Furthermore, a filter to keep only conflicts between passenger cars and vans (i.e., vehicles with a length lower than 7 m), a spatial filter and a filter to identify unrealistic conflicts are applied. The output of this step is a file in the *csv*-format with each line specifying details on individual conflicts, such as $\tau_{\mathrm{TTC}}^{\mathrm{min}}$, $t_{\tau_{\mathrm{TTC}}^{\mathrm{min}}}$ or the indices of the conflicting traffic participants.
3. Scenario representation: in a time step-based coupling of active safety simulation and driving dynamics simulation, concrete scenarios based on individual conflicts were simulated in three dimensions by extracting relevant information from the converted *fzp*-files. This coupled simulation is also referred to as nanoscopic simulation throughout this thesis and combines the MATLAB-based program X-RATE with PC-Crash to exchange the kinematic states of traffic participants, brake commands and more. The development of X-RATE (”Extended Effectiveness Rating of Advanced Driver Assistance Systems”, Kolk, 2018) was part of this thesis work. The tool has been used in a variety of studies (e.g., Gruber, Kolk, et al., 2019; Kolk, Kirschbichler, et al., 2016; Kolk, Sinz, et al., 2016; Kolk, Tomasch, et al., 2018; Smit et al., 2019; Tomasch, Kolk, et al., 2015; Tomasch, Sinz, et al., 2015 or Wimmer, Düring, et al., 2019). The driving dynamics solver PC-Crash (Moser, 2020), offers a validated collision mechanics and

trajectory model (Steffan and Moser, 1996) and is a widely accepted tool for accident reconstruction. To demonstrate the applicability of the solution approach, an exemplary effectiveness study is defined with two different treatments, in which exemplary AEB City systems were simulated for both conflict participants (the traffic participants between which a conflict was detected by SSAM). The goal of the effectiveness study was not to evaluate an existing system, but rather to explore which kind of effectiveness considerations can be conducted meaningfully. In the first treatment (system configuration 1), the safety systems of conflict participants triggered at a TTC threshold of 1.0 s with the full available brake acceleration of $a^{\min} = -8\,\mathrm{m/s^2}$. In the second treatment (system configuration 2), they triggered at an ETTC (Enhanced Time-to-Collision, which considers also potential acceleration and deceleration maneuvers of conflicting vehicles) threshold of 1.5 s if the driver was not already performing an evasion maneuver. Instead of the full available brake acceleration, the systems in the second treatment only braked with the acceleration required to avoid a collision. It is assumed that traffic surrounding the conflict participants had no safety systems installed and did not react when the conflict participants triggered a braking maneuver. The safety systems reacted to the output of a geometric sensor model, featuring a ray-tracing approach, that represents a sensor with a 180° field-of-view opening angle and a 100 m range. The ray-tracing approach emitted vision rays into the space surrounding the detecting vehicles. Intersections of the vision rays with the triangular meshes that represent traffic participants and non-moving objects were calculated using to the Ray-Triangle-Intersection algorithm presented in Möller and Trumbore, 1997, to determine the visibility of the traffic participants. The geometries of vehicles and other traffic participants were represented to the sensors and collision detection algorithms as moving boxes composed of triangular meshes with dimensions equivalent to the lengths, widths and heights of the traffic participants. The purpose of the sensor model is visibility determination, i.e., material properties or effects such as ray reflection are not considered. The results of scenario representation consist of a table that describes general data for each concrete scenario (e.g., whether the simulations led to a collision or not), as well as files containing time series data for each simulated traffic participant. The two available options for simulation were the MiL and SiL approaches. For the purpose of this thesis work, a MiL approach was considered sufficient. The output of this step are tables in the *csv*-format for each simulated conflict that describe the kinematic quantities for each simulated traffic participant (e.g., velocity or position) at each time step, as well as their sensor and safety system status. A further table in the *csv*-format is produced that summarizes general and collision-related information for each concrete scenario. For the scenario representation step, the degree to which visibility obstructions were considered was varied in a sensitivity study, and effects such as changes in the moment of first detection of other vehicles were investigated. Furthermore, the kinetic path driver model was varied which chooses steering angles to follow the trajectories from MTFS and the curve behavior was studied. Finally, the

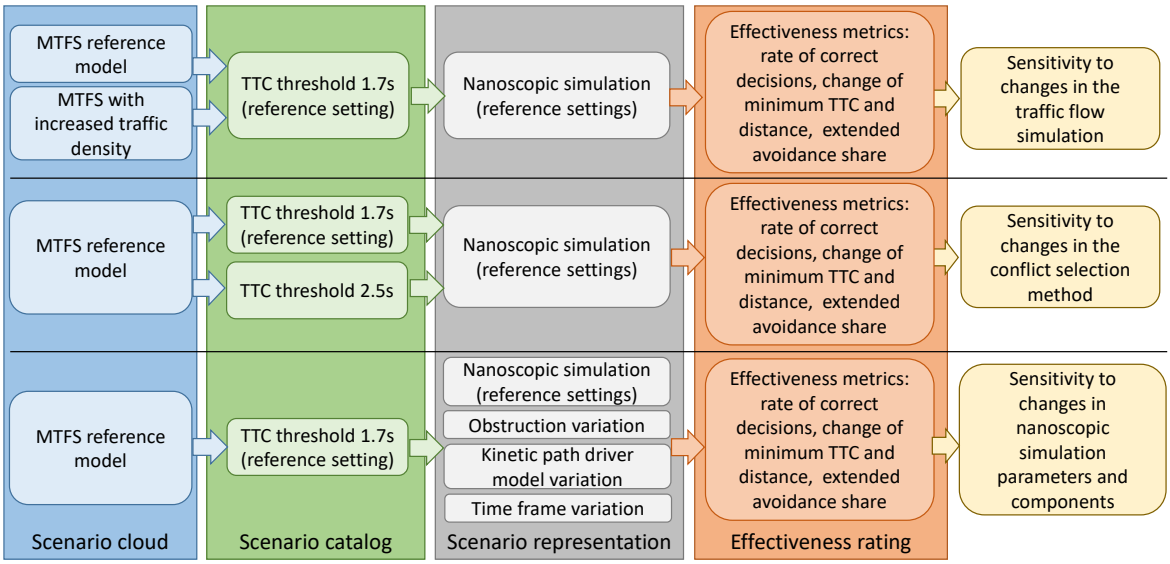

Figure 4.2.: Sensitivity study to answer Q1.3: at various steps in the process depicted in Figure 4.1, components of the method and parameters are varied to gain an understanding of the sensitivity of the result on model choices.

time frame simulated around each conflict was varied.

4. In the last step, results from the *csv*-files from nanoscopic simulation, which were conducted for the exemplary effectiveness study with the two treatments defined in the previous step, were gathered and the effectiveness metrics were calculated. For that purpose, a toolbox based on Python 3.6 was developed. For the effectiveness assessment, effectiveness metrics extracted from the literature were applied insofar as possible and were extended where necessary. One of the extensions that were introduced concerns the avoidance share. The avoidance share metric used in the literature only distinguishes the case that a collision occurs in the baseline and may or may not be avoided in the treatment. When critical scenarios without collisions in the baseline are considered, collisions can still occur in the concrete treatment scenario. Therefore, new categories for all combinations of "collision" and "no collision" in the baseline and treatment were introduced, and a distinction was made whether the collision partners had changed. Another adaption was made based on the "reduction of conflicts" metric E_{conf} by evaluating the median minimum TTC and minimum distance between traffic participants in the treatment. Furthermore, the median collision severity expressed by Δv was evaluated, as well as system response related effectiveness metrics such as the rate of correct decisions, which expresses the proportion of the concrete scenarios, in which the safety system decided not to intervene when the situation was objectively not dangerous, and to intervene when objective danger was present. Objective danger was defined to be present when there was a collision in the baseline.

For the scenario generation, selection and representation step, model assumptions and parameter choices specific to the chosen solution approach were varied in a sensitivity study. This means, for example, that no variation in sensor or safety system parameters was

conducted (such as a variation of the sensor field of view). In addition to other effects, for each variation in the sensitivity study, the system response related effectiveness metrics, change of minimum TTC and minimum distance and extended avoidance share were evaluated and compared. These findings provide knowledge about which model components and parameters should be chosen with care when applying the presented method in prospective effectiveness assessment studies. The chosen variations are summarized in Figure 4.2.

5. Scenario cloud generation

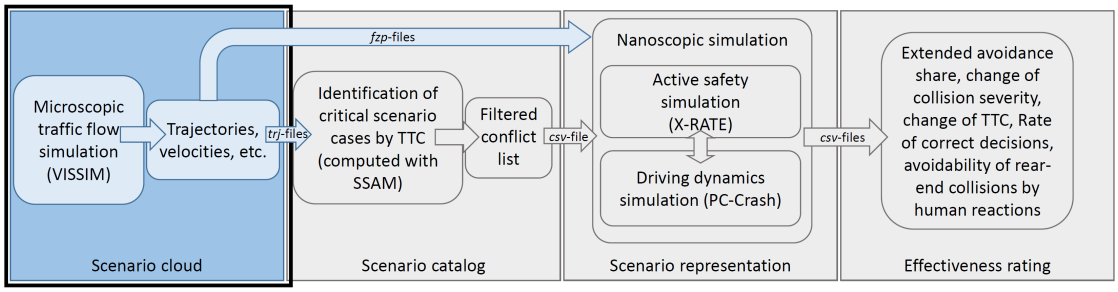

Figure 5.1.: Scenario cloud generation step (marked by the thick black frame): MTFS is used as scenario cloud method to generate traffic scenarios for further use in the solution approach sketched in Chapter 4.

The first step in the effectiveness assessment process, as visualized by Figure 5.1, is the creation of a scenario cloud. The data basis for the creation of the scenario cloud is MTFS. The traffic flow model was developed in Medicus, 2019 and was built using the software VISSIM (Fellendorf and Vortisch, 2010). VISSIM creates files in the *trj* and *fzp*-format, which contain data that describe velocities, accelerations, positions and more for each simulated vehicle for each time step. Once the MTFS model has been defined, the calculation is highly automated such that several simulation runs of the MTFS model can be calculated with different random numbers for each simulation run.

The validity of the MTFS model used in this thesis was investigated by using a multi-step approach in the following way (approach based on Huang et al., 2013, adapted in Medicus, 2019):

Creation of the MTFS model: In a first step, the basic simulation model was created by defining the road network geometry, lane connectivity, traffic densities at the network inflow regions, vehicle routes (paths that vehicles can choose to drive from the inflow region where they were initialized to their destination, the target outflow region), pedestrian crosswalks, bicycle paths, priority rights and traffic signals. Furthermore, the traffic signal programs were defined to replicate the traffic signal programs at the real traffic site. Geo-referenced aerial images from gis.stmk.gv.at were used to model the road geometry as accurately as possible.

Calibration of the MTFS model regarding traffic aspects: In the next step, simulations were conducted and key traffic performance indicators compared to real traffic conditions at the investigated traffic site. On this basis, the model was calibrated to match real traffic as closely as possible regarding the number of vehicles per hour and travel

times. The data for automated detector counts describing the number of vehicles per hour were provided by the City Graz (Austria), for several days during a typical work week in January 2016. The data regarding the travel times were recorded end of June in 2018, using the app "Androsensor" on an Android smartphone. As a step additional to calibration, it is recommended in FGSV, 2006 to compare the simulated results to a second dataset and thereby conduct validation. Since only one aggregated dataset for detector counts and travel times was available, a validation was not possible. The traffic observations that were used to calibrate the model were conducted during the morning rush hour in the city of Graz, during 7:15 am and 8:15 am (morning peak hour). Details can be found in Medicus, 2019. The morning peak hour was selected as it represents the time with the highest traffic density in Graz. The intention was to generate traffic with a high potential for critical scenarios where active safety systems can become active.

Checking the plausibility of the MTFS model regarding safety aspects: A model that is calibrated to match traffic flow related criteria will not necessarily match criteria related to safety aspects (Astarita and Giofré, 2019). The chosen approach is based on Huang et al., 2013, who first calibrated the traffic flow model regarding traffic-related parameters and then regarding the number of conflicts (a scene in which the safety surrogate measure TTC falls below a defined threshold), by comparing the number of simulated conflicts with real conflict observations based on video analysis of an investigated road site. For the model used in this thesis, no conflict counts were available for safety related calibration. Instead, it was possible to apply the following procedures to achieve realistic conflicts: in this step, safety-related parameters were varied in a sensitivity study and calibrated to identify the most plausible results for the number of conflicts. Furthermore, a trajectory based analysis was conducted where individual conflicts were investigated for plausibility. To resolve locations of unusually high conflict density, priority rules were defined and the road geometry adapted. In addition, conflicts at several locations in the road network were simulated in nanoscopic simulation and the velocity profile and positions over time were compared to the same quantities in MTFS. Where large deviations existed, adaptations were made in the MTFS model, such as the introduction of slow down regions or changes in road geometry. Even though traffic observations regarding conflict numbers in real traffic were not available as in the study by Huang et al., 2013, the approaches presented in Section 5.1.3 were able to provide support in the process of checking the plausibility of the MTFS model regarding safety-related aspects.

The following sections are separated into subsections that deal with the above mentioned steps individually.

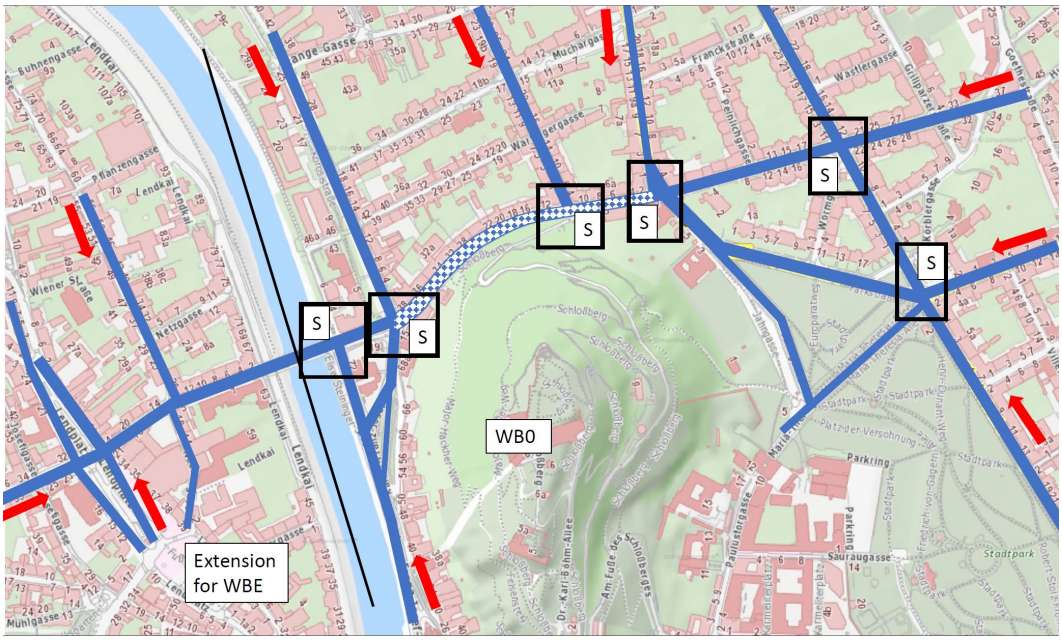

Figure 5.2.: The road segments (dark and solid blue) modeled by the traffic flow simulation models WB0and WBE. The road section "Wickenburggasse" is marked by the checkerboard pattern. The signalized intersections are shown in the black boxes, marked with the letter "S". Inflows are marked by arrows. Illustration adapted from Medicus, 2019. Source of background image: gis.stmk.gv.at

5.1. Method

5.1.1. Creation of the microscopic traffic flow simulation model

In the following, the simulated traffic site is described as well as the driver models (vehicle follow model and lane change model). In MTFS, the lane change and vehicle follow model describe the driving behavior of individual vehicles in relationship to other vehicles, and the route model describes how drivers navigate through the road network to reach their destination. The route model is not directly relevant to the aspects investigated in this thesis and is therefore not further discussed.

5.1.1.1. Description of the traffic site

As the simulated region, the urban road section surrounding the "Wickenburggasse" in the city of Graz (Austria) was chosen, see Figure 5.2, since this road section includes several accident hot spots. The model was first developed in Medicus, 2019 to cover a smaller region (base version WB0 for "Wickenburggasse version 0"). In the base version WB0, the road section "Wickenburggasse" was modeled along with connecting road segments and in total six signalized intersections, which are either directly part of the Wickenburggasse, or connected to the Wickenburggasse by at most one road segment (solid blue roads and road marked by checkerboard pattern in Figure 5.2).

The simulated traffic modes of WB0 include the motorized private transport (passenger cars and trucks), public transport (buses, trams) and vulnerable road users (bicyclists and pedestrians). Traffic can enter the road network of the base version WB0 in total at 9 inflow regions (see arrows in Figure 5.2, not all inflows are shown).

In the next step, the simulation model was extended to the west to also include a further traffic node with high traffic density, the Lendplatz in the city of Graz. The model is extended to the west by the roads marked in solid blue in Figure 5.2, leading to version WBE.

5.1.1.2. Vehicle follow model

The psycho-physical car-follow model by Wiedemann, 1974, implemented in VISSIM, is one of the most widely applied models to describe follow behavior. It describes how one vehicle follows another vehicle and considers the relationship between physical stimuli and psychological reactions of the driving person. The state of the driver model depends on the two dynamic parameters relative velocity v_{rel} and relative distance d_{rel} between the lead and following vehicle. Before explaining Figure 5.3, a few terms are defined:

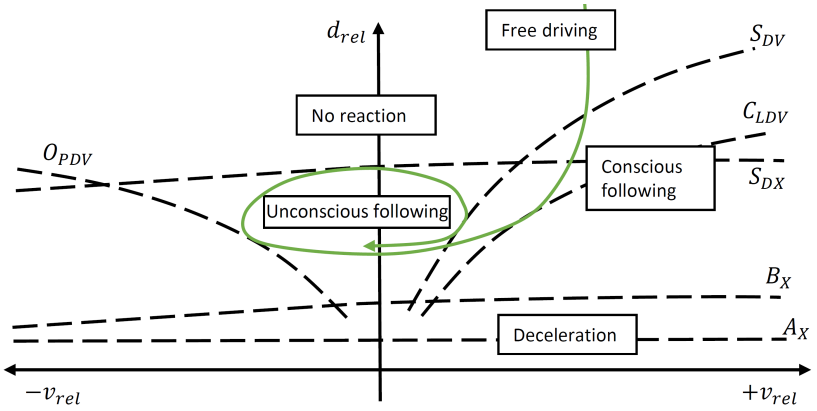

Figure 5.3.: The car-follow model by Wiedemann, 1974. The horizontal axis shows the speed difference between the follow and lead vehicle, while the vertical axis shows the relative distance.

A_X describes the desired distance between stationary vehicles. A_X is independent of v_{rel}.

B_X represents the desired minimal follow distance of the following vehicle at a similar speed as the lead vehicle. It is composed of the constant part A_X and a velocity dependent part. Since the follow distance does not increase proportionally at higher velocities, but rather leads to more risky driving behavior with lower distances, a parabolic relationship between B_X and the velocity is used: $B_X(v_{\text{rel}}) = A_X + (z\ B_{X,mult} + B_{X,add})\sqrt{v_{\text{rel}}}$, where $B_{X,mult}$ and $B_{X,add}$ are free calibration parameters of the driver model and z describes a random value that is normally distributed around 0.5 in the interval $[0, 1]$ with standard deviation 0.15.

S_{DX} describes the upper limit for the distance, before the following vehicle realizes that the distance increases and starts accelerating again. It is usually defined with a factor of 1.5 to 2.5 times B_X, i.e., it depends on v_{rel}.

S_{DV} represents a perception threshold, at which it is assumed that the driver in the follower vehicle notices the lead vehicle and starts to decrease the speed difference (in VISSIM, S_{DV} and C_{LDV} are assumed to be equal, see PTV Planung Transport Verkehr AG, 2017). Depends on v_{rel}.

C_{LDV} represents a reaction threshold for speed differences, at which it is assumed that the driver in the follower vehicle starts a braking maneuver and therefore starts to decelerate further, i.e. decrease the acceleration relative to the lead vehicle even more. Depends on v_{rel}.

O_{PDV} represents the perception threshold at lower speeds when the distance between the vehicles gets higher. Depends on v_{rel}.

On the right side of Figure 5.3, the thresholds for the approach process are shown. When a driver approaches another vehicle which is slower (starting at free driving, Figure 5.3), he starts to notice that the distance to the lead vehicle decreases (crossing the S_{DV} line and transitioning to conscious following), causing him to reduce the speed before C_{LDV} is crossed and therefore also decrease v_{rel}. With lower speed difference, the driver will enter unconscious following and the distance will increase. When the v_{rel} approaches the O_{PDV} threshold, the driver increases the speed again and therefore lowers the distance. This process leads to the spiral shown in Figure 5.3.

In VISSIM, two variants of the follow model by Wiedemann are implemented, namely "Wiedemann 74" and "Wiedemann 99". While Wiedemann 74 only offers three parameters to be changed by the user, Wiedemann 99 offers ten parameters (see PTV Planung Transport Verkehr AG, 2017). The VISSIM manual clearly recommends the Wiedemann 74 for the follow behavior of vehicles and bicycles in urban traffic sites. Therefore, the Wiedemann 74 model was used in Medicus, 2019 and for the MTFS model in this thesis. The Wiedemann 99 model is not explained further.

5.1.1.3. Lane change model

Next to follow behavior, also the lateral behavior is essential to safety-related analysis using MTFS models. Two separate cases are distinguished: necessary and voluntary lane changes. The first case occurs when a vehicle is forced to change lanes by means of route choice to reach their destination, lane number reduction or traffic rules. A voluntary lane change allows vehicles to achieve their desired speed (Hoffmann, 2013). Common lane change models are the ones presented by Sparmann, 1978 or Gipps, 1986.

The lane change model implemented in VISSIM (see Fellendorf and Vortisch, 2010), which is also used for the traffic model in this thesis, distinguishes between voluntary and necessary lane changes. If the route planning module does not already plan a lane change out of the necessity to reach the destination (voluntary lane change), other conditions that could require a necessary lane change are checked. If the vehicle is in follow mode according

to the Wiedemann 74 model described in Section 5.1.1.2, and the other lane offers better conditions for driving (e.g., a higher TTC to the leading vehicle, or a higher possible speed, see Fellendorf and Vortisch, 2010), the lane change model checks whether the change can be conducted safely. If all conditions are fulfilled, the lane change is initiated. A parametric Bézier curve is then fitted between the lanes as the path that the vehicles follow to conduct the lane change. However, there is no check whether the fitted curve can be driven if driving dynamics were considered, for example as is done in nanoscopic simulation.

For necessary lane changes that are required to reach the destination, two additional conditions are considered, based on gap acceptance and the emergency stopping distance (the distance to the emergency stop position of the current lane, i.e., the location where lane changes have to be completed). When the driver intends to change the lane to a lane with another vehicle which will be forced to slow down (forced deceleration), the lane change is only conducted if the forced deceleration is below a specified threshold. Otherwise, an emergency brake is conducted. The acceptable forced deceleration depends on the emergency stopping distance (a free calibration parameter, Fellendorf and Vortisch, 2010).

5.1.2. Calibration of the microscopic traffic flow simulation model regarding traffic aspects

The goal of traffic-based calibration is to change the free parameters of the MTFS model in such a way, that observations on real traffic are matched as closely as possible. The observations that were available for the creation of WB0 and WBE were measurements of travel time and detector counts. Changing the number of vehicles per hour that are generated stochastically at the inflows (see arrows in Figure 5.2), is one way to manipulate the flow of vehicles inside the road network. Other ways to manipulate the flow inside the network include changing the route choices of vehicles, i.e. by changing which percentage of the vehicles generated at the inflows have which destination. For details on how the route choices and inflows were defined, the reader is referred to Medicus, 2019.

5.1.2.1. Calibration regarding detector counts

The first step of traffic based calibration was done to match automated detector counts during the morning peak hour from 7:15 am to 8:15 am. The detector counts measure the number of vehicles per hour for individual lanes. In total, fifteen detectors were installed, see vertically striped bars in Figure 5.4, where each detector measured the vehicles per hour on a specific lane. The observations were done for several workdays and average values were calculated as one aggregated data set for comparison with simulated data. In the simulation model in VISSIM, virtual detectors were defined at the same locations as the real detectors.

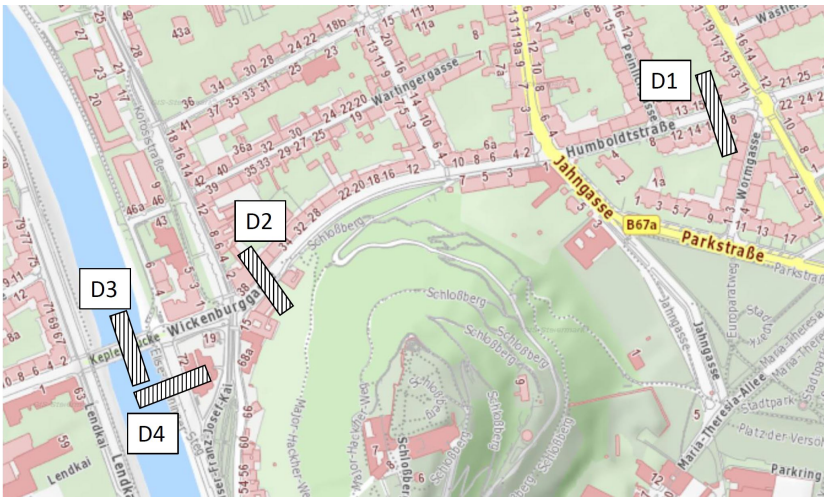

Figure 5.4.: The four detector installations D1, D2, D3 and D4 (bars with black vertical stripes). In total, the vehicles were counted at fifteen lanes (three lanes at D1, four lanes at D2, four lanes at D3 and four lanes at D4).

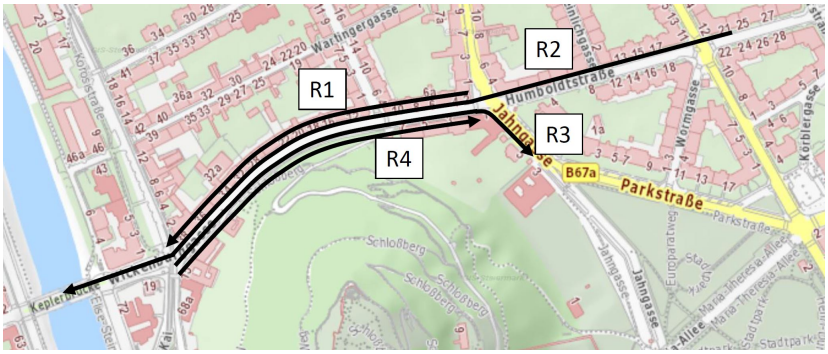

Figure 5.5.: The four defined routes R1, R2, R3 and R4 (black arrows) that were used to calibrate travel times.

The virtual detector counts were compared with the observed detector counts using the GEH error measure:

$$GEH = \sqrt{\frac{2(Fl_{\text{sim}} - Fl_{\text{obs}})^2}{Fl_{\text{sim}} + Fl_{\text{obs}}}}, \tag{5.1}$$

where Fl_{sim} is the simulated vehicle count at a specified location and Fl_{obs} is the observed vehicle count. For a description of the GEH measure, see Archer, 2005. The calibration is done iteratively by trial and error, until GEH reaches the threshold 5, which is recommended by Archer.

For the inflows that were added in the process of extending WB0 to WBE, observed vehicle counts were directly available, i.e., the counts could be used as boundary conditions such that these inflows did not need to be calibrated. Instead, only a calibration of route choices was necessary.

5.1.2.2. Calibration regarding travel times

Once the vehicle counts at detector installations were matched to a satisfying level, the model was calibrated to match vehicle travel times. Four routes were defined (see Figure 5.5) and driven in a test vehicle equipped with a GPS tracker. Two routes led only through the Wickenburggasse, while two longer routes were added to include the Wickenburggasse and further intersections. The same routes were defined in VISSIM as additional output. Each route was driven five times in the morning peak hour, and average values were computed for comparison with average simulated travel times using the error measure "Root Mean Squared Percent Error":

$$RMSPE = \sqrt{\frac{1}{n}\sum_{i=1}^{n}\left|\frac{t_i^{\text{sim}} - t_i^{\text{obs}}}{t_i^{\text{obs}}}\right|^2} \tag{5.2}$$

with t_i^{sim} being the simulated travel time, t_i^{obs} the observed travel time for the route i, and n being the number of routes. This measure is described in more detail by Detering, 2011.

5.1.2.3. Creation of a model with increased traffic density for the sensitivity study

In the course of the sensitivity study in Chapter 9, the change in effectiveness metrics is evaluated for the case that the traffic flow simulation model is changed. For that purpose, the road "Wickenburggasse", see Figure 5.2, in model WBE is selected and traffic in that road is artificially increased by 50 % by manipulating the traffic signal programs at signalized intersections (see green boxes Figure 5.2) and increasing the number of generated vehicles at specific inflow regions, leading to model version WBE50 ("Wickenburggasse extended with 50 % increased traffic"). Since a simple increase of generated vehicles at each inflow region of the simulation would have led to traffic jams, only the routes that lead over the Wickenburggasse were increased by 50 %, while other routes were reduced.

5.1.3. Checking the plausibility of the microscopic traffic flow simulation model regarding safety aspects

Calibration regarding traffic-related aspects (vehicles per hour, travel times) does not necessarily imply that the model is calibrated regarding safety-related aspects. Therefore, the third step of this approach focuses on the safety-related aspects and consists of a trajectory-based analysis and a sensitivity study regarding the number of conflicts to exclude implausible results. The two approaches are explained in the following subsections.

5.1.3.1. Sensitivity study regarding the number of conflicts

For the sensitivity analysis, in a first step, the trajectory data generated by VISSIM is evaluated using the software SSAM (Gettman, Pu, et al., 2008) and filtered according

Figure 5.6.: Historical accident data for the years 2013 to 2016, shown for the Wickenburggasse and connecting roads. The red circles represent accidents between passenger cars, the purple diamonds accidents involving powered two-wheelers, the green squares accidents with cyclists and the orange triangles represent accidents with other mixes of participant types. Data taken from Statistik Austria, 2020 and basemap.at

to a procedure and appropriate thresholds that were identified by Gettman, Pu, et al., 2008 or Sayed et al., 1994. This procedure recommends to consider only conflicts with $0 < \tau_{\mathrm{TTC,S}}^{\mathrm{min}} \leq 1.5\,\mathrm{s}$, maximum velocity $\geq 16.1\,\mathrm{km/h}$, minimum acceleration $> -9.15\,\mathrm{m/s^2}$ and traffic participant length $> 1\,\mathrm{m}$. Furthermore, only conflicts after 900 s of simulated time in MTFS are considered. The resulting conflicts are filtered and a plausibilization is conducted regarding the number of conflicts and their spatial distribution in the network. Furthermore, the simulation animation is checked. For the purpose of the plausibilization of the number of conflicts, and to account for the fact that the number of conflicts can vary between simulation runs (since randomly generated numbers are used in several parts of MTFS, e.g., for the generation of traffic participants, the parameterization of the driver models or the actual execution of driver models), ten simulation runs and average values for the conflict numbers are computed. For the plausibilization of the spatial distribution of conflicts, the conflicts of all ten simulation runs were visualized in the road network and compared to accident hot spot data that were collected in the years 2013 to 2016, see Figure 5.6.

5.1.3.2. Trajectory-based safety analysis

The goal of this procedure is to identify configurations and parameter settings in the MTFS model that lead to unrealistic conflicts that cannot occur in real traffic and to minimize deviations between MTFS and nanoscopic simulation. For this type of analysis, conflicts are extracted from the results of MTFS and recreated in nanoscopic simulation according to the method presented in this thesis work, i.e., by running a conflict analysis in SSAM on the MTFS results, simulating 5 s before and after individual conflicts in nanoscopic

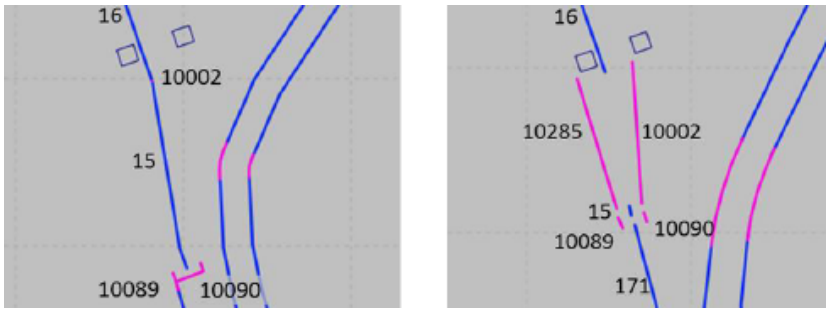

Figure 5.7.: Adaptation of lane and connector geometry, such that unrealistic accumulations of conflicts are avoided.

simulation including driving dynamics simulation and subsequent manual comparison of the trajectories. In nanoscopic simulation, the traffic participants choose their speed by following the acceleration profiles from MTFS. They choose steering angles by using a kinetic path driver model. A special focus is placed on conflicts in areas in the MTFS model where driving around curves, turning maneuvers, high numbers of conflicts with low values for TTC or high numbers of lane changes occur.

VISSIM offers a variety of tools to resolve unrealistic conflicts. In the following, examples how these tools can be applied are described.

One of the applied tools was the definition of conflict areas and priority rules. In locations in the road network where traffic streams can intersect (e.g., at intersections), traffic participants simply follow their route without paying attention to other traffic participants. At signalized intersections, intersections of traffic streams are avoided due to the timing of the traffic signals. If no traffic signals are present, conflict areas and priority rules have to be defined to clarify the priority rights and to avoid conflicts that would not occur in real traffic.

The next tool were geometrical adaptations of the road network of WB0. Several locations in the network of WB0 were identified where a high density of conflicts occurred, such as one location where two lanes merged into one and vehicles had to wait for the traffic lights. Before the adaptation, the vehicles started queuing before the connectors 10089 and 10090 (see Figure 5.7, left), which were too close together, such that conflicts were produced and collisions occurred in nanoscopic simulation. After the adaptation, the connectors were separated into individual lanes 10285 and 10002 and priority rules were defined, such that enough lateral distance between queuing vehicles was available.

Due to their geometrical length, the turning behavior of buses and trucks is different than that of passenger cars, since their turning radius is higher. Vehicles in VISSIM follow the defined paths closely. Therefore, curves with low radii have to be checked in nanoscopic simulation whether they can also be driven by buses or trucks with higher turning radii, without producing unrealistic results. Separate routes were defined for long vehicles that better described their turning behavior.

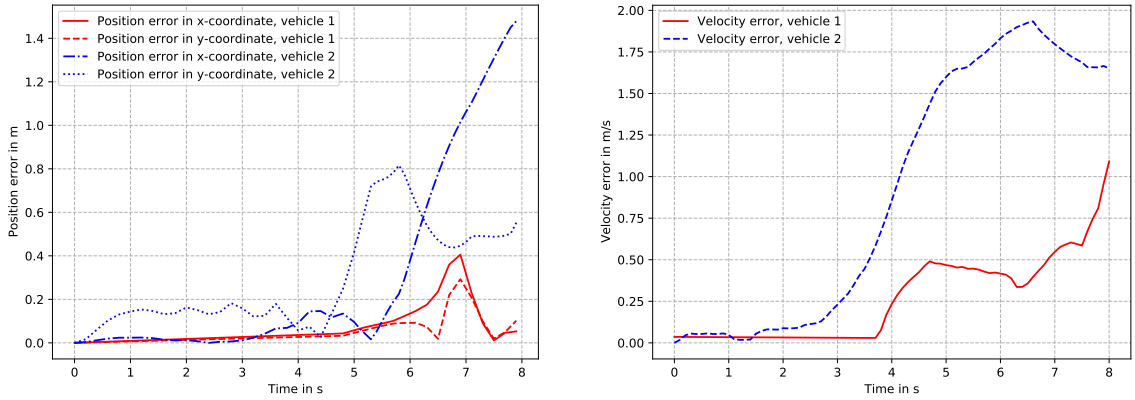

Figure 5.8.: Left: Exemplary error in position (i.e., absolute value per time step of the difference between MTFS and nanoscopic simulation) when representing a conflict in nanoscopic simulation, before the curve speed was adjusted. Right: Exemplary error in velocity.

If velocities in curves are too high, the steering in a vehicle might not able to follow the trajectories from MTFS within reasonable bounds of accuracy and it loses velocity in comparison to MTFS. In version WB0 (see Section 5.1.1) of the traffic flow model, the velocity in certain areas of the MTFS was only limited by each driver's desired maximum velocity. A possible consequence is that vehicles drive around curves in MTFS too fast, such that the trajectory simulated in MTFS is physically not drivable. In particular in conflicts, where driving around curves is involved, there can be high deviations between the trajectory from MTFS and the trajectory in nanoscopic simulation, where driving dynamics are considered. For one such conflict, where two vehicles driving in opposing lanes turned to the same direction at an intersection, the positional error for the center of gravity (i.e., the difference of the x- and y-coordinates at each time step) between nanoscopic simulation and MTFS is shown in Figure 5.8 (left). Furthermore, the velocity error is shown in Figure 5.8 (right). As can be seen, the error after 8 s simulation time in nanoscopic simulation can be up to 1.5 m in the position or up to 2 m/s in the velocity, since the velocity profile in MTFS could not be followed closely enough. Since such driving behavior is unrealistic, several slow down regions were defined for WBE which forced vehicles in MTFS to limit their velocity before they enter the slow down regions.

5.2. Results

5.2.1. Calibration of the microscopic traffic flow simulation model regarding traffic aspects

5.2.1.1. Calibration regarding detector counts and travel times

In Table 5.1, the results of the calibration of the model WBE to reduce the error measure *GEH* are shown. Each of the detector stations D1 to D4 count the vehicles per hour for up

	D1			D2				D3				D4			
Measurement	543	563	308	45	371	262	298	691	259	210	230	212	235	122	454
Simulation	552	554	301	44	368	293	282	736	266	211	239	255	191	167	415
GEH	0.4	0.4	0.4	0.2	0.2	1.8	1.0	1.7	0.4	0.0	0.6	2.8	3.0	3.7	1.9

Table 5.1.: Measured and simulated detector counts in vehicles per hour for the four detector stations D1 to D4 (see Figure 5.4) and computed error measure GEH. Taken from Medicus, 2019.

to four lanes. As can be seen, it was possible to find a network configuration such that the GEH stayed below 5, as recommended in Archer, 2005. This was achieved by manipulating the inflows and route choices (see Medicus, 2019).

Furthermore, a calibration to reduce the error measure RMSPE of the travel time was conducted, with the results shown in Table 5.2. This was mainly achieved by adjusting the distribution of the desired speed and the profiles for accelerating and decelerating which were followed by drivers in the Wickenburggasse. No specific threshold was followed in the calibration for travel times. However, it was attempted to reduce the RMSPE of the travel time as far as possible without violating the GEH threshold.

	R1	R2	R3	R4
Measurement	40.5	110.3	72.8	39.6
Simulation	29.4	88.2	58.3	28.5
RMSPE	27.6	20.2	20.1	28.2

Table 5.2.: Measured and simulated travel times in seconds for the four defined routes R1 to R4, see Figure 5.5. Taken from Medicus, 2019.

5.2.1.2. Creation of a model with increased traffic density for the sensitivity study

For the model WBE50, the inflows, route choices and traffic signals were manipulated to increase the traffic only in the Wickenburggasse by 50 %. The individual lanes of the detector stations D1 to D4 which were defined in MTFS and used to calibrate the MTFS model to real observations were grouped and the vehicle counts for lanes that head in the same direction were summed. Table 5.3 shows the sums of vehicle counts per direction per detector station. Furthermore, the ratios for WBE and WBE50 between the respective vehicle counts is shown. As can be seen, it was possible to increase traffic at detector station D2 (which counts vehicles only for lanes in the Wickenburggasse) by 50 %. However, it was not possible to keep all other vehicle count ratios to 1.0.

	D1	D2		D3		D4
WBE	1407	412	575	1002	450	1028
WBE50	1596	614	878	1011	479	1028
Ratio	1.1	1.5	1.5	1.0	1.1	1.0

Table 5.3.: Vehicles per hour for the detector stations D1 to D4 (see Figure 5.4), grouped and summed by lanes that lead in the same direction. D2 is the detector that measures the traffic directly in the Wickenburggasse. Taken from Medicus, 2019.

5.2.2. Checking the plausibility of the microscopic traffic flow simulation model regarding safety aspects

5.2.2.1. Sensitivity study regarding the number of conflicts

Medicus, 2019 conducted a sensitivity study of the following influencing factors, such that unrealistic parameterizations could be identified and excluded:

- Simulation frequency: number of time steps per second (frequency) with which the simulation is conducted in VISSIM
- Choice of follow model: Wiedemann 74 or Wiedemann 99
- Follow model parameters: three parameters for Wiedemann 74 and ten parameters for Wiedemann 99
- Lane change model parameters: e.g., gap acceptance, maximum number of surrounding vehicles considered by the lane change model or required safety distances

It was found that a change from the Wiedemann 74 to the Wiedemann 99 vehicle follow model resulted in an increase of 84 % of total conflicts (after applying the filter conditions from Section 5.1.3.1). Furthermore, the average value for the lowest TTC reached during the conflicts was decreased from 1.2 s to 1.1 s. When changing from Wiedemann 74 to Wiedemann 99, also a 33 % increase in crossing conflicts and a 172 % increase in lane-change conflicts was observed. The VISSIM manual clearly recommends the Wiedemann 74 for the follow behavior of vehicles and bicycles in urban traffic sites, as the Wiedeman 99 model is mainly suited for traffic sites such as freeways, where a lower number of merging areas (e.g., areas where lane changes occur) than in urban traffic sites are involved. The large increase in lane-change conflicts when using Wiedemann 99 confirms this statement. Therefore, the Wiedemann 74 model was used for vehicles and bicycles in Medicus, 2019 and for the MTFS model in this thesis.

Not only the type of follow model had a large influence on the conflicts, but also the driver model parameters. The largest influence was observed for the parameter A_X, i.e. the desired minimum distance for stationary vehicles. Since no parameterization produced results that seemed particularly unrealistic, simply the default values of VISSIM were used ($A_X = 2\,\text{m}$, $B_{X,add} = 2$, $B_{X,mult} = 3$). The same holds true for the lane change model.

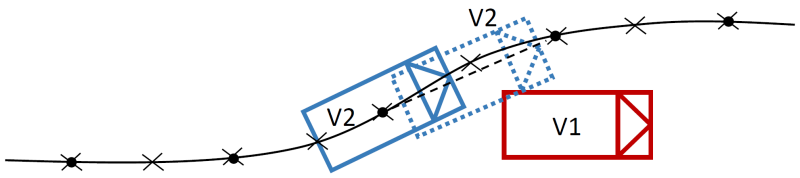

Figure 5.9.: The solid black line represents the planned path of the blue vehicle ($V2$, solid). The blue vehicle's center of gravity locations are marked by the black circles for 5 Hz MTFS simulation frequency and by black crosses for 10 Hz MTFS simulation frequency. Due to linear interpolation of vehicle positions (dotted blue vehicle, $V2$) for the calculation of SSMs when 5 Hz is used, SSAM might detect a collision with vehicle $V1$ which would not occur when a higher simulation frequency were used.

Furthermore, it was found that the number and the severity (i.e., the lowest value reached for TTC per conflict) of conflicts depended on the simulation frequency. The number of conflicts and their severity was the highest with 1 Hz, i.e., one time step per second, and declined when using 5 Hz or 10 Hz. After 10 Hz, the number of conflicts and average severity remained stable. A possible explanation could be that the time step sizes 1 Hz or 5 Hz simply do not offer sufficient temporal resolution for the calculation of SSMs. As an example, within 0.2 s, which corresponds to the time step size at 5 Hz, a vehicle traveling at 15 m/s (54 km/h) in urban traffic would cover 3 m. Within those 3 m, which is more than half a vehicle length if the vehicles are 5 m long, positions during evasion maneuvers are approximated linearly to a 10 Hz resolution by SSAM (Gettman, Pu, et al., 2008) for the calculation of SSMs. Due to the linear interpolation in curved driving, certain cases could be interpreted by SSAM as collisions, see Figure 5.9. This effect is even more pronounced when 1 Hz is used in MTFS. Therefore, 10 Hz was used for the simulation as the number of conflicts became stable at a simulation frequency of 10 Hz or higher.

5.2.2.2. Trajectory-based safety analysis

The trajectory-based safety analysis and subsequent model adaptions as described in the examples in Section 5.1.3.2 led to a reduction in the number of conflicts. When the conflicts are counted after applying the filter conditions described in Section 5.1.3.1, the total number of conflicts was reduced by 14 % (see Medicus, 2019). It was further noted, that crossing conflicts, i.e., conflicts where the vehicles exhibit an absolute value of the relative heading angle $|\theta_{\text{conf}}|$ of more than 85° (see Figure 5.10), were reduced by 60 % (attributable to the introduction of priority rights) and lane-change conflicts were reduced by 42 % (attributable to geometric adaptions of lane connectors). Rear-end conflicts, however, which account for the majority (78 %) of conflicts, were reduced by only 4 % (they are not influenced by any of the adaptations). Next to the number of conflicts, also the average of the lowest TTC reached per conflict was increased from 0.5 s to 1.3 s, i.e., the conflicts were much less severe as compared to before.

By introducing slow down regions to limit the curve speed to more physically realistic

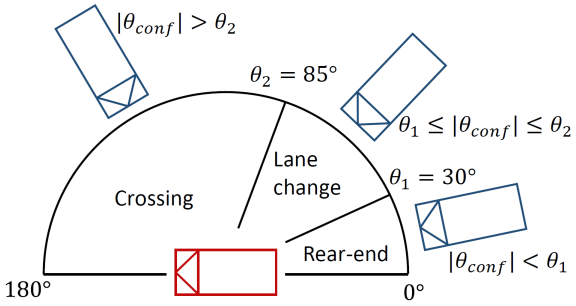

Figure 5.10.: The conflict types as they are defined in Gettman, Pu, et al., 2008. Conflicts with an absolute value of the relative heading angle $|\theta_{\text{conf}}|$ below the threshold $\theta_1 = 30°$ are classified as rear-end conflicts, conflicts with $\theta_1 \leq |\theta_{\text{conf}}| \leq \theta_2$ are classified as lane-change conflicts and conflicts with $|\theta_{\text{conf}}| > \theta_2 = 85°$ are classified as crossing conflicts.

values, it was possible to minimize the velocity and the position error in comparison between MTFS and nanoscopic simulation.

5.3. Conclusions

The following conclusions were found in the process of developing the MTFS models WBE and WBE50:

- Due to the calibration regarding traffic aspects, it was possible to keep the error measure GEH below 5 for each detector station and the error measure $RMSPE$ below 30 % for each route that was used to calibrate the MTFS model WBE towards the observed travel times.
- A sensitivity analysis led to the conclusion that 10 Hz is sufficient to produce a stable number of conflicts.
- For the vehicle follow and lane change model, no unrealistic settings were found, such that the default values in VISSIM were used and the recommendation of the VISSIM manual to use Wiedemann 74 for interurban road sites was followed.
- The trajectory based analysis allowed to reduce the number of conflicts by 14 % and also raised the average detected TTC from 0.5 s to 1.3 s. Geometrical adaptations in the lane network in VISSIM, the definition of priority rights and slow down regions proved to be useful tools to minimize deviations in the trajectories and velocity profiles between MTFS and nanoscopic simulation.

6. Scenario catalog definition

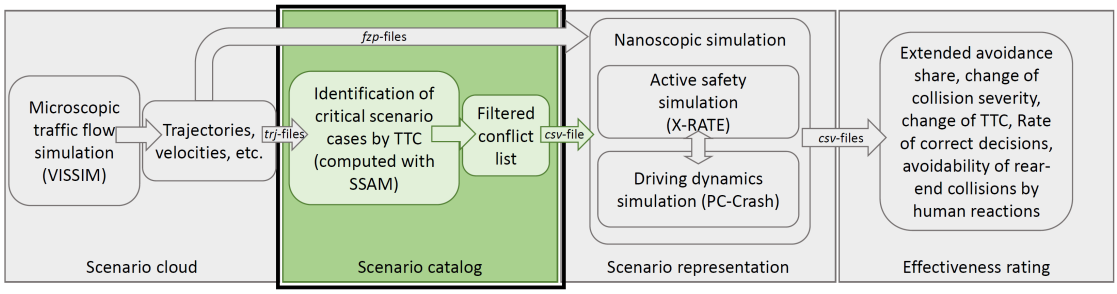

Figure 6.1.: Scenario catalog definition step (marked by the thick black frame): after their generation, MTFS results are analyzed regarding safety surrogate measures such as TTC or PET. Based on this analysis and appropriate conflict selection criteria, conflicts are transferred to nanoscopic simulation, where they are simulated individually.

This chapter describes how a scenario catalog can be defined based on the results of the scenario generation step (Chapter 5), see Figure 6.1. The application of SSAM leads to a comprehensive analysis of *trj*-files created by VISSIM containing conflict related quantities, such as TTC, PET, the maximum of the velocities of the conflict participants during the conflict, the lowest deceleration of any of the conflicting vehicles, or the magnitude of the difference of the velocity vectors of the conflicting vehicles at the time of lowest TTC. The result is a list of conflicts in the *csv*-format. This conflict list contains information such as $\tau_{\mathrm{TTC,S}}^{\mathrm{min}}$ for each conflict, the computed SSMs, the time and location of occurrence and other relevant data that is required to represent the conflict-based concrete scenarios in nanoscopic simulation. Before concrete scenarios can be simulated in nanoscopic simulation, the conflicts calculated by SSAM have to be filtered.

The calculation in SSAM is already highly automated, such that the SSMs can be calculated with one calculation run of SSAM for several *trj*-files without manual intervention.

The method section in this chapter is divided in subsections for the calculation of the SSMs and for the filtering of conflicts to define the scenario catalog. In the following, the additional subscripts X and S are used to distinguish between SSMs calculated by X-RATE (e.g., $\tau_{\mathrm{TTC,X}}$) and SSAM (e.g., $\tau_{\mathrm{TTC,S}}$).

6.1. Method

6.1.1. Calculation of Safety Surrogate Measures

In its $\tau_{TTC,S}$ and $\tau_{PET,S}$ calculation algorithm, SSAM makes use of the fact that the analysis is done after the simulation (see Gettman, Pu, et al., 2008). When calculating the $\tau_{TTC,S}$ and $\tau_{PET,S}$ at a given time step t_n, SSAM projects the vehicles that were simulated in MTFS forward along their trajectories (i.e., also following curves) under the assumption that their current velocity v_{t_n} remains constant (i.e., without consideration of the current acceleration), see Figure 6.2. At each time step t_n, SSAM checks whether a collision occurs within the search interval $\left[t_n,\, t_n + \tau_{TTC}^{max}\right]$, where τ_{TTC}^{max} denotes the defined maximum length of the search interval. This search is conducted for increasing forward projection times t in steps of 0.1 s, starting at 0 up to τ_{TTC}^{max}. For each t, the vehicles are moved along the trajectory that was simulated in MTFS for a distance of tv_{t_n}, until either a collision with another vehicle is found or t reaches τ_{TTC}^{max}. For the purpose of identifying an initial conflict list, SSAM uses a high value of $\tau_{TTC}^{max} = 2.5\,s$. If a collision of projected vehicles is detected, the vehicle pair is then stored in a list with the value of t for $\tau_{TTC,S}^{min}$, creating a new conflict if the vehicle pair was not added before to the list due to a projected collision from a previous time step. If the vehicle pair is already in the conflict list and the newly found $\tau_{TTC,S}$ for this time step is lower than the existing one, then the value for $\tau_{TTC,S}^{min}$ is updated with the new value.

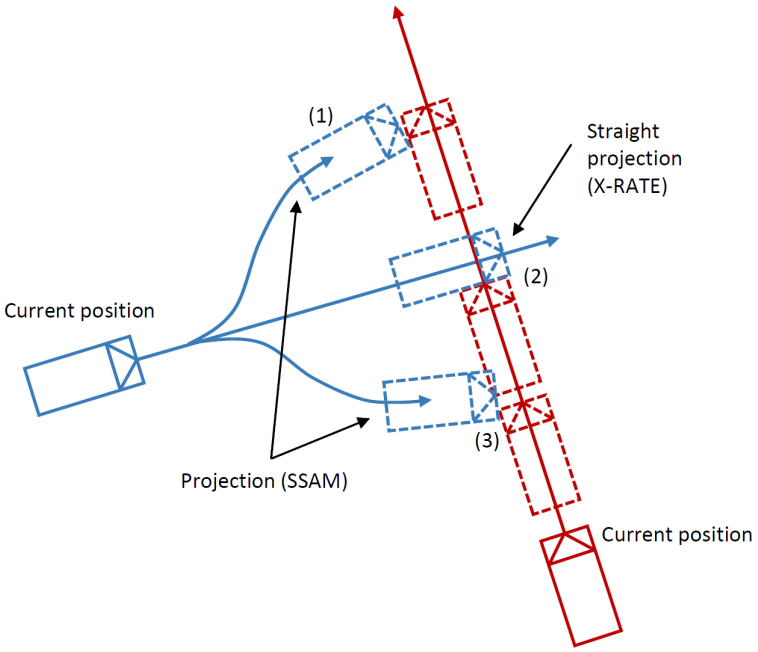

Figure 6.2.: Differences in τ_{TTC} calculation in an exemplary intersection situation. SSAM projects the vehicles forward along the trajectories which were simulated in MTFS. Depending on the trajectories, the $\tau_{TTC,S}$ can be lower (position 3) or higher (position 1) than $\tau_{TTC,X}$ (position 2).

In contrast to using the knowledge on the vehicles trajectories, other studies (e.g., Minderhoud and Bovy, 2001 or Kolk, Kirschbichler, et al., 2016) assume a straight continuation

of movement with the current velocities, i.e., with constant heading angle and constant velocity. This is also the approach, which is implemented in X-RATE. In the general case, i.e., when the trajectories are not perfectly straight, the consequence of the difference in the calculation of $\tau_{\text{TTC}}^{\min}$ is that $\tau_{\text{TTC,X}}^{\min} \neq \tau_{\text{TTC,S}}^{\min}$ (see Figure 6.2). However, the fact that no driving dynamics are considered in MTFS represents another reason why the values $\tau_{\text{TTC,X}}^{\min}$ in nanoscopic simulation can be different to the values $\tau_{\text{TTC,S}}^{\min}$ in the respective conflicts. Nevertheless, SSAM was chosen as the best available option for the calculation of the SSMs due to the following reasons:

- The computation of SSMs in SSAM is highly optimized.
- SSAM is a tool widely accepted and applied for traffic safety analysis in the traffic flow simulation community (see e.g., Dijkstra et al., 2010; Gettman, Pu, et al., 2008; Huang et al., 2013; Kim and Sul, 2009; Vasconcelos et al., 2014).
- The difference to nanoscopic simulation due to the driving dynamics also exists.
- SSAM acts as a pre-filter and conflicts are simulated again in nanoscopic simulation.

Next to the safety surrogate measures, each line in the output file of SSAM in the *csv*-format consists of the following, among other, data points for each conflict (see Gettman, Pu, et al., 2008):

- *trjFile*: input file for SSAM (i.e., output of MTFS), in which the conflict occurred. SSAM can analyze several result files from MTFS in one single call of the SSAM analysis procedure.
- $t_{\tau_{\text{TTC}}^{\min}}$: point in time when the minimum Time-to-Collision $\tau_{\text{TTC,S}}^{\min}$ was reached during the conflict. The value of $t_{\tau_{\text{TTC}}^{\min}}$ is used to identify the data from the VISSIM output which should be extracted to describe the traffic present during the conflict.
- *xMinPET* / *yMinPET*: coordinates where the minimum Post-Encroachment-Time ($\tau_{\text{PET,S}}^{\min}$) was reached during the conflict. These values are used for spatially filtering the conflicts.
- $v^{\max}$: maximum speed reached during the conflict by any of the conflict partners. Used as a criterion for filtering.
- *FirstVID* / *SecondVID*: vehicle index of the first and second participant that were involved in the conflict. Necessary for identification of the time series of the correct vehicles in the MTFS output. These two traffic participants are called *conflict participants*.
- θ_{conf}: the conflict angle θ_{conf} describes the angle that is enclosed by the heading directions of both conflicting traffic participants (Figure 6.3). It is computed by subtracting the heading angle of the first participant (*FirstVID*) minus the heading angle of the second participant (*SecondVID*). It must lie in the interval $[-180°, 180°]$. If not, it is transformed by subtraction or addition of 360°.
- *ConflictType*: based on the absolute value of the conflict angle θ_{conf}, a categorization of conflicts in *rear end*, *lane change* and *crossing* is introduced, see Figure 6.3. This categorization is based on Gettman, Pu, et al., 2008.

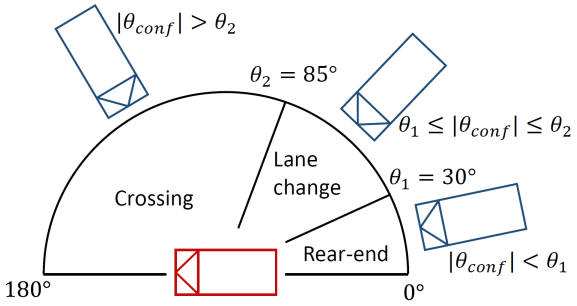

Figure 6.3.: The conflict types as they are defined in Gettman, Pu, et al., 2008. Conflicts with an absolute value of the relative heading angle $|\theta_{\text{conf}}|$ below the threshold $\theta_1 = 30°$ are classified as rear-end conflicts, conflicts with $\theta_1 \leq |\theta_{\text{conf}}| \leq \theta_2$ are classified as lane-change conflicts and conflicts with $|\theta_{\text{conf}}| > \theta_2 = 85°$ are classified as crossing conflicts.

6.1.2. Filtering the results of the conflict analysis

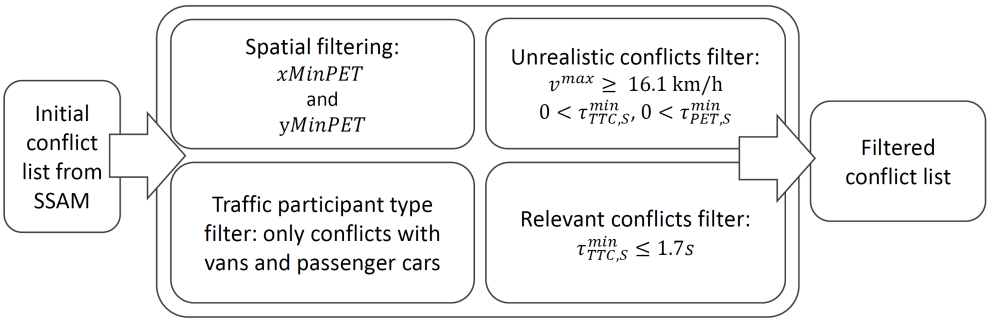

Figure 6.4.: To compile a conflict list for the definition of the scenario catalog, a filter for traffic participant types, for spatial filtering, for unrealistic conflicts and a filter to keep only relevant conflicts are applied.

After calculation of the initial conflict list by SSAM, in the next step, a variety of filters are applied to define a filtered conflict list, based on which the concrete scenarios can be extracted from the MTFS results. An overview on these filters is presented in Figure 6.4. The filters explained in the following can be applied in any order:

Traffic participant type filter: Not all combinations of traffic participant types need to be considered. Initially, the conflict list contains all traffic participant types that were simulated in the MTFS model such as vehicles, cyclists or pedestrians. Depending on which type of traffic participants should be the focus of the effectiveness study, these conflicts need to be filtered to contain only the traffic participants of interest. In the present thesis, the focus lies on conflicts that involve passenger cars and vans (i.e., vehicles with a length lower than 7 m). The nanoscopic simulation includes traffic participants of any type as the surrounding traffic, while the conflict partners are restricted to specific types through this filtering step.

Spatial filtering: To represent a conflict in nanoscopic simulation, it is necessary to extract data from the MTFS output for a time span before and after the occurrence of the conflict, i.e., $t_{\tau^{\min}_{\text{TTC}}}$. For the case that a conflict occurred too close to one of the network boundaries (in- or outflows), there can be less than the required time span available

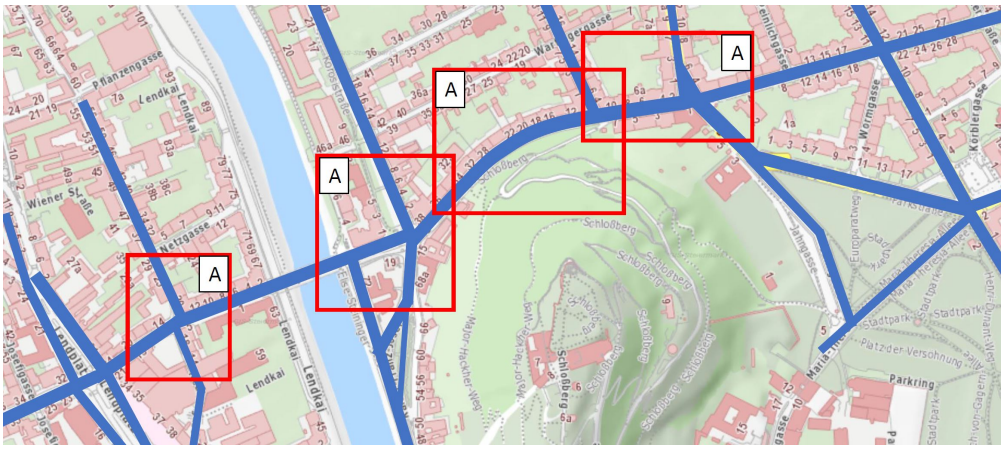

Figure 6.5.: The red boxes, marked by the letter "A", mark the areas from which conflicts are considered. These are areas with high densities of conflicts.

in the output data from MTFS. Therefore, conflicts that occur too close to the road network boundaries are filtered out, leaving only the "inner areas". The location of a conflict can be identified using the output parameters $xMinPET$ and $yMinPET$. In this thesis work, four signalized intersections represented in the MTFS model WBE are focused since they contain accident hot spots, as well as the Wickenburggasse itself (see Figure 6.5).

Unrealistic conflicts filter: Gettman, Pu, et al., 2008 recommends filtering out conflicts in which the velocity lies below a certain threshold. Conflicts with low velocities are identified by the output parameter $v^{\max}$, which should not be below 16.1 km/h (10 miles/h), since the vehicles would already be close to a full stop. Furthermore, Gettman, Pu, et al., 2008 recommends to use only conflicts with non-zero values for $\tau^{\min}_{\mathrm{TTC,S}}$ and $\tau^{\min}_{\mathrm{PET,S}}$, since VISSIM (see Chapter 5) cannot guarantee that no vehicle geometries overlap, e.g., during lane changes, due to the implemented approximation logic in VISSIM. This leads to "virtual accidents" with $\tau^{\min}_{\mathrm{TTC,S}} = 0$ or $\tau^{\min}_{\mathrm{PET,S}} = 0$.

Relevant conflicts filter: Before applying this filter, the list of conflicts contains conflicts with $\tau^{\min}_{\mathrm{TTC,S}}$ up to $\tau^{\max}_{\mathrm{TTC}}$. The aim of this filter is to reduce the conflict list further to contain less conflicts where the safety systems are not expected to activate a braking maneuver. For this purpose, a filter threshold $\tau^{\mathrm{Filt}}_{\mathrm{TTC}}$ is used, such that only conflicts with $\tau^{\min}_{\mathrm{TTC,S}} \leq \tau^{\mathrm{Filt}}_{\mathrm{TTC}}$ are selected for the scenario catalog. In the following, an investigation how $\tau^{\min}_{\mathrm{TTC,S}}$ correlates with $\tau^{\min}_{\mathrm{TTC,X}}$ ($\tau^{\min}_{\mathrm{TTC}}$ as detected by X-RATE in nanoscopic simulation) is conducted. For this analysis, only the first 20 MTFS model runs of WBE were used. Filtering with the highest value $\tau^{\mathrm{Filt}}_{\mathrm{TTC}} = 2.5\,\mathrm{s}$ led to 2 607 conflicts in total.

In Figure 6.6, the values of $\tau^{\min}_{\mathrm{TTC,S}}$ are compared to the values of $\tau^{\min}_{\mathrm{TTC,X}}$ detected by X-RATE in nanoscopic simulation in the baseline. To see whether the two quantities are correlated, a linear regression fit is computed (blue line). This linear regression fit shows a negative intercept of $-0.32\,\mathrm{s}$, with a slope of 1.09. The low correlation coefficient of $r_{corr} = 0.45$ does not indicate a strong linear relationship between $\tau^{\min}_{\mathrm{TTC,S}}$

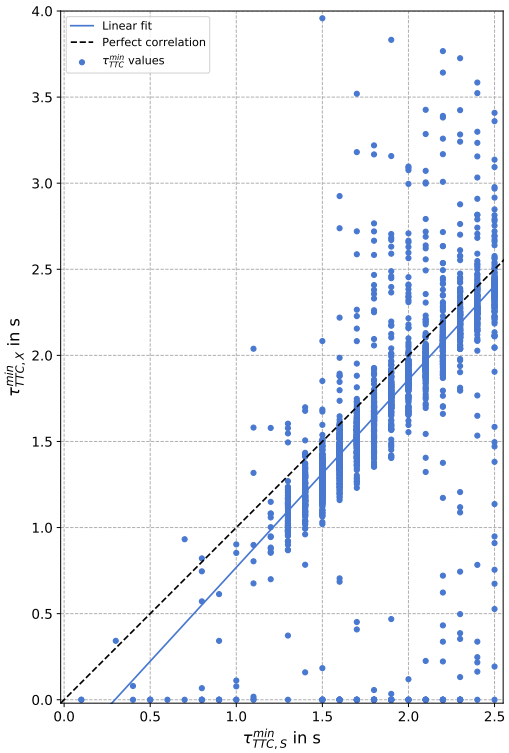

Figure 6.6.: Correlation of $\tau^{\text{min}}_{\text{TTC,S}}$ detected by SSAM (horizontal axis) and $\tau^{\text{min}}_{\text{TTC,X}}$ (vertical axis) between the conflict participants as it was detected by X-RATE in the baseline. The black dashed line shows perfect correlation, while the blue line shows a linear regression fit with $\tau^{\text{min}}_{\text{TTC,X}} = 1.09\,\tau^{\text{min}}_{\text{TTC,S}} - 0.32$ and a correlation coefficient $r_{corr} = 0.45$.

and $\tau^{\text{min}}_{\text{TTC,X}}$. A significant variation of the values around the linear fit can be seen in Figure 6.6. The reason for this variation of $\tau^{\text{min}}_{\text{TTC,X}}$ around the linear fit is the fact that the calculation algorithm for τ_{TTC} deviates between X-RATE and SSAM (see Section 6.1.1) and that a kinetic path driver model has to be used to follow the trajectories computed in MTFS (see later chapters). However, $\tau^{\text{min}}_{\text{TTC,S}}$ can be still used a preliminary filter, even if there is low correlation between $\tau^{\text{min}}_{\text{TTC,S}}$ and $\tau^{\text{min}}_{\text{TTC,X}}$, if the effectiveness metrics are designed in such a way that irrelevant conflicts are neglected. Therefore, a value of 0.2 s is added to the highest trigger threshold of the two investigated systems ($\tau^{\text{Trig}}_{\text{ETTC}} = 1.5\,\text{s}$) to account for the variation of $\tau^{\text{min}}_{\text{TTC,X}}$, leading to $\tau^{\text{Filt}}_{\text{TTC}} = 1.7\,\text{s}$, which is used as a preliminary value for the exemplary effectiveness study, and in the sensitivity study in Chapter 9, the dependence of the effectiveness metrics on $\tau^{\text{Filt}}_{\text{TTC}}$ is investigated.

6.2. Results and discussion

6.2.1. Analysis of conflicts in the MTFS model WBE

For the generation of MTFS results, 50 runs of the model WBE were calculated in total, as this number of model runs leads to a number of conflicts that fulfills the requirement "High

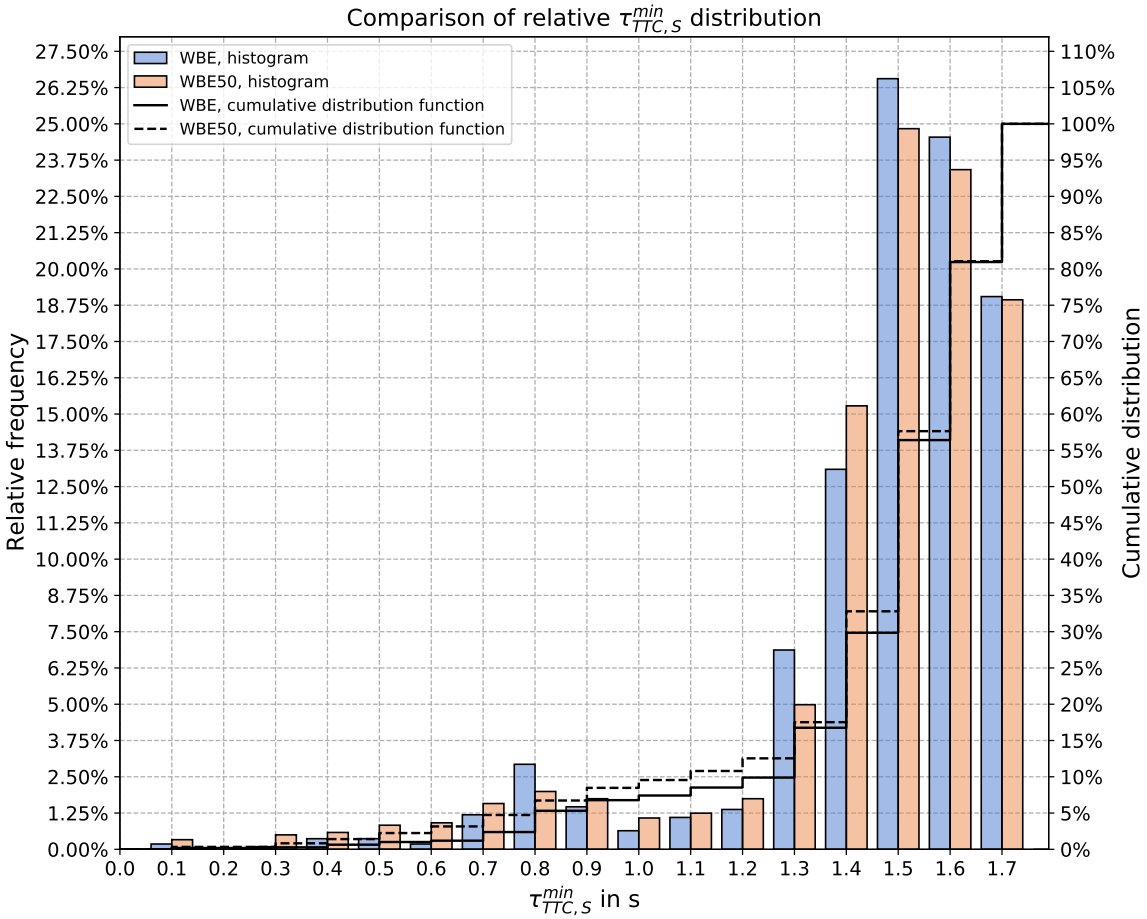

Figure 6.7.: Relative frequency of occurrence (solid bars) for the values of $\tau^{\min}_{\mathrm{TTC,S}}$ for WBE and WBE50. Each bar B shows the count of conflicts with $e_l \leq \tau^{\min}_{\mathrm{TTC,S}} < e_l + 0.1\,\mathrm{s}$, divided by the total number of conflicts for the respective MTFS model, where e_l is the left interval limit in steps of 0.1. The bars are centered around their respective left interval limits. The lines show the cumulative distribution function of the $\tau^{\min}_{\mathrm{TTC,S}}$ values in the intervals $e_l \leq \tau^{\min}_{\mathrm{TTC,S}} < e_l + 0.1\,\mathrm{s}$.

number of concrete scenarios". When applying the software SSAM to the 50 model runs, in total 95 412 conflicts are identified as the initial conflict list with $\tau^{\min}_{\mathrm{TTC,S}} \leq \tau^{\max}_{\mathrm{TTC}} = 2.5\,\mathrm{s}$, which represents the upper limit of SSAM for the conflict search algorithm. Then, the filter procedure described in Section 6.1.2 is applied. For the spatial filter, only conflicts in the Wickenburggasse as well as in the Neubaugasse and adjoining intersections are kept, see Figure 6.5. This leaves 12 366 conflicts. In the next steps, the unrealistic conflicts and traffic participant type filters are applied. As a final filter, the relevant conflicts filter is applied, such that only conflicts with $\tau^{\min}_{\mathrm{TTC,S}} \leq \tau^{\mathrm{Filt}}_{\mathrm{TTC}} = 1.7\,\mathrm{s}$ are kept. This leaves 2 760 conflicts in the final conflict list for the 50 model runs.

According to the classification specified in Section 6.1.1, the conflicts can be separated into 2 516 (91.1 %) rear-end, 186 (6.7 %) lane change and 58 (2.1 %) crossing conflicts, i.e., the majority of conflicts is of rear-end type.

The distribution of the values for $\tau^{\min}_{\mathrm{TTC,S}}$ is shown in Figure 6.7. It can be seen that only

few conflicts (187 out of 2760 conflicts, i.e., 6.8 %) exhibit a $\tau_{TTC,S}^{min} < 1.0\,s$, while the largest proportion lies between 1.0 s and 1.7 s. The distribution shown in Figure 6.7 is influenced by the driver model parameters chosen for the MTFS model, as discussed in Medicus, 2019.

6.2.2. Analysis of conflicts in the MTFS model WBE50

MTFS model	*Rear-end conflicts*	*Lane-change conflicts*	*Crossing conflicts*	*Total conflicts*
WBE	50.3 (91.1 %)	3.7 (6.7 %)	1.2 (2.1 %)	55.2
WBE50	53.9 (90.8 %)	3.9 (6.6 %)	1.5 (2.5 %)	59.3
Relative increase WBE to WBE50	+7.0 %	+5.9 %	+27.6 %	+7.4 %

Table 6.1.: Number of conflicts per simulated hour (each MTFS model run represents one hour of traffic) and relative increase of conflicts per hour between the MTFS models. The numbers in parentheses represent the proportion in the total number of conflicts per hour of the respective MTFS model.

To analyze the model WBE50, the same filters as described in Section 6.2 were applied to define the scenario catalog. The original conflict analysis with a coarse filter of $\tau_{TTC}^{max} = 2.5\,s$ led to a total of 105 990 conflicts. After filtering, such that $\tau_{TTC,S}^{min} \leq 1.7\,s$ for all conflicts, 2 964 conflicts are left, which represents a 7.4 % increase in the total number of conflicts in comparison to WBE, see Table 6.1. The biggest relative increase can be seen for the crossing conflicts (27.6 %), and the lowest increase for the lane-change conflicts (5.9 %). Among the conflicts in WBE50, 2 693 (90.8 %) are of rear-end type, according to the classification in Section 6.1.1, while 197 (6.6 %) are lane change conflicts and 74 (2.4 %) are crossing conflicts. With a maximum difference for each conflict type of 0.4 % of the total conflicts, this distribution is very similar to the conflict type distribution of WBE.

In Figure 6.7, the distributions of $\tau_{TTC,S}^{min}$ values of WBE and WBE50 are compared in a histogram of the relative frequency and cumulative distribution. As can be seen, the proportion of conflicts with $\tau_{TTC,S}^{min} \leq 1.2\,s$ is slightly higher for WBE50 (12.6 % of the total conflicts, i.e., 372 of 2 964) than for WBE (9.9 % of the total conflicts, i.e., 274 of 2 760), while conflicts with higher $\tau_{TTC,S}^{min}$ are less common in relation to the total number of conflicts. This means that the increased traffic in the road section "Wickenburggasse" led to more severe conflicts.

6.3. Conclusions

The following conclusions were found when analyzing the results of the conflict analysis:

- The majority of conflicts in the investigated MTFS models WBE (validated reference MTFS model) and WBE50 (traffic density artificially increased by 50 % increase in a selected road), representing the traffic at the morning peak hour between 7:15 am

and 8:15 am at an inner-urban traffic site, were rear-end conflicts (91.1 % and 90.8 %, respectively).

- Applying the filtering procedure to the model WBE50 (traffic density artificially increased by 50 % increase in a selected road) leads to 7.4 % more conflicts (in total, 59.28 conflicts per simulated hour) as for the validated reference MTFS model WBE, while the biggest increase of 27.6 % relative to WBE was observed for crossing conflicts.
- The distribution of the type of conflicts remained very similar between the MTFS models WBE (91.1 %, 6.7 % and 2.1 % for rear-end, lane-change and, respectively, crossing conflicts) and WBE50 (90.8 %, 6.6 % and 2.5 % for rear-end, lane-change and, respectively, crossing conflicts).
- The distribution of $\tau_{\mathrm{TTC,S}}^{\mathrm{min}}$ indicates that the increased traffic in WBE50 led to proportionally more severe conflicts.

7. Scenario representation

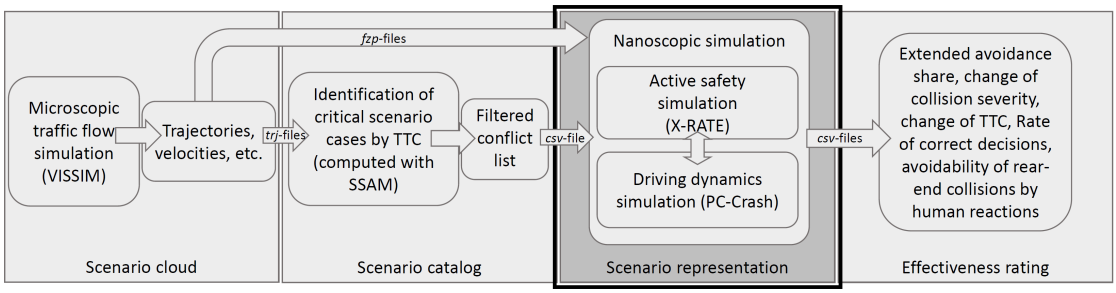

Figure 7.1.: Scenario representation step (marked by the thick black frame): in the third step, the output generated by Microscopic Traffic Flow Simulation (MTFS) and the conflict analysis based on Safety Surrogate Measure (SSM) is used to define individual concrete scenarios for nanoscopic simulation, where driving dynamics and ADAS can be considered.

This chapter describes how a representation of scenarios can be achieved in nanoscopic simulation, using the outputs of the previous steps *scenario generation* and *scenario catalog definition*. In the chosen solution approach, it forms the third step in the assessment process, see Figure 7.1.

7.1. Method

For the following sections, a vehicle and a sensor coordinate system are introduced, denoted by the superscripts V (vehicle) and S (sensor), in addition to the global coordinate system denoted by the superscript G (global). The origin of the vehicle coordinate system $\vec{O}_i^V$ of the vehicle with index i is located in the center of gravity $\vec{X}_{\mathrm{COG},i}^V$ of the vehicle which is assumed to be located at half the length, i.e., $l/2$, and half the width, i.e., $w/2$, of the vehicle (see Figure 7.2). The longitudinal vehicle coordinate direction x faces to the front of the vehicle, while the lateral vehicle coordinate y-direction faces to the left as seen from the driver's view, see Figure 7.2. The z-axis is assumed to be facing up (not shown in the figure). The sensor with index j is located at a fixed position $\vec{X}_{\mathrm{S},j}^V$ on the vehicle (see Figure 7.2), i.e., if the vehicle changes its orientation then the sensor is rotated in the same manner.

In this method section, first, an overview on nanoscopic simulation is given, containing an explanation of the simulation framework X-RATE and the individual steps that need to be executed to conduct the time step wise simulation of concrete scenarios. Among these steps, the preparation of concrete scenarios based on conflicts, the sensor model, the strategy

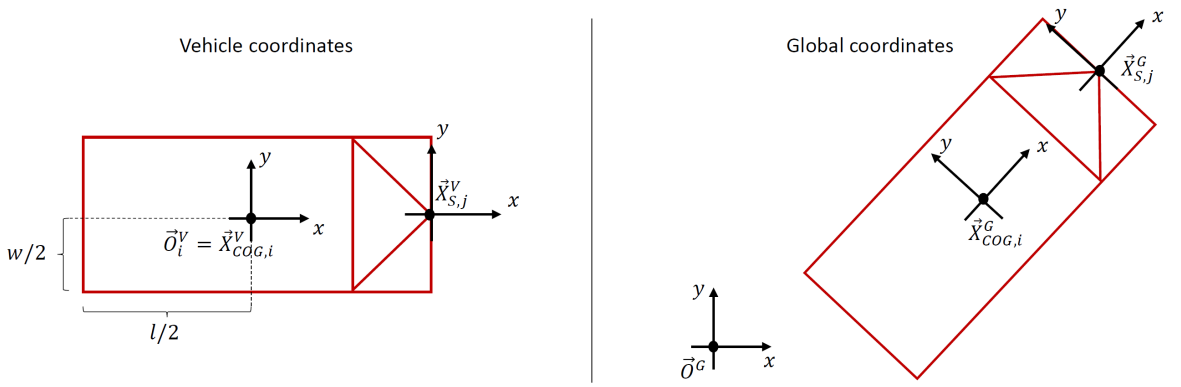

Figure 7.2.: Definition of the global coordinate system (origin $\vec{O}^G$), vehicle coordinate system (origin $\vec{O}_i^V$ at the vehicle's center of gravity $\vec{X}_{\mathrm{COG},i}^V$) and sensor coordinate system (origin at $\vec{X}_{\mathrm{S},j}^V$ or $\vec{X}_{\mathrm{S},j}^G$). The sensor is placed at a fixed location on the vehicle.

model, the application of the kinetic path driver model and the collision model are explained in more detail in individual subsections. In addition, the scenery model is explained.

7.1.1. Overview on nanoscopic simulation

7.1.1.1. The simulation framework X-RATE

Figure 7.3 shows the factors that influence the course of actions during a scenario in the form of a modular framework, which are the basis for the implementation of the tool X-RATE.

On the highest level, there is the *simulation control* layer that prepares concrete scenarios as individual simulations, executes them one by one and collects results for the assessment step. The simulation control layer conducts the simulations in an automated way for the full scenario catalog, without the need for manual intervention for a defined conflict list, as long as the MTFS results are available in an arbitrary storage location on the computer or network, and once all simulation settings have been configured.

A concrete scenario is described in nanoscopic simulation through the following models, which are in turn comprised of several sub-models (a similar sub-division is presented in Page et al., 2015):

Infrastructure model: within this thesis, the infrastructure is represented in nanoscopic simulation only as the road, which consists of an indefinitely large flat surface. The real traffic site simulated in the MTFS models WBE and WBE50 exhibits a slight inclination (less than one meter change in altitude over 200 meter distance), which is neglected in nanoscopic simulation. Vehicles cannot "hit" a road boundary, since such a boundary is not considered.

Scenery model: intended to represent the weather, lighting conditions and static objects that are primarily relevant as sight obstructions to sensor vision such as houses, trees and more.

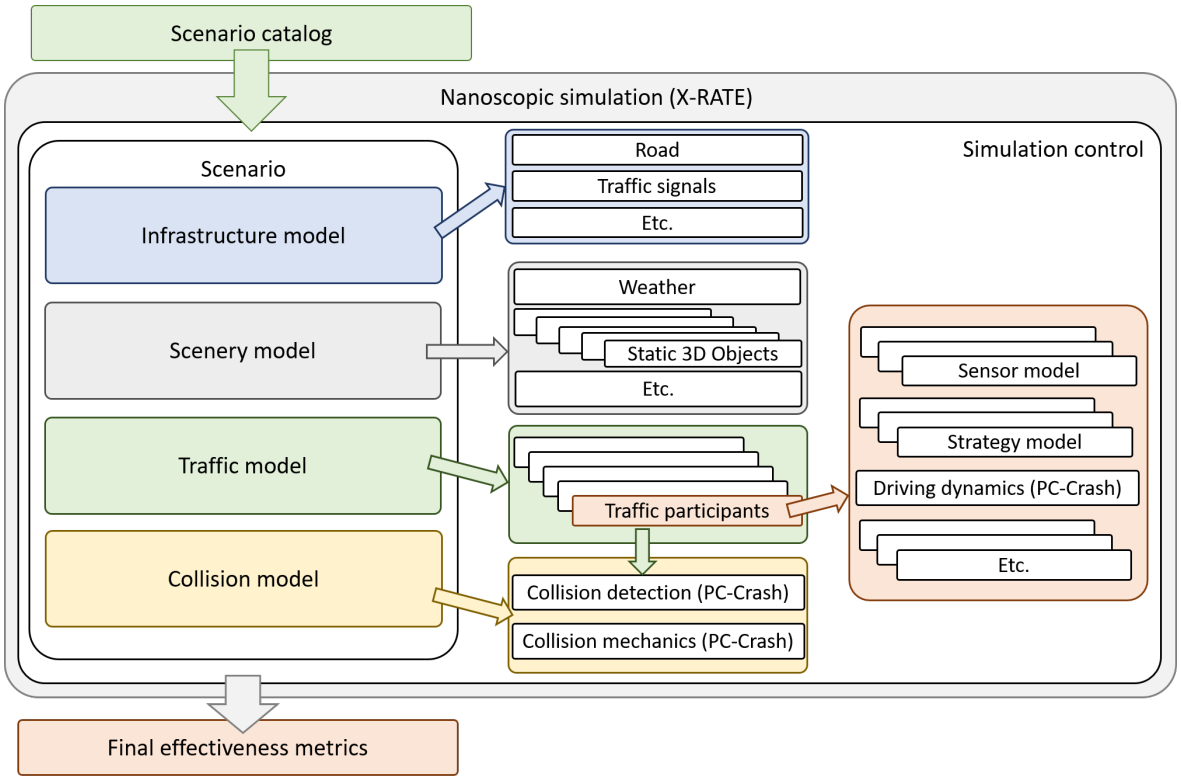

Figure 7.3.: Modular structure of the program framework for nanoscopic simulation. The highest level is the simulation control, which receives concrete scenarios from the catalog. The infrastructure, scenery and traffic model reflect the concrete scenarios. If a collision occurs, its consequences are calculated by the collision model. Figure based on Page et al., 2015 and Sander, 2017.

Traffic model: describes dynamic objects, that might change their position and orientation in space, i.e., traffic participants such as vehicles, pedestrians, bicycles and more. This model provides an interface to the MTFS simulation software VISSIM to import scenario data. The interface to VISSIM takes over the role of the scenario source.

Collision model: during the simulation, PC-Crash checks whether the geometries of any of the simulated traffic participants intersect (collision detection). If a collision is detected, the collision model is applied to calculate collision-related quantities for further evaluation. In the case of the present thesis work, a momentum based collision model that approximates the crash-phase as a phase with infinitely short duration.

The behavior of each traffic participant in turn is described by several other sub-models of the traffic model, such as:

Sensor model: this model represents the perception mechanisms of the sensors that are used by the active safety systems to gather information on the scenery. In the present thesis work, a geometric sensor model is used to determine the visibility of traffic participants through ray-tracing.

Strategy model: the strategy model describes that part of the safety system, which responds to the input provided by the sensors, by triggering appropriate counter measures if a critical situation in traffic is encountered. In the present thesis, a braking maneuver is triggered to avoid frontal collisions.

Driving dynamics model: responsible model for representation of the physical effects during the driving process. This model considers kinetic driving including three dimensional motion (see Section 2.3.1.2), suspension and tire characteristics, and tire slip by coupling X-RATE with PC-Crash. The model also includes the description of movement of two-wheelers (motorbikes or bicycles) or pedestrians.

7.1.1.2. Simulation process of individual conflicts

The algorithm that simulates individual concrete scenarios works in a time step-wise fashion and is shown in Figure 7.4. Depending on the type of the simulated traffic participant, different actions are executed. Only the conflict vehicles have a safety system installed, i.e., only for them, the sensor and strategy model is executed. Kinetic vehicles are simulated with full driving dynamics in PC-Crash, while kinematic vehicles, being only relevant as sight obstructions, are considered only in MATLAB, such that their driving states represent an exact replay of their driving states in MTFS. The performed actions are explained in the following:

Preparation of concrete scenarios based on conflicts: each concrete scenario is prepared by extracting time series data from the MTFS simulation results, setting the initial status of traffic participants, and setting trajectories of vehicle fronts and acceleration

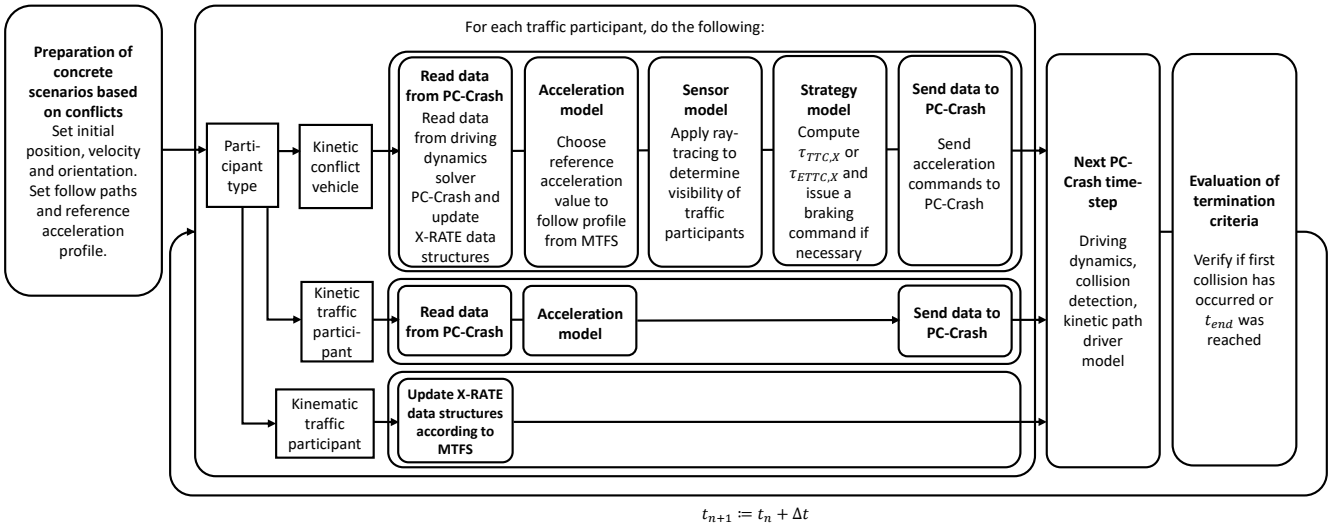

Figure 7.4.: The simulation process that is repeated for every concrete scenario.

profiles from MTFS as follow paths and reference acceleration profiles in nanoscopic simulation.

Read data from PC-Crash / Update X-RATE data structures according to MTFS: if this is not the first time step simulated for this concrete scenario, for each kinetically simulated traffic participant, results on the last time step of driving dynamics simulation are requested from PC-Crash over the OLE (Object Linking and Embedding) programming interface. This includes the positions of the centers of gravity of traffic participants, their accelerations, velocities, velocity directions and the orientation in space. Data structures in X-RATE are updated with the new information on the traffic participants' status. This includes updating the rotation matrices which are needed for coordinate transformations (see Appendix C.1). Furthermore, the local mesh model coordinates of traffic participants, using the participants' current positions and orientations, are transformed to the global coordinate system. For kinematic traffic participants, the data structures in X-RATE are updated to represent a replay of MTFS.

Sensor model: at this step, the visibility of traffic participants is determined. This step is only executed for conflict vehicles.

Acceleration model: the acceleration model provides acceleration commands by using the acceleration values that were simulated in the corresponding time step in MTFS. Commands by the acceleration model can be overwritten by the strategy model in the same time step.

Strategy model: the sensor data is transferred to the strategy model which represents the active safety system logic. This model processes the sensor data, calculates $\tau_{\mathrm{TTC,X}}$ or $\tau_{\mathrm{ETTC,X}}$ and decides whether it is necessary to intervene in the driving process by braking. This step is only executed for conflict vehicles.

Send data to PC-Crash: transfer of acceleration commands to PC-Crash over the OLE interface.

Next PC-Crash time step: start of calculation of the next time step. Based on the path

provided by the MTFS simulation, steering angles have to be chosen to follow this path, which is done by the kinetic path driver model implemented in PC-Crash. Furthermore, the collision detection and collision mechanics calculation are conducted.

Evaluation of termination criteria: check whether the termination criteria are fulfilled, i.e. check whether the maximum simulation time t_{end} was reached or whether a collision has occurred. Since $t_{\text{sim}} = 5\,\text{s}$, $t_{\text{end}} = 10\,\text{s}$ is defined. If the criteria are not fulfilled, the next nanoscopic simulation time step is executed.

The simulation is conducted with a fixed time step size $\Delta t = 15\,\text{ms}$. Since the driving dynamics solver PC-Crash Version 11.0 (see User's and technical manual Moser, 2020) only offers time step sizes of 15 ms, 60 ms and 300 ms for the communication with other software over the OLE-interface, the shortest time step $\Delta t = 15\,\text{ms}$ is chosen to reach the highest possible computational accuracy. A vehicle moving with 13.8 m/s (50 km/h) in urban traffic can change its position by a maximum of around 20 cm within 15 ms. This inaccuracy is accounted for by the safety zone (denoted by d_{SZ}), which is considered in the sensor and strategy model for collision detection. Furthermore, with a time step of 60 ms, when starting at $t = 0$, the simulation would iterate over the steps $t = 180\,\text{ms}$ and $t = 240\,\text{ms}$. If a certain threshold is met at $t = 190\,\text{ms}$, the next time step where the system could react would be $t = 240\,\text{ms}$, leading to a total delay due to the simulation time step of 50 ms. This delay is random, depending on the type of threshold, its value and distance to the next time step. To decrease the influence of unwanted randomness, a time step as small as possible is chosen, i.e., 15 ms.

7.1.2. Preparation of concrete scenarios based on conflicts

Before any simulation is conducted, a time frame $I = \left[t_{\tau_{\text{TTC}}^{\min}} - t_{\text{sim}},\ t_{\tau_{\text{TTC}}^{\min}} + t_{\text{sim}}\right]$ is defined that is considered for each conflict. In the exemplary effectiveness study, $t_{\text{sim}} = 5\,\text{s}$ is chosen as a starting value. However, it is not clear whether five seconds are necessary or if it is sufficient to simulate a shorter time frame around $t_{\tau_{\text{TTC}}^{\min}}$. Therefore, in a sensitivity study in Chapter 9, the length of this time frame before and after $t_{\tau_{\text{TTC}}^{\min}}$ is shortened to 3.5 s and 2 s to investigate the effect on the results of the nanoscopic simulation, when safety systems trigger their emergency maneuvers and, in particular, whether the resulting effectiveness metrics are different.

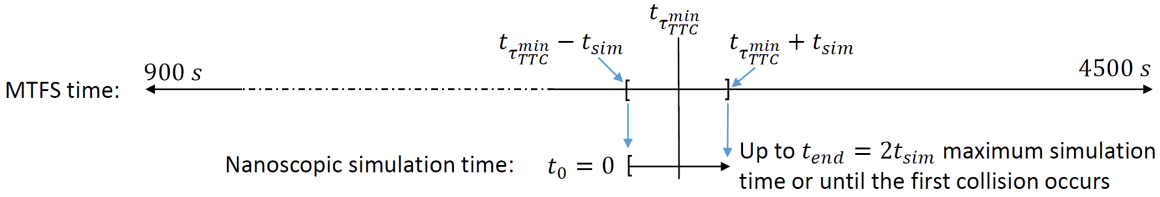

Figure 7.5.: Representation of the time intervals in MTFS and nanoscopic simulation. The initial status for each concrete scenario at $t_0 = 0$ in nanoscopic simulation corresponds to $t_{\tau_{\text{TTC}}^{\min}} - t_{\text{sim}}$ in the MTFS results.

For each conflict, the first step in concrete scenario preparation consists of loading the *fzp*-file of the respective MTFS model run, in which the conflict occurred, into the MATLAB memory. Then, the traffic participants that need to be simulated are determined. In the next step, each of those traffic participants is placed in nanoscopic simulation such that it's initial center of gravity, which is chosen to be at exactly half the vehicle length and width of the participant, corresponds to the center of gravity at $t_{\tau_{\mathrm{TTC}}^{\min}} - t_{\mathrm{sim}}$ in MTFS. The same is done for the initial orientation and velocity. The start $t_0 = 0$ of nanoscopic simulation then corresponds to the lower limit of the time interval $I = \left[t_{\tau_{\mathrm{TTC}}^{\min}} - t_{\mathrm{sim}},\ t_{\tau_{\mathrm{TTC}}^{\min}} + t_{\mathrm{sim}}\right]$ in MTFS, see Figure 7.5. Furthermore, the nanoscopic simulation ends either at $t_{\mathrm{end}} = 2t_{\mathrm{sim}}$ or at t_{imp} (the time of occurrence of the first collision). Finally, the participants' geometrical and physical properties are set in PC-Crash and X-RATE and the simulation of this concrete scenario is started.

7.1.2.1. Description of VISSIM output

Before a concrete scenario can be represented in nanoscopic simulation, the appropriate part of the MTFS result data has to be extracted and processed. The output of the MTFS tool VISSIM can be written, among other formats, in *fzp*- and *trj*-format. The *trj*-format is a binary format and is required by SSAM for further conflict analysis, while the text-based *fzp*-format can be read by X-RATE. Since reading large text-based files suffered from low performance, the *fzp*-data is stored after the first time it is loaded in the binary *mat*-format (*MATLAB* data file format) which can be loaded more efficiently by MATLAB. The *fzp*-file contains a header with general information on the simulation, as well as the main section with time step-based information for each simulated traffic participant. Each line after the header of the *fzp*-file contains information for one vehicle and one time step. The lines are sorted primarily by the time step and secondarily by the traffic participant index. The information that can be extracted from the *fzp*-file is required for setting up the individual concrete scenarios in nanoscopic simulation:

- Timestamp t_n of the current simulation time step
- Traffic participant index i
- Speed $v_i(t_n)$ at the end of the current time step in km/h
- Acceleration $a_i(t_n)$ during the current time step in $\mathrm{m/s^2}$
- Global coordinates $\vec{F}_i^G(t_n)$ of the front edge of the participant i at the end of the time step in meter
- Global coordinates $\vec{R}_i^G(t_n)$ of the rear edge of the participant at the end of the time step in meter
- Vehicle length l_i in meter
- Vehicle width w_i in meter

The coordinates of each participant's front and rear are used to compute the coordinates of the center of gravity of this participant: $\vec{X}_{\mathrm{COG},i}^G(t_n) = \vec{R}_i^G(t_n)/2 + \vec{F}_i^G(t_n)/2$. Fur-

thermore, the participants' current heading direction $\theta_i(t_n)$ is computed by $\theta_i(t_n) = atan2(X^{x,G}_{\text{COG},i}(t_n), X^{y,G}_{\text{COG},i}(t_n))$, where $atan2$ is the 2-argument-arctangent.

7.1.2.2. Determination of traffic participants to be simulated

In nanoscopic simulation of a concrete scenario, not all traffic participants need to be simulated that were present in MTFS in the road network during the conflict. There are two reasons that can make it necessary to simulate a traffic participant which is part of the surrounding traffic, i.e., a participant that is not a conflict participant. One reason is that a participant could become involved in a collision, in the case that one of the conflict participants triggers an emergency maneuver, and the other reason is when the participant poses a sight obstruction.

Based on the definition of the temporal scope I, the following steps are conducted in X-RATE to determine the list of traffic participants to be simulated:

1. Assemble a list of traffic participants P that were present in the road network during I. Data must be available for the full interval I for a traffic participant to be included in P. For each traffic participant that was present in the simulated road network during the temporal scope I, the time series data described in the previous subsection is extracted from the MTFS output.
2. Reduce this list P to P_{close} to include only those traffic participants that come within a certain range (denoted by the event horizon, H) to the conflict participants, such that the computation time in nanoscopic simulation is shortened by considering only the most relevant participants. For the parameter H, the value $H = 100\,\text{m}$ was chosen, since the highest range of any simulated sensor in this thesis was 100 m, which is considered suitable for urban traffic. The list P_{close} is computed by evaluating the following conditions for each time step $t_n \in I$ for each participant in P with participant index i:

$$d(\vec{X}^G_{\text{COG},i}(t_n), \vec{X}^G_{\text{COG},i_1}(t_n)) < H \qquad \text{or} \qquad d(\vec{X}^G_{\text{COG},i}(t_n), \vec{X}^G_{\text{COG},i_2}(t_n)) < H, \tag{7.1}$$

   where $d(\vec{X}^G_{\text{COG},i}(t_n), \vec{X}^G_{\text{COG},j}(t_n))$ is the distance between two participants' centers of gravity $\vec{X}^G_{\text{COG},i}$ and $\vec{X}^G_{\text{COG},j}$ with indices i and j at time t_n. The indices i_1 and i_2 refer to the two conflict participants (they correspond to $FirstVID$ and $SecondVID$ in the SSAM output, see Section 6.1.1). If one of the two conditions in Equation 7.1 evaluates true for a participant with index i at any time step t_n, the participant with index i is added to the list P_{close} since it comes within the event horizon H.
3. Apply further reduction of P_{close} to generate P_{crit}, which contains only traffic participants that have a collision course, i.e., fall below a certain threshold $\tau^{\text{Crit}}_{\text{TTC}}$ for $\tau_{\text{TTC,S}}$. If $\tau_{\text{TTC,S}}$ between a conflict participant and another traffic participant lies above the threshold of $\tau^{\text{Crit}}_{\text{TTC}} = 3\,\text{s}$, then the other participant was only simulated as sight obstruction by being placed kinematically (see Section 2.3.1.1) at the positions that were

simulated in MTFS, to save computation time. For all traffic participants in P_{crit}, the kinetic model (Section 2.3.1.2) is used with full simulation of driving dynamics. The value $\tau_{\text{TTC}}^{\text{Crit}} = 3\,\text{s}$ for filtering participants that might come into contact with the conflict participants represents a very conservative choice. To put this into perspective: Gettman, Pu, et al., 2008 used the limits 1.0 s to 1.5 s for $\tau_{\text{TTC,S}}$ to define a light conflict. For the τ_{TTC} calculation, the method employed by SSAM is used (i.e. $\tau_{\text{TTC,S}}$), which assumes that the current velocity of a traffic participant remains constant and projects its COG-positions forward along the already known path, see Section 6.1.1.

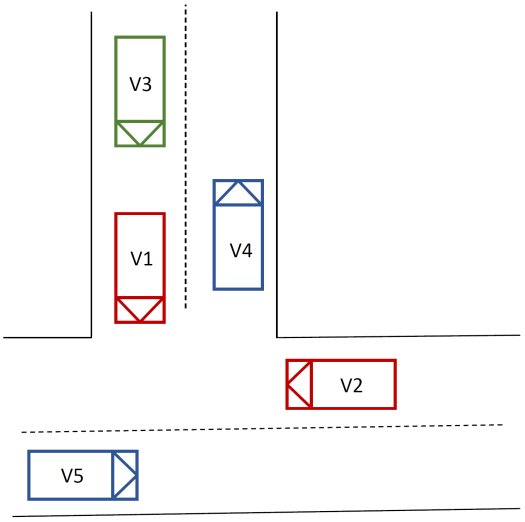

Figure 7.6.: V1 and V2 are the conflict participants (kinetic simulation). V3 (contained in P_{crit}, kinetic simulation) follows V1 and could come very close to V1 if V1 were to suddenly initiate a brake maneuver. V4 and V5 are contained in P_{close} and are considered only as sight obstructions (kinematic simulation).

In Chapter 9, a sensitivity study is conducted that investigates whether consideration of the traffic participants in P_{close} has an influence on the effectiveness metrics and whether the sensor in one of the conflict participants can detect the other conflict participant earlier, if the participants in P_{close} as sight obstructions are omitted from simulation.

7.1.2.3. Representation of traffic participants

In nanoscopic simulation, the traffic participants were approximated and represented geometrically by a mesh with triangular faces and the geometry of a box. In the MTFS model, each traffic participant was generated in VISSIM with a box-shaped geometry as well. Fifteen different combinations of values for length and width were manually pre-defined for the MTFS model to represent the most common types of passenger cars, vans and busses. When a new traffic participant is generated in MTFS, one of these combinations is selected randomly, according to its type, and used as the participant's dimensions. The dimensions l (length) and w (width) in nanoscopic simulation for passenger cars, vans, trucks and buses were defined equal to the dimensions of the corresponding vehicles in MTFS. Since height was not defined in the MTFS model, a representative value of 1.5 m was chosen for passenger

cars in nanoscopic simulation which is an average value for modern vehicles. For buses and trucks, a height of 3 m was used. The values were calculated using information from the websites www.automobiledimension.com and www.car.info. Pedestrians were simulated with dimensions $l/w/h = 0.44/0.6/1.8\,\mathrm{m}$ for length, width and height (average values for males in OECD countries, OECD, 2009), while the values $l/w/h = 1.73/0.64/1.8\,\mathrm{m}$ were used for cyclists (bicycle dimensions corresponding to a modern city bike, the height corresponds to the average male's height in OECD countries).

Using the volume $V = lwh$ of the box shape, the traffic participants' mass m (required for the calculation of Δv in the collision model, see Section 7.1.5.2) was calculated by $m = \rho V$ with the following values for the density ρ:

- Passenger cars: $\rho_{car} = 115\,\mathrm{kg/m^3}$
- Buses, trucks: $\rho_{bus,\,truck} = 175\,\mathrm{kg/m^3}$

These values were calculated as average values based on several common vehicle models, using information from the websites www.automobiledimension.com and www.car.info. Furthermore, the collision model required appropriate values for the moments of inertia I_{xx}, I_{yy} and I_{zz}, for which the calculation formulas suggested by PC-Crash (Moser, 2020 and Burg and Moser, 2017) were used. I.e., the moment of inertia in the vertical axis I_{zz} was calculated by $I_{zz} = 0.127\,mBl$ for passenger cars, where B refers to the wheelbase (the distance between the front and rear axle). For buses and trucks, PC-Crash calculates the moment of inertia by $I_{zz} = m(l^2 + w^2)/12$ (Burg and Moser, 2017). Based on I_{zz}, the other moments of inertia were calculated: $I_{yy} = I_{zz}$ and $I_{xx} = 0.3 I_{zz}$ (Burg and Moser, 2017).

7.1.3. Sensor model

At the start of the simulation of the scenario catalog, several mesh models need to be loaded into MATLAB to represent the geometry of the three dimensional static objects that should be considered by the sensor model. The static objects of the scenery (houses and parking cars, see Section 7.1.7) are defined in a separate file in the *xml*-format that stores nodal mesh coordinates in a local mesh coordinate system, a nodal connectivity list that describes the triangulation of the mesh, the position, orientation and scaling of static objects. Using the positions and orientations in space of non-moving objects such as buildings, the nodal mesh coordinates can be transformed for each object to the reference coordinate system (global coordinate system, see Appendix C.1.

At the start of the simulation of each individual concrete scenario, the mesh models that represent the box-shaped geometry of the traffic participants need to be loaded into the MATLAB memory. They are stored in the *xml*-format in the form of nodal coordinate lists in the local vehicle coordinate system and lists of triangular faces, which are composed of three node indices each.

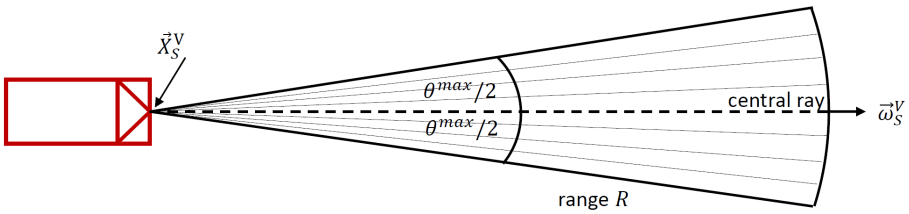

Figure 7.7.: Top view of the sensor field of view with a forward facing sensor. The opening angle θ^{max} extends by $\theta^{max}/2$ in spherical coordinates to the left and right of the central vision ray, of which the direction is given by the sensor orientation $\vec{\omega}^S$.

In the following subsections, the parameters describing the sensor model are explained, while more details on the calculation can be found in Appendix C. Then, a description how the model determines the visibility of traffic participants is provided.

The sensor model is applied at every time step of the nanoscopic simulation.

7.1.3.1. Description of the sensor model

With the chosen approach, "vision rays" are cast into the three dimensional virtual surrounding of the vehicle, based on a rasterization of the field of view in spherical coordinates, to calculate intersections of vision rays with static objects from the scenery or traffic participants. The field of view has the shape of a circle sector (see Figure 7.7). Each vision rays lies on the same plane, located in three dimensional space. This allows a simple determination which of the objects is visible to a vision ray, by searching for the closest intersection point for each vision ray.

The field of view of each sensor is characterized geometrically through the following few parameters:

Sensor position ($\vec{X}_S^V$): The position of the sensor S installed on the vehicle is denoted by $\vec{X}_S^V$ and is specified in the vehicle coordinate system. It is the origin of the sensor coordinate system. For the exemplary study defined in the solution approach, in each vehicle that is equipped with a safety system in nanoscopic simulation, a singular sensor is placed directly in the middle of the front of the vehicle, in a height of 0.5 m above the ground.

Sensor orientation ($\vec{\omega}_S^V$): The angles that represent the rotation of the central sensor ray are defined relative to the vehicle coordinate system. They are given in Euler angles in the zyx-convention (see Lengyel, 2012). The orientation is chosen to be $\vec{\omega}_S^V = (0, 0, 0)$, such that the sensor faces forward in the same direction as the vehicle. Since the sensor is fixed on the vehicle, the field of view is rotated when the vehicle is rotated.

Horizontal opening angle ($\theta^{\max}$): Describes the extent of the sensor field of view, which extends by $\theta_{\max}/2$ to the left and right of the central ray, see Figure 7.7. In this thesis

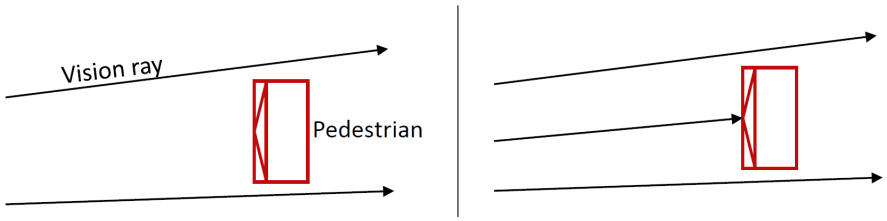

Figure 7.8.: Left: the pedestrian is missed by the sensor vision rays due to a too low value for N^h_{rays}. Right: N^h_{rays} was chosen sufficiently high. At least one vision ray hits the pedestrian, even though the position of the pedestrian relative to the detecting vehicle is the same as in the left image.

work, no vertical opening angle is considered, i.e., with the consequence that all sensor rays lie within one plane.

Range (R): Describes how far each "vision ray" extends at most from the sensor origin. In spherical coordinates, this corresponds to the radius. The range R is constant over the whole range of angles that are covered by the sensor field of view (see Figure 7.7). The range R and horizontal opening angle $\theta^{\max}$ are two of the most influential factors for the capability of a sensor to see objects. They are the major parameters that define the field of view. For the exemplary study defined in the solution approach, the values $R = 100\,\text{m}$ and $\theta^{\max} = 180^\circ$ were chosen, as was also done in Sander and Lubbe, 2018, offering a large field of view that represents high performing sensors.

Horizontal resolution (N^h_{rays}): The number of rays that cover the horizontal opening angle $\theta^{\max}$ is denoted by N^h_{rays}. A uniform spacing of vision rays in angular coordinates is assumed. With the choice $N^h_{\text{rays}} = 2\theta^{\max}$ for the horizontal resolution and $\theta^{\max} = 180^\circ$, a distance of

$$2\pi R \frac{\theta^{\max}}{360} \frac{1}{N^h_{\text{rays}}} = 0.87\,\text{m}$$

was covered between sensor vision rays in the maximum available range of 100 m. The simulated pedestrians were 0.44 m wide in their shortest dimension, which means that they could theoretically be missed by the sensor in certain circumstances, even if they are in the sensor field of view and their visibility is not obstructed by other objects (see Figure 7.8). However, at a distance of approximately 50 m between pedestrian and vehicle, the distance between vision rays becomes lower than the shortest dimension of the pedestrian, i.e., at least one ray is guaranteed to hit the pedestrian if his visibility is not obstructed and if the pedestrian is located within the field of view of the sensor. A vehicle traveling with a velocity of 50 km/h (which is the maximum allowed velocity in the urban traffic site simulated in the MTFS model) in a distance of 50 m towards a pedestrian is still $\tau_{\text{TTC}} = 3.6\,\text{s}$ away from a collision, which is still early enough to trigger active safety measures. Since vehicles are much larger and since they are the primary concern in the thesis, the chosen resolution N^h_{rays} was regarded to be fully sufficient.

7.1.3.2. Detection of traffic participants

Figure 7.9 shows several different variations to which degree a traffic participant can be visible to a sensor: the view on vehicle 1 is fully blocked by a static object or another traffic participant (in the example of Figure 7.9, the view is blocked by a wall). If a vision ray hits an object or traffic participant, it is not followed further such that objects or traffic participants farther away cannot be seen by that ray. Vehicle 2 is hit by at least one ray. Vehicle 3 is fully visible, while vehicle 4 is on the edge of the sensor's field of view. In this case, the opening angle of the sensor is not sufficient to fully include the object. Vehicle 5 is further away from the sensor than the range R, thus not detectable to the sensor.

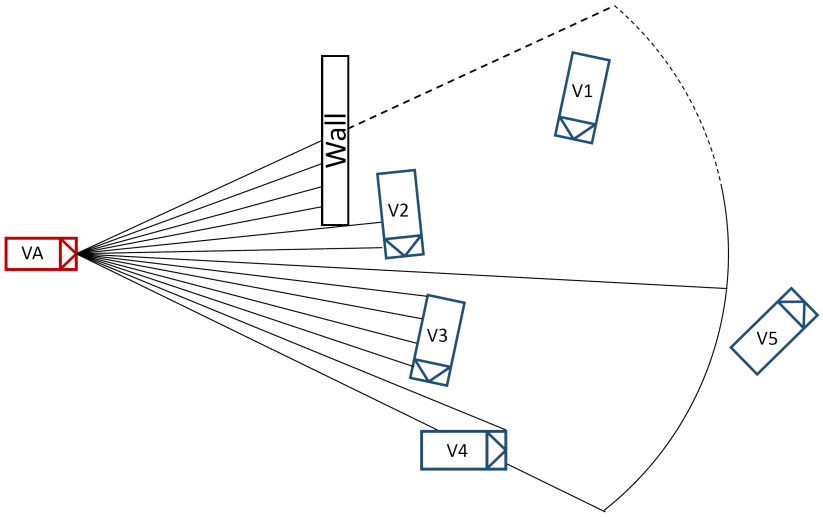

Figure 7.9.: Different degrees of visibility of traffic participants to a sensor. The sensor in vehicle VA cannot see $V1$, because the view is blocked. $V2$ is partially hidden. $V3$ is fully visible. $V4$ is partially inside the field of view. $V5$ is outside the field of view.

The sensor algorithm differentiates between two different states: *detection* and *classification*. Such a distinction is also made in an exemplary effectiveness study in Wimmer, Düring, et al., 2019, where state-of-the-art active safety simulation toolboxes, including X-RATE, are compared. When at least one vision ray hits a traffic participant, it is considered *detected* (e.g., $V2$ in Figure 7.9). For *classification*, a traffic participant must be detected and fully in view, i.e., it must lie within the opening angle and range R. Furthermore, it was assumed that there existed a delay (the acquisition time t_{acq}) between the point in time when a traffic participant is first detected until the point in time when the sensor actually registered this object as classified, i.e., until the safety system is allowed to react to the traffic participant. A value of $t_{\text{acq}} = 0.2\,\text{s}$ was chosen for the acquisition time in accordance to Wimmer, Düring, et al., 2019, where this time span is denoted by the term classification delay. In the study Wimmer, Düring, et al., 2019, $t_{\text{acq}} = 0.2\,\text{s}$ was assumed without conducting validation to real systems. However, the introduction of the acquisition time was necessary since the above described sensor model cannot determine which proportion of the traffic participant is visible, i.e., statements such as "50 % of the traffic participant are visible" are not possible. Furthermore, it is unlikely that real systems can immediately react to a threat at the first

moment when a part of the threat first becomes visible. However, within 0.2 s, a vehicle traveling at 50 km/h moves around 2.7 m. If a vehicle with 5 m length was previously hidden from the sensor's view, more than 50 % of that vehicle could then be visible. Since no references other than Wimmer, Düring, et al., 2019 could be found in the literature regarding the time required by different sensors or the proportion of traffic participants that must be visible to reach classification, 0.2 s (or more than 50 % visibility for a 5 m vehicle traveling at 50 km/h), $t_{\mathrm{acq}} = 0.2\,\mathrm{s}$ is assumed to be reasonable. For real systems, this parameter will on depend several details in the implementation of the detection algorithms and the hardware capabilities.

7.1.4. Strategy model

In this thesis, for the purpose of comparison of effectiveness results, two system configurations are defined. Each configuration leads to one treatment, where both conflict participants are equipped with an active safety system with the same system configuration.

For both system configurations, a safety zone d_{SZ} is considered. The safety zone is based on the concept in the studies Sander, 2017 and Sander and Lubbe, 2018. The detecting vehicle's geometry is virtually enlarged by a fixed distance (Sander, 2017 uses $d_{\mathrm{SZ}} = 0.2\,\mathrm{m}$) in direction normal to each vehicle side (i.e., front, back and sides). This ensures that the system also predicts the presence of a collision course if traffic participants pass each other very closely, when a collision course would not be detected without the safety zone. Furthermore, $d_{\mathrm{SZ}} = 0.2\,\mathrm{m}$ accounts for possible inaccuracies introduced by the simulation step, i.e., for the maximum distance that is traveled within one simulation time step, since a vehicle moving with 13.8 m/s (50 km/h) in urban traffic can change its position by a maximum of around 0.2 m within the minimum simulation step $\Delta t = 15\,\mathrm{ms}$, based on the restriction by PC-Crash (Moser, 2020).

The following subsections justify and explain how the safety systems were configured.

7.1.4.1. System configuration and trigger condition

The task of the strategy model is to use the information on the scenery and other traffic participants provided by the sensors to determine whether a collision is imminent or not, and if the time window to avoid this collision becomes too narrow for the driver to react properly, an emergency maneuver must be initiated. Basically, an emergency maneuver can consist of one of the following maneuvers, or a combination thereof: braking, accelerating and lateral avoidance by steering. Since the execution of steering and (positive) acceleration maneuvers by safety systems is not considered in this thesis, the strategy is defined in such a way that an emergency braking maneuver is triggered when lateral evasion by the driver can be excluded and if a collision is imminent.

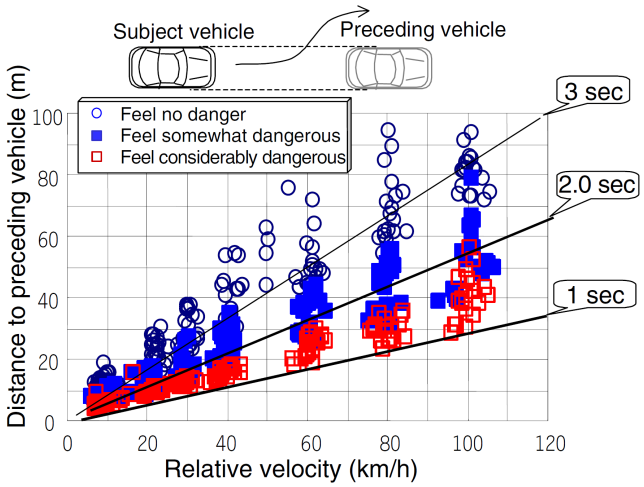

Figure 7.10.: Measurements for relative velocity and distance at the moment of lateral evasion maneuver initiation in a driving simulator study, and a rating of how the test subjects felt about their maneuver. The lines represent various levels of τ_{TTC} at the time of maneuver initiation. Image taken from Kodaka et al., 2003.

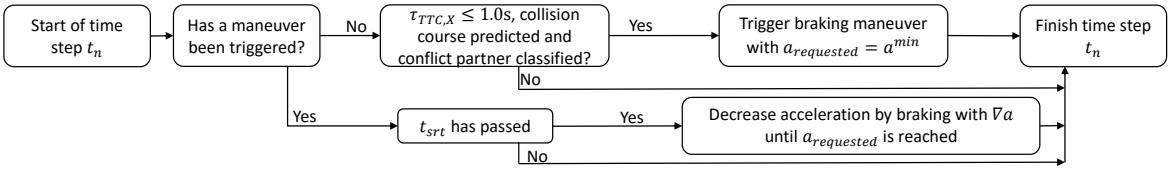

Figure 7.11.: Decision graph of the emergency strategy of system configuration 1. As soon as a collision course is detected and $\tau_{\mathrm{TTC,X}}$ falls below 1.0 s, the system initiates a full brake maneuver. ∇a denotes the brake gradient, expressing the decrease of acceleration per second.

As a guideline to define an appropriate moment to trigger emergency braking maneuvers, the results in the driving simulator study by Kodaka et al., 2003 are used. As can be seen in Figure 7.10, no driver initiated a lateral evasion maneuver below the limit of $\tau_{\mathrm{TTC}} = 1.0\,\mathrm{s}$, while the limit between "feel somewhat dangerous" and "feel considerably dangerous" lay around 1.5 s to 2.0 s. Kodaka et al., 2003 also found that drivers would conduct lateral maneuvers in the category "feel considerably dangerous" extremely rarely in daily traffic. Hence, $\tau_{\mathrm{TTC}}^{\mathrm{Trig}} = 1.0\,\mathrm{s}$ as the latest possible moment when drivers would start a lateral evasion is used to define the first system configuration (system configuration 1), and it is appropriate to request the full available brake force at this point, i.e., $a_{\mathrm{requested}} = a^{\mathrm{min}}$ (Winner, 2015a). After triggering the brake command, the system response time (t_{srt}) has to pass, which is the time needed from fulfillment of the trigger condition until the brakes start building up brake force. The value $t_{\mathrm{srt}} = 0.2\,\mathrm{s}$ is used in accordance with Wimmer, Düring, et al., 2019. This parameter is used to account for the time that various subsystems of real systems require to execute the commands given by the decision algorithm. The strategy of system configuration 1 is visualized in Figure 7.11. The algorithm used to calculate $\tau_{\mathrm{TTC,X}}$ in nanoscopic simulation is explained in Appendix D.1.

Junietz, 2019 provides a comprehensive review of safety surrogate measures other than τ_{TTC}.

Examples of further safety surrogate measures applicable in longitudinally acting systems (e.g., braking systems) include extensions of τ_{TTC} (e.g., by involving possible deceleration maneuvers in the calculation), the required deceleration to avoid an accident (Karlsson et al., 2004) or the Brake Threat Number BTN (Brannstrom et al., 2008). Early AEB systems equipped in passenger cars operate based on τ_{TTC} thresholds. More modern systems may use extensions of τ_{TTC}, the required deceleration or other more advanced safety surrogate measure which also incorporate the difficulty with which an accident can be avoided (Junietz, 2019). Therefore, instead of braking with the full brake force at the earliest moment when lateral evasion by the driver can safely be excluded, a less severe strategy is followed for system configuration 2, where the braking maneuver is initiated earlier, but only with as much brake acceleration as is required to avoid the collision. This acceleration value is denoted in the following by $a_{required}$, and a version of $a_{required}$ that is adjusted for the system response time t_{srt} is denoted by $a^{adj}_{required}$. The algorithms for the calculation of $a_{required}$ and $a^{adj}_{required}$ are explained in Appendix D.3. When initiating a system intervention earlier than with system configuration 1, the strategy must consider that the driver might already be braking or evading laterally. As a way to consider possible braking before system activation, e.g., when following another vehicle in a rear-end situation, a modification of $\tau_{TTC,X}$ is used, namely the Enhanced Time-to-Collision (ETTC), see Winner, 2015a, denoted in the following by $\tau_{ETTC,X}$. If the acceleration is non-zero and stays constant, $\tau_{ETTC,X}$ decreases linearly with the decrease of the actual time that is left before a collision occurs, unlike $\tau_{TTC,X}$, which would decrease non-linearly with the passage of time, see Figure 7.12. Next to this

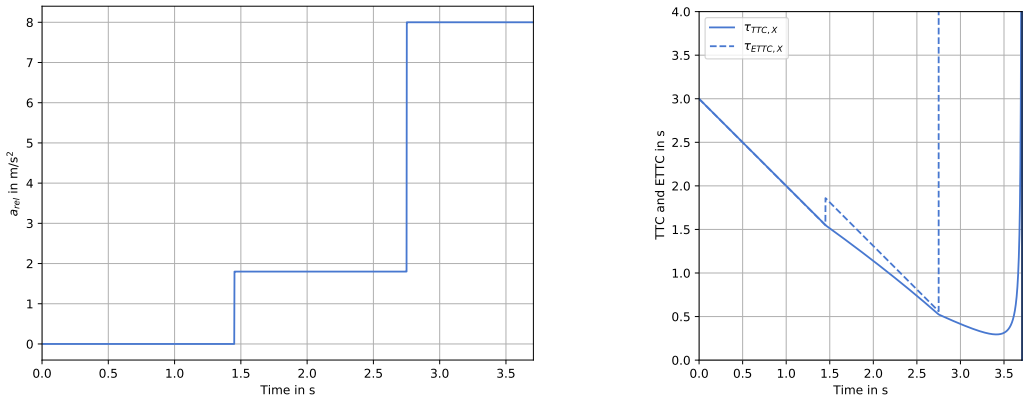

Figure 7.12.: Left: relative acceleration a_{rel} in an exemplary rear-end conflict. The driver first brakes insufficiently to avoid a collision, then starts a full brake maneuver. Right: corresponding values for $\tau_{TTC,X}$ and $\tau_{ETTC,X}$. Once the collision is avoided by sufficient braking, $\tau_{ETTC,X}$ does not exist.

advantage, $\tau_{ETTC,X}$ seems to be a better predictor than $\tau_{TTC,X}$ for the moment when human drivers start braking maneuvers, as was investigated by Chen et al., 2016, who compared $\tau_{TTC,X}$ and $\tau_{ETTC,X}$ values for braking maneuvers in NDS data and found a lower variation of $\tau_{ETTC,X}$ values for given velocities. For this system configuration, the threshold $\tau^{Trig}_{ETTC} = 1.5\,s$ is used, as this value still lies within the category "feel considerably dangerous" identified in Kodaka et al., 2003 but is closer to "feel somewhat dangerous", see Figure 7.10.

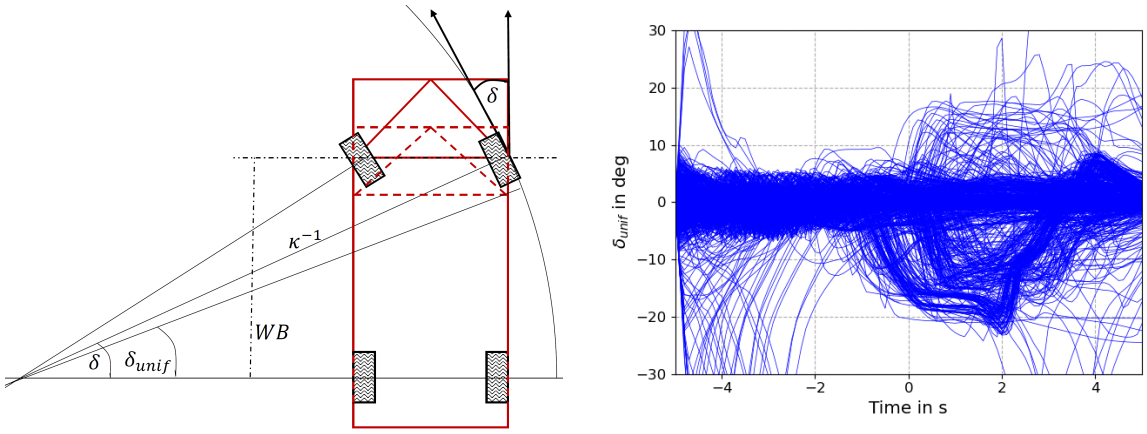

Figure 7.13.: Left: the steering angle δ of the outer front wheel is transformed to the curvature κ and then transformed back to the unified steering angle δ_{unif} of an exemplary vehicle (dashed red vehicle contour), driving a trajectory with the same curvature. Right: δ_{unif} for all conflicts simulated in nanoscopic simulation.

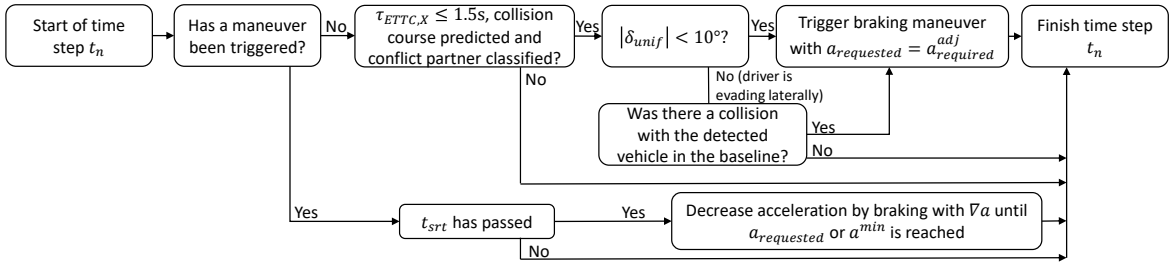

Figure 7.14.: Decision graph of the emergency strategy of system configuration 2. As soon as a collision course is detected, if $\tau_{\text{ETTC,X}}$ falls below 1.5 s and if the driver is not attempting lateral evasion, the system decreases the acceleration down to $a_{\text{requested}} = a_{\text{required}}$. ∇a denotes the brake gradient, expressing the decrease of acceleration per second.

Furthermore, the second system is configured in such a way that no braking maneuver is initiated if the driver already attempts lateral evasion. To identify such evasion attempts, the steering angle δ of the vehicle's outer front wheel is considered. However, since the vehicles simulated in nanoscopic simulation were of different length, and had a different wheelbase WB (distance between the front and rear axle), the steering angle δ is transformed to the curvature κ of the current driving trajectory by $\kappa = \sin(\delta)/WB$ (Figure 7.13, left) and then transformed back to the unified steering angle δ_{unif} of an exemplary vehicle with a unified wheelbase $WB_{\text{unif}} = 3.5\,\text{m}$ by $\delta_{\text{unif}} = \arcsin(\kappa WB_{\text{unif}})$. As a limit for $|\delta_{\text{unif}}|$ to identify lateral evasion attempts, the value 10° is used, as this represents a threshold that is surpassed in the most common evasion maneuvers, see Figure 7.13 (right). Furthermore, knowledge from the baseline is used to determine whether a collision occurred despite a lateral maneuver with δ_{unif} above 10°. Therefore, if the primary trigger condition is fulfilled ($\tau_{\text{ETTC,X}} \leq 1.5\,\text{s}$), an emergency maneuver is triggered if $|\delta_{\text{unif}}| < 10°$ or if there was a collision in the baseline. The strategy of system configuration 2 is visualized in Figure 7.14. The algorithm used to calculate $\tau_{\text{ETTC,X}}$ in nanoscopic simulation is explained in Appendix D.2.

For both system configurations, after t_{srt} has passed, the system checks whether the ac-

celeration a_{driver} due to braking or acceleration commands by the driver is higher than $a_{\text{requested}}$. If this is the case, then the current acceleration is reduced by the brake system until either the minimum possible brake acceleration (a^{min}) or $a_{\text{requested}}$ are reached. Otherwise, no action needs to be taken at this time step as the driver is already braking with a lower acceleration.

The MTFS models WBE and WBE50 were validated to traffic metrics observed in dry road conditions with sunny weather. Therefore, according to G. Müller and S. Müller, 2015 and Warner et al., 1983, under such conditions, a coefficient of friction of $\mu = 0.815$ can be assumed, leading to $a^{\text{min}} = -\mu g = -8\,\text{m/s}^2$ for the minimum brake acceleration, where $g \approx 9.81\,\text{m/s}^2$ is the standard acceleration of gravity. For simplicity, a linear decrease of brake acceleration is assumed. Such a linear decrease is also used in Wimmer, Düring, et al., 2019.

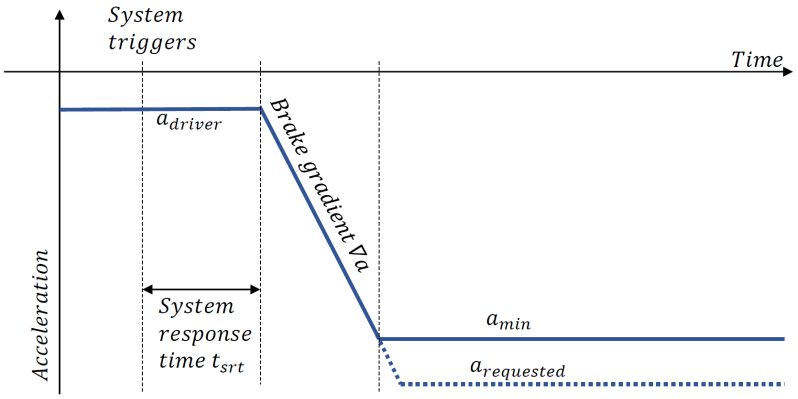

Figure 7.15.: Braking maneuver. A linear decrease of the acceleration is assumed. Before the maneuver is initiated by the safety system, the driver might have already been braking (i.e., $a_{\text{driver}} \neq 0$). The safety system requests an acceleration $a_{\text{requested}}$ and achieves a minimum possible acceleration a^{min}, based on road friction conditions.

The amount by which the acceleration can be reduced per time interval is expressed by the brake gradient (∇a). Burg and Moser, 2017 present a list of typical values for the time from brake start until the full brake force on dry road conditions is reached for several types of vehicles. For passenger cars, the build-up time ranges between 0.2 s and 0.4 s. Therefore, a value of 0.2 s was assumed. This time span is used to compute the constant brake gradient assumed for all active safety systems in nanoscopic simulation: $\nabla a = \frac{a^{\text{min}}}{0.2\,\text{s}} = \frac{-8\,\text{m/s}^2}{0.2\,\text{s}} = -40\,\text{m/s}^3$. The course of the acceleration over time during an emergency brake maneuver is shown in Figure 7.15.

Once a braking maneuver has been triggered, the vehicle continues to brake to a full stop, without re-evaluating the concrete scenario, until a termination criterion has been reached for the simulation of this concrete scenario, i.e., either a collision occurs or the maximum simulation time has been reached.

7.1.5. Collision model

For the collision model parameters, values are specified at the beginning of the simulation of the scenario catalog within the tools used in this thesis work. The parameters do not depend on the collision configuration or the collision partners.

7.1.5.1. Collision detection

The algorithm responsible for collision detection uses the polygon intersection routine by the Hodgman and Sutherland algorithm (Sutherland and Hodgman, 1974). At each time step during the simulation, the algorithm first performs a preliminary low-cost (in terms of computation times) calculation to determine whether a collision is possible, by checking whether the distances of the centers of gravity to each other are in their sum smaller than the sum of the largest dimension of each vehicle. If a collision cannot be excluded by the preliminary checks, two dimensional vehicle polygons are calculated as projections of the three dimensional vehicles to the horizontal plane. This is done by considering only the bottom rectangle of the box-shaped geometries by which traffic participants are represented and neglecting the vertical coordinate of the vertices. The Hodgman and Sutherland algorithm is then applied to determine whether an overlap of the polygons exists and to find its shape.

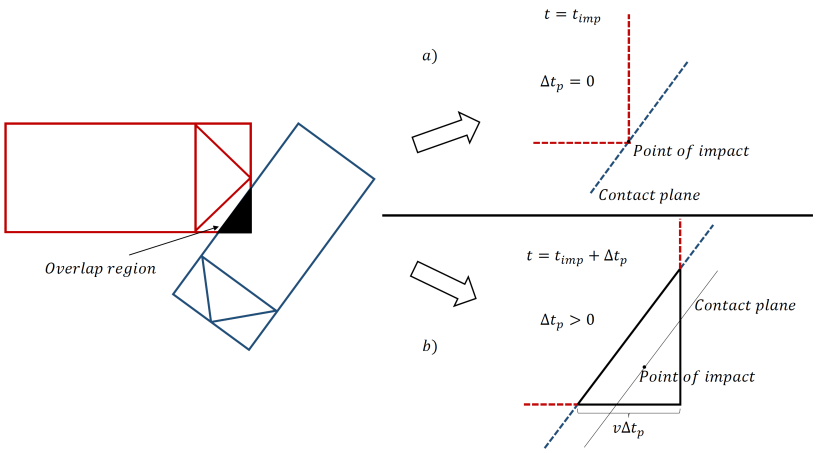

Figure 7.16.: Collision detection. If the penetration depth Δt_p is set to 0 (Figure a), there will be no overlap between vehicle polygons, otherwise they continue to travel for a short amount of time (Figure b), in which case the red vehicle penetrates the blue vehicle's geometry for a distance of $v\Delta t_p$, where v is the red vehicle's velocity at time of first impact t_{imp}.

Collision detection for the momentum-based impact model (see Section 7.1.5.2) is influenced by the parameter Δt_p (*penetration depth*), which is defined as the time interval after first contact, for which the vehicles continue to travel in their path of motion, before the collision is regarded detected. If $\Delta t_p = 0$ is chosen for the collision model, the collision is detected at the moment of first contact, i.e., a minimal part of the geometry is contacting, see a) in Figure 7.16. An investigation on suitable choices for Δt_p can be found in the blogpost The

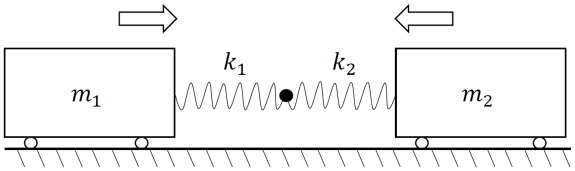

Figure 7.17.: Simple one dimensional harmonic oscillator model used in The Virtual CRASH Team, 2017 for the derivation of Δt_p. Two blocks with m_1 and m_2 collide and are dampened by two springs with stiffness k_1 and k_2.

Virtual CRASH Team, 2017. Through a simple one dimensional harmonic oscillator model (see Figure 7.17), they derived an estimate

$$\Delta t_p = \sqrt{\frac{\frac{k_1 k_2}{k_1+k_2}}{\frac{m_1 m_2}{m_1+m_2}}} \tag{7.2}$$

for the penetration depth, where m_1 and m_2 are the masses of two colliding solid blocks which are dampened by two springs with stiffness values k_1 and k_2. In The Virtual CRASH Team, 2017, they then generalize the model to two dimensions, assume vehicle mass, length and width distributions to represent typical properties of modern vehicles and conduct a Monte Carlo simulation for different collision configurations (rear-end collision, side impact, two vehicles moving in opposing directions and colliding frontally). The most frequently occurring value for Δt_p was around 0.03 s. Therefore, in this thesis work, $\Delta t_p = 0.03\,\mathrm{s}$ is used as an approximation and replacement for a detailed calculation of the deformations of the vehicles that occur during a collision.

7.1.5.2. Collision mechanics

For the calculation of collisions, a model based on momentum conservation equations is used. This model is described in more detail in Appendix E and is based on the works by Kudlich, 1966 and Slibar, 1966. The input parameters for this collision model are the positions $\vec{X}_{\mathrm{COG},i}$ and orientations $\vec{\omega}_{V,i}$ of the colliding traffic participants, the velocity directions $\vec{v}_{\mathrm{COG},i}$ of their centers of gravity, their angular velocities $\vec{\gamma}_i$, their masses m_i and their moments of inertia $I_{xx,i}$, $I_{yy,i}$ and $I_{zz,i}$ about their respective axis, with $i \in \{1, 2\}$ being the colliding traffic participants' indices. Furthermore, the impact model specific parameters inter-vehicle friction μ_{IV}, coefficient of restitution ϵ, point of impact POI and the orientation of the contact plane are required.

For the definition of the POI, the geometrical rule from Kolk, Sinz, et al., 2016 is used which uses the center of gravity of the area for which the traffic participant polygons overlap (see Figure 7.16) as the POI. The inter-vehicle friction μ_{IV} is a parameter that strongly influences whether a collision is a sliding collision or a locked collision (see Kolk, Sinz, et al., 2016). Marine, 2007 discusses the consequences of parameter choices and concludes that the inter-vehicle friction is a parameter for which it is very difficult to find a general rule.

Funk et al., 2004 have conducted practical testing for low-speed crashes (below 10 km/h) and came up with approximate values of 0.4 to 0.5 for the inter-vehicle friction μ_{IV}, which, however, does not allow conclusions for crashes at higher speeds. The value 0.5 is used in this thesis for all crashes. The coefficient of restitution ϵ was assumed to have a low value of $\epsilon = 0.115$, which was identified by Cannon, 2001 to be appropriate for collisions where the crash impulse direction is close to parallel to the longitudinal axis of vehicles. This is the case for rear-end and frontal crashes. As was discussed in the conflict analysis in Section 6.2, the majority of conflicts (around 90 %) were of rear-end type, justifying the choice $\epsilon = 0.115$. This choice was used for all collision configurations.

The outputs of the impact model described in detail in Appendix E are the post-crash velocity $\vec{v}^{\,p}_{\mathrm{COG},i}$ and post-crash angular velocity $\vec{\gamma}^{\,p}_i$ (superscript p for "post-crash"). Based on $\vec{v}^{\,p}_{\mathrm{COG},i}$, the collision induced velocity change

$$\Delta v_i = \sqrt{(v^x_{\mathrm{COG},i} - v^{p,x}_{\mathrm{COG},i})^2 + (v^y_{\mathrm{COG},i} - v^{p,y}_{\mathrm{COG},i})^2 + (v^z_{\mathrm{COG},i} - v^{p,z}_{\mathrm{COG},i})^2}$$

is computed.

7.1.6. Kinetic path driver model

The trajectories of traffic participants (positions of the centers of gravity over time) driven in MTFS were generated without the consideration of driving dynamics. Therefore, to recreate a conflict from MTFS in nanoscopic simulation, a kinetic path driver model needs to be applied to translate the trajectories (in the following referred to as paths) into actual steering commands for each simulation time step.

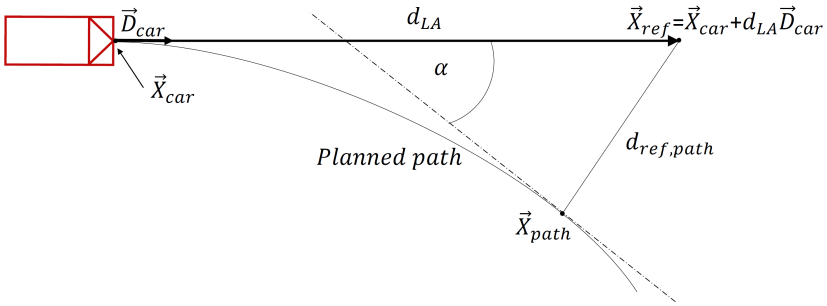

Figure 7.18.: Based on the anchor point $\vec{X}_{\mathrm{ref}}$, a look-ahead distance d_{LA} and the vehicle's heading direction $\vec{D}_{\mathrm{car}}$, a reference point $\vec{X}_{\mathrm{ref}}$ is defined and is projected onto the planned path to get $\vec{X}_{\mathrm{path}}$. The angle α and distance $d_{\mathrm{ref,\,path}}$ are used as inputs for the kinetic path driver model.

In the kinetic path driver model that is used for nanoscopic simulation and is implemented in PC-Crash (Moser, 2020), a look-ahead time t_{LA} is defined, leading to a look-ahead distance $d_{\mathrm{LA}} = t_{\mathrm{LA}} v$ (with v being the current velocity). Directly before the vehicle's anchor point $\vec{X}_{\mathrm{car}}$, in distance d_{LA}, the reference point $\vec{X}_{\mathrm{ref}}$ is defined (see Figure 7.18), i.e., $\vec{X}_{\mathrm{ref}} = \vec{X}_{\mathrm{car}} + d_{\mathrm{LA}}\vec{D}_{\mathrm{car}}$, where $\vec{D}_{\mathrm{car}}$ denotes the vehicle's heading direction. The point $\vec{X}_{\mathrm{path}}$ is defined as the point

on the planned path closest to $\vec{X}_{\text{ref}}$. Based on α and the distance between $\vec{X}_{\text{ref}}$ and $\vec{X}_{\text{path}}$, the kinetic path driver model then decides according to defined rules how to choose the steering angle δ_{steer}, such that the vehicle's anchor point $\vec{X}_{\text{car}}$ comes as close as possible to the path. The functional basis of the kinetic path driver model (shown in Figure 7.18) is based on Kondo, 1953; Kondo and Ajimine, 1968. Further kinetic path driver models can be found in Plöchl and Edelmann, 2007. In this thesis work, the kinetic path driver model is limited such that $|\delta_{\text{steer}}| \leq \delta_{\text{steer}}^{\max}$, where $\delta_{\text{steer}}^{\max}$ is the mechanical limit how far the outside front wheel can be turned at most. Furthermore, the rate of change $\dot{\delta}_{\text{steer}}$ of the steering angle δ_{steer} is limited by a maximum steering velocity $\dot{\delta}_{\text{steer}}^{\max}$, representing the drivers' and the vehicles' limits to change the steering angle: $\left|\dot{\delta}_{\text{steer}}\right| \leq \dot{\delta}_{\text{steer}}^{\max}$. For this thesis, the values $\delta_{\text{steer}}^{\max} = 30\,\text{deg}$ and $\dot{\delta}_{\text{steer}}^{\max} = 90\,\text{deg/s}$ are used for passenger cars, vans and buses. The value $\delta_{\text{steer}}^{\max} = 30\,\text{deg}$ represents a typical value for modern passenger cars. It was computed based on data from www.automobiledimension.com and www.car.info for several vehicles through a one-track model, i.e., as an average of the values $\delta_{\text{steer}}^{\max} = \arcsin\left(\kappa^{\max} WB\right)$, where WB is the wheelbase and $\kappa^{\max}$ the curvature (i.e., the inverse of the radius) of the vehicle's turning circle. The same was done analogously to verify the value $\delta_{\text{steer}}^{\max} = 30\,\text{deg}$ for larger vehicles such as buses, by using data for the Citaro buses by Mercedes Benz (see mercedes-benz-bus.com). The value $\dot{\delta}_{\text{steer}}^{\max} = 90\,\text{deg/s}$ corresponds to the highest steering wheel velocity (assuming a steering ratio of 15:1) found in Breuer, 1998, where 841 "Moose-Tests" were evaluated, which is a test conducted to study vehicle and driver behavior in extreme evasion maneuvers.

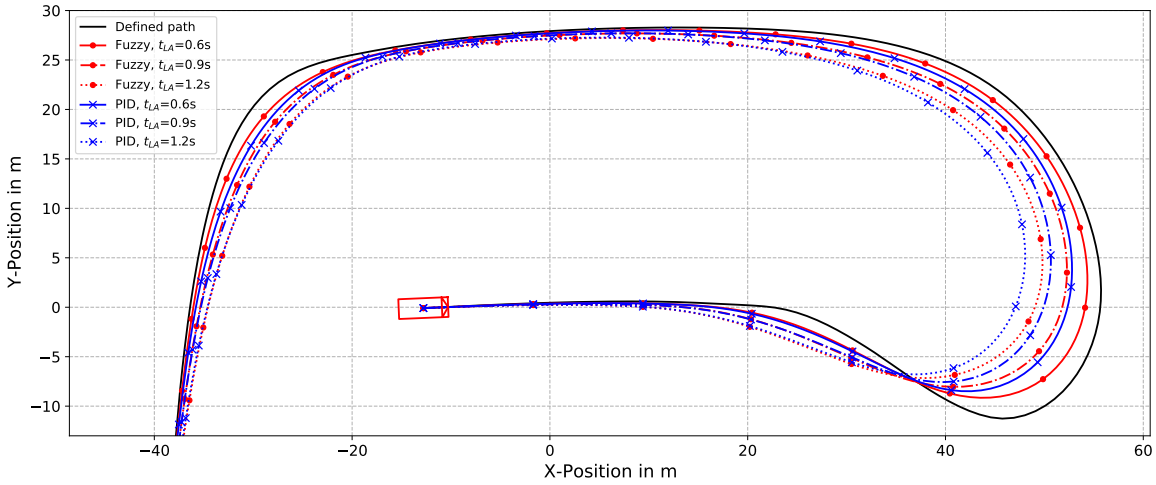

Figure 7.19.: Comparison of the settings $t_{\text{LA}} \in \{0.6\,\text{s}, 0.9\,\text{s}, 1.2\,\text{s}\}$ for the fuzzy and the PID kinetic path driver models offered by PC-Crash. The solid black line without markers is the defined path, which is not necessarily physically drive-able, while the other lines represent simulated trajectories of the center of gravity of the vehicle.

PC-Crash offers one kinetic path driver model which is based on a PID-controller, and one which is based on a fuzzy logic (Moser, 2020). In Figure 7.19, various simulated trajectories for different kinetic path driver models (fuzzy and PID-controller) and settings for t_{LA} are compared to the defined path. In this figure, the fuzzy model shows the best overall agreement with the follow path for a look-ahead distance of 0.6 s, and showed

very stable steering behavior. Therefore, for the exemplary effectiveness study, the fuzzy model was used for the simulation of conflicts with the setting $t_{\mathrm{LA}} = 0.6\,\mathrm{s}$. The effect on the effectiveness metrics of choosing the settings $t_{\mathrm{LA}} = 0.9\,\mathrm{s}$ and $t_{\mathrm{LA}} = 1.2\,\mathrm{s}$ with the fuzzy model in comparison to $t_{\mathrm{LA}} = 0.6\,\mathrm{s}$ is investigated in a sensitivity study in Section 9.4. In general, longer look-ahead distances led to cutting of corners, while a lower look-ahead distance resulted in closer following of the path, but in some cases, e.g., with $t_{\mathrm{LA}} = 0.4\,\mathrm{s}$, the side effect of traffic participants oscillating right and left to the path could be observed, because the resulting steering maneuvers were too violent. Furthermore, the best agreement with paths is achieved when the anchor point is set to the middle of the vehicle front and when the positions of the vehicle front $\vec{F}_i^G(t_n)$ are defined as the paths, instead of $\vec{X}_{\mathrm{COG},i}$. The result is that the kinetic path driver model tries to steer in such a way that the vehicle front comes as close as possible to the path.

7.1.7. The scenery model

The scenery was represented in this thesis in nanoscopic simulation by the following components:

Static objects as sight obstructions: In the case of the present thesis, the considered static objects include buildings and parking cars (it was assumed that 100 % of all parking spots were occupied) wherever they were able to limit the visibility of other traffic participants, i.e., particularly at intersections. Since they are only relevant for the consideration of sight obstruction, static objects were represented in as little detail as possible, e.g., by quadrangular and planar surfaces, to represent the front of a building. Individual walls of buildings were approximated by two triangles each, to form their quadrangular surface. The geometrical details of the facades were neglected. No collisions of traffic participants with the static objects were possible. Since several prospective effectiveness assessment studies omit the consideration of static objects (e.g., J. M. Scanlon et al., 2017 considers sight obstructions for accidents close to intersections only by other traffic participants, but not static objects), the effects of this omission are investigated in the sensitivity study.

Road and weather conditions: Dry road conditions with sunny weather were assumed, since this is the environmental condition for which the driver behavior in the MTFS models was validated. Simulated sensors are not affected in any way by the weather conditions. Since the road site represented in the model described in Chapter 5 showed low differences in height (less than 0.7 m per 100 m length), the road was assumed to be two dimensional. This height difference was calculated by considering the two intersections Neubaugasse / Keplerstraße and Humboldtstraße / Bergmanngasse. Both intersections were included in the MTFS model and the spatial conflict filter. They were the intersections that were farthest apart (900 m of airline) and it is possible to travel from the intersection Humboldtstraße / Bergmanngasse to the other going only

down hill. There was a difference in elevation of only 6 m between the intersections, according to data from daftlogic.com. The small amount of inclination was considered by limiting the maximum velocity and acceleration for cyclists, for which it is directly considered in the MTFS and is considered to be negligible for engine powered vehicles. Road surface roughness was not considered in a detailed way in any of the models. The assumed road friction plays the most important role among all properties of the road and weather, since it limits the deceleration that can be reached by emergency brake maneuvers.

Lighting conditions: The lighting conditions did not influence the simulation and were therefore not further specified.

7.1.8. Summary of the method

The previous sections presented how nanoscopic simulation of the conflicts that were identified in the scenario catalog definition step can be achieved. Furthermore, the simulated safety systems are described. Table 7.1 gives an overview of all parameter values involved in nanoscopic simulation, chosen for the exemplary effectiveness study.

Parameter	*Value*	*Parameter*	*Value*
Concrete scenario preparation		**Collision model**	
Simulated time frame I	$\left[t_{\tau_{\text{TTC}}^{\min}} - t_{\text{sim}},\ t_{\tau_{\text{TTC}}^{\min}} + t_{\text{sim}}\right]$, $t_{\text{sim}} = 5\,\text{s}$	Δt_p	0.03 s
H	100 m	μ_{IV}	0.5
$\tau_{\text{TTC}}^{\text{Crit}}$	3 s	ϵ	0.115
Traffic participant dimensions $l/w/h$	from MTFS if available, else: 0.44/0.6/1.8 m (pedestrians) 1.73/0.64/1.8 m (cyclists) $h = 3$ m (buses, trucks) $h = 1.5$ m (passenger cars, vans)	Contact plane angle	Geometric rule (Kolk, Sinz, et al., 2016)
Traffic participant mass and density ($m = lwh\rho$)	$\rho_{car} = 115\,\text{kg/m}^3$ $\rho_{bus,truck} = 175\,\text{kg/m}^3$ $m_{pedestrian} = 80\,\text{kg}$ $m_{cyclist} = 90\,\text{kg}$	POI	Geometric rule (Kolk, Sinz, et al., 2016)
I_{xx}, I_{yy}, I_{zz}	$0.127\,mBl$ (passenger cars, vans) $I_{zz} = m(l^2 + w^2)/12$, $I_{yy} = I_{zz}$, $I_{xx} = 0.3 I_{zz}$ (buses, trucks)	**Kinetic path driver model**	
Sensor model		$\delta_{\text{steer}}^{\max}$	45 deg (passenger cars, vans) 55 deg (buses, trucks)
$\vec{X}_S^V$	$(l/2, 0, 0.5\,\text{m})$	$\dot{\delta}_{\text{steer}}^{\max}$	90 deg/s (passenger cars, vans) 150 deg/s (buses, trucks)
$\vec{\omega}_S^V$	$(0, 0, 0)$	t_{LA}	0.6 s
$\theta^{\max}$	180°	**Strategy model**	
R	100 m	$\tau_{\text{TTC}}^{\text{Trig}}$ and $\tau_{\text{ETTC}}^{\text{Trig}}$	1.0 s, respectively 1.5 s
N_{rays}^h	$2\theta^{\max}$	t_{srt}	0.2 s
t_{acq}	0.2 s	$a^{\min}$	$8\,\text{m/s}^2$
Infrastructure model		$a_{\text{requested}}$	$a^{\min}$, respectively $a_{\text{required}}^{\text{adj}}$
μ (road friction)	0.815	∇a	$40\,\text{m/s}^3$
		d_{SZ}	0.2 m

Table 7.1.: Summary of parameters used in the models involved in nanoscopic simulation.

7.2. Results and discussion

In this result section, the method proposed in the solution approach is applied to simulate the scenario catalog as the baseline, using 50 model runs of the MTFS model WBE and

thereby to demonstrate the applicability of the approach.

In the following subsections, an investigation on *collision events* is presented, which are collisions (as detected by PC-Crash, see Section 7.1.5.1) that occur in nanoscopic simulation, since a kinetic path driver model needs to be applied to follow the trajectories from MTFS. Since the MTFS trajectories cannot be followed exactly in nanoscopic simulation, traffic participants that pass each other closely without collision in MTFS, might collide in nanoscopic simulation. The time of occurrence of collision events, the type of the collisions and their severity depend on the parameterization of the kinetic path driver model. These dependencies, and the dependency of the effectiveness metrics, are investigated in detail in the sensitivity study in Section 9.4. Since MTFS is designed to not produce collisions by definition, and because the collision events in nanoscopic simulation are rather artifacts of the specific approach presented in this thesis work, it is not valid to treat those collision events as if they would correspond to accidents in real traffic (hence the new term "collision events"). The collision events occurred either between the two conflict participants (denoted in the following figures by "Both collision partners are conflict vehicles"), or between one of the conflict participants and a traffic participant from surrounding traffic (denoted by "One collision partner is a conflict vehicle").

Furthermore, the movement of conflict participants relative to each other is examined to investigate the field of view of simulated sensors. Next to the two conflict participants, between 0 to around 10 other traffic participants in P_{crit} and between 0 and 15 other traffic participants in P_{close} were considered, with a total of at most 25 traffic participants that matched the participant filtering criteria.

7.2.1. Impact locations and the time of occurrence of collision events

In total, 230 collision events were detected in the baseline when simulating the 2760 conflicts detected for the 50 MTFS model runs in nanoscopic simulation, which amounts to 4.6 collision events per hour of simulated time and 55.2 conflicts per hour of simulated time.

The first investigation on collision events considers their time of occurrence in nanoscopic simulation (i.e., t_{imp}) in relation to $t_{\tau_{\text{TTC}}^{\min}}$. A kernel density estimate of the differences $t_{\text{imp}} - t_{\tau_{\text{TTC}}^{\min}}$ is shown in Figure 7.20, such that the value 0 on the horizontal axis corresponds to $t_{\tau_{\text{TTC}}^{\min}}$ in MTFS. It can be seen that, for the concrete scenarios, where only one collision partner was a conflict participant, t_{imp} is not necessarily correlated to $t_{\tau_{\text{TTC}}^{\min}}$, since the differences of the impact time $t_{\text{imp}} - t_{\tau_{\text{TTC}}^{\min}}$ show no major peaks in density (solid line). The concrete scenarios with both collision partners being conflict participants (dashed line in Figure 7.20) instead show a major peak in density around 0 s to 0.5 s difference and one peak in density at 3 s to 4 s difference to $t_{\tau_{\text{TTC}}^{\min}}$. The collision events that contributed to the peak around 0 s to 0.5 s can be attributed to the occurrence of the conflict that defines the concrete scenario, i.e., the fact that $\tau_{\text{TTC,S}}^{\min}$ was reached at that moment. The conflicts that contributed to the peak around

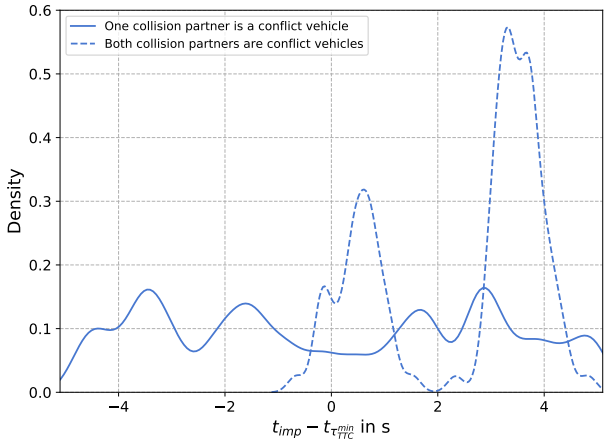

Figure 7.20.: Horizontal axis: difference between the impact time t_{imp} and $t_{\tau_{\text{TTC}}^{\text{min}}}$, i.e. $t_{\text{imp}} - t_{\tau_{\text{TTC}}^{\text{min}}}$. The value 0 on the horizontal axis corresponds to $t_{\tau_{\text{TTC}}^{\text{min}}}$ in MTFS. Vertical axis: kernel density estimates (see for example Rosenblatt, 1956) of the distribution of the values $t_{\text{imp}} - t_{\tau_{\text{TTC}}^{\text{min}}}$. As kernel function, the normal distribution with a bandwidth of $h = 0.1$ was used. The solid line shows the density of collision events where only one of the collision partners was a conflict participant, while the dashed line ("Both collision partners are conflict vehicles") shows the density of collision events where both collision partners were conflict vehicles.

3 s to 4 s are all situations that occur very similarly to the one shown in Figure 7.21, even at similar coordinates. This might be due to the kinetic path driver model not following the MTFS trajectory closely enough in that particular situation and motivates to study the influence of kinetic path driver model parameters on the occurrence of collision events.

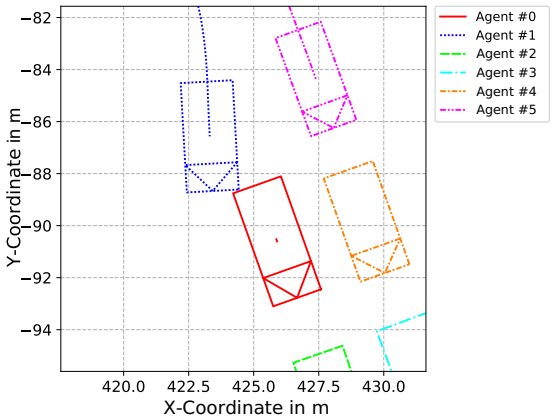

Figure 7.21.: Top view of the vehicle positions in one of the collision events, where both collision partners were conflict participants (blue and red vehicle in the middle of the figure), including other surrounding traffic (colored rectangles) and their trajectories (colored lines).

The second investigation considers the locations of impact on the vehicle geometries and the severity of the impacts. In 93 % of the collision events, the Δv was below 10 km/h, and in 73 % of the collisions events, the Δv was below 5 km/h, i.e., the majority of collisions were of minor severity and with low velocities. Figure 7.22 shows the locations of the points of impact (*POI*, see Section 7.1.5.2), scaled to the geometry of an exemplary vehicle with

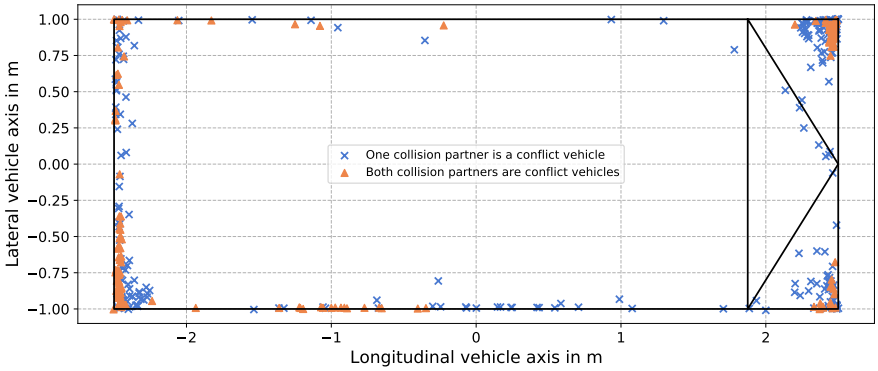

Figure 7.22.: The location of the points of impact (POI_{scaled}) for collision events, scaled to the dimensions of an exemplary vehicle with length 5 m and width 2 m. The blue crosses ("One collision partner is a conflict vehicle") show the collision events where only one of the collision partners was a conflict participant, while the orange triangles ("Both collision partners are conflict vehicles") show the collision events where both were conflict vehicles.

5 m length and 2 m width. Since the individual vehicles in the simulation had different dimensions, the coordinates of the points of impact were scaled to match the dimensions of the exemplary vehicle, such that $POI^x_{\text{scaled}} = \frac{5}{2}\frac{2POI^x}{l}$ and $POI^y_{\text{scaled}} = \frac{2POI^y}{w}$, where POI^x and POI^y are the x- and y-coordinates of the POI in the respective local vehicle coordinate systems and l and w are the colliding vehicles' length and width. It can be seen, that in most collision events, only the corners of the vehicles were involved, such as in the conflict that is shown in Figure 7.21. This further agrees with the observation that collision events are caused by differences to MTFS in the kinetic path driver model, leading for example to concrete scenarios where overtaking and lane change maneuvers can lead to intersecting vehicle corners. There are no notable differences in the impact locations between concrete scenarios where only one or both conflict participants are involved.

7.2.2. Movement of the conflict participants

Firstly to visualize the movement of conflict participants in nanoscopic simulation relative to each other, secondarily to better understand in which parts of the sensors' fields of view (180° opening angle and 100 m range) the respective other conflict participants were located and, thirdly, to better understand how the sensors were suited to detect other traffic participants, the trajectories (the positions of the center of gravity over time) of conflict participants were transformed into the local vehicle coordinate systems of the detecting vehicles (in this case they are also conflict participants) and are shown in Figure 7.23. This means that if vehicles A and B are the conflict participants (with their respective vehicle coordinate systems V_A and V_B), the trajectory of B was transformed into the coordinate system of vehicle A, i.e., $\vec{X}^{V_A}_{\text{COG},B} = R^{V_A}(\vec{X}^{G}_{\text{COG},B} - \vec{X}^{G}_{\text{COG},A})$, with R^{V_A} being the transformation matrix from G to V_A, and vice versa, i.e., $\vec{X}^{V_B}_{\text{COG},A} = R^{V_B}(\vec{X}^{G}_{\text{COG},A} - \vec{X}^{G}_{\text{COG},B})$. The sensors' fields of view are shown as the circular arches in Figure 7.23. It can be seen that either the other vehicle remained

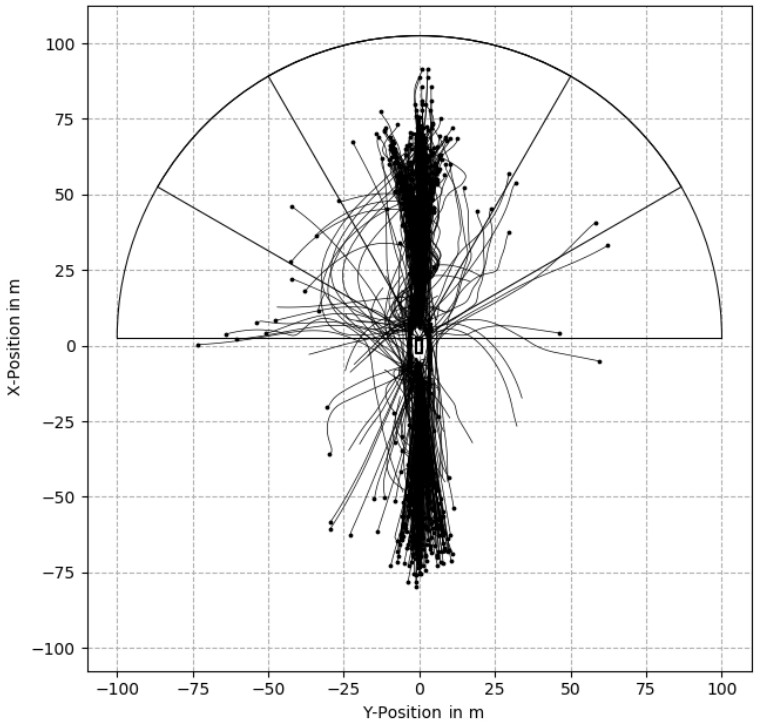

Figure 7.23.: Relative movement of conflict participants in nanoscopic simulation. For each conflict and each conflict participant A, the trajectory of the other conflict participant B was transformed into the coordinate system of the sensor of vehicle A (and vice versa). Three circle sectors are overlaid for exemplary purposes to represent the fields of view of sensors with 60°, 120° and 180° opening angle and 100 m range.

behind the sensor (i.e., an opening angle larger than 180° or a backward facing sensor is required), or, for the majority of the conflicts that occur in front of the sensor, a lower opening angle of 60° would be sufficient. Most conflicts occurred within longitudinal traffic, which reflects the fact that around 90 % of the conflicts are of rear-end type (see Section 6.2). To be able to react also in the crossing conflicts, a large opening angle is required. For the vast majority of the concrete scenarios, even a range of 75 m would be sufficient such that the sensors can see the other conflict participant at the beginning of the simulation.

7.3. Conclusions

The following conclusions were found when analyzing the results of the baseline simulation for 50 MTFS model runs, i.e., 2760 conflicts:

- In the baseline, collisions can occur, which are then called *collision events* (in total, 230, or 4.6 per hour of simulated time). These collision events can occur between any of the simulated traffic participants in nanoscopic simulation: between the conflict participants or between one of the traffic participants in the surrounding traffic - even with bicyclists or pedestrians.

- These collision events occur since a kinetic path driver model has to be used in nanoscopic simulation, which invariably leads to deviations from the MTFS trajectory. They are treated as unsystematic artifacts of the presented solution approach and do not necessarily correspond to the characteristics of accidents in real traffic. Nevertheless, keeping this in mind for the present thesis work, while it is still valid to consider system response related effectiveness metrics, also metrics related to the collision severity or the avoidance potential are investigated, primarily to demonstrate the opportunities of methods in future studies that generate traffic stochastically and can also produce validated collisions with characteristics (such as pre-crash trajectories, impact locations and collision severities) corresponding to accidents in real traffic.
- Most of the collision events were collisions where the corners of the vehicle geometries intersected.
- The collision events, where only one participant is a conflict participant, occur randomly with little evidence for correlation to $t_{\tau_{\mathrm{TTC}}^{\mathrm{min}}}$.
- In collision events, where both vehicles were conflict participants, the impact time of collision events concentrated around $t_{\tau_{\mathrm{TTC}}^{\mathrm{min}}}$ and in a cluster between 3 s and 4 s after $t_{\tau_{\mathrm{TTC}}^{\mathrm{min}}}$, which can be attributed to a low-speed lane-change conflict at a specific location.
- Plotting the trajectories of the conflict participants in relative sensor coordinates and comparing them to the fields of view of various sensors (60°, 120° and 180°) suggests that, in the majority of the investigated conflicts, using the lowest opening angle (60°) would not lead to differences in the visibility of traffic participants. Nevertheless, a 180° opening angle is used to also cover crossing conflicts as good as possible.

8. Effectiveness rating

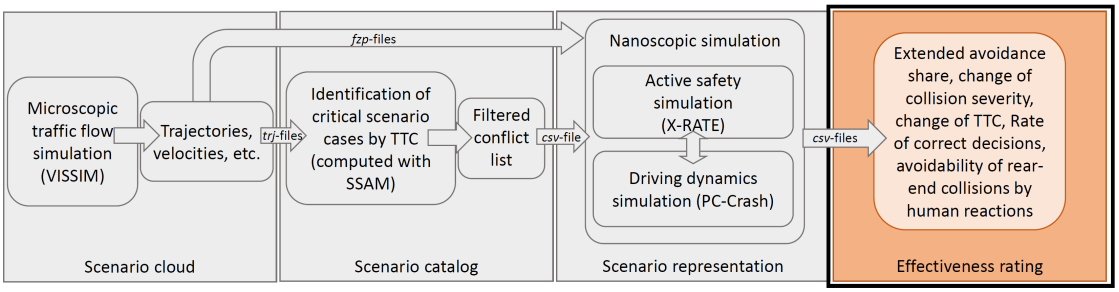

Figure 8.1.: Effectiveness rating step: results from nanoscopic simulation are processed to calculate effectiveness metrics, which are functions that aim to objectively describe to which extent the introduction of the safety system has made traffic safer.

In the following chapter, various effectiveness metrics and functions are discussed that are applied to the results from nanoscopic simulation. The calculation of effectiveness metrics forms the final step "Effectiveness rating" (Figure 8.1) in the solution approach presented in Chapter 4.

In this thesis, the notion of *monotonicity* as property of effectiveness metrics is introduced and it is used as a necessary requirement for a valid effectiveness metric. Monotonicity is defined as follows: if the safety benefit of system A in a specific aspect is greater than that of system B according to a *monotonous* metric E, then the value of the effectiveness metric for A must be greater than for B. This is defined as *positive correlation* of a monotonous effectiveness metric. A *negatively correlated* monotonous metric becomes smaller for greater safety benefits.

8.1. Method

8.1.1. Accident avoidance rates and changes in collision partners

The most basic form of defining the accident avoidance rate is given by

$$E_{\text{av}} := \frac{\text{number of collisions in the baseline that were avoided}}{|S_C|},$$

with $S_C := \{s \in S,$ such that a collision occurs in the concrete scenario $s\}$ and S being the scenario catalog. This metric was applied, for example, in the studies Eichberger, Tomasch,

				Treatment	
				Collision	No collision
Baseline	Collision	**Collision partner was changed**	Yes	*Changed collision*	*Avoided collision*
			No	*Unchanged collision*	
	No collision			*New collision*	*No collision*

Table 8.1.: Categorization of collision partner configurations.

Rohm, Hirschberg, and Steffan, 2011; Kolk, Kirschbichler, et al., 2016; Kusano and Gabler, 2011; Sander, 2017. E_{av} is monotonous, i.e. if system A avoids a higher proportion of collisions than system B, it is considered safer, and is therefore positively correlated with an increase in safety.

In this thesis work, the classic accident avoidance metric E_{av} is extended to also consider a potential change in collision partners (*changed collision*) between the baseline and treatment, or the occurrence of *new collisions*. This extension could not be found in the literature and can be applied when the surrounding traffic is considered. An example for a scenario with changing collision partners would be where a vehicle L brakes due to a conflict with a vehicle X, but the driver in a third vehicle F did not react appropriately (see Figure 8.2).

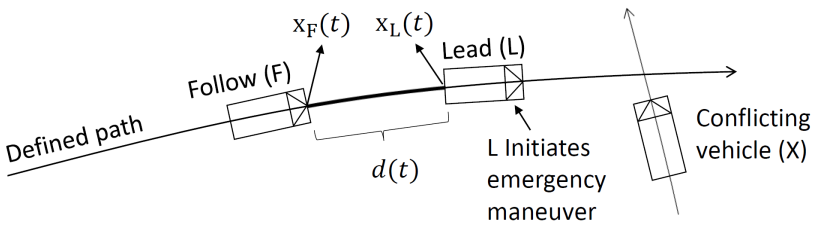

Figure 8.2.: An example of how a potential collision is avoided, leading to a new dangerous situation with a previously uninvolved traffic participant. Vehicle F follows vehicle L, who initiates an emergency brake maneuver in response to a potential collision with vehicle X. x_L and x_F denote the displacement along the defined path, while d denotes the relative distance between the traffic participants.

Table 8.1 presents the nomenclature for various combinations of configurations of collision partners in the baseline and treatment simulation: if a concrete scenario results in a collision in the baseline and in the treatment simulation, then the collision is termed either an *unchanged collision* or *changed collision*, depending on whether the collision occurred between the same or different traffic participants in the baseline and treatment simulation. The term *avoided collision* is used when a concrete scenario resulted in a collision in the baseline, but did not in the treatment simulation. A collision is considered to be a *new collision*, if a collision occurred only in the treatment, but not in the baseline simulation. In the following, the symbol N_{av} denotes the number of collisions in the baseline that were avoided, N_{new} denotes the number of concrete scenarios in S^{TR} with new collisions, N_{unch} denotes the number of concrete scenarios in S^{TR} with unchanged collisions and N_{ch} denotes the number of concrete scenarios in S^{TR} with changed collisions. Summing N_{av}, N_{unch} and N_{ch} yields

the total number of concrete scenarios with collisions in the baseline:

$$N_{\text{av}} + N_{\text{unch}} + N_{\text{ch}} = |S_C| \,. \tag{8.1}$$

Dividing Equation 8.1 by $|S_C|$ leads to:

$$\underbrace{\frac{N_{\text{av}}}{|S_C|}}_{:=E_{\text{av}}} + \underbrace{\frac{N_{\text{unch}}}{|S_C|}}_{:=E_{\text{unch}}} + \underbrace{\frac{N_{\text{ch}}}{|S_C|}}_{:=E_{\text{ch}}} = 1, \tag{8.2}$$

which allows the definition of the proportion of concrete scenario with respective collision partner configurations in the total number of collisions in the baseline as the effectiveness metrics E_{av}, E_{unch} and E_{ch} to express how the original baseline collisions have changed. Furthermore, the relationship

$$N_{\text{new}} + N_{\text{unch}} + N_{\text{ch}} = \left|S_C^{\text{TR}}\right| . \tag{8.3}$$

holds. Dividing Equation 8.3 by the right-hand-side $\left|S_C^{\text{TR}}\right|$ leads to:

$$\underbrace{\frac{N_{\text{new}}}{\left|S_C^{\text{TR}}\right|}}_{:=E_{\text{new}}} + \frac{N_{\text{unch}}}{\left|S_C^{\text{TR}}\right|} + \frac{N_{\text{ch}}}{\left|S_C^{\text{TR}}\right|} = 1,$$

such that the proportion of new collisions in the number of treatment collisions $\left|S_C^{\text{TR}}\right|$ can be expressed by the metric E_{new}.

For E_{ch}, lower numbers are better, since involving surrounding traffic in conflicts and thereby endangering other traffic participants to avoid a collision should not be an option (i.e. the metric is negatively correlated). At the same time, E_{unch} should also be as low as possible, since if both metrics E_{unch} and E_{ch} are low (close to 0), this means a high proportion (close to 1) of avoided collisions E_{av}, see Equation 8.2. These three metrics should be discussed mutually to accurately describe the change of collision partner configurations. If there is no collision in the baseline, then the metrics E_{av}, E_{ch} and E_{unch} are undefined.

Values of E_{new} close to 1 mean that a large proportion of the collisions in the treatment treatment simulation occurred only due to the activation of an emergency maneuver. This is in any case highly undesirable, thus lower values of E_{new} are better in terms of safety (i.e. the metric is negatively correlated). However, it is possible that the introduction of the safety system led to new collisions, while in other concrete scenarios, a collision was avoided. Hence, when discussing E_{new}, E_{av} should also be discussed.

8.1.2. System response categories and related metrics

Helmer, 2014 presented an effectiveness metric that expresses in how many concrete scenarios a safety system has decided correctly. A decision is considered *correct*, either when the situation is objectively dangerous and the system reacts, or when the situation is objectively

		System response	
		Activation	None
Objective danger	Yes	*True positive (TP)*	*False negative (FN)*
	No	*False positive (FP)*	*True negative (TN)*

Table 8.2.: Categorization of safety system responses. The term *objective danger* refers to what is regarded as dangerous by the criteria and their activation thresholds defined in the system specification. Based on a table in Helmer, 2014.

not dangerous and the system does not trigger. This leads to the categorization in *true/false positive/negative* decisions (see also Stehman, 1997), as shown in Table 8.2. Among other possibilities for the definition of objective danger, the specification of the safety system is used as a basis within this thesis work. An emergency brake system aims to avoid collisions or mitigate their consequences. Therefore, when a situation leads to a collision in the baseline simulation, this constitutes a situation where the system should definitely react (independent of whether it *can* react - a situation might be objectively dangerous, but the sight of the conflicting traffic participant might be occluded). Thus, the prevalence of a collision in the baseline is used as a sufficient requirement for objective danger. Furthermore, the safety systems described in Chapter 7 also use a safety zone: if the systems' algorithm predicts that two traffic participants will get within 0.2 m to each other (not necessarily leading to a collision), it will also initiate an emergency maneuver. Therefore, intrusion into the safety zone is also used as a sufficient requirement for objective danger (as was done for example in Sander, 2017).

Once the correct category in Table 8.2 has been identified for each investigated concrete scenario, the rate of correctly treated situations is calculated according to Kleinbaum et al., 2010 (also termed "accuracy" in Chicco and Jurman, 2020; Stehman, 1997):

$$E_{\text{corr}} = \frac{TP + TN}{TP + TN + FN + FP}$$

where TP, TN, FN and FP denote the number of concrete treatment scenarios in the respective class of system responses. Furthermore, the number of positive concrete scenarios (the objectively dangerous concrete scenarios where a system activation should take place) is denoted by $n^+ = TP + FN$. Analogously, $n^- = TN + FP$. The value of E_{corr} ranges between 0 and 1. The value of E_{corr} should be as close to 1 as possible (positively correlated). A high value for E_{corr} expresses that the system has a low rate of false decisions, i.e. it activates when it should and does not when it should not. In the present thesis, the criteria for the determination of objective danger and system activation are related to the conflict, i.e., a baseline situation is only treated as dangerous if the distance between the conflicts participants is below the defined threshold or if there is a collision between the primary conflict participants. Activations are only counted if the first activation by any of the primary conflict partners in the treatment simulation was triggered for the other primary conflict vehicle.

In Yerushalmy, 1947, a metric for the sensitivity (the proportion of true positives among the positive concrete scenarios)

$$E_{\text{sens}} = \frac{TP}{n^+}$$

was first presented, next to the metric for the specificity (the proportion of true negatives among the negative concrete scenarios):

$$E_{\text{spec}} = \frac{TN}{n^-}.$$

These are metrics which are commonly evaluated in the literature to describe the performance of classifiers in binary classification tasks, i.e., tasks where a system should categorize samples into one of two possible classes (positive or negative). Both metrics range from 0 to 1. If E_{sens} is close to 1, that means almost no false negative activations occurred. Analogously, the same holds true for E_{spec} and false positives. Furthermore, the Matthews correlation coefficient

$$E_{\text{MCC}} = \frac{TP \cdot TN - FP \cdot FN}{\sqrt{(TP+FP)(TP+FN)(TN+FP)(TN+FN)}}$$

and its normed variant (i.e., transformed to the unit interval $[0, 1]$)

$$E_{\text{MCC}}^{\text{norm}} = \frac{E_{\text{MCC}} + 1}{2}$$

are discussed in Chicco and Jurman, 2020. They constructed several exemplary datasets, some of them with notable imbalances in the identified categories (e.g., $TN \geq 90\,\%$), and concluded that E_{MCC} and $E_{\text{MCC}}^{\text{norm}}$ were the most informative of metrics, among several others, including E_{corr}. The values of $E_{\text{MCC}}^{\text{norm}}$ range from 0 to 1, with 0 representing perfect misclassification (i.e., the system never activated in a dangerous situation and vice versa) and 1 representing perfect classification. The value 0.5 represents random classification. In this thesis, the metrics E_{corr}, E_{sens}, E_{spec} and $E_{\text{MCC}}^{\text{norm}}$ are used to analyze the safety benefit of the investigated safety systems, as well as E_{TP}, E_{TN}, E_{FN} and E_{FP}, which correspond to the respective numbers TP, TN, FN and FP, divided by $TP + TN + FN + FP$. The false decisions (E_{FN} and E_{FP}) should be as close as possible to 0, while the true decisions (E_{TN} and E_{TP}) should be as high as possible.

8.1.3. Change in minimum TTC and minimum distance between traffic participants

If a collision has been avoided, it may still be a very close situation, where traffic participants passed each other by a very short distance. To complement the avoidance-related metrics in Section 8.1.1, the minimum distance (i.e., $d^{\min}$) and minimum TTC (i.e., $\tau_{\text{TTC},X}^{\min}$) between conflict participants during concrete scenarios are investigated. This is done also as a replacement for the metric E_{conf} (Section 2.4.3) which describes the ratio of the number of conflicts between baseline and treatment.

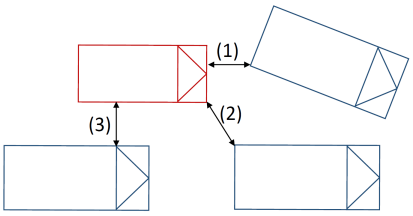

Figure 8.3.: Calculation of $d^{\min}$ based on Pirzadeh, 1999. All three cases, how the minimum distance can occur, are considered: between node to edge (1), node to node (2) and edge to edge (3).

For the calculation of $d^{\min}$, the rotating caliper method for convex polygons by Pirzadeh, 1999 is used. It computes the minimum distance between two convex polygons and deals with all three possibilities how the minimum distance can occur, see Figure 8.3 (right): node to edge (1), node to node (2) and edge to edge (3). For the calculation of $d^{\min}$, the x- and y-coordinates of the bottom of the box-shaped traffic participant geometry are used as polygons.

To express how a safety system contributes to the safety of a vehicle by increasing $d^{\min}$ and $\tau^{\min}_{\mathrm{TTC,X}}$ between the conflict participants in dangerous situations (for the definition of objective danger, see Section 8.1.2), the values $f_{\mathrm{eff}}(s)$ and $f_{\mathrm{eff}}(TR(s))$ are investigated, where f_{eff} denotes $d^{\min}$ or $\tau^{\min}_{\mathrm{TTC,X}}$ as the effectiveness functions, evaluated between the conflict participants, and $TR(s)$ denotes the treatment situation corresponding to the concrete scenario s. The values $f_{\mathrm{eff}}(s)$ and $f_{\mathrm{eff}}(TR(s))$ are then aggregated for all $s \in S_{\mathrm{dang}}$, where S_{dang} denotes the set of concrete baseline scenarios with a dangerous situation. Since $d^{\min}$ and $\tau^{\min}_{\mathrm{TTC,X}}$ lie on an ordinal scale (e.g., an increase of $d^{\min}$ from 1 m to 2 m does not necessarily imply the same safety benefit as increasing $d^{\min}$ from 19 m to 20 m), taking the mean of the values $f_{\mathrm{eff}}(s)$ and $f_{\mathrm{eff}}(TR(s))$ or computing the differences $f_{\mathrm{eff}}(TR(s)) - f_{\mathrm{eff}}(s)$ is not a valid operation (see Krapp and Nebel, 2011). However, it is valid to compute location metrics such as the 25 %-, 50 %- and 75 %-quartiles $\mathrm{Q}^{25\,\%}_{S_{\mathrm{dang}}}$, $\mathrm{Q}^{50\,\%}_{S_{\mathrm{dang}}}$ and $\mathrm{Q}^{75\,\%}_{S_{\mathrm{dang}}}$. In the following, the median $\mathrm{Q}^{50\,\%}_{S_{\mathrm{dang}}}$ is used for the aggregation of $f_{\mathrm{eff}}(s)$ and $f_{\mathrm{eff}}(TR(s))$. The median represents the numeric value that separates the higher half from the lower half of the values $f_{\mathrm{eff}}(s)$ with $s \in S_{\mathrm{dang}}$. For example, if $f_{\mathrm{eff}}(s)$ evaluates for an exemplary effectiveness function f_{eff} to 0.3, 0.4, 0.45, 0.5, 0.8, for dangerous scenarios $s \in S_{\mathrm{dang}}$ with $|S_{\mathrm{dang}}| = 5$ (uneven number of concrete scenarios), the median would evaluate to 0.45. If an even number of dangerous scenarios is considered, for example $|S_{\mathrm{dang}}| = 4$, with $f_{\mathrm{eff}}(s)$ evaluating to 0.3, 0.4, 0.45, 0.5, then the median would be computed as the average of the middle values 0.4 and 0.45, i.e., $\mathrm{Q}^{50\,\%}_{S_{\mathrm{dang}}}(f_{\mathrm{eff}}(s)) = \frac{0.4+0.45}{2}$ (see for example Krapp and Nebel, 2011). This allows the definition of the following metrics:

$$E^{\mathrm{dang},BL}_{\mathrm{TTC},50\,\%} := \mathrm{Q}^{50\,\%}_{S_{\mathrm{dang}}}(\tau^{\min}_{\mathrm{TTC,X}}(s)),$$
$$E^{\mathrm{dang},TR}_{\mathrm{TTC},50\,\%} := \mathrm{Q}^{50\,\%}_{S_{\mathrm{dang}}}(\tau^{\min}_{\mathrm{TTC,X}}(TR(s))).$$

The same is done for $d^{\min}$ as the effectiveness function, leading to the metrics $E^{\mathrm{dang},BL}_{\mathrm{dist},50\,\%}$ and $E^{\mathrm{dang},TR}_{\mathrm{dist},50\,\%}$. Collisions in concrete scenarios s or $TR(s)$ are counted as $\tau^{\min}_{\mathrm{TTC,X}} = 0$ and

$d^{\min} = 0$. The distribution of the values $f_{\text{eff}}(s)$ and $f_{\text{eff}}(TR(s))$ is not known and can contain significant outliers. Since S_{dang} consists of concrete scenarios with collisions or situations where the minimum distance is lower than 0.2 m, the metric $E^{\text{dang},BL}_{\text{dist},50\,\%}$ will lie between 0 and 0.2 m. Using the simplified relationship $\tau_{\text{TTC,X}} = \frac{x_{\text{rel}}}{v_{\text{rel}}}$, it can be seen that the metric $E^{\text{dang},BL}_{\text{TTC},50\,\%}$ will lie below 0.2 s in the worst case, for velocities above 1 m/s. Furthermore, the metrics $E^{\text{dang},TR}_{\text{TTC},50\,\%}$ and $E^{\text{dang},TR}_{\text{dist},50\,\%}$ are positive. They are positively correlated, since increasing $\tau^{\min}_{\text{TTC,X}}$ and $d^{\min}$ in the treatment is associated with an increase in the safety benefit.

8.1.4. Effectiveness metrics related to the collision severity

In Section 2.4.2, several effectiveness metrics related to the collision severity that are commonly applied in the literature were presented. These are defined as the mean value of the change of Δv or v_c. However, since Δv or v_c also lie on the ordinal scale, analogous to $d^{\min}$ or $\tau^{\min}_{\text{TTC,X}}$, only location metrics such as the median of values in the treatment or baseline are used in this thesis as effectiveness metrics.

In the following, the notations $f_{p_1}(s)$ and $f_{p_2}(s)$ are used to express an effectiveness function such as Δv_{p_1} and Δv_{p_2}, respectively evaluated for the conflict participants p_1 and p_2 in the concrete scenario s. The notation $Q^{50\,\%}_{S_C}(f_{p_1}(s), f_{p_2}(s))$ is used to express the median of all values $f_{p_1}(s)$ and $f_{p_2}(s)$ for all concrete scenarios s in the scenario catalog S_C. The median of the collision severity in the baseline or treatment is calculated by

$$E^{\text{BL},50\,\%}_{\Delta v} := Q^{50\,\%}_{S_C}(\Delta v_{p_1}(s),\, \Delta v_{p_2}(s)) \tag{8.4}$$

$$E^{\text{TR},50\,\%}_{\Delta v} := Q^{50\,\%}_{S^{TR}_C}(\Delta v_{p_1}(TR(s)),\, \Delta v_{p_2}(TR(s))). \tag{8.5}$$

In Sander and Lubbe, 2018, the metric $E^{\text{TR},50\,\%}_{\Delta v}$ was compared for different treatments to $E^{\text{BL},50\,\%}_{\Delta v}$ to investigate the influence of intersection AEB systems in reducing the average collision severity. These metrics are positive in value, theoretically without an upper limit.

Since E_{av}, E_{new} or E_{ch} only describe the relative change in accident numbers between collision partner configurations, several metrics can be defined analogously that also express the average severity of collisions in the respective collision partner configurations:

$$E^{\text{new},50\,\%}_{\Delta v} := Q^{50\,\%}_{S^{\text{new}}}(\Delta v_{p_1}(TR(s)),\, \Delta v_{p_2}(TR(s))), \tag{8.6}$$

$$E^{\text{ch},50\,\%}_{\Delta v} := Q^{50\,\%}_{S^{\text{ch}}}(\Delta v_{p_1}(TR(s)),\, \Delta v_{p_2}(TR(s))), \tag{8.7}$$

$$E^{\text{unch},50\,\%}_{\Delta v} := Q^{50\,\%}_{S^{\text{unch}}}(\Delta v_{p_1}(TR(s)),\, \Delta v_{p_2}(TR(s))), \tag{8.8}$$

with S^{new} being the set of all concrete scenarios where a new collision occurs in the treatment, S^{ch} being the set of all concrete scenarios where the collision partners are not the same in the treatment as in the baseline, i.e., changed collisions, and S^{unch} being the set of all concrete scenarios where the collision partners remained the same in the treatment as in the baseline, i.e., unchanged collisions. Lower values of $E^{\text{TR},50\,\%}_{\Delta v}$, $E^{\text{new},50\,\%}_{\Delta v}$, $E^{\text{ch},50\,\%}_{\Delta v}$ and $E^{\text{unch},50\,\%}_{\Delta v}$ indicate higher safety effects, i.e. they are negatively correlated.

8.1.5. Investigation on the convergence of effectiveness metrics

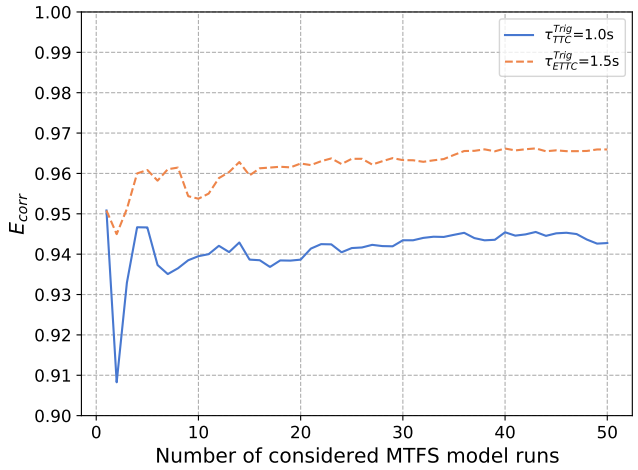

Figure 8.4.: Convergence of the metric E_{corr}, comparing two safety systems that triggered at different thresholds $\tau_{\text{TTC}}^{\text{Trig}}$.

In general, if the sample size is increased, more powerful statistical conclusions can be drawn on the underlying population (Bourier, 2013). In the context of effectiveness assessment and this thesis, the convergence of effectiveness metrics due to the use of a higher number of MTFS model runs, i.e., a higher number of investigated conflicts, is investigated. Convergence is said to be achieved, when the value of the metric does not change significantly when considering a higher sample size. In this thesis, convergence is presented through graphs that display an increasing number of MTFS model runs that were considered in the calculation of the metric on the horizontal axis and the value of the metric on the vertical axis. The stability of the convergence is verified visually through such graphs. For an example, see Figure 8.4. The less the metric is changing for a higher sample size, the more can the value of the metric be seen as a final value. In this example, the metric stayed at a similar level even at a low number of MTFS model runs (less than 10).

8.1.6. Summary of the method

Table 8.3 summarizes the effectiveness metrics described and introduced in this chapter and lists their theoretical upper and lower limits and the direction of correlation with increasing safety benefits. Each of the listed metrics is evaluated for the exemplary effectiveness study in the following sections.

Effectiveness metric	*Lower limit*	*Upper limit*	*Correlation*
E_{av}	0	1	+
E_{new}	0	1	-
E_{ch}	0	1	-
E_{unch}	0	1	-
E_{corr}, E_{sens}, E_{spec}, $E_{\text{MCC}}^{\text{norm}}$	0	1	+
E_{FP}, E_{FN}	1	0	-
E_{TP}, E_{TN}	0	1	+
$E_{\text{TTC},50\,\%}^{\text{dang},BL}$	0	less than 0.2 s for velocities above 1 m/s	none
$E_{\text{dist},50\,\%}^{\text{dang},BL}$	0	0.2 m	none
$E_{\text{TTC},50\,\%}^{\text{dang},TR}$, $E_{\text{dist},50\,\%}^{\text{dang},TR}$	0	none	+
$E_{\Delta v}^{\text{BL},50\,\%}$	0	none	none
$E_{\Delta v}^{\text{TR},50\,\%}$	0	none	-
$E_{\Delta v}^{\text{new},50\,\%}$, $E_{\Delta v}^{\text{ch},50\,\%}$, $E_{\Delta v}^{\text{unch},50\,\%}$	0	none	-

Table 8.3.: Overview on effectiveness metrics. A positive correlation (+) signifies that when two safety systems A and B are compared, and the metric exhibits a higher value for A, then the safety benefit of A is higher than of B. For negative correlation (-), the situation is vice versa. Some metrics have no theoretical upper or lower limit, marked by the word "none".

8.2. Results and discussion

In the following subsections, each of the effectiveness metrics presented in Section 8.1 is evaluated for the exemplary effectiveness study defined in the solution approach. This effectiveness study compares two treatments. In the first treatment, both conflict participants' AEB systems were configured with $\tau_{\text{TTC}}^{\text{Trig}} = 1.0\,\text{s}$ and $a_{\text{requested}} = a^{\min} = -8\,\text{m/s}^2$ (system configuration 1), and in the second treatment, they were configured with $\tau_{\text{ETTC}}^{\text{Trig}} = 1.5\,\text{s}$, $a_{\text{requested}} = a_{\text{required}}^{\text{adj}}$ and to not trigger if the driver is evading successfully laterally (system configuration 2), see Section 7.1.4. To investigate the convergence of the effectiveness metrics in relation to the number of MTFS model runs which are considered in the computation of the effectiveness metrics, convergence plots as described in Section 8.1.5 are analyzed. The results shown in graphs and tables are computed when considering all 50 model runs of the MTFS model WBE, which contained in total 2 760 conflicts (the minimum number of conflicts per MTFS model run was 33, and the maximum was 75).

Results of this exemplary effectiveness study are discussed and compared to the literature. However, it has to be noted, that the comparability of results for effectiveness metrics in the categories "accident avoidance rates and changes in collision partners" and "effectiveness metrics related to the collision severity" is limited. This is due to the fact that collision events are artifacts of the coupling between MTFS and nanoscopic simulation and do not necessarily resemble the characteristics (such as pre-crash trajectories, impact locations and collision severities) of accidents in real traffic.

8.2.1. System response categories and related metrics

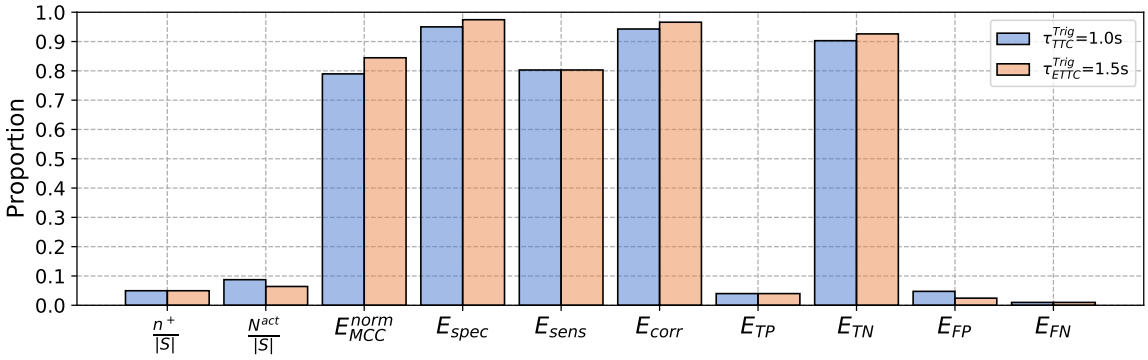

Figure 8.5.: Metrics related to the system response categories (false/true positive/negative), the proportion $\frac{n^+}{|S|}$ of dangerous baseline situations in the number of concrete scenarios in the scenario catalog S, and the proportion $\frac{N^{act}}{|S|}$ of system activations in $|S|$.

As can be seen in Figure 8.5 by the proportion $N^{\text{act}}/|S|$ ($N^{\text{act}} = TP + FP$ denotes the number of concrete treatment scenarios with system activations), a braking maneuver was activated in more concrete scenarios (8.7 % vs. 6.4 % of the investigated conflicts) by system configuration 1 ($\tau_{\text{TTC}}^{\text{Trig}} = 1.0\,\text{s}$) than configuration 2 ($\tau_{\text{ETTC}}^{\text{Trig}} = 1.5\,\text{s}$). In a significant number of concrete scenarios, the vehicles were already braking when the system with configuration 1 activated a braking maneuver (e.g., around 40 % of the vehicles already braked with less than $1\,\text{m/s}^2$, see Figure 8.6, left). With system configuration 1, the current acceleration is not considered in the TTC calculation. Hence, several activations can occur that would not have been necessary, which explains the higher number of activations for system configuration 1.

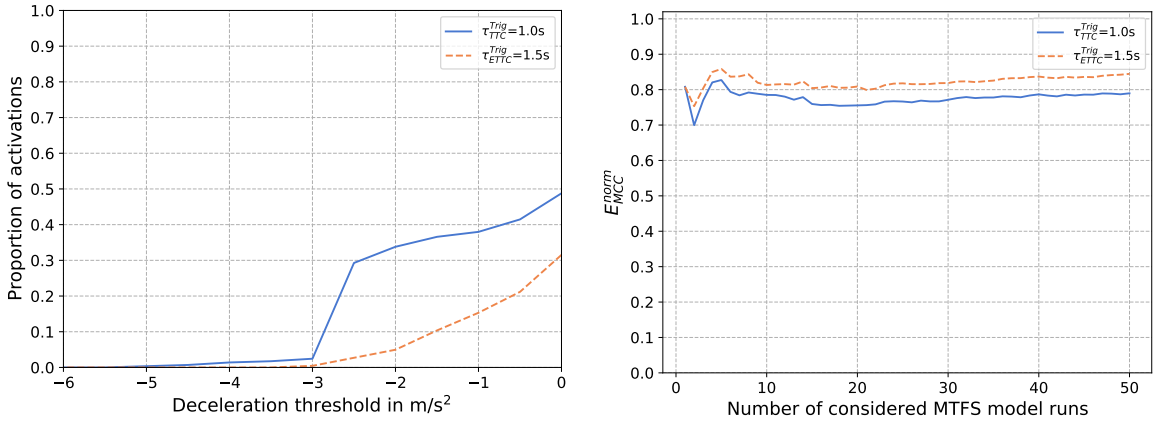

Figure 8.6.: Left: proportion of concrete scenarios where the vehicle activating an emergency brake maneuver was already braking with a longitudinal acceleration below a certain threshold. Right: convergence of the metric $E_{\text{MCC}}^{\text{norm}}$ in dependence on the number of considered MTFS model runs.

Due to the higher number of system activations with configuration 1, there was a higher proportion E_{FP} of conflicts in the total number of conflicts with false positive responses than

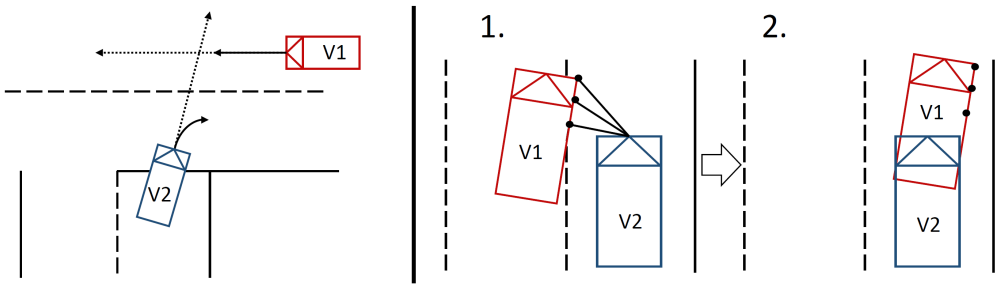

Figure 8.7.: Left: an example for a situation where the turning vehicle showed a false positive system response. The blue vehicle ($V2$) intended to turn right at an intersection (solid arc), while the red vehicle ($V1$) intended to travel straight ahead (solid straight arrow). Right: situation with false negative system response. The red vehicle ($V1$) tries to change to the lane of the blue vehicle ($V2$), leading to a collision event.

with configuration 2 (4.7 % vs. 2.4 %, Figure 8.5), while the number of conflicts with true positive and false negative system responses remained equal. This led to the sensitivity E_{sens}, i.e., the system's ability to detect dangerous situations, being equal, while the specificity E_{spec}, i.e., the system's ability to classify a non-dangerous situation as such, was higher for system configuration 2 (97.4 % vs. 95.0 %). Finally, the normed correlation coefficient $E_{\text{MCC}}^{\text{norm}}$ was higher for system configuration 2 than for configuration 1 (84.5 % vs. 79.0 %, see Figure 8.6, right), as well as the proportion of correct decisions E_{corr} (96.6 % vs. 94.3 %, see Figure 8.6). Since less false positive activations occur with system configuration 2, even though the trigger threshold is higher ($\tau_{\text{ETTC}}^{\text{Trig}} = 1.5\,\text{s}$ vs. $\tau_{\text{TTC}}^{\text{Trig}} = 1.0\,\text{s}$), this system configuration is to be preferred according to the metrics investigated in this section.

The convergence of the metrics related to the system response categories was excellent. One example is given in Figure 8.6 (right), where the convergence of $E_{\text{MCC}}^{\text{norm}}$ is shown. The metrics E_{sens}, E_{spec} and E_{corr} converged similary well. Their convergence graphs are shown in Figure F.1 in the appendix. Steady values are achieved even when only 10 MTFS simulation runs are considered in the computation of the metrics. Therefore, each of the discussed metrics is also considered for the sensitivity analysis.

Detailed analysis of the conflicts in which the system decisions were categorized as "false positive" or "false negative" offers the opportunity to better understand consequences of details in the implementation of the systems. When investigating false positives, situations such as the one depicted in Figure 8.7 (left) can be identified. In this example, the TTC algorithm of system configuration 1 predicted a possible collision, since a straight continuation of movement is assumed, while configuration 2 did not activate since steering was involved and no collision in the baseline was identified. The false negative decisions were situations exclusively such as the one depicted in Figure 8.7 (right). In this situation, the red vehicle $V1$ tried to change the lane to the lane of the blue vehicle $V2$, which led to a collision event (2.). The blue vehicle $V2$ was not in the field of view of the red vehicle's sensor (vehicle $V1$), therefore its safety system could not react to the presence of the blue vehicle $V2$ (false negative - no activation even though it would have been necessary). The sensor in the blue

vehicle $V2$ was able to detect several points on the red vehicle $V1$ (1.), but not detect the full vehicle, such that no classification could be reached. Thus, the blue vehicle $V2$ did not react either, even though it should have activated to avoid a collision (false negative).

Very little actual estimates of metrics such as the sensitivity E_{sens} (measuring how often the system activates in a dangerous situation) or specificity E_{spec} (measuring how often the system does not activate in a non-dangerous situation) of AEB systems exist in the literature. One of the few who provide related estimates is Helmer, 2014, who used stochastic scenario generation to evaluate a preventive pedestrian collision avoidance system. He considered several types of related effectiveness metrics, e.g., the number of system interventions per avoided accident or the number of false positive warnings per warning issued. He evaluated these metrics in dependence of the system activation threshold. However, since the metrics in this section are defined differently, they cannot be compared. Helmer, 2014 acknowledges the trade-off that is invariably connected to activating an emergency maneuver early: earlier activation thresholds will lead to more system activations, possibly avoiding more accidents, but there will also be more situations where activation was not strictly necessary (false positive). Without providing estimates of the extent of the effect, Parasuraman and Riley, 1997 concluded that automation disuse, e.g., in the form of high false-positive rates, can lead to users mistrusting the automation and turning it off, which would negate the intended safety effect. As was shown, depending on the specific system configuration and implementation, incorrect system responses such as false positives and false negatives will definitely occur, and the method presented in this thesis is a first step in filling the gap in research on methods that are suited to identify concrete scenarios where false system responses occur, to estimate the sensitivity and specificity.

8.2.2. Accident avoidance rates and changes in collision partners

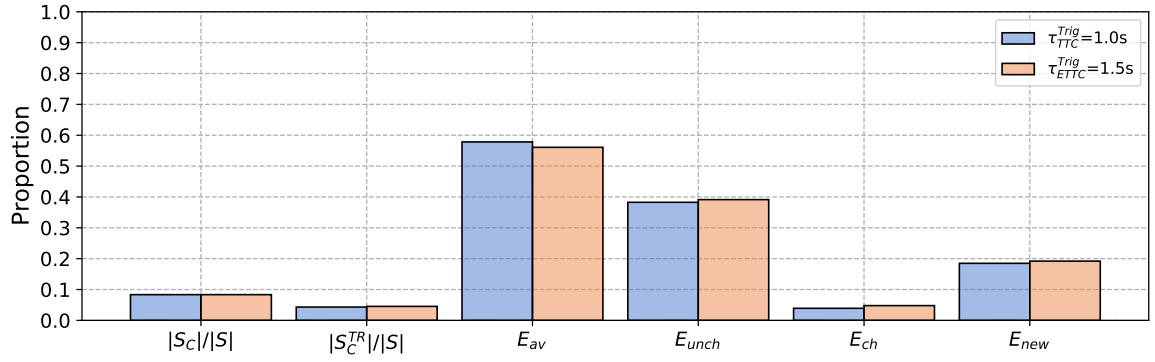

Figure 8.8.: The proportions of baseline ($|S_C|/|S|$) and treatment ($|S_C^{TR}|/|S|$) collisions and metrics related to collision avoidance and the change of collision partner configurations.

In total, collision events occurred in 8.3 % of the conflicts in the baseline, and they were reduced by the systems such that a collision occurred only in 4.3 % (system configuration 1, $\tau_{\text{TTC}}^{\text{Trig}} = 1.0\,\text{s}$) and respectively 4.5 % (system configuration 2, $\tau_{\text{ETTC}}^{\text{Trig}} = 1.5\,\text{s}$) of the conflicts in

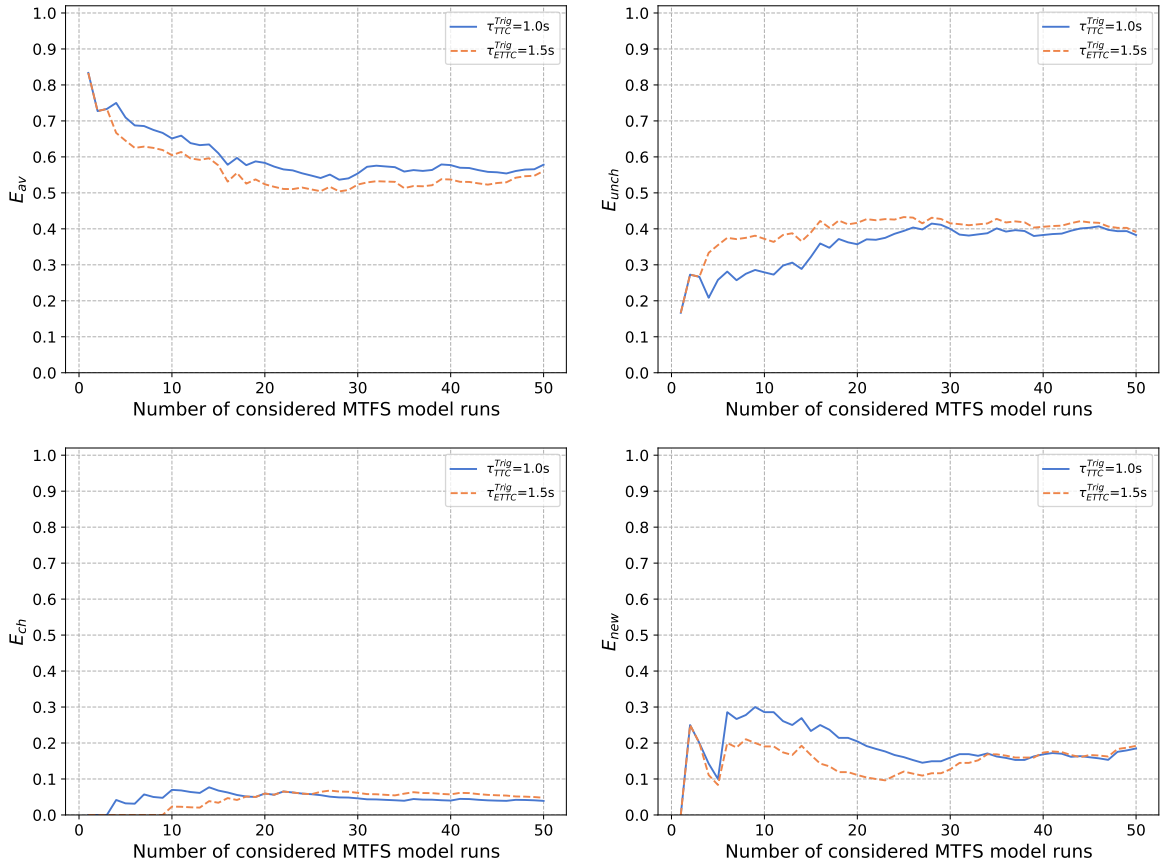

Figure 8.9.: Convergence of metrics related to collision avoidance and change of collision partner configurations.

the treatment, as can be seen by $|S_C|/|S|$ and $|S_C^{TR}|/|S|$ in Figure 8.8. System configuration 1 showed a higher avoidance potential E_{av} (57.8 % vs. 56.1 %). A possible explanation is that system configuration 1 led to more conflicts with activations than configuration 2, see previous subsection. Since it avoided less collisions, system configuration 2 left the collision partner configuration in a higher proportion of baseline collisions unchanged (metric E_{unch}, 39.1 % vs. 38.3 %). The proportion of baseline collisions where the collision partners were changed to involve previously uninvolved traffic participants was slightly higher for system configuration 2 (4.8 % vs. 3.9 %). The proportions of the treatment collisions that were new collisions were very similar (metric E_{new}, 18.5 % for system configuration 1 vs. 19.2 % for system configuration 2). The similar values in E_{new} and E_{ch} indicate that a similar number of collisions are introduced with other traffic participants that were previously not involved, under the assumption that those other traffic participants do not react to the triggered emergency maneuvers. To summarize these results, it can be noted that the main difference, in the light of the metrics investigated in this section, consists in the slightly higher (57.8 % vs. 56.1 %) collision avoidance potential by system configuration 1.

The convergence of the metrics E_{av}, E_{unch} and E_{ch} in relation to the number of considered MTFS model runs stabilized at around 20 MTFS model runs (Figure 8.9). Most conflicts where a collision could not be avoided by the active safety system with configuration 2, but by configuration 1, are of the same type as shown in Figure 8.10. In this example, the

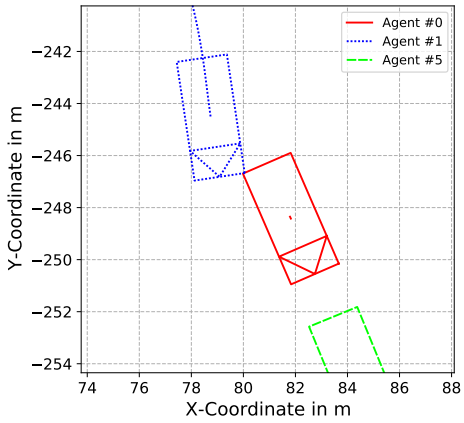

Figure 8.10.: An example for a conflict that was avoided by system configuration 1, but not configuration 2.

blue vehicle (agent #1) tried to change the lane to the lane on its right at an intersection, but this maneuver led to a collision at low velocity with the red vehicle (agent #0). The computation algorithm of $a^{\text{adj}}_{\text{required}}$ tries to predict the relative distance and velocity between the vehicles to predict a_{required} at the moment when the requested brake acceleration can been reached. However, in the given example, the triggering vehicle accelerated directly after triggering, leading to the actual velocity being higher than the predicted velocity, such that the estimated $a^{\text{adj}}_{\text{required}}$ was not low enough to avoid the collision. In real vehicles, the current acceleration used to predict the velocity and distance could be replaced by an assumed maximum driver acceleration, to consider the worst case.

For the metric E_{new}, stability can be observed upwards from 30 MTFS model runs. This is due to the fact that the metric $E_{\text{new}} = \frac{N_{\text{new}}}{|S_C^{\text{TR}}|}$ is computed as the proportion of new collisions in the treatment, which are less than the collisions in the baseline. Due to the sufficient convergence behavior of E_{av}, E_{ch} and E_{unch}, and since differences in these metrics can be seen, each of these metrics is also considered for the sensitivity analysis. As the convergence of E_{new} was inferior and the difference between the systems minimal, it is not considered in the sensitivity studies. The absolute numbers of conflicts in the respective collision partner configurations can be found in Appendix F.2.

To compare the results to the literature, Table 8.4 summarizes the crash reduction rates found in several studies. If available, retrospective studies are preferred for comparison, as they represent real world benefits of safety systems instead of predicted benefits. Otherwise, prospective simulative studies are used.

In the following, the studies listed in Table 8.4 are described: in Cicchino, 2017, a list of current vehicle models is presented, along with the type of systems that are installed in those vehicles. Cicchino distinguishes the following categories: FCW only (Forward Collision Warning, i.e., a system that emits a warning to the driver that a frontal collision is imminent), low-speed AEB (AEB systems that autonomously initiate a brake maneuver at speeds up to 30.4 km/h) and AEB + FCW (systems that first warn the driver and then autonomously

Study	*Study type*	*System type*	*Conflict type*	*Data basis*	*Reduction rate*
Cicchino, 2017	Retro-spective	low-speed AEB	rear-end	45 000 injury crash involvements	43 %
		AEB + FCW			50 %
Isaksson-Hellman and Lindman, 2015b		low-speed AEB		165 000 insured vehicle years	25 % to 29 %
Isaksson-Hellman and Lindman, 2015a		AEB + FCW		335 000 insured vehicle years	38 % to 45 %
Fildes et al., 2015		AEB + FCW		meta analysis	38 %
J. M. Scanlon et al., 2017	Pros-spective	Intersection AEB	crossing	448 reconstructed real accidents	25 % to 59 %
Sander and Lubbe, 2018		Intersection AEB		792 reconstructed real accidents	79 %
Bareiss et al., 2019		Intersection AEB		501 reconstructed real accidents	18 % to 84 %
Present thesis		AEB	all conflict types	MTFS	56.1 % to 57.8 %

Table 8.4.: Comparison of crash reduction rates found for comparable systems in retrospective studies in the literature and the present study. No studies investigating intersection accidents could be found.

initiate a brake maneuver if the driver did not react and the collision course still persists). The details of the vehicles' individual strategies are not further analyzed. The vehicles in MTFS were involved in conflicts at all speeds up to the maximum speed allowed at the simulated road sections, such that Cicchino's results for both the low-speed AEB and AEB + FCW must be combined. Analyzing more than 45 000 injury crash involvements from police reports in the U.S., Cicchino, 2017 finds reduced rear-end striking crash involvement rates of 43 % for low-speed AEB and 50 % reduction for AEB + FCW. Based on Swedish insurance data, it was concluded in Isaksson-Hellman and Lindman, 2015b, that the presence of low-speed AEB systems (operating at up to 30.4 km/h) led to 25 % to 29 % fewer rear-end collisions than in cars without the system. Furthermore, in Isaksson-Hellman and Lindman, 2015a, it was concluded that the presence of AEB + FCW systems that operate at speeds up to 50 km/h resulted in 38 % to 45 % fewer rear-end crashes as in vehicles without such systems. A meta analysis by Fildes et al., 2015 reports 38 % reduction by AEB + FCW systems in rear-end crashes.

For estimates of the collision avoidance potential in crashes of the crossing conflict type, only prospective simulation studies can be found. In Sander and Lubbe, 2018, a 120° and 180° sensor paired with an AEB is simulated that brakes as soon as the comfort threshold of $5\,\mathrm{m/s^2}$ for a_{required} is surpassed. For the 180° sensor, which was also used in this thesis, a collision avoidance potential of 79 % was found. This result is based on 792 reconstructed real accidents with straight crossing paths of the colliding vehicles. Both vehicles were equipped with a safety system, as was done also in this thesis. In J. M. Scanlon et al., 2017, 448 reconstructed straight crossing path accidents and in Bareiss, 2019, 501 reconstructed left turn across path/opposite direction crashes were investigated. In both studies, sensors with

120° opening angle were simulated, and both vehicles were equipped with a safety system. J. M. Scanlon et al., 2017 found an estimated reduction rate of 25 % to 59 % for a τ_{TTC}-based system and Bareiss, 2019 found a reduction rate of 18 % to 84 % for an τ_{ETTC}-based system, depending on the remaining system configuration.

To compare the avoidance potential found in this thesis to the literature, an average of the reduction rates is first computed for each conflict type investigated in the literature studies. Then, an average of the averages for each conflict type is computed, weighted by the proportion of the conflict types for WBE, since conflicts of all types are used to compute E_{av}. Since the lane-change conflict type is not represented in Table 8.4, it is omitted from the weighted average. This leads to an aggregated crash reduction rate of 38.8 % (worst-case) to 41.6 % (best-case). In this section, it was found that 56.1 % to 57.8 % of collisions in the baseline were avoided (expressed by E_{av}), which represents an overestimation when comparing with the literature. These numbers for E_{av} are based on the assumption of an ideal sensor and safety system which always operates as defined in Section 7.1, simulated for sunny weather and dry road conditions. The performance of safety systems in real vehicles might for example be influenced by the weather, lighting and road conditions, sensor detection errors, sensor pollution and more. As long as such effects are not considered, an overestimate such as the one found in this thesis is possible. For the other metrics E_{ch} or E_{new}, no estimates can be found.

8.2.3. Change in minimum TTC and minimum distances

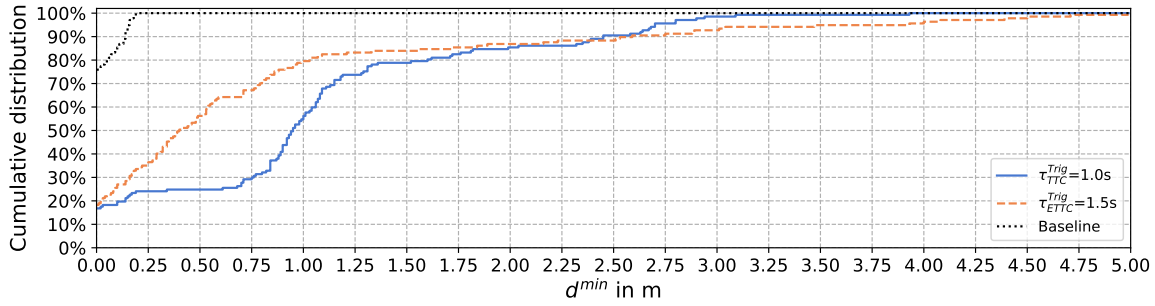

Figure 8.11.: Cumulative distribution of d^{min} in the baseline and the two treatments. The vertical axis represents the quantiles. Collisions are counted as zero values.

The capability of the safety systems to increase d^{min} and $\tau_{\mathrm{TTC,X}}^{\mathrm{min}}$ in dangerous situations is expressed by the metrics $E_{\mathrm{dist,50\,\%}}^{\mathrm{dang},TR}$ and $E_{\mathrm{TTC,50\,\%}}^{\mathrm{dang},TR}$. These metrics are represented in the cumulative distribution graphs in Figure 8.11 and Figure 8.12, by the values on the horizontal axis that correspond to the 50 %-mark (i.e., the median) on the vertical axis. If the corresponding value on the horizontal axis for a specific quantile (e.g., 50 % or 25 %) is higher for one of the system configurations, this indicates a higher safety benefit of this system configuration in comparison to the other.

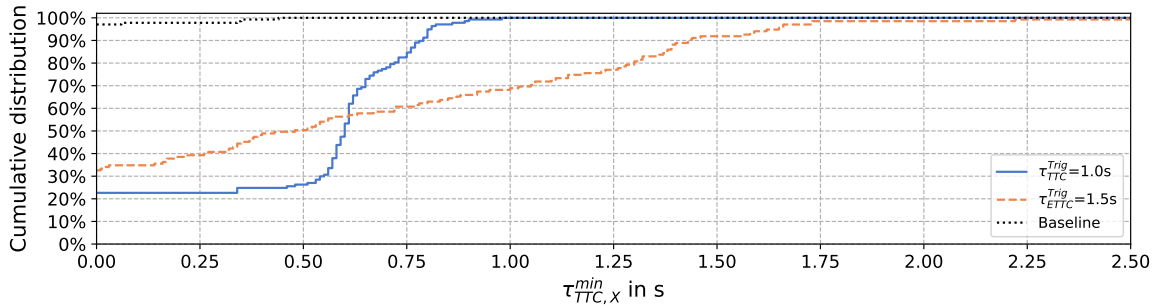

Figure 8.12.: Cumulative distribution of $\tau^{\text{min}}_{\text{TTC,X}}$ in the baseline and the two treatments. Collisions are counted as zero values.

As can be seen in Figure 8.11, the metric $E^{\text{dang},TR}_{\text{dist},50\,\%}$ was higher for system configuration 1 (0.95 m vs. 0.40 m), i.e., in 50 % of dangerous situations, system configuration 1 had a higher effectiveness in increasing the distance between conflict partners. One reason why $E^{\text{dang},TR}_{\text{dist},50\,\%}$ was lower for system configuration 2 is that this system triggers its braking maneuvers with only as much deceleration as is required to avoid a potential collision. This led to a "goal-braking" behavior that left only 1 m or less in around 80 % of dangerous situations.

Also the metric $E^{\text{dang},TR}_{\text{TTC},50\,\%}$ was higher for system configuration 1 (0.60 s vs. 0.48 s), i.e., system configuration 1 was better able to increase $\tau^{\text{min}}_{\text{TTC,X}}$ reached between the conflicts partners. However, the values $\tau^{\text{min}}_{\text{TTC,X}}(TR(s))$ were distributed over a notably larger range with system configuration 2, as can be seen by the flat increase of the corresponding curve in Figure 8.12, since $\tau_{\text{ETTC,X}}$, based on which configuration 2 triggered its maneuvers, is not necessarily correlated to $\tau_{\text{TTC,X}}$. Furthermore, in around 43 % of the dangerous situations, configuration 2 led to a higher $\tau^{\text{min}}_{\text{TTC,X}}$.

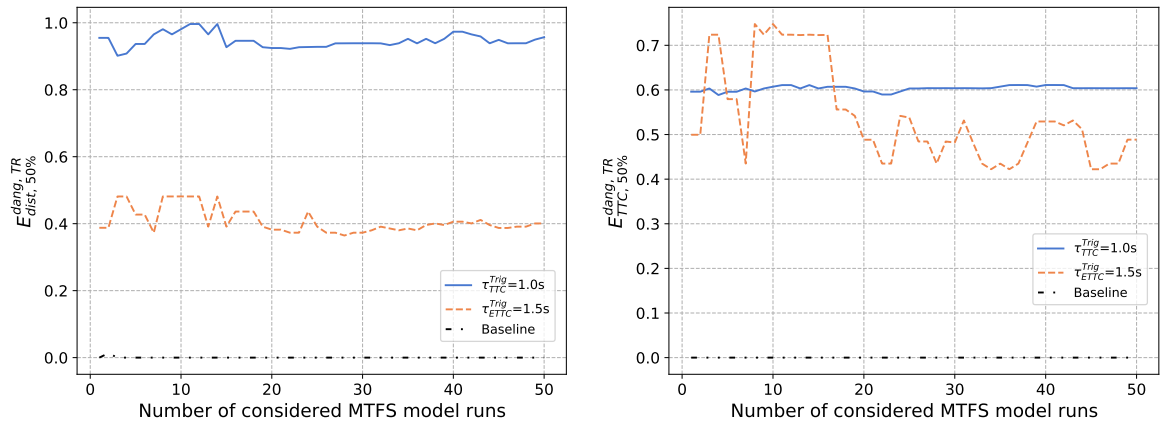

Figure 8.13.: Convergence of the metrics $E^{\text{dang},TR}_{\text{dist},50\,\%}$ (left) and $E^{\text{dang},TR}_{\text{TTC},50\,\%}$ (right) in dependence on the number of considered MTFS model runs, compared to the respective baseline metrics $E^{\text{dang},BL}_{\text{dist},50\,\%}$ and $E^{\text{dang},BL}_{\text{TTC},50\,\%}$.

In Figure 8.13 (left), it can be seen that the convergence of the metric $E^{\text{dang},TR}_{\text{dist},50\,\%}$ becomes stable for both system configurations after consideration of around 20 simulation runs of the MTFS model. Figure 8.13 (right) shows that the convergence of $E^{\text{dang},TR}_{\text{TTC},50\,\%}$ is reached

very early (below 10 MTFS model runs) for system configuration 1, while for configuration 2, the metric oscillates between 0.43 s to 0.53 s when considering between 20 to 50 MTFS model runs. The fact that the values $\tau^{\min}_{\mathrm{TTC},X}(TR(s))$ show a flat increase for configuration 2 (Figure 8.12, right) represents a possible explanation for the inferior convergence.

As a conclusion, system configuration 1 offered the better safety benefit in increasing $d^{\min}$. For the majority of cases, the analogous holds true for $\tau^{\min}_{\mathrm{TTC},X}$, but there were several situations where configuration 2 increased $\tau^{\min}_{\mathrm{TTC},X}$ to a higher degree. Since early convergence occurred, and since a difference in the metrics could be observed, the metrics are further discussed in the sensitivity analysis.

No comparable results for the effectiveness metrics $E^{\mathrm{dang},TR}_{\mathrm{dist},50\,\%}$ and $E^{\mathrm{dang},TR}_{\mathrm{TTC},50\,\%}$ can be found in the literature.

8.2.4. Effectiveness metrics related to the collision severity

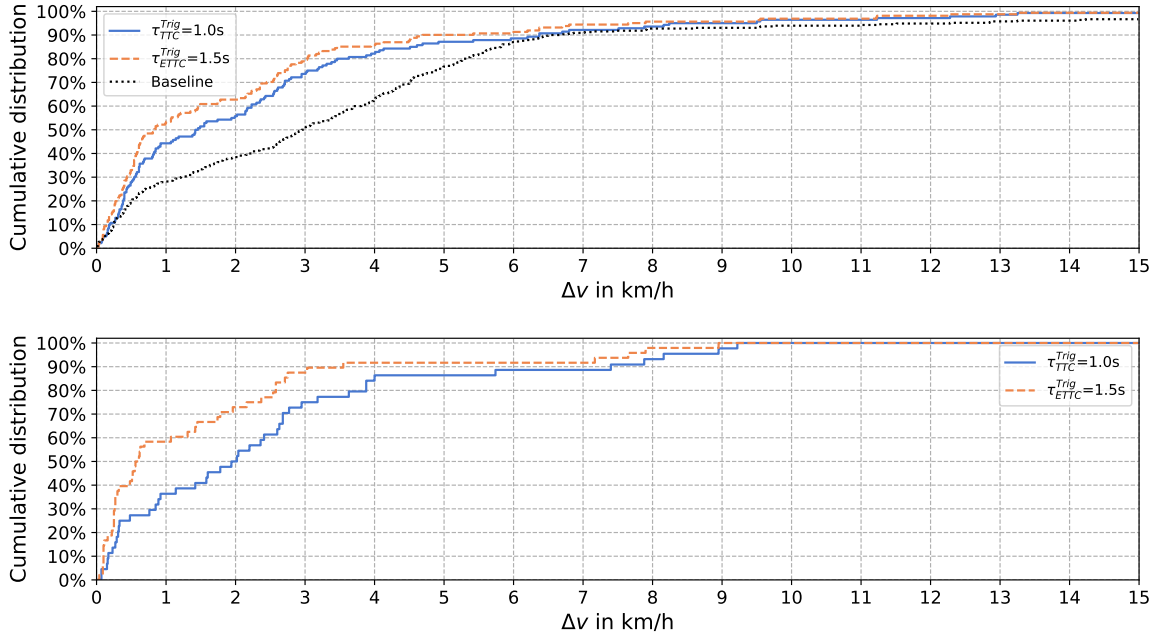

Figure 8.14.: Upper: Cumulative distribution of Δv for the baseline and the treatments. Lower: Cumulative distribution of Δv in the treatments in new collisions (i.e., a collision occurred in the treatment, but not in the baseline). The value on the horizontal axis corresponding to 50 % on the vertical axis represents the median, i.e., $E^{\mathrm{BL},50\,\%}_{\Delta v}$ and $E^{\mathrm{TR},50\,\%}_{\Delta v}$ in the upper figure, and $E^{\mathrm{new},50\,\%}_{\Delta v}$ in the lower figure.

When considering 50 MTFS model runs, there were 119 collisions in the treatment for system configuration 1, and 131 collisions in the treatment for configuration 2. The cumulative distribution graph of baseline values for Δv in Figure 8.14 (upper graph) shows that the largest proportion of collisions were of low severity (75 % of collisions had $\Delta v < 5\,\mathrm{km/h}$). The collisions that remained in the treatment, when using system configuration 2, were of lower severity than with system configuration 1 (0.8 km/h vs. 1.4 km/h). For the metric

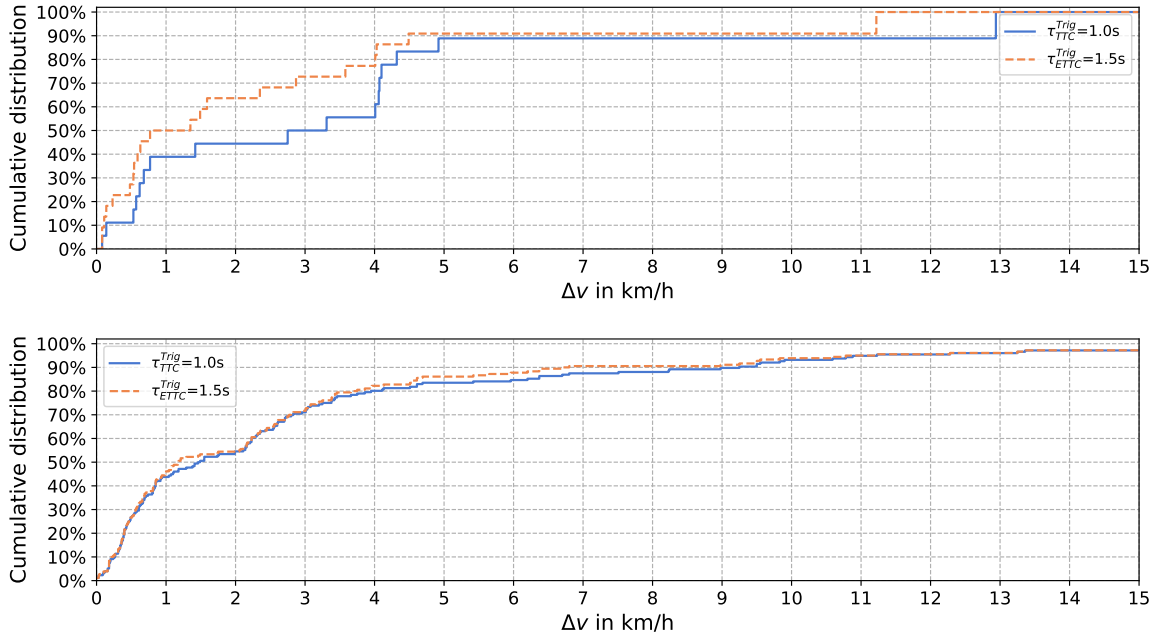

Figure 8.15.: Upper: Cumulative distribution of Δv in the treatments in changed collisions (i.e., the collision partners were different in the baseline and treatment). Lower: Cumulative distribution of Δv in the treatments in unchanged collisions (i.e., the collision partners remained the same in the baseline and treatment). The value on the horizontal axis corresponding to 50 % on the vertical axis represents the median, i.e., $E_{\Delta v}^{\mathrm{ch},50\,\%}$ in the upper figure, and $E_{\Delta v}^{\mathrm{unch},50\,\%}$ in the lower figure.

$E_{\Delta v}^{\mathrm{TR},50\,\%}$ and the other collision related metrics, lower values are better. Furthermore, the new collisions had a lower severity with system configuration 2 (0.6 km/h vs. 2.0 km/h, Figure 8.14, lower graph), as well as the changed collisions (1.1 km/h vs. 3.0 km/h, Figure 8.15, upper graph) and unchanged collisions (1.2 km/h vs. 1.5 km/h, Figure 8.15, lower graph).

The convergence behavior (see Figure 8.16) of the metrics $E_{\Delta v}^{\mathrm{TR},50\,\%}$, $E_{\Delta v}^{\mathrm{new},50\,\%}$, $E_{\Delta v}^{\mathrm{ch},50\,\%}$ and $E_{\Delta v}^{\mathrm{unch},50\,\%}$ was very unstable, even at high numbers of considered MTFS model runs. Thus, they are not further considered in the sensitivity study.

Not many studies exist in the literature that evaluate the change of Δv. In Kusano and Gabler, 2012, a prospective case-by-case simulation of 1 396 reconstructed rear-end collisions was conducted. They investigated three system configurations: FCW only (warning at $\tau_{\mathrm{TTC}}^{\mathrm{Trig}} = 1.7\,\mathrm{s}$), FCW with pre-crash brake assist (driver deceleration is doubled, starting at $\tau_{\mathrm{TTC}}^{\mathrm{Trig}} = 0.8\,\mathrm{s}$) and FCW combined with pre-crash brake assist and autonomous braking (starting at $\tau_{\mathrm{TTC}}^{\mathrm{Trig}} = 0.45\,\mathrm{s}$). They found that the configuration that includes the autonomous braking can avoid 7.7 % of the considered collisions, and can reduce the median Δv in the baseline (i.e., $E_{\Delta v}^{\mathrm{BL},50\,\%}$) from 17 km/h to 11.3 km/h in the treatment (i.e., $E_{\Delta v}^{\mathrm{TR},50\,\%}$). In Sander and Lubbe, 2018, where an AEB for straight crossing path accidents was investigated, it was found that the median Δv can be reduced from 19 km/h ($E_{\Delta v}^{\mathrm{BL},50\,\%}$) to 11 km/h to 13 km/h ($E_{\Delta v}^{\mathrm{TR},50\,\%}$). In the present thesis, the values $E_{\Delta v}^{\mathrm{BL},50\,\%} = 3.0\,\mathrm{km/h}$ and $E_{\Delta v}^{\mathrm{TR},50\,\%} = 1.4\,\mathrm{km/h}$ ($\tau_{\mathrm{TTC}}^{\mathrm{Trig}} = 1.0\,\mathrm{s}$) to $E_{\Delta v}^{\mathrm{TR},50\,\%} = 0.8\,\mathrm{km/h}$ ($\tau_{\mathrm{ETTC}}^{\mathrm{Trig}} = 1.5\,\mathrm{s}$) were identified. These values differ significantly to the literature results. The most fundamental difference is represented by

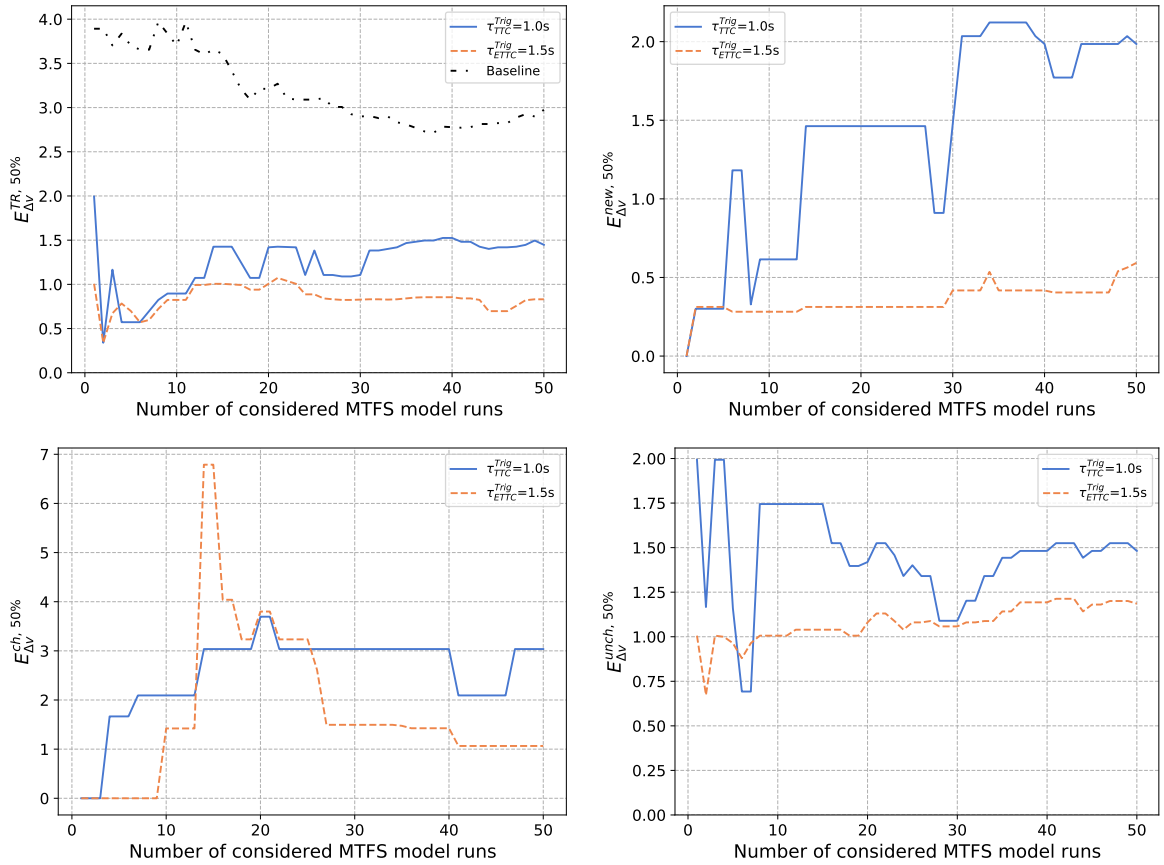

Figure 8.16.: Convergence of effectiveness metrics related to the collision severity in the treatment (upper left graph), in new collisions (upper right graph), in changed collisions (lower left graph) and unchanged collisions (lower right graph).

the fact, that reconstructed real accidents were used in the literature studies, while the collisions in this thesis were artifacts of the coupling approach. A further difference that has to be mentioned is that in Kusano and Gabler, 2012, the systems included a FCW system, which was not considered in this thesis. Furthermore, the system in Kusano and Gabler, 2012 activated the pre-crash brake assist or autonomous braking later ($\tau_{\mathrm{TTC}}^{\mathrm{Trig}} = 0.8\,\mathrm{s}$ and $\tau_{\mathrm{TTC}}^{\mathrm{Trig}} = 0.45\,\mathrm{s}$) than the systems investigated in this thesis. In addition, the collisions investigated in this thesis (230 in the baseline and around 130 in the treatments) were fewer and of considerably lower severity in the baseline, while 792 collisions were investigated in Sander and Lubbe, 2018, and 1 396 in Kusano and Gabler, 2012, leading to a higher statistical power of the results in the literature.

8.2.5. Summary of the convergence of effectiveness metrics

Table 8.5 summarizes the number of MTFS model runs that were required to achieve stable values for the effectiveness metrics. Metrics that use a fraction of the total number of conflicts as basis for the computation, or where the values used for their calculation show a high variance, showed in general a slower convergence than for example proportions of the

Effectiveness metric	*Number of model runs required to reach convergence*	*Effectiveness metric*	*Number of model runs required to reach convergence*
E_{corr}	< 10	$E_{\Delta v}^{\text{TR},50\,\%}$	> 50
$E_{\text{MCC}}^{\text{norm}}$	< 10	$E_{\Delta v}^{\text{new},50\,\%}$	> 50
E_{sens}, E_{spec}	< 10	$E_{\Delta v}^{\text{ch},50\,\%}$	> 50
E_{TP}, E_{FP}, E_{TN}, E_{TN}	< 10	$E_{\Delta v}^{\text{unch},50\,\%}$	> 50
E_{new}	30	$E_{\text{dist},50\,\%}^{\text{dang},TR}$	20
E_{av}	20	$E_{\text{TTC},50\,\%}^{\text{dang},TR}$	20 to 50
E_{unch}	20		
E_{ch}	20		

Table 8.5.: This table shows the number MTFS of model runs that were required to reach convergence in various effectiveness.

total considered conflicts, such as E_{corr}. In particular, slow convergence can be observed for metrics related to the collision severity within collision partner configurations ($E_{\Delta v}^{\text{new},50\,\%}$, $E_{\Delta v}^{\text{ch},50\,\%}$, $E_{\Delta v}^{\text{unch},50\,\%}$ or $E_{\Delta v}^{\text{TR},50\,\%}$). Therefore, collision related metrics will not be investigated further.

8.3. Conclusions

The following conclusions were found when analyzing the results for the effectiveness metrics:

- To achieve convergence of the metrics related to system responses ($E_{\text{MCC}}^{\text{norm}}$, E_{corr}, E_{sens}, E_{spec}, E_{TP}, E_{FP}, E_{TN} and E_{TN}), the metrics related to the change in minimum distances and the TTC ($E_{\text{dist},50\,\%}^{\text{dang},TR}$ and $E_{\text{TTC},50\,\%}^{\text{dang},TR}$) and several of the metrics related to the avoidance potential and changes in collision partner configurations (E_{av}, E_{unch} and E_{ch}), 20 MTFS model runs are considered to be sufficient.
- The convergence of metrics that express the collision severity in collision partner configuration groups ($E_{\Delta v}^{\text{TR},50\,\%}$, $E_{\Delta v}^{\text{new},50\,\%}$, $E_{\Delta v}^{\text{ch},50\,\%}$ and $E_{\Delta v}^{\text{unch},50\,\%}$) was unstable even when considering 50 MTFS model runs. The system that triggers at $\tau_{\text{ETTC}}^{\text{Trig}} = 1.5\,\text{s}$ led to slightly lower (better) values for those metrics.
- The system that triggers based on $\tau_{\text{TTC}}^{\text{Trig}} = 1.0\,\text{s}$ triggers in more situations (8.7 % vs. 6.4 %) than the system that triggers at $\tau_{\text{ETTC}}^{\text{Trig}} = 1.5\,\text{s}$.
- The number of conflicts where the system response was categorized as "true positive" was equal for both configurations, but the system that triggers at $\tau_{\text{ETTC}}^{\text{Trig}} = 1.5\,\text{s}$ produced only half as many false positive responses (4.7 % vs. 2.4 %), which also led to a higher specificity E_{spec} (97.4 % vs. 95.0 %) and Matthew's correlation coefficient $E_{\text{MCC}}^{\text{norm}}$ (84.5 % vs. 79.0 %).

- The system that triggers based on $\tau_{\mathrm{TTC}}^{\mathrm{Trig}} = 1.0\,\mathrm{s}$ avoids slightly more collisions (57.8 % vs. 56.1 %) in the baseline that occurred between either conflict participants or a conflict participant and surrounding traffic.
- The system that triggers based on $\tau_{\mathrm{ETTC}}^{\mathrm{Trig}} = 1.5\,\mathrm{s}$ (4.8 %) led to slightly more changed collisions than the system that triggers at $\tau_{\mathrm{ETTC}}^{\mathrm{Trig}} = 1.5\,\mathrm{s}$(3.9 %).
- The goal braking behavior as consequence of using $a_{\mathrm{requested}} = a_{\mathrm{required}}^{\mathrm{adj}}$ for the system that triggers at $\tau_{\mathrm{ETTC}}^{\mathrm{Trig}} = 1.5\,\mathrm{s}$ led to a lower median of the minimum distance reached between the conflict participants in the treatment (0.95 m with $\tau_{\mathrm{TTC}}^{\mathrm{Trig}} = 1.0\,\mathrm{s}$ vs. 0.40 m with $\tau_{\mathrm{ETTC}}^{\mathrm{Trig}} = 1.5\,\mathrm{s}$). The same holds true for the median of the minimum TTC (0.60 s with $\tau_{\mathrm{TTC}}^{\mathrm{Trig}} = 1.0\,\mathrm{s}$ vs. 0.48 s with $\tau_{\mathrm{ETTC}}^{\mathrm{Trig}} = 1.5\,\mathrm{s}$), but the system that triggers at $\tau_{\mathrm{ETTC}}^{\mathrm{Trig}} = 1.5\,\mathrm{s}$ led to several situations where the benefit in increasing the minimum TTC was higher than for the system that triggers at $\tau_{\mathrm{TTC}}^{\mathrm{Trig}} = 1.0\,\mathrm{s}$.
- Since the accident avoidance potential and the reduction in collision severity are similar, the system that triggers at $\tau_{\mathrm{ETTC}}^{\mathrm{Trig}} = 1.5\,\mathrm{s}$ would be preferred for implementation in real vehicles as it led only to half as many false positive system responses in conflicts with $\tau_{\mathrm{TTC,S}}^{\mathrm{min}} \leq 1.7\,\mathrm{s}$.

9. Sensitivity study

Sensitivity study	*Variations*
Variation in the traffic density in the MTFS model	WBE and WBE50 for scenario generation
Variation in the conflict filter threshold for scenario catalog definition	$\tau_{\mathrm{TTC}}^{\mathrm{Filt}} = 0.5\,\mathrm{s}$ to $\tau_{\mathrm{TTC}}^{\mathrm{Filt}} = 2.5\,\mathrm{s}$, in steps of 0.1 s
Variation in the presence of static objects and surrounding traffic	Variation 1: all visibility obstructions, variation 2: without static objects, variation 3: without static objects and without traffic participants in P_{close}
Variation in the look-ahead time of the kinetic path driver model	$t_{\mathrm{LA}} = 0.6\,\mathrm{s}$, $t_{\mathrm{LA}} = 0.9\,\mathrm{s}$ and $t_{\mathrm{LA}} = 1.2\,\mathrm{s}$
Variation in the simulated time before and after $t_{\tau_{\mathrm{TTC}}^{\mathrm{min}}}$	5 s, 3.5 s and 2 s

Table 9.1.: The conducted sensitivity studies and the investigated parameter variations.

The goal of this chapter is to identify the sensitivity of the effectiveness metrics in dependence on specific influencing factors. The focus lies on influencing factors that are specific to the effectiveness assessment methodology which is presented in this thesis, and includes variations in the scenario generation (MTFS model WBE vs. WBE50), scenario catalog definition (filtering with different values for $\tau_{\mathrm{TTC}}^{\mathrm{Filt}}$) and scenario representation step (with and without presence of visibility obstructions, variation of the look-ahead time for the kinetic path driver model, variation of the simulated time frame before and after $t_{\tau_{\mathrm{TTC}}^{\mathrm{min}}}$). These influencing factors were identified in the previous chapters. The influencing factors and the investigated variations are summarized in Table 9.1.

As a basis for comparison, the baseline established in Chapter 7 and the exemplary effectiveness study presented in chapter 8 are evaluated considering only the first 20 MTFS model runs of the 50 MTFS model runs that were originally used for the exemplary effectiveness study. For each variation of an influencing factor, the same system configurations are simulated as for the exemplary effectiveness study, and the effectiveness metrics that are related to the avoidance potential (E_{av}, E_{ch} and E_{unch}), the system responses ($E_{\mathrm{MCC}}^{\mathrm{norm}}$, E_{corr}, E_{sens}, E_{spec}, E_{TP}, E_{FP}, E_{TN} and E_{TN}) and the change in d^{min} and $\tau_{\mathrm{TTC,X}}^{\mathrm{min}}$ ($E_{\mathrm{dist,\,50\,\%}}^{\mathrm{dang},\,TR}$ and $E_{\mathrm{TTC,\,50\,\%}}^{\mathrm{dang},\,TR}$) are evaluated and compared to the comparison basis.

9.1. Variation in the traffic density in the MTFS model

9.1.1. Objective and method

In this section, as a variation of the exemplary effectiveness study, the MTFS model WBE is replaced by the version WBE50, where the traffic density in the road section "Wickenburggasse" is increased by 50 %, to determine the influence of the traffic density at the selected road site on the effectiveness metrics. As listed in the conclusions in Section 6.3, the main consequences of the increased traffic density in the model WBE50 were an increase of 7.4 % in the total conflicts after filtering compared to WBE, a proportional increase in conflicts with $\tau_{\mathrm{TTC,S}}^{\mathrm{min}} \leq 1.2\,\mathrm{s}$ and an increase in crossing conflicts by 27.6 %.

9.1.2. Results and discussion

9.1.2.1. System response categories and related metrics

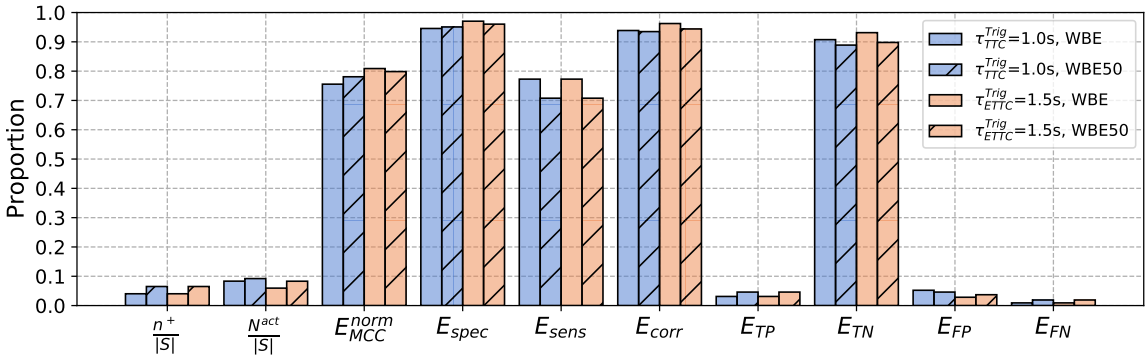

Figure 9.1.: Metrics related to the system response categories (false/true positive/negative), the proportion $\frac{n^+}{|S|}$ of dangerous baseline situations in the number of concrete scenarios in the scenario catalog S, and the proportion $\frac{N^{\mathrm{act}}}{|S|}$ of system activations in $|S|$.

Figure 9.1 shows that exchanging the MTFS model WBE by the model WBE50 with increased traffic density led to an increase of dangerous situations ($\frac{n^+}{|S|}$, 4.0 % vs. 6.5 % of the respective total conflicts). Consequently, also the proportion of conflicts with activations increased by 0.9 % for configuration 1 ($\tau_{\mathrm{TTC}}^{\mathrm{Trig}} = 1.0\,\mathrm{s}$) and by 2.3 % for configuration 2 ($\tau_{\mathrm{ETTC}}^{\mathrm{Trig}} = 1.5\,\mathrm{s}$). The increase in activations for both configurations occurred due to a higher percentage of crossing conflicts. In particular for configuration 2, several false positive activations occurred in those crossing conflicts, such as in the situation shown in Figure 9.2. In this case, as well as in several other crossing conflicts, the active safety system of the blue vehicle triggered a braking maneuver, since at some point of the turning maneuver of the red vehicle, a collision course existed that also fulfilled the other conditions necessary for triggering. The blue vehicle did not decelerate, leading to τ_{ETTC} and $\tau_{\mathrm{TTC,X}}$ being equal and the τ_{ETTC} did fall below 1.5 s, but not below 1.0 s. Hence, the system with configuration 2 activated a braking maneuver, but the system with configuration 1 did not. Therefore, for

such crossing conflicts, considering the acceleration in the calculation of τ_{ETTC} for system configuration 2 did not provide an advantage over configuration 1 in terms of E_{FP}. The higher threshold did therefore lead to an earlier activation. A solution for real vehicles is to employ collision detection algorithms, which are capable of detecting, tracking and predicting turning behavior of other vehicles to avoid system activations such as the one in the discussed situation.

All the changes in the other metrics are consequences of the increased number of false positive activations.

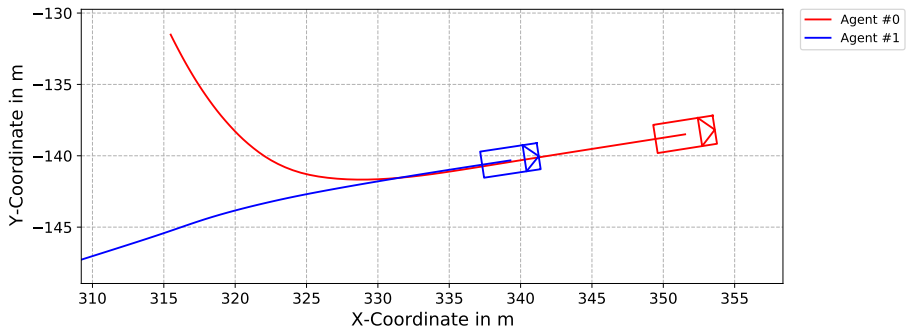

Figure 9.2.: A crossing conflict (baseline), where the red vehicle (agent #0) turns into the same lane as the blue vehicle (agent #1). In the treatment, the safety system in the blue vehicle detected a collision course and triggered a braking maneuver with system configuration 2.

9.1.2.2. Accident avoidance rates and changes in collision partners

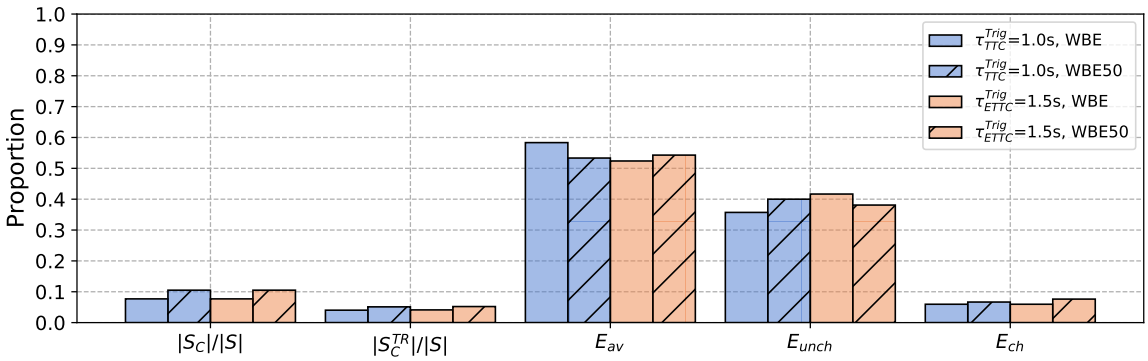

Figure 9.3.: The proportions of baseline ($|S_C|/|S|$) and treatment ($|S_C^{TR}|/|S|$) collisions and metrics related to collision avoidance and the change of collision partner configurations.

As can be seen in Figure 9.3, the proportional number of collisions in the baseline $|S_C|/|S|$ increased when using the MTFS model WBE50 instead of WBE (10.5 % for WBE50 vs. 7.7 % for WBE, representing an increase by 25 %). A possible explanation is the increase in conflicts with lower $\tau_{\mathrm{TTC,S}}^{\mathrm{min}}$, i.e., an increase in conflicts with higher severity. Furthermore, on average, more vehicles in WBE50 (on average 11.7) than in WBE (on average 10.2) matched the filter criteria explained in Section 7.1.2.2 to generate the list of traffic participants to be considered

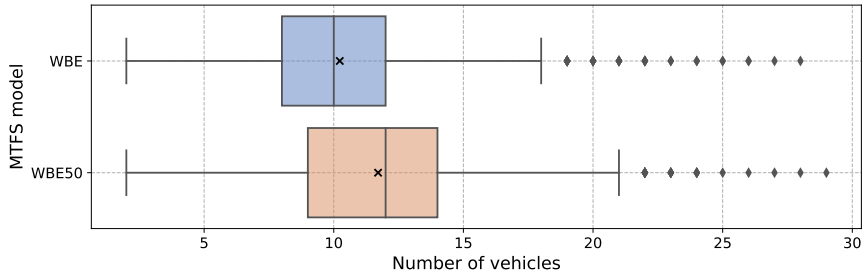

Figure 9.4.: Boxplots of the number of vehicles that were considered in nanoscopic simulation of individual conflicts, comparing WBE and WBE50.

in nanoscopic simulation, see Figure 9.4, which led to more opportunities for collision events to occur.

The proportion $|S_C^{TR}|/|S|$ of collisions in the treatment increased by around 1 % (around 5 % for WBE50 vs. around 4 % for WBE). A difference can be observed for the accident avoidance potential E_{av} (58.3 % for WBE vs. 53.3 % for WBE50 with configuration 1, and 52.4 % for WBE vs. 54.3 % for WBE50 with configuration 2) and the related metrics E_{unch} (35.7 % for WBE vs. 40.0 % for WBE50 with configuration 1, and 41.7 % for WBE vs. 38.1 % for WBE50 with configuration 2) and E_{ch} (6.0 % for WBE vs. 6.7 % for WBE50 with configuration 1, and 6.0 % for WBE vs. 7.6 % for WBE50 with configuration 2), see Figure 9.3. However, since these metrics varied in the exemplary effectiveness study in a corridor of around 5 % even at a higher number of considered MTFS model runs (more than 30), the differences are considered to not be significant, i.e., the increase in the traffic density did not have an impact on the collision avoidance potential.

9.1.2.3. Changes in minimum TTC and minimum distances

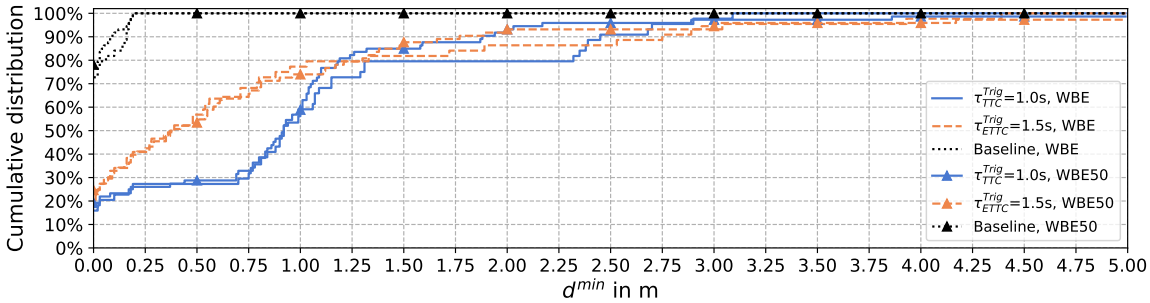

Figure 9.5.: Cumulative distribution of d^{min} in the baseline and the two treatments. The vertical axis represents the quantiles. Collisions are counted as zero values.

The metric $E_{\text{dist},50\,\%}^{\text{dang},TR}$ remained on a very similar level when exchanging the MTFS model WBE by WBE50: for configuration 1, it remained at 0.92 m, and for configuration 2, it changed from 0.37 m to 0.39 m, see Figure 9.5. The analogous holds true for the metric $E_{\text{TTC},50\,\%}^{\text{dang},TR}$, which was changed from 0.58 s to 0.60 s for configuration 1 and from 0.43 s to

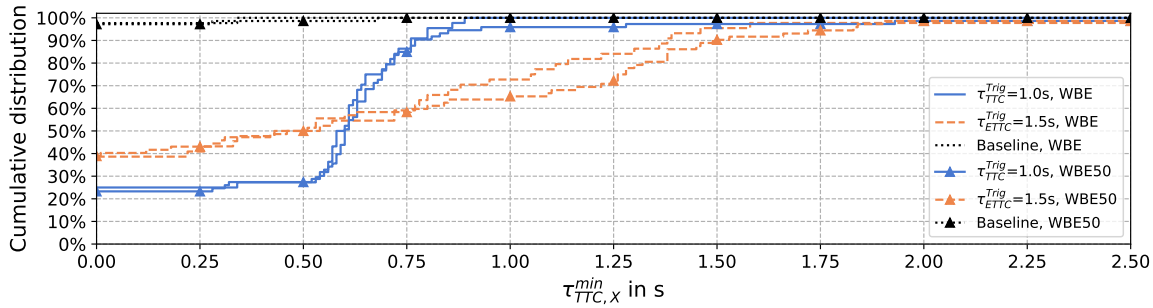

Figure 9.6.: Cumulative distribution of $\tau^{\text{min}}_{\text{TTC,X}}$ in the baseline and the two treatments. Collisions are counted as zero values.

0.46 s for configuration 2 (less than 0.03 s difference). A difference in d^{min} between the MTFS models can be seen only for the upper quantiles. For example, in around 30 % of the cases, the systems were able to leave more distance between the conflict partners when using WBE compared to WBE50. The situation was reversed for $\tau^{\text{min}}_{\text{TTC,X}}$, since system configuration 2 in particular led to higher values for $\tau^{\text{min}}_{\text{TTC,X}}$ in the treatment, when using WBE50. This indicates that for most situations, the safety benefit remains on the same level regarding $\tau^{\text{min}}_{\text{TTC,X}}$, while for a certain proportion of the situations, the safety benefit was higher when the traffic density is higher, i.e., when more conflicts with a higher severity (lower TTC) occur.

9.1.3. Conclusions

The following conclusions regarding the effect on the effectiveness results were found when the MTFS model WBE is replaced by WBE50:

- For system configuration 2 ($\tau^{\text{Trig}}_{\text{ETTC}} = 1.5\,\text{s}$), i.e., for the system that triggers at $\tau^{\text{Trig}}_{\text{ETTC}} = 1.5\,\text{s}$, a higher proportion of conflicts with false positive activations ($E_{\text{FP}} = 3.7\,\%$ for WBE50 vs. $E_{\text{FP}} = 2.8\,\%$) occurred when using the model WBE50. In particular, this is the case for crossing conflicts, of which more occurred in WBE50. For several crossing conflicts, using τ_{ETTC} as trigger criterion offered no benefit regarding E_{FP} and related metrics. This increase in false positive activations represents the aspect of the effectiveness where the increase in traffic density had the largest impact.
- The increased traffic density led to more vehicles (on average, 11.7 vehicles for WBE50 and 10.2 vehicles for WBE) being considered per conflict in nanoscopic simulation and a proportional increase of collision events in the baseline (25 % increase) and treatment (16 % increase for both system configurations).
- No significant change in the avoidance potential E_{av}, E_{unch} or E_{ch} could be observed when the traffic density is increased. A significant change is thereby understood in the sense that the differences are lower than the variation of the metrics in the exemplary effectiveness study.

- No significant change in $E^{\text{dang},TR}_{\text{dist},50\,\%}$ and $E^{\text{dang},TR}_{\text{TTC},50\,\%}$ could be observed when increasing the traffic density, although higher values for $\tau^{\text{min}}_{\text{TTC,X}}$ and lower values for d^{min} could be observed in the upper quantiles (e.g., 75 %) when using the model WBE50.

The results suggest, that for the investigated traffic site and represented time of day (morning peak hour), the traffic density is of minor influence on most of the effectiveness metrics.

9.2. Variation in the conflict filter threshold for scenario catalog definition

9.2.1. Objective and method

For the exemplary effectiveness study, the threshold $\tau^{\text{Filt}}_{\text{TTC}} = 1.7\,\text{s}$ was used as a filter to identify the conflicts to form the scenario catalog, i.e., only conflicts that fulfill the condition $\tau^{\text{min}}_{\text{TTC,S}} \leq 1.7\,\text{s}$ were considered. Since $\tau^{\text{Filt}}_{\text{TTC}}$ is a parameter which is specific for the method presented in this thesis, the consequences of choosing different values (from 0.5 up to 2.5 s) are investigated in this section.

To investigate the influence of $\tau^{\text{Filt}}_{\text{TTC}}$, the baseline and both treatments (with the same system configurations as in the previous sections) are simulated for all conflicts up to $\tau^{\text{Filt}}_{\text{TTC}} = 2.5\,\text{s}$, which was the maximum of values for $\tau^{\text{min}}_{\text{TTC,S}}$, among the conflicts included in the analysis by SSAM. As input, the first 20 simulation runs that were simulated for the MTFS model WBE were used. To investigate the influence of $\tau^{\text{Filt}}_{\text{TTC}}$ on the effectiveness metrics, the value of $\tau^{\text{Filt}}_{\text{TTC}}$ is increased in steps of 0.1 s from 0.5 s up to a maximum value of 2.5 s. For each increase of $\tau^{\text{Filt}}_{\text{TTC}}$, the number of conflicts considered in the scenario catalog increases, and for each such newly defined scenario catalog, the effectiveness metrics are recalculated. Filtering with the highest value $\tau^{\text{Filt}}_{\text{TTC}} = 2.5\,\text{s}$ led to 2 607 conflicts in total, representing an increase by the factor 2.39 compared to filtering with $\tau^{\text{Filt}}_{\text{TTC}} = 1.7\,\text{s}$. The dependence of the effectiveness metrics on $\tau^{\text{Filt}}_{\text{TTC}}$ is then visualized in graphs with the threshold $\tau^{\text{Filt}}_{\text{TTC}}$ on the horizontal axis and the metrics on the vertical axis. The following aspects are investigated in the following subsections:

- How the activations of the safety systems correlated with $\tau^{\text{min}}_{\text{TTC,S}}$ and the influence of $\tau^{\text{Filt}}_{\text{TTC}}$ on effectiveness metrics related to the system response categories.
- The influence of $\tau^{\text{Filt}}_{\text{TTC}}$ on the number of collision events in the baseline and treatment and on the effectiveness metrics related change of collision partner categories.
- The influence of $\tau^{\text{Filt}}_{\text{TTC}}$ on effectiveness metrics related to the change of d^{min} and $\tau^{\text{min}}_{\text{TTC}}$ in dangerous situations.

9.2.2. Results and discussion

9.2.2.1. System response categories and related metrics

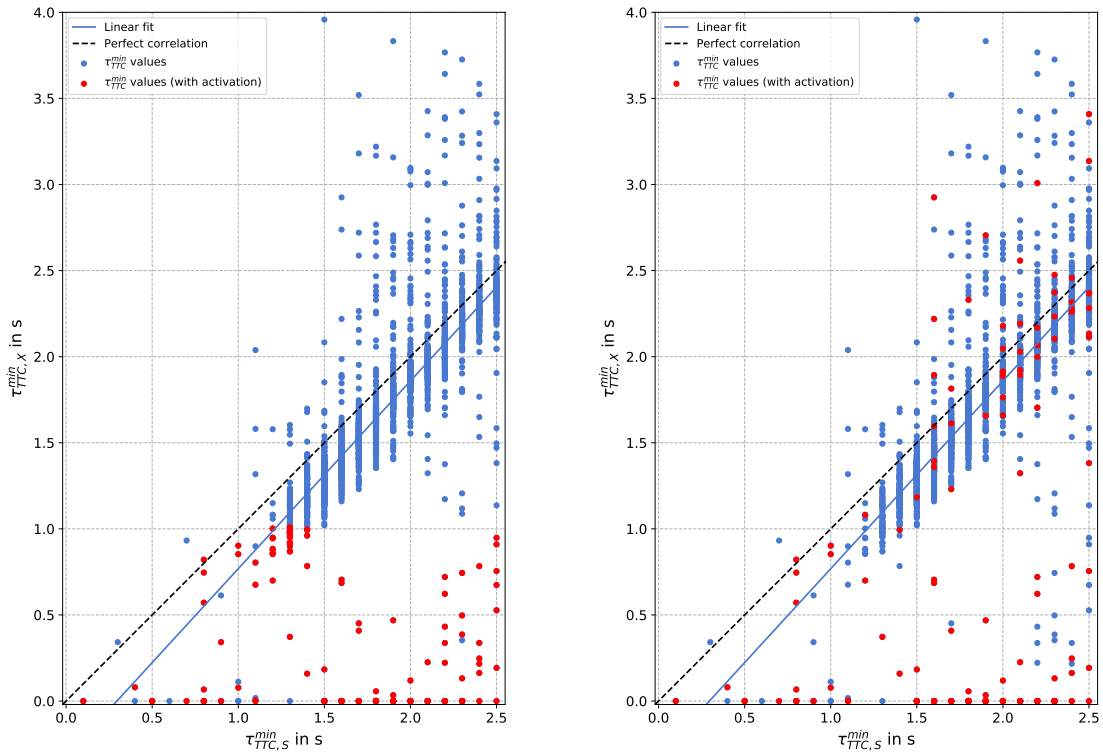

Figure 9.7.: Correlation of $\tau^{\text{min}}_{\text{TTC,S}}$ detected by SSAM (horizontal axis) and $\tau^{\text{min}}_{\text{TTC,X}}$ (vertical axis) between the conflict participants as it was detected by X-RATE in the baseline. The conflicts where a system activated an emergency maneuver are marked red. The black dashed line shows perfect correlation, while the blue line shows a linear regression fit with $\tau^{\text{min}}_{\text{TTC,X}} = 1.09\,\tau^{\text{min}}_{\text{TTC,S}} - 0.32$ and correlation coefficient $r_{corr} = 0.45$. Left: system activations (red markers) for system configuration 1 with $\tau^{\text{Trig}}_{\text{TTC}} = 1.0\,\text{s}$. Right: system activations (red markers) for system configuration 2 with $\tau^{\text{Trig}}_{\text{ETTC}} = 1.5\,\text{s}$.

To investigate in which conflicts an activation of a safety system occurred, in dependence of $\tau^{\text{min}}_{\text{TTC,S}}$, the values of $\tau^{\text{min}}_{\text{TTC,S}}$ are compared in Figure 9.7 to the values of $\tau^{\text{min}}_{\text{TTC,X}}$, detected by X-RATE in nanoscopic simulation. The conflicts where the systems activated for the other conflict participant are marked red. The conflicts on the line $\tau^{\text{min}}_{\text{TTC,X}} = 0$ were collision events, since the TTC between the colliding vehicles is 0. In Figure 9.7 (left), the activations for system configuration 1 with $\tau^{\text{Trig}}_{\text{TTC}} = 1.0\,\text{s}$ are marked. It can be seen that the system with configuration 1 activated in almost all of the conflicts with $\tau^{\text{min}}_{\text{TTC,X}} \leq 1.0\,\text{s}$, as could be expected. In some conflicts with $\tau^{\text{min}}_{\text{TTC,X}} \leq 1.0\,\text{s}$, even on the line $\tau^{\text{min}}_{\text{TTC,X}} = 0$, there was no activation - these are conflicts with false negative system responses. An example for such a conflict is when the driver tried to change to a lane where another vehicle was present. In such lane change conflicts, it can occur that for each of both involved vehicles, the other vehicles is not fully in the sensors' fields of view, leading to a false negative system response (see Section 8.2.1). Furthermore, there were also activations in conflicts with $\tau^{\text{min}}_{\text{TTC,S}} \geq 1.0\,\text{s}$. However, as can be seen in Figure 9.8, the proportion of conflicts with activations, evaluated for the intervals $e_r - 0.1 \leq \tau^{\text{min}}_{\text{TTC,S}} < e_r$, stabilized at around 5 % to 10 %,

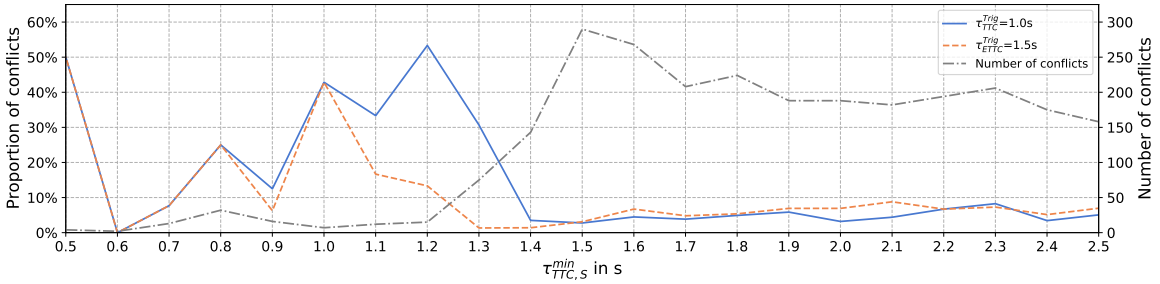

Figure 9.8.: This figure shows, in steps of 0.1 s for the interval boundaries e_r, the number of conflicts in which a safety system activated for a conflict participant and for which $e_r - 0.1 \leq \tau^{\text{min}}_{\text{TTC,S}} < e_r$ holds, divided by the total number of conflicts in the intervals $e_r - 1 \leq \tau^{\text{min}}_{\text{TTC,S}} < e_r$ (left horizontal axis labels). The total number of conflicts in each interval is shown by the axis labels on the right horizontal axis.

starting at $\tau^{\text{min}}_{\text{TTC,S}} = 1.4\,\text{s}$, i.e., such activations in conflicts with higher values for $\tau^{\text{min}}_{\text{TTC,S}}$ took place only in a small percentage of conflicts. This leads to the conclusion that, for systems based on a $\tau^{\text{min}}_{\text{TTC,X}}$ threshold, although system activations become less common, the higher $\tau^{\text{min}}_{\text{TTC,S}}$ is in a given conflict, $\tau^{\text{min}}_{\text{TTC,S}}$ does not allow perfect prediction whether a safety system will activate or not in a specific conflict. This is due to the existing difference between the τ_{TTC} calculation algorithms in SSAM and X-RATE and due to the kinetic path driver model in nanoscopic simulation. The activations with system configuration 2, based on τ_{ETTC}, took place at a broad range of $\tau^{\text{min}}_{\text{TTC,X}}$ reached during the conflicts, see Figure 9.7 (right). This suggests that for the system based on the τ_{ETTC} threshold, prediction of activations is even more difficult by considering $\tau^{\text{min}}_{\text{TTC,S}}$.

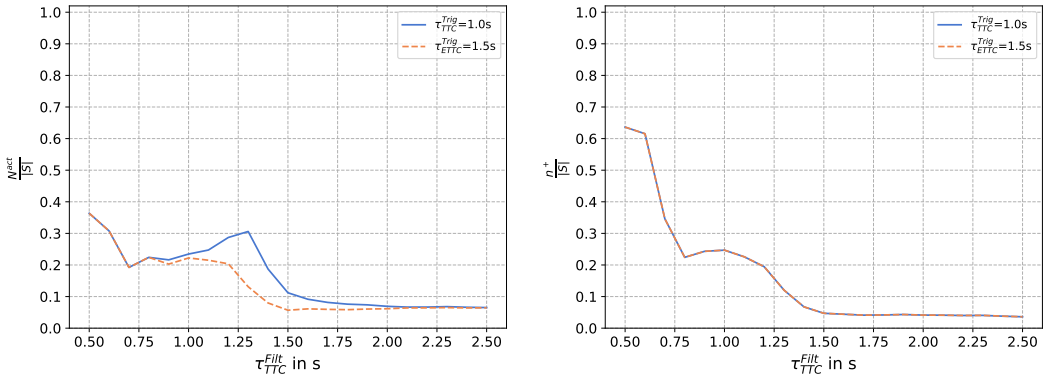

Figure 9.9.: Left: proportion $\frac{N^{\text{act}}}{|S|}$ of conflicts with system activations in the total number of conflicts with $\tau^{\text{min}}_{\text{TTC,S}} \leq \tau^{\text{Filt}}_{\text{TTC}}$. Right: proportion $\frac{n^+}{|S|}$ of conflicts with objective objective danger in the total number of conflicts with $\tau^{\text{min}}_{\text{TTC,S}} \leq \tau^{\text{Filt}}_{\text{TTC}}$.

When filtering with $\tau^{\text{Filt}}_{\text{TTC}}$ less than around 2.0 s, system configuration 1 ($\tau^{\text{Trig}}_{\text{TTC}} = 1.0\,\text{s}$) triggered in proportionally more conflicts $\tau^{\text{min}}_{\text{TTC,S}} \leq \tau^{\text{Filt}}_{\text{TTC}}$ than configuration 2 ($\tau^{\text{Trig}}_{\text{ETTC}} = 1.5\,\text{s}$), see $\frac{N^{\text{act}}}{|S|}$ in Figure 9.9 (left). Finally, with $\tau^{\text{Filt}}_{\text{TTC}} \leq 2.0\,\text{s}$, this proportion stabilized at around 6.4 % (168 of 2607 conflicts at $\tau^{\text{Filt}}_{\text{TTC}} = 2.5\,\text{s}$) for both system configurations. In contrast, the proportion $\frac{n^+}{|S|}$ of dangerous situations that occurred, stabilized when filtering with values 1.5 s to 2.5 s for $\tau^{\text{Filt}}_{\text{TTC}}$ and reached a value of 3.6 % with $\tau^{\text{Filt}}_{\text{TTC}} = 2.5\,\text{s}$ (94 of 2607 conflicts), see

Figure 9.9 (right).

A stable proportion E_{TP} of around 3.1 % of the total conflicts was classified as true positive when filtering with $\tau_{\mathrm{TTC}}^{\mathrm{Filt}} = 2.5\,\mathrm{s}$ for both system configurations (82 true positive responses for both system configurations, see Figure 9.10, upper left), while a stable proportion E_{FP} of around 3.4 % of the total conflicts was classified as false positive when filtering with $\tau_{\mathrm{TTC}}^{\mathrm{Filt}} = 2.5\,\mathrm{s}$ for both system configurations (88 for configuration 1 and 86 for configuration 2), see Figure 9.10 (upper right). Regrading the proportion E_{FP} of conflicts with false positive activations, system configuration 2 ($\tau_{\mathrm{ETTC}}^{\mathrm{Trig}} = 1.5\,\mathrm{s}$) performed better by activating in less conflicts where it was not necessary to activate, for conflicts with $0.75\,\mathrm{s} \leq \tau_{\mathrm{TTC,S}}^{\mathrm{min}} \leq 2.0\,\mathrm{s}$. Consequently, the proportion E_{TN} in the total conflicts was better (higher) for system configuration 2, see Figure 9.10 (lower left), while it stabilized at $\tau_{\mathrm{TTC}}^{\mathrm{Filt}} = 2.5\,\mathrm{s}$ at around 93 % for both configurations (2425 of 2607 conflicts). The proportion E_{FN} of false negative system responses converged to around 0.5 % (12 out of 2607 conflicts for both system configurations) at $\tau_{\mathrm{TTC}}^{\mathrm{Filt}} = 2.5\,\mathrm{s}$.

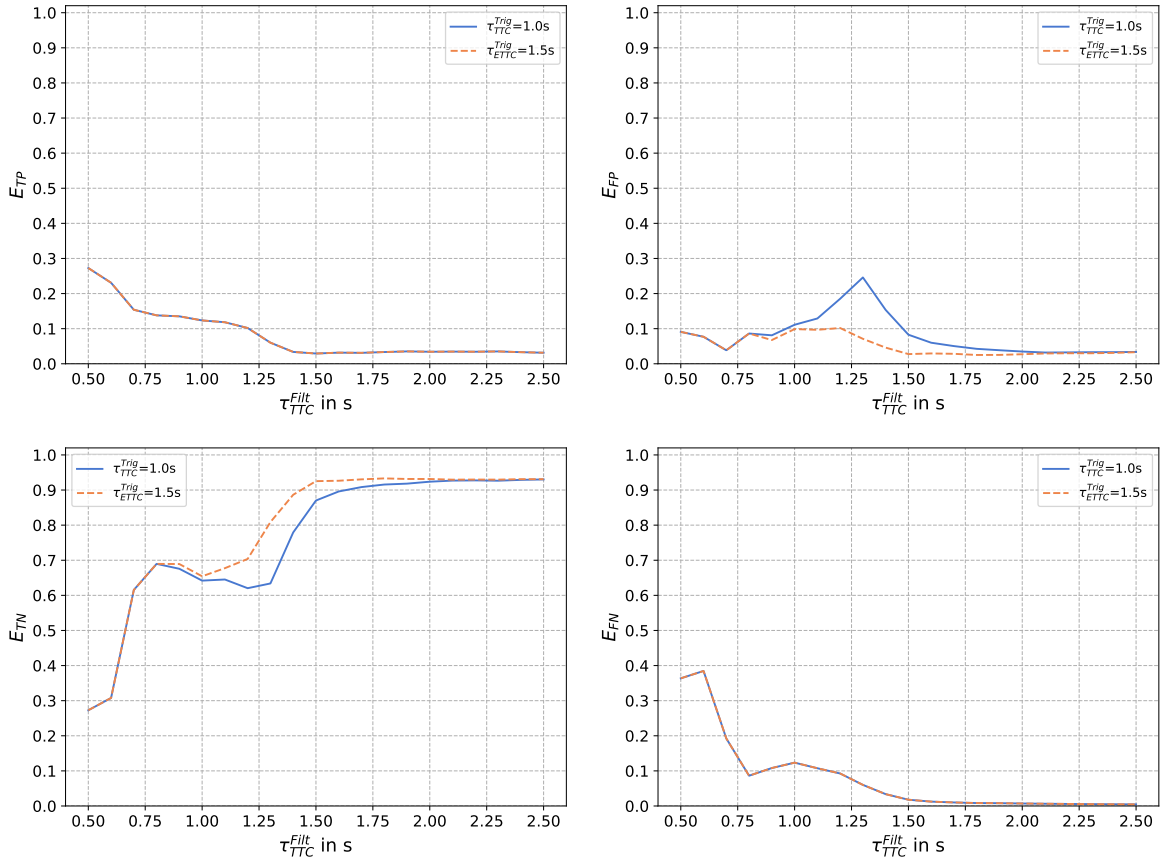

Figure 9.10.: Upper left and right: E_{TP}, respectively E_{FP}. Lower left and right: E_{TN}, respectively E_{FN}. The metrics were computed based on all conflicts with $\tau_{\mathrm{TTC,S}}^{\mathrm{min}} \leq \tau_{\mathrm{TTC}}^{\mathrm{Filt}}$.

The proportion of true positive responses E_{TP} and false negative responses E_{FN} remained on a very similar level for any value of $\tau_{\mathrm{TTC}}^{\mathrm{Filt}}$. Furthermore, since E_{FN} and E_{FP} did not converge to 0, there remained a certain proportion of conflicts that are persistently treated incorrectly. Examples for such consistently incorrectly treated situations are crossing conflicts, where

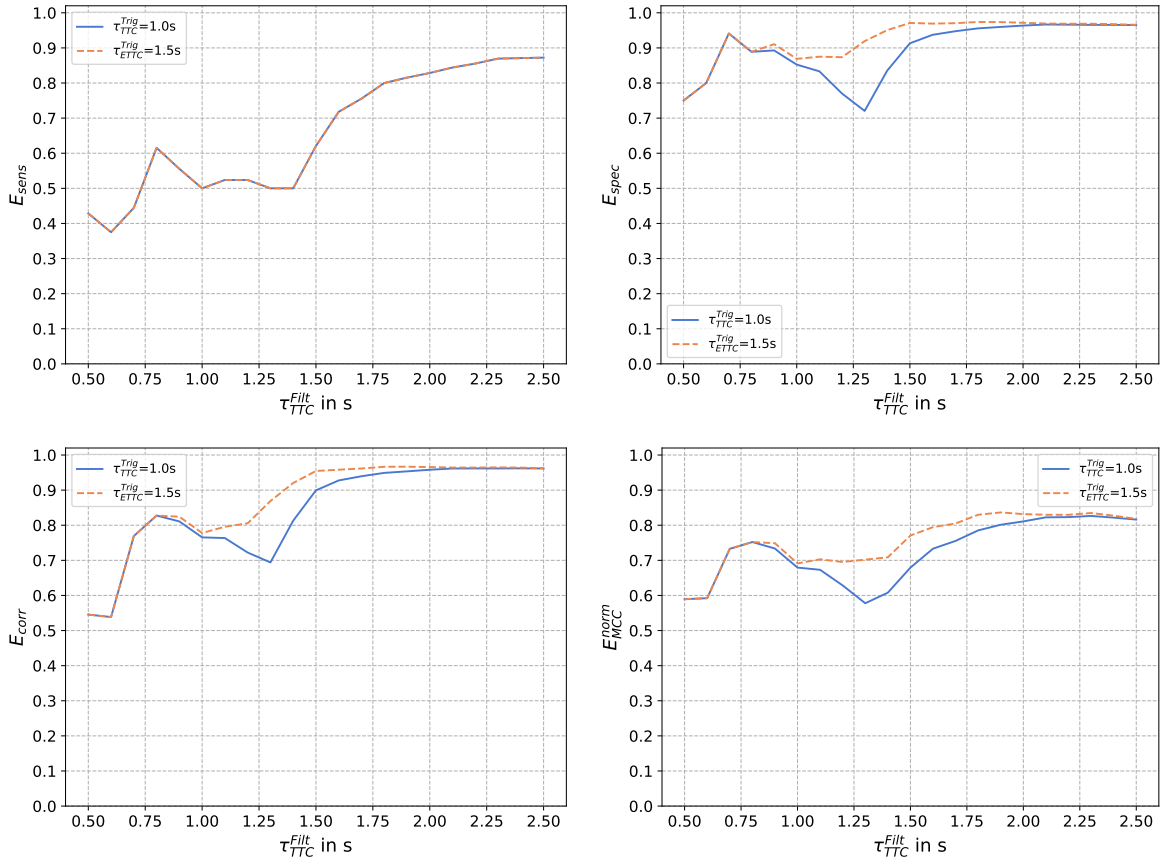

Figure 9.11.: Upper left and right: E_{sens}, respectively E_{spec}. Lower left and right: E_{corr}, respectively $E_{\text{MCC}}^{\text{norm}}$. The metrics were computed based on all conflicts with $\tau_{\text{TTC,S}}^{\text{min}} \leq \tau_{\text{TTC}}^{\text{Filt}}$.

the simple sensor model is not sufficient to correctly predict the driving in curves of other traffic participants (false positive activations), see Section 8.2.1 in the exemplary effectiveness study, or lane-change conflicts where the sensor model cannot perceive traffic participants in the adjacent lane and where the kinetic path driver model leads to a collision event (false negative activations).

Two metrics that are not expressed as a proportion of the total conflict number, but instead as a proportion of a subset of all conflicts, are the metrics E_{sens} and E_{spec}. The sensitivity, see Figure 9.11 (upper left), is defined as $E_{\text{sens}} = \frac{TP}{TP+FN}$, i.e., the proportion of conflicts with dangerous situations where the system activated. Since both E_{TP} and E_{FN} showed similar values, also E_{sens} showed the same values for both configurations. Based on this metric, both system configuration performed equally well in detecting dangerous situations. However, E_{sens} reached a stable value of 87.2 % only for $\tau_{\text{TTC}}^{\text{Filt}} \geq 2.3\,\text{s}$, while E_{spec} started stabilizing earlier at around 96.5 % for $\tau_{\text{TTC}}^{\text{Filt}} \geq 2.0\,\text{s}$.

The rate of correct decisions E_{corr}, see Figure 9.11 (lower left), stabilized to 96.2 % for E_{corr} for both system configurations, while the normed Matthew's correlation coefficient $E_{\text{MCC}}^{\text{norm}}$ (Figure 9.11, lower right) stabilized to 81.6 % for system configuration 1 and 81.8 % for system configuration 2. This is a consequence of the proportion $\frac{N^{\text{act}}}{|S|}$ of activations stabilizing

at $\tau_{\text{TTC}}^{\text{Filt}} \geq 2.0\,\text{s}$. However, a notable difference both in E_{corr} and $E_{\text{MCC}}^{\text{norm}}$ can be observed between the two system configurations when filtering with $0.75\,\text{s} \leq \tau_{\text{TTC}}^{\text{Filt}} \leq 2.0\,\text{s}$, where the proportion of true negative responses E_{TN} and false positive responses E_{FP} deviated, see Figure 9.10 (upper left and lower right). While E_{corr} reached a stable level, $E_{\text{MCC}}^{\text{norm}}$ seemed to be more sensitive to the small differences in the response categories (the maximum difference $\tau_{\text{TTC}}^{\text{Filt}} = 2.5\,\text{s}$ in TN, TP, FP or FN between both configurations was 2 conflicts).

The proportions E_{TP}, E_{TN}, E_{FP}, E_{FN}, or also the metric E_{spec}, converged to very similar values when filtering with $\tau_{\text{TTC}}^{\text{Filt}} = 2.0\,\text{s}$ or more. This shows that there was no major difference between the two system configurations for less severe conflicts with $\tau_{\text{TTC,S}}^{\text{min}} \geq 2.0\,\text{s}$. Differences between the two system configurations can be mainly seen for conflicts with $\tau_{\text{TTC,S}}^{\text{min}} \leq 2.0\,\text{s}$, where the system configuration 2 ($\tau_{\text{ETTC}}^{\text{Trig}} = 1.5\,\text{s}$) performed better by not activating when it was not necessary to activate. The derived metrics E_{corr}, $E_{\text{MCC}}^{\text{norm}}$, E_{sens} and E_{spec} lead to the same conclusions on the safety benefits of the systems.

9.2.2.2. Accident avoidance rates and changes in collision partners

The steadily growing number $|S_C|$ in Figure 9.12 (left) shows that even at values of 1.5 s to 2.5 s for $\tau_{\text{TTC}}^{\text{Filt}}$, additional collision events occurred in the baseline. Furthermore, Figure 9.12 (right) shows that these collision events represented a stable proportion $|S_C|/|S|$ of the total conflicts at values of 1.5 s to 2.5 s for $\tau_{\text{TTC}}^{\text{Filt}}$, with 8.4 % (up to 220 of 2607 conflicts) at $\tau_{\text{TTC}}^{\text{Filt}} = 2.5\,\text{s}$. The activation of the safety systems led to a decrease in the proportion

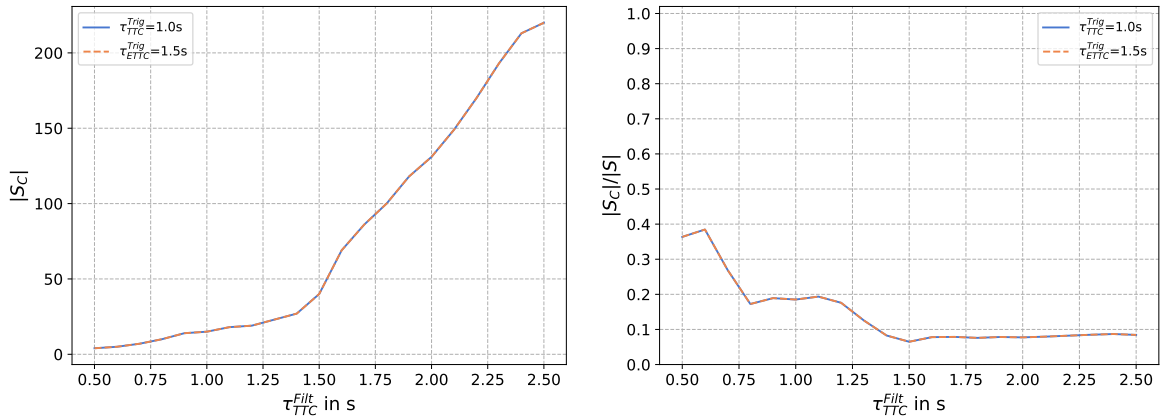

Figure 9.12.: Absolute number of baseline collisions (left) and proportion of baseline collisions (right) in the total number of conflicts when filtering with increasing values of $\tau_{\text{TTC}}^{\text{Filt}}$.

of collisions $|S_C^{TR}|/|S|$ in the treatment, as can be seen in Figure 9.13 (upper right). For both system configurations, 80 collisions were left in the treatment. System configuration 1 showed a better performance in terms of the avoidance metric $E_{\text{av}} = 69.1\,\%$, as can be seen in Figure 9.13 (lower left) for $\tau_{\text{TTC}}^{\text{Filt}} = 2.5\,\text{s}$, while for system configuration 2, only 66.4 % of the collisions in the baseline could be avoided. In 27.3 % (system configuration 1) and 29.5 % (system configuration 2) of the conflicts where a collision occurred in the baseline, a

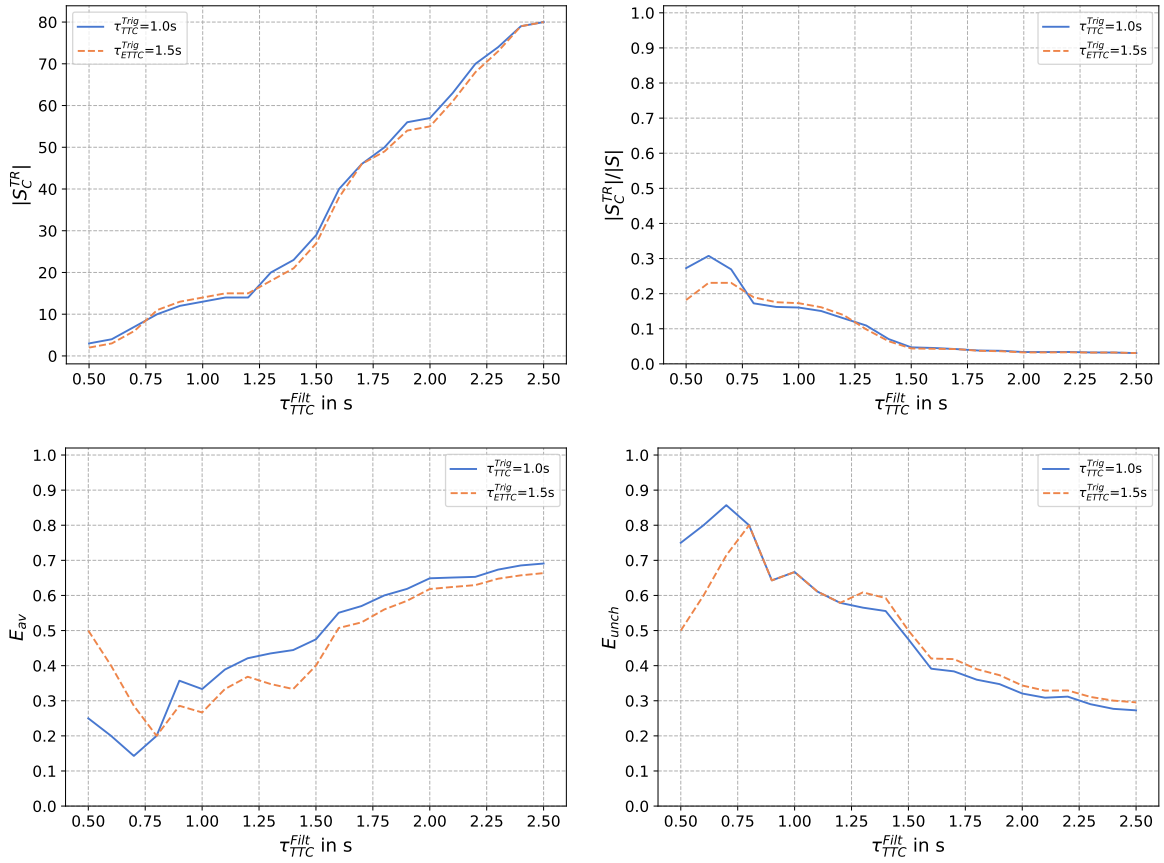

Figure 9.13.: Absolute number of treatment collisions (upper left) and proportion of treatment collisions (upper right) in the total number of conflicts and when filtering with increasing values of $\tau_{\text{TTC}}^{\text{Filt}}$. Lower left and right: E_{av}, respectively E_{unch}, computed based on all conflicts with $\tau_{\text{TTC,S}}^{\text{min}} \leq \tau_{\text{TTC}}^{\text{Filt}}$.

collision occurred between the same traffic participants in the treatment, see metric E_{unch} in Figure 9.13 (lower right). Both E_{av} and E_{unch} did not converge. Furthermore, in a stable proportion of around 3.6 % (system configuration 1) and 4.1 % (system configuration 2) of conflicts with collisions in the baseline, the collision partners were changed (metric E_{ch} in Figure 9.14).

Since the avoidance related metrics varied in the exemplary effectiveness study in a corridor of around 5 % even at more than 30 considered MTFS model runs, the differences between the system configurations for $\tau_{\text{TTC}}^{\text{Filt}} = 2.5\,\text{s}$ are considered to not be significant. However, a notable difference can be observed from around $\tau_{\text{TTC}}^{\text{Filt}} = 1.0\,\text{s}$ to 1.5 s, where system configuration 1 performed by around 10 % better than the other system. Most of those conflicts were situations where the braking vehicle accelerated directly after triggering the brake maneuver, but before the brake delay and lag time had passed. This small increase in velocity had the consequence that the calculated $a_{\text{required}}^{\text{adj}}$ was too low to avoid an accident. Furthermore, the lack of convergence shows on the one hand that the systems showed significantly better avoidance potential at values for $\tau_{\text{TTC}}^{\text{Filt}}$ close to 2.5 s, i.e., in less severe conflicts, than at lower values. On the other hand, it shows that it might be necessary to consider conflicts with $\tau_{\text{TTC,S}}^{\text{min}}$ even higher than 2.5 s to reach a stable value for E_{av}.

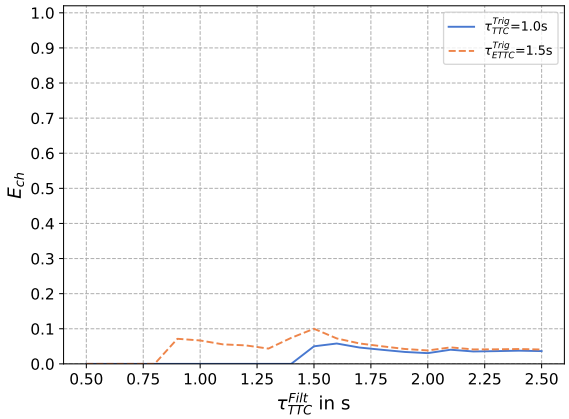

Figure 9.14.: E_{ch}, computed based on all conflicts with $\tau_{\text{TTC,S}}^{\text{min}} \leq \tau_{\text{TTC}}^{\text{Filt}}$.

9.2.2.3. Changes in minimum TTC and minimum distances

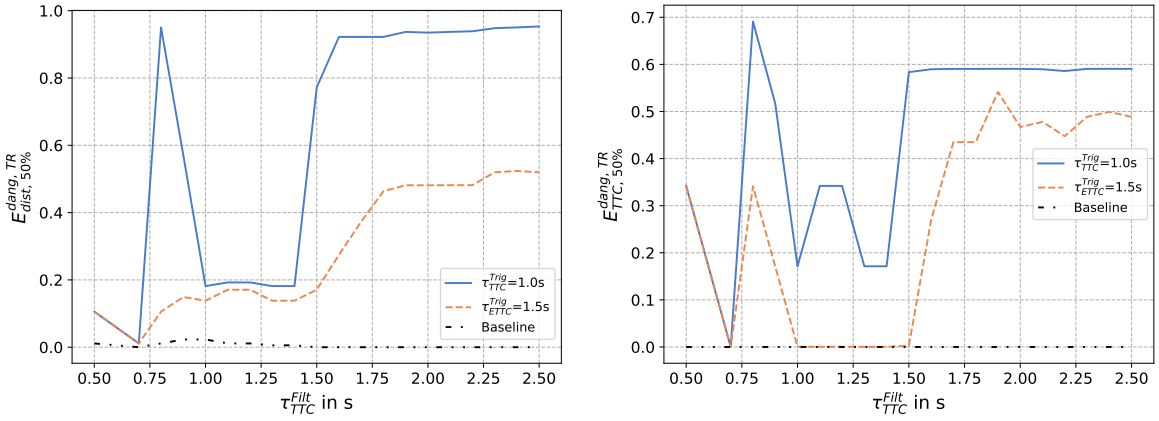

Figure 9.15.: Convergence of the metrics $E_{\text{dist,50\,\%}}^{\text{dang},\,TR}$ (left) and $E_{\text{TTC,50\,\%}}^{\text{dang},\,TR}$ (right) in dependence on the conflict filter threshold $\tau_{\text{TTC}}^{\text{Filt}}$, compared to the respective baseline metrics $E_{\text{dist,50\,\%}}^{\text{dang},\,BL}$ and $E_{\text{TTC,50\,\%}}^{\text{dang},\,BL}$.

When filtering with $\tau_{\text{TTC}}^{\text{Filt}} = 2.5\,\text{s}$, system configuration 1 ($\tau_{\text{TTC}}^{\text{Trig}} = 1.0\,\text{s}$) provided a higher safety benefit than configuration 2 ($\tau_{\text{ETTC}}^{\text{Trig}} = 1.5\,\text{s}$) at $\tau_{\text{TTC}}^{\text{Filt}} = 2.5\,\text{s}$ in terms of $E_{\text{dist,50\,\%}}^{\text{dang},\,TR}$ (0.95 m for system configuration 1 vs. 0.52 m for system configuration 2) and $E_{\text{TTC,50\,\%}}^{\text{dang},\,TR}$ (0.59 s for system configuration 1 vs. 0.49 s for system configuration 2), i.e., the median of d^{min} and $\tau_{\text{TTC,X}}^{\text{min}}$ in treatment situations was significantly higher (i.e., the differences between the metrics is higher than the variation of the metrics in the exemplary effectiveness study at high numbers of MTFS model runs). The same advantage of system configuration 1 in increasing d^{min} and $\tau_{\text{TTC,X}}^{\text{min}}$ was also observed in the exemplary study, since the system with this configuration braked with a fixed deceleration, instead of $a_{\text{requested}} = a_{\text{required}}^{\text{adj}}$, which led to goal braking behavior, as can be seen with configuration 2. For both metrics and system configurations, the metrics stabilized before $\tau_{\text{TTC}}^{\text{Filt}} = 2.0\,\text{s}$, see Figure 9.15. For system configuration 1, stabilization was observable even at around $\tau_{\text{TTC}}^{\text{Filt}} = 1.6\,\text{s}$.

9.2.3. Conclusions

The following conclusions regarding the influence on the effectiveness results were found when varying the conflict filter threshold $\tau_{\mathrm{TTC}}^{\mathrm{Filt}}$:

- For the metrics E_{TP}, E_{TN}, E_{FP}, E_{FN}, E_{spec}, E_{corr}, $E_{\mathrm{MCC}}^{\mathrm{norm}}$, $E_{\mathrm{dist,\,50\,\%}}^{\mathrm{dang},\,TR}$, $E_{\mathrm{TTC,\,50\,\%}}^{\mathrm{dang},\,TR}$, convergence could be observed starting at $\tau_{\mathrm{TTC}}^{\mathrm{Filt}} = 2.0\,\mathrm{s}$. That means that $\tau_{\mathrm{TTC}}^{\mathrm{Filt}} = 1.7\,\mathrm{s}$, as used in the exemplary study, was not sufficient to reach a final estimate of the effectiveness. At $\tau_{\mathrm{TTC}}^{\mathrm{Filt}} = 2.0\,\mathrm{s}$, 1 692 conflicts met the filter criteria, which represents an increase by 55 %, compared to filtering with $\tau_{\mathrm{TTC}}^{\mathrm{Filt}} = 1.7\,\mathrm{s}$.
- The values for the avoidance related metrics E_{av}, E_{unch} and E_{ch} did not stabilize, indicating that it was easier to avoid collisions in conflicts with $\tau_{\mathrm{TTC,S}}^{\mathrm{min}}$ close to 2.5 s, and that even more of the less severe conflicts should be included in the scenario catalog.
- In conflicts with $\tau_{\mathrm{TTC,S}}^{\mathrm{min}} \geq 1.5\,\mathrm{s}$, the systems triggered a braking maneuver in a constant and stable proportion of around 5 % to 10 % of the total conflicts in the intervals $e_r - 0.1 \leq \tau_{\mathrm{TTC,S}}^{\mathrm{min}} < e_r$, but activations are less common than in conflicts with $\tau_{\mathrm{TTC,S}}^{\mathrm{min}} \leq 1.5\,\mathrm{s}$ (both system configurations). As a consequence, using $\tau_{\mathrm{TTC}}^{\mathrm{Filt}} = 1.7\,\mathrm{s}$, or even a higher threshold, was not enough to find all conflicts where the systems would activate.
- When using $\tau_{\mathrm{TTC,S}}^{\mathrm{min}}$ as predictor, prediction of the conflicts in which a system based on $\tau_{\mathrm{ETTC,X}}$ will activate is even more difficult than for systems that trigger based on $\tau_{\mathrm{TTC,X}}$.
- Further harmonization between the τ_{TTC} calculation algorithms would be one step that leads to higher predictability in which conflicts the systems would activate, possibly allowing further concentration of the assessment of safety systems on concrete scenarios in which they are intended to be active.
- When considering conflicts with $\tau_{\mathrm{TTC,S}}^{\mathrm{min}}$ up to the highest available value 2.5 s, activations took place at around 6.4 % of the conflicts, around 3.1 % of all conflicts led to true positive system responses and around 3.4 % led to false positive system responses. False negative responses occurred only in around 0.5 % of the conflicts. This was observable for both system configurations, and the metrics converged to very similar values (only up to 0.1 % difference). Convergence started at around $\tau_{\mathrm{TTC}}^{\mathrm{Filt}} = 2.0\,\mathrm{s}$.
- In terms of E_{FP} and E_{TN}, and consequently E_{spec}, $E_{\mathrm{MCC}}^{\mathrm{norm}}$ and E_{corr}, system configuration 2 (based on τ_{ETTC}) performed better for conflicts with $0.75\,\mathrm{s} \leq \tau_{\mathrm{TTC,S}}^{\mathrm{min}} \leq 2.0\,\mathrm{s}$.
- When filtering with only $\tau_{\mathrm{TTC}}^{\mathrm{Filt}} = 1.4\,\mathrm{s}$, system configuration 1 had a notable advantage in terms of E_{av} (44.4 % for configuration 1 and 33.3 % for configuration 2), due to conflicts where the $a_{\mathrm{required}}^{\mathrm{adj}}$ was insufficient due to an acceleration maneuver directly after reaching the trigger threshold.

To summarize these conclusions, it can be said, that advantages in the safety effect of one system configuration over the other can mainly be seen in conflicts with a severity of $\tau_{\mathrm{TTC,S}}^{\mathrm{min}} \leq 2.0\,\mathrm{s}$. Therefore, an interesting alternative for future effectiveness studies would

be to define several scenario catalogs with conflicts in disjoint intervals of $\tau^{\min}_{\mathrm{TTC,S}}$, e.g., $0 < \tau^{\min}_{\mathrm{TTC,S}} \leq 1.0\,\mathrm{s}$ and $1.0\,\mathrm{s} < \tau^{\min}_{\mathrm{TTC,S}} \leq 2.0\,\mathrm{s}$, and to analyze the effectiveness metrics separately for each interval, instead of considering all conflicts from 0 to a defined threshold.

Furthermore, to reach a final estimate of the effectiveness, in particular for the avoidance related metrics, conflicts with $\tau^{\min}_{\mathrm{TTC,S}}$ as high as possible should be considered.

9.3. Variation in the presence of static objects and surrounding traffic

9.3.1. Objective and method

The objective of this sensitivity study is to investigate to which degree the presence of visibility obstructions influences the effectiveness metrics, and how the moment of first detection and classification is influenced by the visibility obstructions.

For this visibility study, the presence of static objects is switched off as a first variation (the variations are denoted as obstruction configurations) of the exemplary study defined in the solution approach, while a second variation switches off both the static objects as well as surrounding kinematic vehicles. These kinematic vehicles are the vehicles that were included in P_{close}, but not P_{crit} (see Section 7.1.2), and were considered to be primarily relevant as sight obstructions. For this sensitivity study, 20 model runs of the model WBE were investigated.

9.3.2. Results and discussion

9.3.2.1. Change of effectiveness metrics

The effectiveness metrics related to system response categories are shown in Figure 9.16. As can be seen, when the system configuration is fixed and the visibility obstructions are changed, there were no differences in the effectiveness metrics. The same holds true for the avoidance related metrics (see Figure 9.17) and the metrics $E^{\mathrm{dang},TR}_{\mathrm{dist},50\,\%}$ and $E^{\mathrm{dang},TR}_{\mathrm{TTC},50\,\%}$ (see Figure 9.18 and Figure 9.19).

The closer in terms of $\tau^{\min}_{\mathrm{TTC,X}}$ or $d^{\min}$ two vehicles get to each other, the less space between them is available and the lower is the probability that there is an obstruction of visibility between the vehicles. As the results suggest, the available time and space before and around the conflicts is sufficient such that sight obstructions are not relevant, at least in the urban scenario that is simulated in the MTFS model. It has to be noted that the majority of conflicts were rear-end conflicts (more than 90 %), where little opportunity for sight interruption exists.

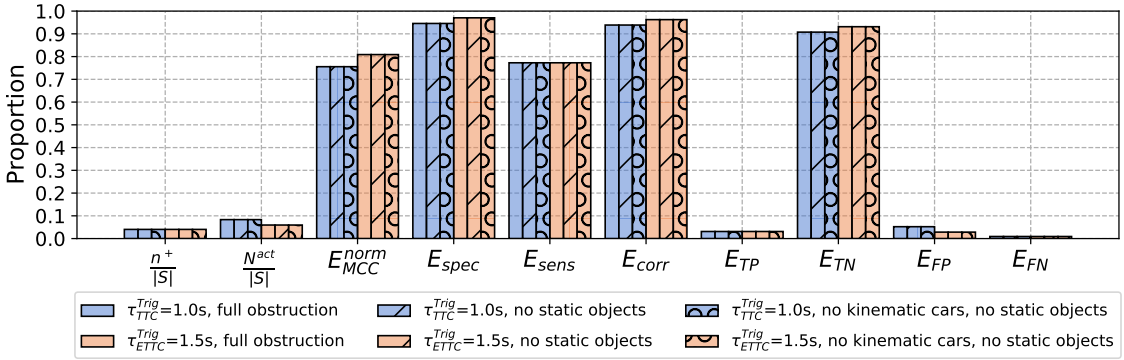

Figure 9.16.: Metrics related to the system response categories (false/true positive/negative), the proportion $\frac{n^+}{|S|}$ of dangerous baseline situations in the number of concrete scenarios in the scenario catalog S, and the proportion $\frac{N^{act}}{|S|}$ of system activations in $|S|$.

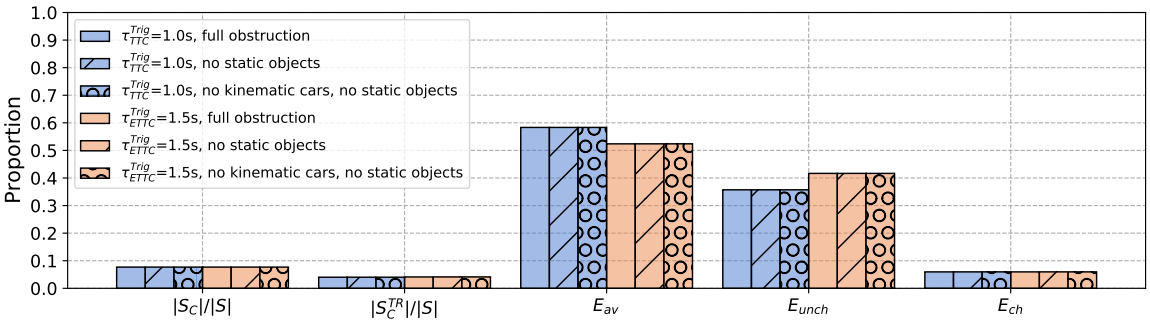

Figure 9.17.: The proportions of baseline ($|S_C|/|S|$) and treatment ($|S_C^{TR}|/|S|$) collisions and metrics related to collision avoidance and the change of collision partner configurations.

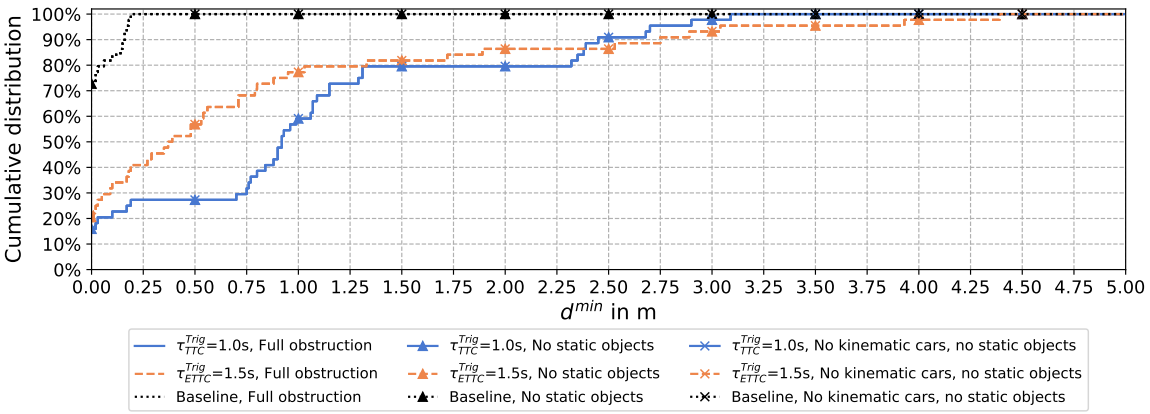

Figure 9.18.: Cumulative distribution of $d^{\min}$ in the baseline and the two treatments. The vertical axis represents the quantiles. Collisions are counted as zero values.

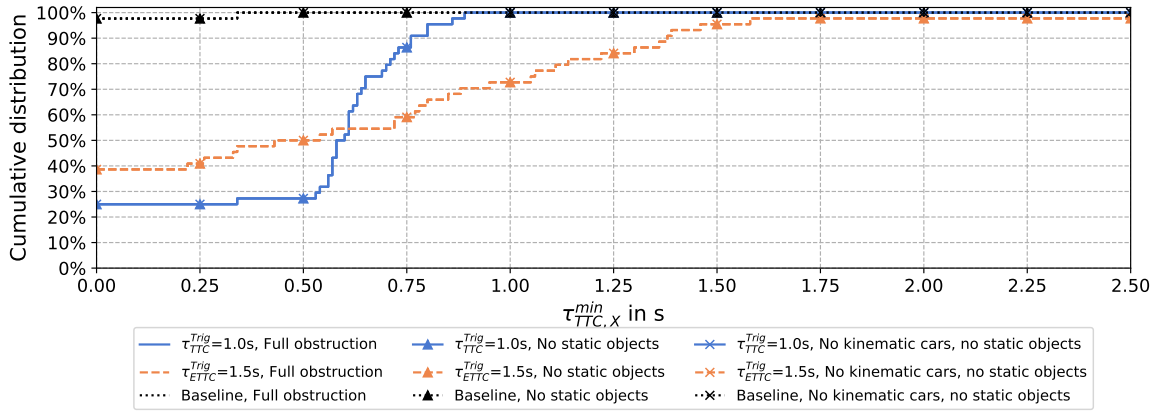

Figure 9.19.: Cumulative distribution of $\tau^{\text{min}}_{\text{TTC,X}}$ in the baseline and the two treatments. Collisions are counted as zero values.

9.3.2.2. Change in the visibility of conflict participants

For all obstruction configurations, the sensors were able to detect the other conflict participant in at least 99.5 % of the investigated conflicts, see Table 9.2. A classification could be reached in at least 98.4 % of all conflicts (for classification, the other conflict vehicle must be detected for at least 0.2 s and it must be fully in view). In some conflicts, when comparing to the full obstruction configuration (i.e., static objects and surrounding kinematic vehicles are considered), there was a difference in the time of first detection and classification (3.7 % to 7.8 %). In the conflicts in which there was a difference, the other conflict participant could be detected on average −1.66 s to −1.45 s earlier than when considering the full obstruction. When considering also the conflicts that did not contain a change in the time of first detection for the calculation of the mean, the other conflict participant can be detected and classified on average 0.1 s earlier when no static objects and kinematic cars are considered. When kinematic cars are considered without static objects, this difference in the mean is only 0.07 s.

Obstruction configuration	*Number of conflicts with detections*	*Number of conflicts with classifications*	*Number of conflicts with a difference in time of first detection*	*Number of conflicts with a difference in time of first classification*	*Mean difference in time of first detection*	*Mean difference in time of first classification*
Full	1087 (99.5 %)	1075 (98.4 %)	-	-	-	-
No static objects	1088 (99.6 %)	1076 (98.5 %)	40 (3.7 %)	56 (5.2 %)	−1.66 s	−1.57 s
No kinematic cars, no static objects	1090 (99.8 %)	1078 (98.7 %)	69 (6.4 %)	85 (7.8 %)	−1.45 s	−1.47 s

Table 9.2.: Changes in the visibility of conflict participants. The numbers in parentheses show the proportions in the total number of conflicts (1 092). The difference in time of first detection and classification is computed in relation to the full obstruction configuration. The calculation of the mean difference in time of first detection and classification included only those conflicts where the difference was not 0. A negative difference in the time of first detection and classification indicates that the other conflict participant was detected earlier.

In 21.7 % of the investigated crossing conflicts and in only 3.1 % of other conflicts, omitting the static objects as sight obstructions made a difference in the time of first detection. I.e., the probability, that the time of first detection changes when not considering static objects, is around 7 times higher for crossing conflicts than in other conflicts. When omitting both the static objects and kinematically simulated traffic participants (i.e., participants in P_{close}), the respective proportions are 26 % and 5.7 %.

9.3.3. Conclusions

The following conclusions were found in the sensitivity study that varies the presence of visibility obstructions:

- An interesting finding of the visibility study in this section is that the effectiveness metrics were fully unaffected when omitting the static objects and kinematic vehicles, i.e., such visibility obstructions can be omitted from the simulation for the investigated traffic site.
- For the majority of the conflicts (more than 98.4 %), between obstruction configurations, there was no difference in the moment in time when the other conflict vehicle is first detected or classified, or whether the other conflict vehicle can be detected or classified at all.
- For the remaining conflicts, where sight obstructions led to a difference in the time of first detection or classification, the other vehicle can be detected or classified on average around 1.5 s earlier when reduced sight obstructions were considered. As was shown, the detections occurred still early enough such that the effectiveness metrics were not influenced.
- The probability that the visibility obstructions had an influence on the moment in time when the other conflict vehicle is first detected or classified was 7 times higher in crossing conflicts than in other conflicts, but only a small portion of the investigated conflicts were of crossing type (2.1 %). Even if the visibility obstructions were not important for the investigated traffic site, they might play a role at intersections with different geometries, e.g., where the walls of buildings or fences are closer to the driving lanes.

9.4. Variation in the look-ahead time of the kinetic path driver model

9.4.1. Objective and method

Due to the results in Chapter 7, the kinetic path driver model used in nanoscopic simulation is considered to be of major influence on the occurrence of collision events. The kinetic path

driver model is influenced by the look-ahead time t_{LA}, see Section 7.1.6. The simulations for the exemplary effectiveness study and the other sensitivity studies in the present chapter were conducted with a look-ahead time $t_{\mathrm{LA}} = 0.6\,\mathrm{s}$. For this section, the additional values $t_{\mathrm{LA}} = 0.9\,\mathrm{s}$ and $t_{\mathrm{LA}} = 1.2\,\mathrm{s}$ are investigated in addition to $t_{\mathrm{LA}} = 0.6\,\mathrm{s}$. For this analysis, 20 model runs of the MTFS model WBE are used. In the following, the differences in the trajectories and the occurrence of collision events in nanoscopic simulation due to a change in t_{LA} are investigated, followed by an investigation of the change of the effectiveness metrics related to the system response categories, the avoidance potential and the reduction of d^{min} and $\tau^{\mathrm{min}}_{\mathrm{TTC,X}}$. For the investigations in this section, the first 20 model runs of the MTFS model WBE were used.

9.4.2. Results and discussion

9.4.2.1. Differences in trajectories in nanoscopic simulation

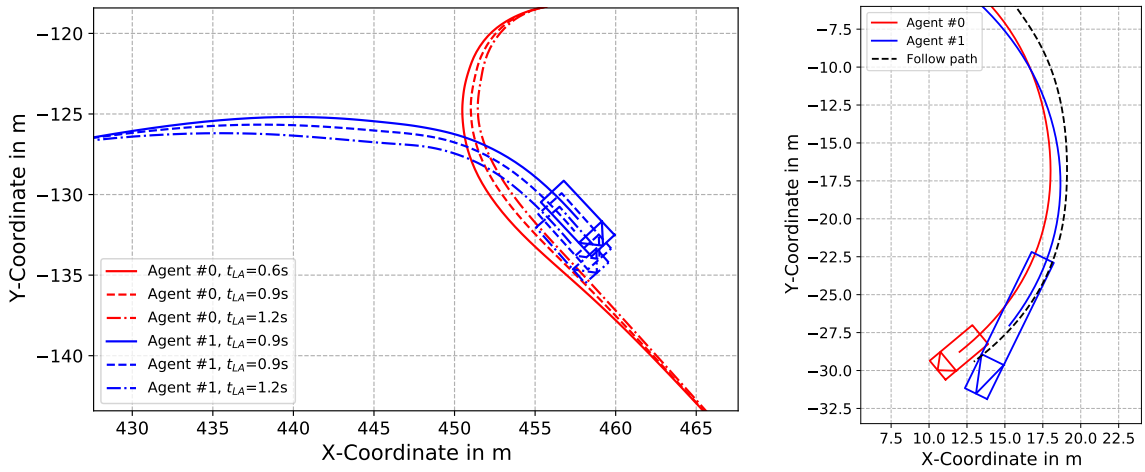

Figure 9.20.: Left: comparison of trajectories in a crossing conflict. The solid lines represent the setting $t_{\mathrm{LA}} = 0.6\,\mathrm{s}$ for the fuzzy model, while the dashed line represents $t_{\mathrm{LA}} = 0.9\,\mathrm{s}$ and the dotted line represents $t_{\mathrm{LA}} = 1.2\,\mathrm{s}$. No collision events occurred. Right: comparison of trajectories for different vehicle geometries, when both vehicles (red passenger car and blue bus) start with their vehicle front at the same initial position.

An example how the parameter t_{LA} influences the resulting trajectories in nanoscopic simulation is the crossing conflict shown in Figure 9.20 (left). In this conflict, a corner-cutting effect for higher look-ahead times is clearly visible, together with smoother curves with higher curve radii. Furthermore, it can be seen that vehicles travel farther if the corners are cut, since less distance needs to be traveled in the curve. This allows the vehicles to more closely follow the acceleration and velocity profiles that are prescribed by MTFS. This effect can make the difference between collision or no collision, and explains the loose correlation between $\tau^{\mathrm{min}}_{\mathrm{TTC,X}}$ and $\tau^{\mathrm{min}}_{\mathrm{TTC,S}}$, see Section 9.2.2.1, since distances and velocities as variables involved in the $\tau_{\mathrm{TTC,X}}$ calculation are both affected by t_{LA}.

In addition to differences in the trajectories when t_{LA} is changed, differences in the trajectories can also result due to differences in the vehicle model, in particular, the vehicle's length and wheelbase. Furthermore, the trajectories resulting from the kinetic path driver model depend on other parameters that influence the driving dynamics, such as the vehicle mass or moment of inertia. In Figure 9.20 (right), the trajectory of a small passenger car (red solid line) is compared to the trajectory of a bus (blue solid line), where both vehicles tried to follow the same follow path (black dashed line) with the same setting for t_{LA}, with the same initial position of the vehicle front, and the same limitations of the driver model (maximum steering velocity and maximum steering angle). As can be seen, there can be up to 1 m difference in the position of the center of gravity.

When considering the differences in the resulting trajectories due to changes in t_{LA} and the vehicle geometries, the question remains which trajectory is the most plausible trajectory. Since kinetic driving dynamics are not considered in MTFS, it is not guaranteed that trajectories from MTFS can be driven by real vehicles. Due to that reason, trajectory-based safety analysis was conducted in the validation step of the MTFS model, see Section 5.1.3.2. This was done by minimizing the deviation between the MTFS trajectories and the trajectories in nanoscopic simulation. However, since trajectories also depended on the vehicle model, as the example in this section shows, the trajectories in MTFS should be validated individually for each vehicle model that was used, to achieve the most plausible results, instead of using a global value for t_{LA} for any vehicle model. In the best case, the validation is supported by comparing the trajectories in MTFS and nanoscopic simulation to recorded trajectories from traffic observation studies that were conducted at the simulated traffic site.

9.4.2.2. Changes in collision events

For a selected lane-change conflict, Figure 9.21 shows the trajectories (positions of the centers of gravity) for the two conflict participants (red and blue) and an additional vehicle of the surrounding traffic (green). In this conflict, a collision event occurred between the red and the green vehicle from the surrounding traffic when the setting $t_{\mathrm{LA}} = 1.2\,\mathrm{s}$ is used. This is one example where a higher look-ahead time, i.e., smoother trajectories, led to an additional collision event. For the lower settings for t_{LA}, the green and red vehicles were able pass without a collision event. In other conflicts, collision events that occurred for $t_{\mathrm{LA}} = 0.6\,\mathrm{s}$, did not occur with the higher look-ahead times.

To investigate at which time in nanoscopic simulation the collision events occurred, the kernel density estimates (KDE) of the values $t_{\mathrm{imp}} - t_{\tau_{\mathrm{TTC}}^{\mathrm{min}}}$ for collision events in the baseline, categorized by the individual settings for t_{LA}, are shown in Figure 9.22 (left and right). For $t_{\mathrm{LA}} = 0.6\,\mathrm{s}$, an increased density of collision events between both conflict participants can be observed at 3 s to 4 s after $t_{\tau_{\mathrm{TTC}}^{\mathrm{min}}}$ (Figure 9.22, left). As was noted in Section 7.2.1, the conflicts that contributed to the peak around 3 s to 4 s are all situations that occur very similarly to the one shown in Figure 9.23, even at similar coordinates. This peak dissolved for higher values

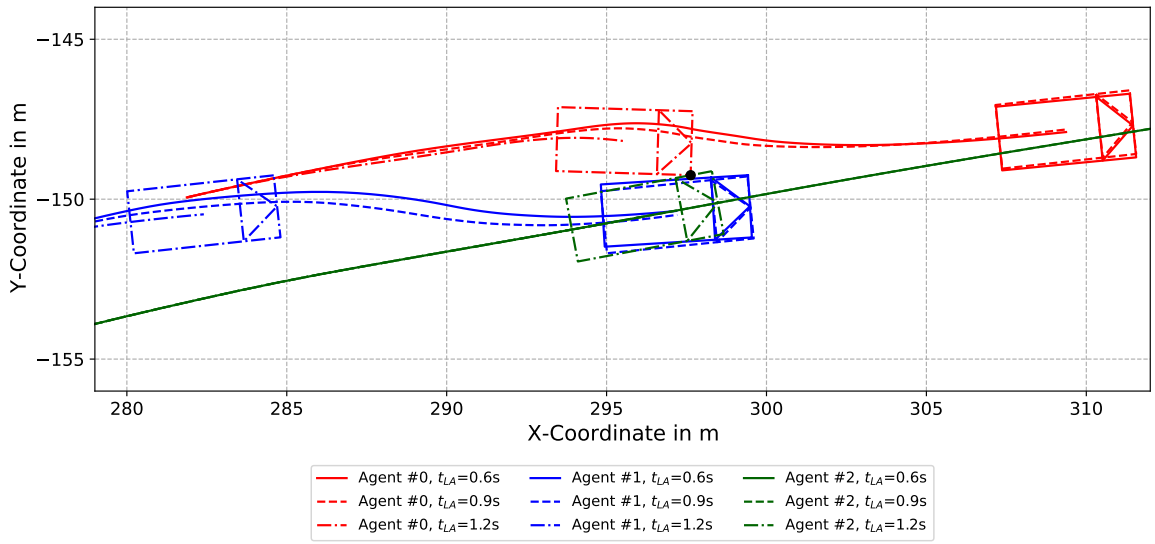

Figure 9.21.: Comparison of trajectories in a lane change conflict, for different settings for t_{LA}. The red and blue vehicles are the conflict participants, while the vehicle are part of the surrounding traffic. For $t_{\mathrm{LA}} = 0.6\,\mathrm{s}$ and $t_{\mathrm{LA}} = 0.9\,\mathrm{s}$, no collisions occurred. For $t_{\mathrm{LA}} = 1.2\,\mathrm{s}$, a collision occurred between the red and green vehicle (black dot).

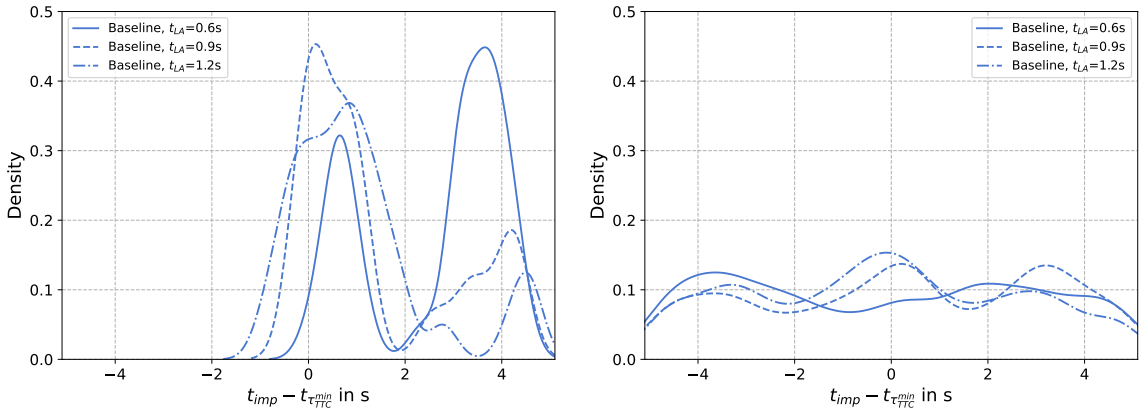

Figure 9.22.: Horizontal axis: difference between the impact time t_{imp} and $t_{\tau_{\mathrm{TTC}}^{\mathrm{min}}}$, i.e. $t_{\mathrm{imp}} - t_{\tau_{\mathrm{TTC}}^{\mathrm{min}}}$. The value 0 on the horizontal axis then corresponds to $t_{\tau_{\mathrm{TTC}}^{\mathrm{min}}}$ in MTFS. Vertical axis: kernel density estimates of the distribution of the values on the horizontal axis (see for example Rosenblatt, 1956). As kernel function, the normal distribution with a bandwidth of $h = 0.1$ was used. Left figure: Collision events where both collision partners were conflict participants. Right figure: Only one of both collision partners was a conflict participant.

of t_{LA}, as the vehicles started steering earlier, leading to larger curve radii such that the vehicle corners did not intersect. Therefore, the collisions contributing to the peak in density at 3 s to 4 s became less common. Further peaks in the density of collision events are still visible for all settings for t_{LA} in the left figure directly around $t_{\tau_{\mathrm{TTC}}^{\mathrm{min}}}$, i.e., 0 on the horizontal axis. Furthermore, it can be noticed that collision events with only one conflict participant involved seemed to be distributed more uniformly on the horizontal axis (Figure 9.22, right).

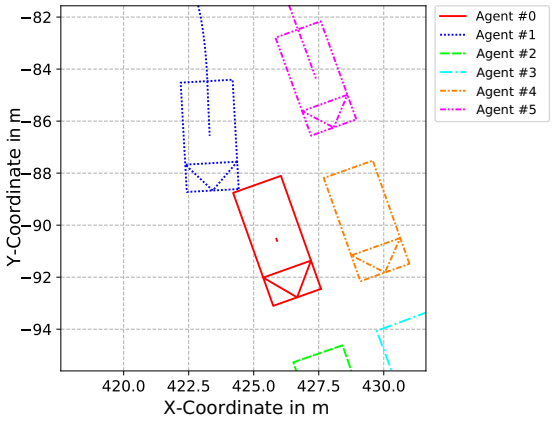

Figure 9.23.: Top view of the vehicle positions in one of the collision events, where both collision partners were conflict participants (red and blue vehicle in the middle of the figure, i.e., agents #0 and #1), including other surrounding traffic (colored rectangles) and their trajectories (colored lines).

Baseline variation	*One collision partner is a conflict participant*	*Both collision partners are conflict participants*	*Total collisions*
$t_{\mathrm{LA}} = 0.6\,\mathrm{s}$	53	31	84
$t_{\mathrm{LA}} = 0.9\,\mathrm{s}$	56 (+5.6 %)	20 (−35.4 %)	76 (−9.5 %)
$t_{\mathrm{LA}} = 1.2\,\mathrm{s}$	58 (+9.4 %)	28 (−9.7 %)	86 (+2.3 %)

Table 9.3.: Number of collisions where only one conflict participant was involved, number of collisions between conflict participants and total number of collisions in the baseline. The numbers on parentheses show the relative change compared to the setting $t_{\mathrm{LA}} = 0.6\,\mathrm{s}$.

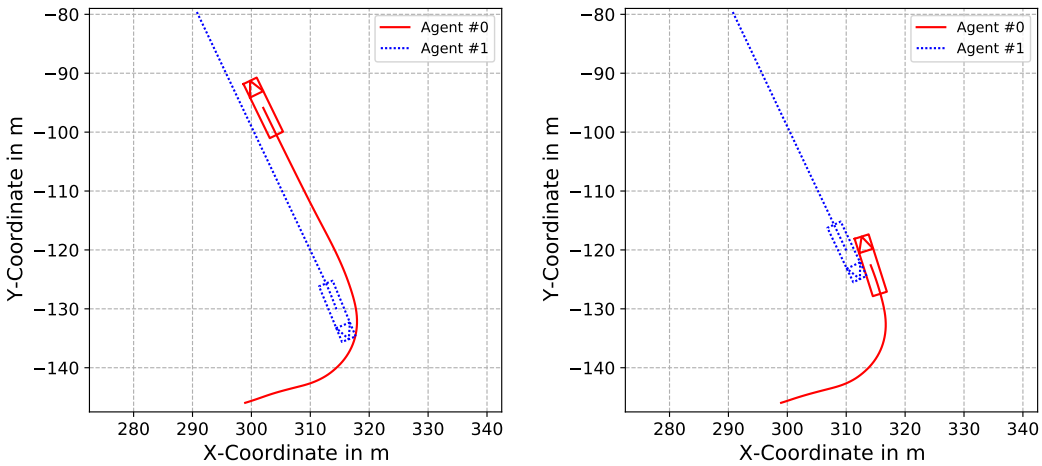

Figure 9.24.: Left: baseline simulation of a conflict with $t_{\mathrm{LA}} = 0.9\,\mathrm{s}$, where the red vehicle (solid, agent #0) turns left, but is able to pass. Right: the same conflict in the baseline simulation with $t_{\mathrm{LA}} = 1.2\,\mathrm{s}$. In this concrete scenario, a collision event occurred with the blue vehicle (dotted, agent #1).

In Table 9.3, it can be seen that the number of collision events between the conflict participants was reduced by 35 % by setting t_{LA} to 0.9 s, since several collisions such as the one in Figure 9.23 were avoided. However, with $t_{\mathrm{LA}} = 1.2\,\mathrm{s}$, the number of collision events

between the conflict participants increased again. This is due to the smoother trajectories, that did not allow other vehicles to pass in some concrete scenarios, such as the ones shown in Figure 9.24 or Figure 9.21. Furthermore, the number of collisions where only one collision partner is a conflict participant stayed on a similar level.

These results show that as a consequence of the changes in the trajectories presented in the previous section, the time of occurrence and number of collision events are influenced as well by t_{LA}. Since MTFS is designed to produce trajectories free of collisions, the collision events in nanoscopic simulation are seen as an artifact of the presented method. It was not possible to remove all collision events with any of the settings for t_{LA}, although a minimum can be observed for $t_{\mathrm{LA}} = 0.9\,\mathrm{s}$. The findings motivate for further research on kinetic path driver models, in which the different vehicle geometries are considered. As was mentioned in Medicus, 2019, trajectory-based safety analysis for MTFS is still in its infancy and requires further research. Using data from traffic observation studies such as in the roundD dataset (Krajewski, Moers, et al., n.d.), the highD dataset (Krajewski, J. Bock, et al., 2018) or the TUBS road user dataset (Plachetka et al., 2018), where detailed time series data for positions or velocities and more are provided for real traffic, could provide additional opportunities for safety-related validation.

9.4.2.3. System response categories and related metrics

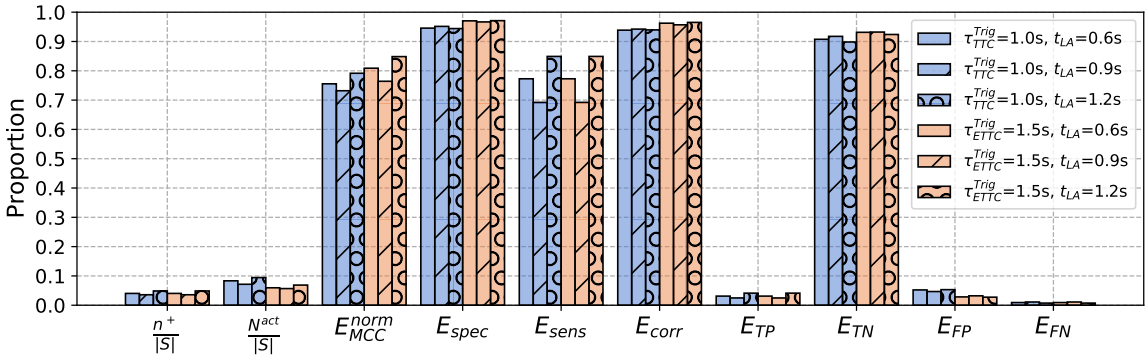

Figure 9.25.: Metrics related to the system response categories (false/true positive/negative), the proportion $\frac{n^+}{|S|}$ of dangerous baseline situations in the number of concrete scenarios in the scenario catalog S, and the proportion $\frac{N^{\mathrm{act}}}{|S|}$ of system activations in $|S|$.

With the setting $t_{\mathrm{LA}} = 1.2\,\mathrm{s}$, dangerous situations occurred in 4.9 % of the conflicts, see $\frac{n^+}{|S|}$ in Figure 9.25, which was higher than for the other settings (4.0 % for $t_{\mathrm{LA}} = 0.6\,\mathrm{s}$ and 3.6 % for $t_{\mathrm{LA}} = 0.9\,\mathrm{s}$). The proportion $\frac{N^{\mathrm{act}}}{|S|}$ of conflicts with activations increased proportionally to $\frac{n^+}{|S|}$ with system configuration 1 ($\frac{N^{\mathrm{act}}}{|S|} = 8.3\,\%$, 7.1 % and 9.4 % for $t_{\mathrm{LA}} = 0.6\,\mathrm{s}$, 0.9 s and 1.2 s, respectively), while it also increased proportionally for system configuration 2 ($\frac{N^{\mathrm{act}}}{|S|} = 6.0\,\%$, 5.6 % and 6.3 % for $t_{\mathrm{LA}} = 0.6\,\mathrm{s}$, 0.9 s and 1.2 s, respectively).

The most notable difference in the metrics related to the system response categories can

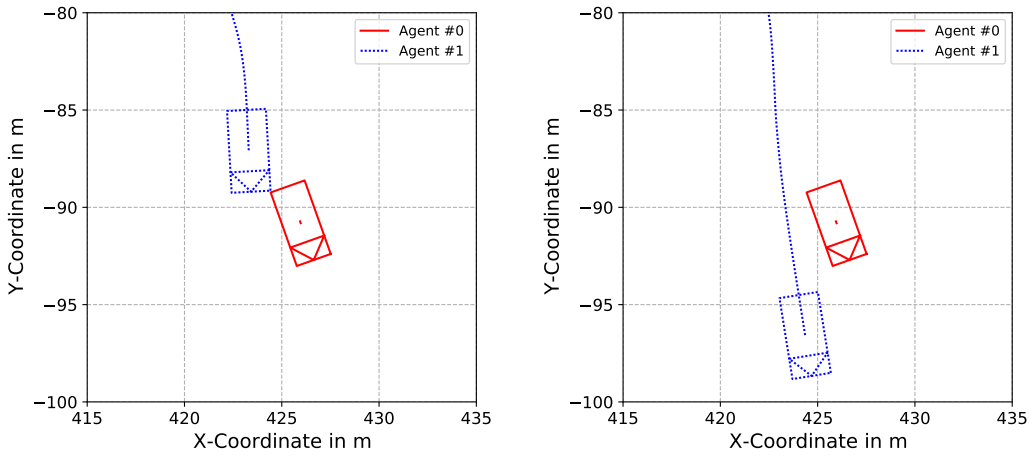

Figure 9.26.: Treatment simulations with system configuration 2 ($\tau_{\mathrm{ETTC}}^{\mathrm{Trig}} = 1.5\,\mathrm{s}$) of a type of conflict that contributed to several false negative system responses. The blue vehicle (dotted, agent #1) tries to change to the lane to its right to pass the red vehicle (solid, agent #0). Left: treatment simulation with $t_{\mathrm{LA}} = 0.6\,\mathrm{s}$. The blue vehicle activated a brake maneuver, but the collision was not avoided. Right: treatment simulation with $t_{\mathrm{LA}} = 0.9\,\mathrm{s}$. The blue vehicle is able to pass, but it entered the safety zone of 0.2 m.

be seen for E_{sens} and $E_{\mathrm{MCC}}^{\mathrm{norm}}$, which is a consequence of differences in the proportions E_{FN} and E_{TP} of conflicts with false negative and true positive responses, see Table 9.4. The false negative responses with $t_{\mathrm{LA}} = 0.9\,\mathrm{s}$ can be attributed to a certain type of conflict shown in Figure 9.26, which occurred several times in a similar way, at the same location in the road site. In this type of conflict, one vehicle tried to change to the lane to its right. With $t_{\mathrm{LA}} = 0.6\,\mathrm{s}$, it was not possible to pass the standing vehicle without a collision at the corners of the vehicles' geometries. Its safety systems activated, but it was not possible to avoid the collision, leading to the conflict being categorized as true positive. With $t_{\mathrm{LA}} = 0.9\,\mathrm{s}$, the vehicle was able to pass, but not without entering the safety zone of 0.2 m. Since the safety zone was entered when the waiting vehicle was no longer fully in view of the sensor of the passing vehicle, no braking maneuver was triggered, leading to the conflict being categorized as false negative. With $t_{\mathrm{LA}} = 1.2\,\mathrm{s}$, the safety zone was not entered, leading to the conflict being categorized as true negative. In absolute numbers, both systems showed a false negative response in 10 conflicts for $t_{\mathrm{LA}} = 0.6\,\mathrm{s}$, 12 conflicts for $t_{\mathrm{LA}} = 0.9\,\mathrm{s}$ and 8 conflicts for $t_{\mathrm{LA}} = 1.2\,\mathrm{s}$, see Table 9.4, i.e., the maximum difference in the number of conflicts with false negative responses was only 4, although this difference had a notable impact on E_{sens} and $E_{\mathrm{MCC}}^{\mathrm{norm}}$.

The discussed conflict demonstrates how the kinetic path driver model led to the same conflict being categorized as true positive, false negative and true negative, depending only on the setting of t_{LA}. This shows how differences in the kinetic path driver model that lead to differences in the vehicle positions being displaced by as little as 0.2 m (inside or outside the safety zone), can have a notable impact on effectiveness metrics such as E_{sens} or $E_{\mathrm{MCC}}^{\mathrm{norm}}$, which in turn underlines the necessity for validation of the kinetic path driver model and validation of the trajectories in MTFS to real traffic observation studies.

System configuration	t_{LA}	E_{spec}	E_{sens}	E_{TP}	E_{TN}	E_{FP}	E_{FN}
$\tau_{\mathrm{TTC}}^{\mathrm{Trig}} = 1.0\,\mathrm{s}$	0.6	94.6 %	77.3 %	3.1 % (34)	90.8 % (991)	5.2 % (57)	0.9 % (10)
	0.9	95.2 %	69.2 %	2.5 % (27)	91.8 % (1001)	4.7 % (51)	1.1 % (8)
	1.2	94.4 %	84.9 %	4.1 % (45)	89.8 % (980)	5.3 % (58)	0.7 % (12)
$\tau_{\mathrm{ETTC}}^{\mathrm{Trig}} = 1.5\,\mathrm{s}$	0.6	97.0 %	77.3 %	3.1 % (34)	93.1 % (1017)	2.8 % (57)	0.9 % (10)
	0.9	96.7 %	69.2 %	2.5 % (27)	93.2 % (1017)	3.2 % (51)	1.1 % (8)
	1.2	97.1 %	84.9 %	4.1 % (45)	92.4 % (1008)	2.7 % (58)	0.7 % (12)

Table 9.4.: The metrics E_{sens}, E_{spec}, E_{TP}, E_{TN}, E_{FP} and E_{FN}. Absolute conflict counts with system responses in the respective categories are shown in parentheses. In total, 1 092 conflict were investigated.

9.4.2.4. Accident avoidance rates and changes in collision partners

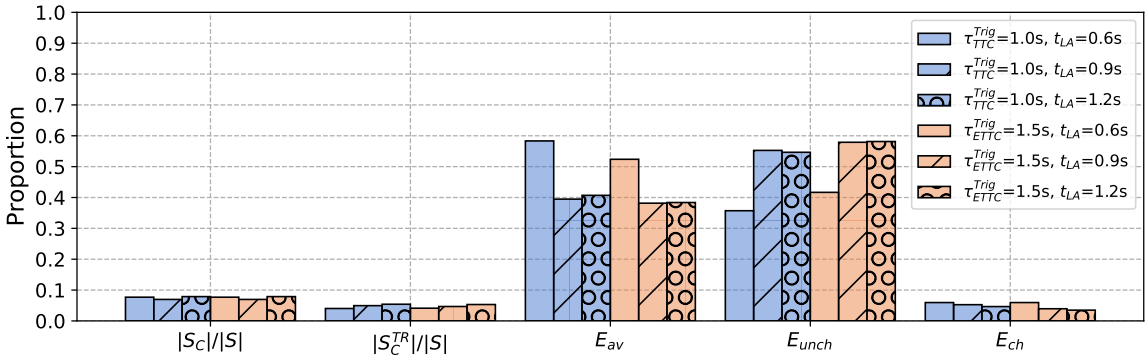

Figure 9.27.: The proportions of baseline ($|S_C|/|S|$) and treatment ($|S_C^{TR}|/|S|$) collisions and metrics related to collision avoidance and the change of collision partner configurations.

As was found in Section 9.4.2.2, the number of collision events in the baselines was 84 for $t_{\mathrm{LA}} = 0.6\,\mathrm{s}$, 76 for $t_{\mathrm{LA}} = 0.9\,\mathrm{s}$ and 86 for $t_{\mathrm{LA}} = 1.2\,\mathrm{s}$, i.e., it was lowest for $t_{\mathrm{LA}} = 0.9\,\mathrm{s}$. However, the proportion of remaining treatment collisions in the total number of conflicts increased to around 5.4 % with increasing t_{LA}, as can be seen by $|S_C^{TR}|/|S|$ in Figure 9.27. With the higher settings for t_{LA}, i.e., $t_{\mathrm{LA}} = 0.9\,\mathrm{s}$ and $t_{\mathrm{LA}} = 1.2\,\mathrm{s}$, there was a drop in the avoidance potential down to 39.5 % and 40.7 % for $t_{\mathrm{LA}} = 0.9\,\mathrm{s}$ and $t_{\mathrm{LA}} = 1.2\,\mathrm{s}$ with system configuration 1 or 38.2 % and 38.4 % for $t_{\mathrm{LA}} = 0.9\,\mathrm{s}$ and $t_{\mathrm{LA}} = 1.2\,\mathrm{s}$ with system configuration 2. Inspection of the avoided conflicts reveals that while there were certain conflicts that were avoided by both system configurations for all settings of t_{LA}, there were also several conflicts that were avoided for example by system configuration 1 and $t_{\mathrm{LA}} = 0.9\,\mathrm{s}$, but not with $t_{\mathrm{LA}} = 1.2\,\mathrm{s}$, and vice versa. Therefore, it is difficult to derive a general statement on the influence of t_{LA} on the avoidance potential, and puts the avoidance potential that was found in the exemplary study in Chapter 8 in perspective. While the exemplary study overestimates E_{av} in comparison to the literature (56.1 % to 57.8 % for $t_{\mathrm{LA}} = 0.6\,\mathrm{s}$ and 50 MTFS model runs), the results found in the present sensitivity study (38.2 % to 40.7 % for $t_{\mathrm{LA}} = 0.9\,\mathrm{s}$ and $t_{\mathrm{LA}} = 1.2\,\mathrm{s}$ and 20 MTFS model runs) come closer to the weighted average of reduction rates found in the literature (38.8 % to 41.6 %, see

Section 8.2.2). The dependency on t_{LA} further highlights the necessity for validation of trajectories in nanoscopic simulation and MTFS to trajectories from real traffic observation studies. An alternative is the co-simulation between MTFS and nanoscopic simulation, see Nalic et al., 2019.

In the majority of conflicts, in which a collision in the baseline was not avoided in the treatment, the collision partners remained unchanged, see E_{unch} in Figure 9.27 (55.3 % and 54.7 % for $t_{\mathrm{LA}} = 0.9\,\mathrm{s}$ and $t_{\mathrm{LA}} = 1.2\,\mathrm{s}$ with system configuration 1 or 57.9 % and 58.1 % for $t_{\mathrm{LA}} = 0.9\,\mathrm{s}$ and $t_{\mathrm{LA}} = 1.2\,\mathrm{s}$ with system configuration 2), while E_{ch} decreased for higher settings of t_{LA} (5.3 % and 4.7 % for $t_{\mathrm{LA}} = 0.9\,\mathrm{s}$ and $t_{\mathrm{LA}} = 1.2\,\mathrm{s}$ with system configuration 1 or 3.9 % and 3.5 % for $t_{\mathrm{LA}} = 0.9\,\mathrm{s}$ and $t_{\mathrm{LA}} = 1.2\,\mathrm{s}$ with system configuration 2).

9.4.2.5. Changes in minimum TTC and minimum distances

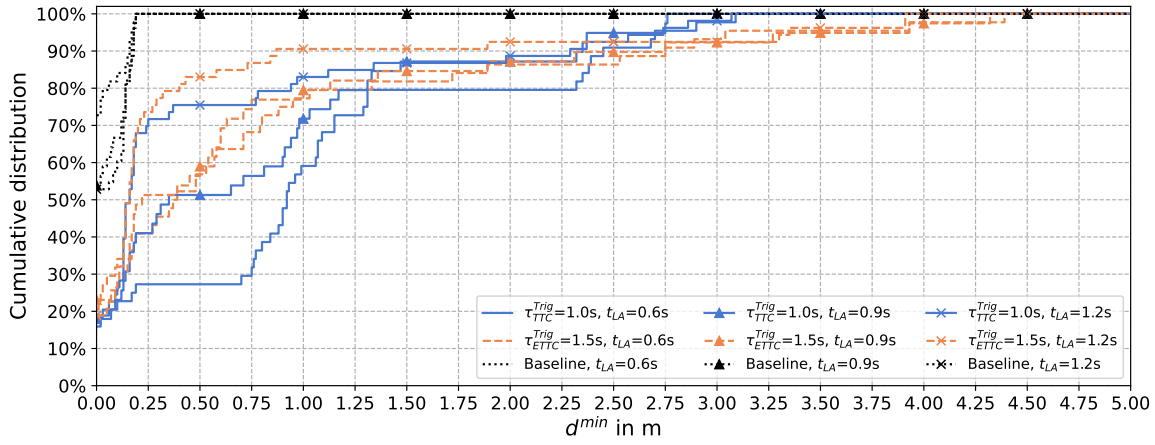

Figure 9.28.: Cumulative distribution of d^{min} in the baseline and the two treatments. The vertical axis represents the quantiles. Collisions are counted as zero values.

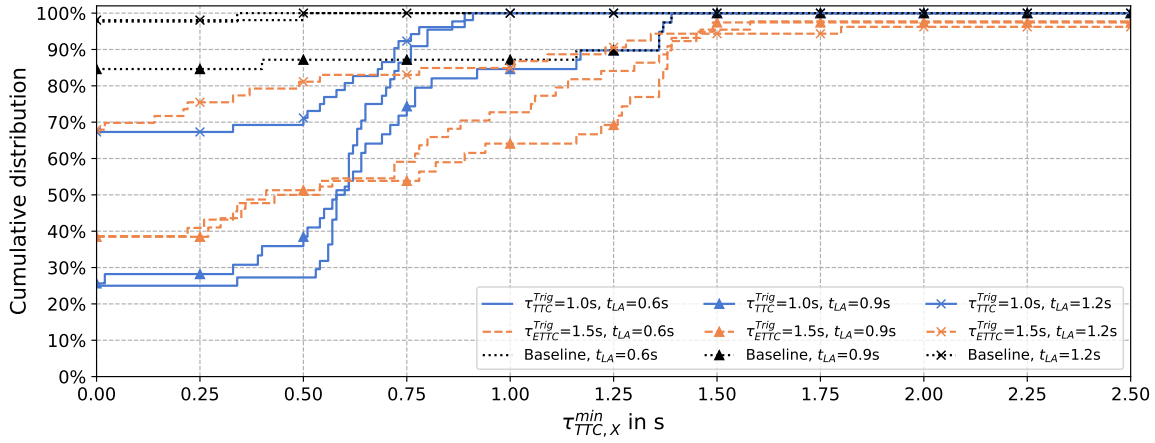

Figure 9.29.: Cumulative distribution of $\tau^{\mathrm{min}}_{\mathrm{TTC,X}}$ in the baseline and the two treatments. Collisions are counted as zero values.

As a general trend when increasing t_{LA}, it can be seen in Figure 9.28, that in the majority of

System configuration	t_{LA}	$E^{\mathrm{dang},TR}_{\mathrm{dist},50\,\%}$ in m	$E^{\mathrm{dang},TR}_{\mathrm{TTC},50\,\%}$ in s
$\tau^{\mathrm{Trig}}_{\mathrm{TTC}} = 1.0\,\mathrm{s}$	0.6	0.92	0.58
	0.9	0.35	0.58
	1.2	0.16	0.00
$\tau^{\mathrm{Trig}}_{\mathrm{ETTC}} = 1.5\,\mathrm{s}$	0.6	0.39	0.43
	0.9	0.22	0.41
	1.2	0.16	0.00

Table 9.5.: The metrics $E^{\mathrm{dang},TR}_{\mathrm{dist},50\,\%}$ and $E^{\mathrm{dang},TR}_{\mathrm{TTC},50\,\%}$ for the investigated system configurations and settings of t_{LA}.

the cases, the values for d^{min} in the treatments were lower for both system configurations (i.e., the lines for higher values of t_{LA} are above the lines for lower values of t_{LA} in Figure 9.28). This can also be seen in Table 9.5 by the medians, expressed by the metric $E^{\mathrm{dang},TR}_{\mathrm{dist},50\,\%}$. This means, that with a higher look-ahead time t_{LA}, a less pronounced safety effect in terms of increasing the minimum distance d^{min} was possible.

A similar effect can be observed for the values of $\tau^{\mathrm{min}}_{\mathrm{TTC,X}}$ in the treatments, see Figure 9.29. Furthermore, for the highest setting for t_{LA}, the median of $\tau^{\mathrm{min}}_{\mathrm{TTC,X}}$, i.e., the metrics $E^{\mathrm{dang},TR}_{\mathrm{TTC},50\,\%}$, even evaluated to 0, as can also be seen in Table 9.5. This means that in the majority of conflicts with dangerous situations, the systems did not provide a safety benefit when using $t_{\mathrm{LA}} = 1.2\,\mathrm{s}$. Again, this dependency on t_{LA} highlights the necessity for validation of trajectories in nanoscopic simulation and MTFS to trajectories from real traffic observation studies.

9.4.3. Conclusions

The following conclusions were found in the sensitivity study that investigates the influence of the look-ahead time:

- Increasing t_{LA} leads to smoother trajectories and cutting of corners, i.e., lower maximum curvatures of trajectories. In general, the vehicles start steering earlier than with $t_{\mathrm{LA}} = 0.6\,\mathrm{s}$.
- In the trajectory-based safety analysis of the MTFS model, the trajectories in MTFS and the parameterization of the kinetic path driver model in nanoscopic simulation should be validated for each vehicle model individually. This includes a validation to parameters that influence the vehicle dynamics, such as the length, wheelbase or vehicle mass.
- A minimum in the number of collision events in the baseline between the conflict participants was found for the setting $t_{\mathrm{LA}} = 0.9\,\mathrm{s}$, with which 35 % less collisions occurred (20 instead of 31), than with the setting $t_{\mathrm{LA}} = 0.6\,\mathrm{s}$, which was used in the exemplary effectiveness study. It has to be noted that this result is only valid when using the fuzzy model implemented in PC-Crash.

- Collision events with surrounding traffic occurred at any time during the simulation, for any setting for t_{LA}.
- Changes in the parameter t_{LA} impacted all categories of effectiveness metrics significantly, i.e., the differences in the metrics were higher than the variation of the metrics observed in the exemplary effectiveness study. Further research on kinetic path driver models is needed, paired with validation to trajectories from traffic observation studies for different vehicle geometries. The influence of t_{LA} on the effectiveness metrics suggests that, without validation to real trajectories, the resulting values for the metrics are best compared with literature by considering value ranges (e.g., the system configuration that triggers at $\tau_{\mathrm{TTC}}^{\mathrm{Trig}} = 1.0\,\mathrm{s}$ leads to an avoidance potential of 40 % to 58 %).
- The metrics E_{sens} and $E_{\mathrm{MCC}}^{\mathrm{norm}}$ were impacted the most by the increase in t_{LA}. For example, for both system configurations, E_{sens} was found to be 69.2 % with $t_{\mathrm{LA}} = 0.9\,\mathrm{s}$ and 84.9 % with $t_{\mathrm{LA}} = 1.2\,\mathrm{s}$, since the false negative and true positive system responses occurred with different proportions in the total number of conflicts, for different settings of t_{LA}.
- With the three different settings for t_{LA}, a specific conflict was once treated as true positive, once as false negative and once as true negative. This demonstrates the impact which changes in the trajectory of as little as 0.2 m can have.
- The collision avoidance potential E_{av}, and consequently the related metric E_{unch}, were significantly influenced by t_{LA}. The metric E_{av} dropped from 58.3 % for system configuration 1 ($\tau_{\mathrm{TTC}}^{\mathrm{Trig}} = 1.0\,\mathrm{s}$) and $t_{\mathrm{LA}} = 0.6\,\mathrm{s}$ down to around 40 % for $t_{\mathrm{LA}} = 0.9\,\mathrm{s}$ and $t_{\mathrm{LA}} = 1.2\,\mathrm{s}$, and from 52.4 % for system configuration 2 ($\tau_{\mathrm{ETTC}}^{\mathrm{Trig}} = 1.5\,\mathrm{s}$) and $t_{\mathrm{LA}} = 0.6\,\mathrm{s}$ down to around 38 % for $t_{\mathrm{LA}} = 0.9\,\mathrm{s}$ and $t_{\mathrm{LA}} = 1.2\,\mathrm{s}$.
- While the exemplary study overestimates E_{av} (56.1 % to 57.8 % for $t_{\mathrm{LA}} = 0.6\,\mathrm{s}$ and 50 MTFS model runs), the numbers for the collision avoidance potential found in this sensitivity study (38.2 % to 40.7 % for $t_{\mathrm{LA}} = 0.9\,\mathrm{s}$ and $t_{\mathrm{LA}} = 1.2\,\mathrm{s}$ and 20 MTFS model runs) come closer to the weighted average of reduction rates found in the literature (38.8 % to 41.6 %, see Section 8.2.2).
- The metrics $E_{\mathrm{dist,\,50\,\%}}^{\mathrm{dang},\,TR}$ and $E_{\mathrm{TTC,\,50\,\%}}^{\mathrm{dang},\,TR}$, measuring the median of d^{min} and $\tau_{\mathrm{TTC,X}}^{\mathrm{min}}$ in the treatment, were significantly influenced by t_{LA}. For system configuration 1 ($\tau_{\mathrm{TTC}}^{\mathrm{Trig}} = 1.0\,\mathrm{s}$), the metric $E_{\mathrm{dist,\,50\,\%}}^{\mathrm{dang},\,TR}$ dropped from 0.92 with $t_{\mathrm{LA}} = 0.6\,\mathrm{s}$ down to 0.16 with $t_{\mathrm{LA}} = 1.2\,\mathrm{s}$, and the metric $E_{\mathrm{TTC,\,50\,\%}}^{\mathrm{dang},\,TR}$ dropped from 0.58 with $t_{\mathrm{LA}} = 0.6\,\mathrm{s}$ down to 0 with $t_{\mathrm{LA}} = 1.2\,\mathrm{s}$. For system configuration 2 ($\tau_{\mathrm{ETTC}}^{\mathrm{Trig}} = 1.5\,\mathrm{s}$), the metric $E_{\mathrm{dist,\,50\,\%}}^{\mathrm{dang},\,TR}$ dropped from 0.39 with $t_{\mathrm{LA}} = 0.6\,\mathrm{s}$ down to 0.16 with $t_{\mathrm{LA}} = 1.2\,\mathrm{s}$, and the metric $E_{\mathrm{TTC,\,50\,\%}}^{\mathrm{dang},\,TR}$ dropped from 0.43 with $t_{\mathrm{LA}} = 0.6\,\mathrm{s}$ down to 0 with $t_{\mathrm{LA}} = 1.2\,\mathrm{s}$.

It has to be noted that this parameter study is not exhaustive and includes only one parameter in the variation, while there are several other ways how the steering behavior can be changed. For example, by changing the of the kinetic path driver model (fuzzy vs. PID-model) or by defining a rule to choose the parameter t_{LA} individually for each vehicle model. However, the dependency of the trajectories and the effectiveness metrics

on t_{LA} suffices to demonstrate the importance of the validation of the kinetic path driver model. Since all of the investigated effectiveness metrics changed when changing t_{LA}, all of the metrics will be affected when such a validation to real traffic observation studies is conducted. In addition, the number of collision events that involve surrounding traffic, or the number of collision events that occurred between conflict participants at 3 s to 4 s after $t_{\tau_{\mathrm{TTC}}^{\mathrm{min}}}$, should decrease, since such collision events should simply appear as additional conflicts in MTFS when the trajectories both in MTFS and nanoscopic simulation are validated to the same validation target.

9.5. Variation in the simulated time before and after the time of minimum TTC

9.5.1. Objective and method

As discussed in Section 7.2.1, collision events occurred throughout the whole simulated time frame $I = \left[t_{\tau_{\mathrm{TTC}}^{\mathrm{min}}} - t_{\mathrm{sim}},\ t_{\tau_{\mathrm{TTC}}^{\mathrm{min}}} + t_{\mathrm{sim}}\right]$ with $t_{\mathrm{sim}} = 5\,\mathrm{s}$. The value $t_{\mathrm{sim}} = 5\,\mathrm{s}$ was chosen for the exemplary effectiveness study as a starting value. Therefore, it remains to be seen, whether shortening the simulated time frame impacts the effectiveness metrics, as the safety systems react to the presence of a collision course. The earliest activating strategy among the investigated safety systems is defined to activate at $\tau_{\mathrm{ETTC}}^{\mathrm{Trig}} = 1.5\,\mathrm{s}$. To include the earliest point in time when a system can react, at least this value of 1.5 s should be included before $t_{\tau_{\mathrm{TTC}}^{\mathrm{min}}}$. As $\tau_{\mathrm{TTC,X}}^{\mathrm{min}}$ and $\tau_{\mathrm{ETTC,X}}^{\mathrm{min}}$ are only loosely correlated to $\tau_{\mathrm{TTC,S}}^{\mathrm{min}}$, at least 2 s before $t_{\tau_{\mathrm{TTC}}^{\mathrm{min}}}$ are considered. Therefore, as the first variation, $t_{\mathrm{sim}} = 2\,\mathrm{s}$ is chosen, resulting in 4 s total length of I. As an additional variation for the time frame, $t_{\mathrm{sim}} = 3.5\,\mathrm{s}$ is investigated. For this sensitivity study, the first 20 model runs of WBE are used. For each of the newly defined time frames, the baseline has to be simulated again.

In the first subsection, the number of collision events and their time of occurrence is investigated. Then, the influence of the simulated time frame length on the effectiveness metrics is investigated.

9.5.2. Results and discussion

9.5.2.1. Changes in collision events

A decrease from 10 s to 7 s or to 4 s in the length of the simulated time around conflicts corresponds to a reduction of 30 % or 60 % of the simulated time, respectively. In Section 7.2.1, it was found that collision events between one conflict participant and surrounding traffic occurred uniformly distributed over the simulated time. It could therefore be suspected that the number of such collision events would be reduced by the same amount as the simulated

Baseline variation	*One collision partner is a conflict participant*	*Both collision partners are conflict participants*	*Total collisions*
Simulated time: 10 s	53	31	84
Simulated time: 7 s	31 (−41.5 %)	20 (−35.4 %)	51 (−39.2 %)
Simulated time: 4 s	10 (−81.1 %)	12 (−61.2 %)	22 (−73.8 %)

Table 9.6.: Number of collisions where only one conflict participant was involved, number of collisions between conflict participants and total number of collisions in the baseline. The numbers on parentheses show the relative change compared to baseline with a simulated time of 10 s.

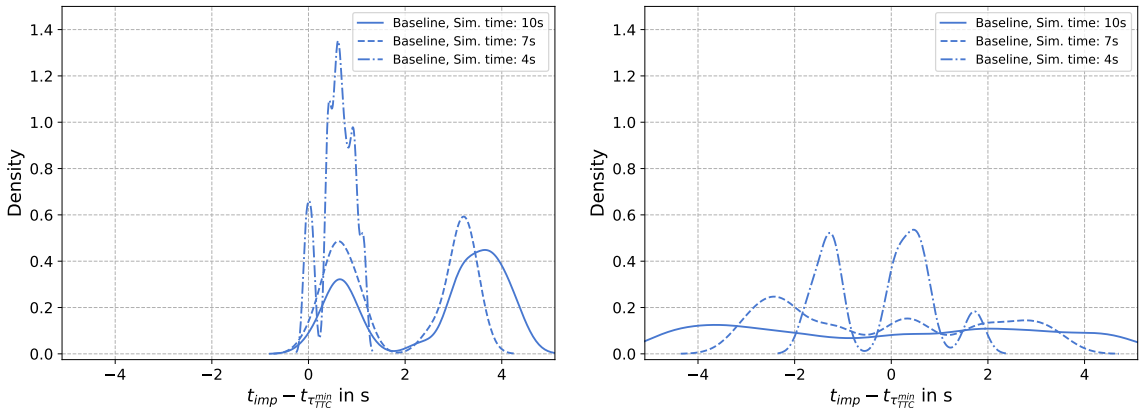

Figure 9.30.: Horizontal axis: difference between the impact time t_{imp} and $t_{\tau_{\text{TTC}}^{\min}}$, i.e. $t_{\text{imp}} - t_{\tau_{\text{TTC}}^{\min}}$. The value 0 on the horizontal axis then corresponds to $t_{\tau_{\text{TTC}}^{\min}}$ in MTFS. Vertical axis: kernel density estimates of the distribution of the values on the horizontal axis (see for example Rosenblatt, 1956). As kernel function, the normal distribution with a bandwidth of $h = 0.2$ was used. Left figure: Collision events where both collision partners were conflict participants. Right figure: Only one of both collision partners was a conflict participant.

time frame length. However, as is shown in Table 9.6, a reduction in the number of collision events can be observed for collision events with only one conflict participant, and also for collision events where both collision partners were a conflict participant. This reduction was in both types of collision events even higher than the reduction of the total length of the simulated time.

Individual inspection of collision events showed that all collision events that occurred with 4 s time frame length also occurred with 7 s and 10 s time frame length, and all collision events that occurred with 7 s time frame length also occurred with 10 s time frame length. Furthermore, they occurred at the same time in relation to $t_{\tau_{\text{TTC}}^{\min}}$. This means that shortening the simulated time frame length simply removes collision events, and if a collision events remains, it occurs at the same time as with the longer time frame.

When investigating the time of occurrence of collision events between conflict participants, i.e., the impact time t_{imp} in relation to $t_{\tau_{\text{TTC}}^{\min}}$, it can be seen in Figure 9.30 (left), that the peak in density around 3 s to 4 s remained for the time frame with length 7 s, but disappeared when the simulated time is limited to a maximum of 2 s after $t_{\tau_{\text{TTC}}^{\min}}$. This is a logical consequence

of the fact that the simulation did simply last not long enough to include those collisions. For the time frame of 4 s length, the collision events between the conflict participants occurred either at the moment when $\tau^{\min}_{\mathrm{TTC,S}}$ was reached, or up to around 1.0 s afterwards. In Figure 9.30 (right), it can be seen, that when using a simulated time frame of a length of 7 s, collision events where only one collision partner was a conflict participant occurred at any time during the simulation, with a small peak in density between 2 s to 3 s before $t_{\tau^{\min}_{\mathrm{TTC}}}$. The 10 collision events that occurred with 4 s simulated time frame length, where only one collision partner was a conflict participant, occurred clustered shortly after $t_{\tau^{\min}_{\mathrm{TTC}}}$ and around 1 s to 2 s before $t_{\tau^{\min}_{\mathrm{TTC}}}$, see Figure 9.30 (right).

9.5.2.2. System response categories and related metrics

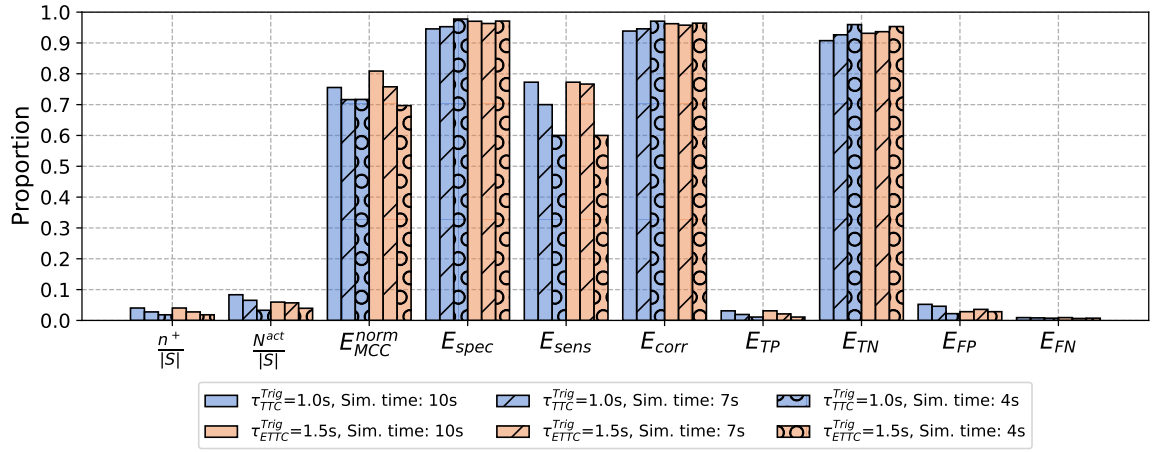

Figure 9.31.: Metrics related to the system response categories (false/true positive/negative), the proportion $\frac{n^+}{|S|}$ of dangerous baseline situations in the number of concrete scenarios in the scenario catalog S, and the proportion $\frac{N^{\mathrm{act}}}{|S|}$ of system activations in $|S|$.

The proportion $\frac{n^+}{|S|}$ of dangerous situations between the conflict participants decreased from 4.0 % to 2.8 % and 1.8 % when shortening the simulated time to 7 s and 4 s, respectively, see Figure 9.31. This corresponds to a reduction by 30 % and 65 %, respectively, as compared to the reduction of the time frame length by 30 % and 60 %. In parallel to fewer occurring collision events, also the proportion $\frac{N^{\mathrm{act}}}{|S|}$ with system activations decreased from 8.3 % to 6.5 % and 3.3 % for system configuration 1 ($\tau^{\mathrm{Trig}}_{\mathrm{TTC}} = 1.0\,\mathrm{s}$), and from 6.0 % to 5.7 % and 3.9 % for system configuration 2 ($\tau^{\mathrm{Trig}}_{\mathrm{ETTC}} = 1.5\,\mathrm{s}$). To investigate the reasons for the reduction in activations, the time of activation in relation to $t_{\tau^{\min}_{\mathrm{TTC}}}$ is visualized in Figure 9.32 as a graph of the kernel density estimate of the values $t_{\mathrm{acti}} - t_{\tau^{\min}_{\mathrm{TTC}}}$, where t_{acti} is the time when the system activation conditions were fulfilled, such that the systems triggered. As can be seen in Figure 9.32 (left and right), the majority of system activations for both configurations took place shortly before $t_{\tau^{\min}_{\mathrm{TTC}}}$, i.e., close to $t_{\mathrm{acti}} - t_{\tau^{\min}_{\mathrm{TTC}}} = 0$. Furthermore, since the collision events that occurred at around 3 s to 4 s after $t_{\tau^{\min}_{\mathrm{TTC}}}$ with a simulation time frame length of 10 s or 7 s did not occur when using a simulation time frame of 4 s length, also the corresponding

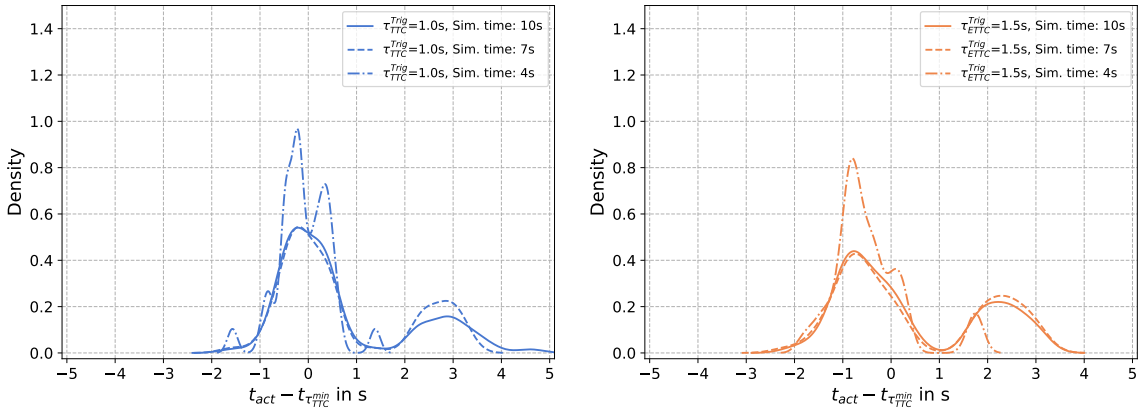

Figure 9.32.: Horizontal axis: difference between the time t_{acti} when the system activation conditions were fulfilled and $t_{\tau_{\text{TTC}}^{\min}}$, i.e. $t_{\text{acti}} - t_{\tau_{\text{TTC}}^{\min}}$. The value 0 on the horizontal axis then corresponds to $t_{\tau_{\text{TTC}}^{\min}}$ in MTFS. Only system activations for the other conflict participant are shown. Vertical axis: kernel density estimates of the distribution of the values on the horizontal axis (see for example Rosenblatt, 1956). As kernel function, the normal distribution with a bandwidth of $h = 0.1$ was used. Left figure: Activations by system configuration 1. Right figure: Activations by system configuration 2.

system activations were not necessary any longer. This led to the disappearance of the corresponding peaks in Figure 9.32 (left and right) at 2 s to 3 s after $t_{\tau_{\text{TTC}}^{\min}}$ when using a simulation time frame of 4 s length.

While the proportion E_{FN} of conflicts with false negative activations was very similar (between 0.6 % and 0.9 %), the proportion E_{TP} of conflicts with true positive activations decreased from 3.1 % to 2.1 % and 1.1 % for both system configurations, as there were fewer dangerous situations. Therefore, at a shorter simulated time frame, the false negative activations corresponded to a larger proportion in $FN + TP$ in the computation of the metric $E_{\text{sens}} = \frac{TP}{FN+TP}$, which decreased for both system configurations from 77.3 % to 60.0 %. These changes are also reflected in $E_{\text{MCC}}^{\text{norm}}$, which was reduced for system configuration 1 from 0.76 to 0.72 for the shortest simulation time frame of 4 s. For system configuration 2, $E_{\text{MCC}}^{\text{norm}}$ was reduced from 0.81 to 0.70.

The proportion E_{TN} of true negative system responses increased from 90.8 % to 96.0 % for system configuration 1 and from 93.1 % to 95.3 % for configuration 2 when shortening the simulation time frame to 4 s. For system configuration 1, the proportion E_{FP} of conflicts with false positive system responses decreased from 5.2 % to 2.2 % when the time frame was shortened to 4 s, which was not the case for configuration 2, where E_{FP} ranged between 2.8 % and 3.6 %, see Figure 9.31. Since the relative changes in E_{TN} or E_{FP} were not as large as for example for E_{TP}, the specificity E_{spec} was impacted not as much as the sensitivity E_{sens}.

Since the metrics related to system response categories were influenced significantly by t_{sim} and the resulting length of the simulated time frame, the question arises how to correctly choose the simulated time frame around conflicts. In the present thesis, the simulation is started at a fixed time before $t_{\tau_{\text{TTC}}^{\min}}$. Either reaching a certain time span after $t_{\tau_{\text{TTC}}^{\min}}$ or

the occurrence of a collision were used as the stop criterion for nanoscopic simulation. When starting the nanoscopic simulation 5 s before $t_{\tau_{\mathrm{TTC}}^{\min}}$, the earliest activation took place -1.37 s before $t_{\tau_{\mathrm{TTC}}^{\min}}$ for system configuration 1, and -1.80 s before $t_{\tau_{\mathrm{TTC}}^{\min}}$ for configuration 2. In addition, no collision event between conflict participants occurred earlier than that. This indicates that 2 s before $t_{\tau_{\mathrm{TTC}}^{\min}}$ are sufficient to include the earliest point in time when an activation or a collision event occurs, even when considering the sensor acquisition time of 0.2 s. Since all investigated effectiveness metrics either depend on collision events, accompanying dangerous situations or system activations, considering only 2 s before $t_{\tau_{\mathrm{TTC}}^{\min}}$ would leave the effectiveness metrics unaffected, as long as the maximum time simulated after $t_{\tau_{\mathrm{TTC}}^{\min}}$ remains at 5 s.

As was concluded in the previous sensitivity study on the kinetic path driver model, validation of the trajectories in MTFS and nanoscopic simulation to the same validation target (e.g., results from real traffic observation studies) should leave only collision events between conflict participants, in the case that such collision events still occur. They would also occur in close temporal vicinity to $t_{\tau_{\mathrm{TTC}}^{\min}}$. If that is the case, the effectiveness metrics that measure the safety benefit in regard to the conflict participants would not be impacted if the simulation is stopped as soon as a collision or dangerous situation is no longer possible between the conflict participants, or if an activation for the other conflict participant can no longer occur. This could serve as an alternative stopping criterion for future studies, which involve the aforementioned trajectory validation. If interactions between vehicles activating a brake maneuver and the surrounding traffic are of interest, it might be necessary to consider longer simulation time frames. Vehicles in the surrounding traffic might not be able to react to the emergency maneuver, which might produce further dangerous situations. To measure the consequences of system activations on the surrounding traffic or the traffic flow in general, it could even be necessary to couple nanoscopic simulation and MTFS more directly on a time step by time step basis without distinction of individual conflicts, since interruptions due to emergency maneuvers might propagate through the traffic flow, causing traffic jams and new conflicts several seconds or perhaps even minutes after a system activation.

9.5.2.3. Accident avoidance rates and changes in collision partners

The proportion $|S_C|/|S|$ of baseline collisions decreased with shorter simulated time frames from 7.7 % to 2.0 %. Correspondingly, with a shorter simulated time frame, the proportion $|S_C^{TR}|/|S|$ of treatment collisions decreased from 4.0 % to 1.1 % for system configuration 1 and from 4.1 % to 1.2 % for system configuration 2.

The effectiveness metric E_{av} showed a variation between 45.5 % (4 s simulated time frame, both system configurations) and 58.3 % (10 s simulated time frame) for system configuration 1 or 56.9 % for system configuration 2 (7 s simulated time frame). However, as the number of collisions in the baseline was 22 for 4 s simulated time frame length, avoiding one more

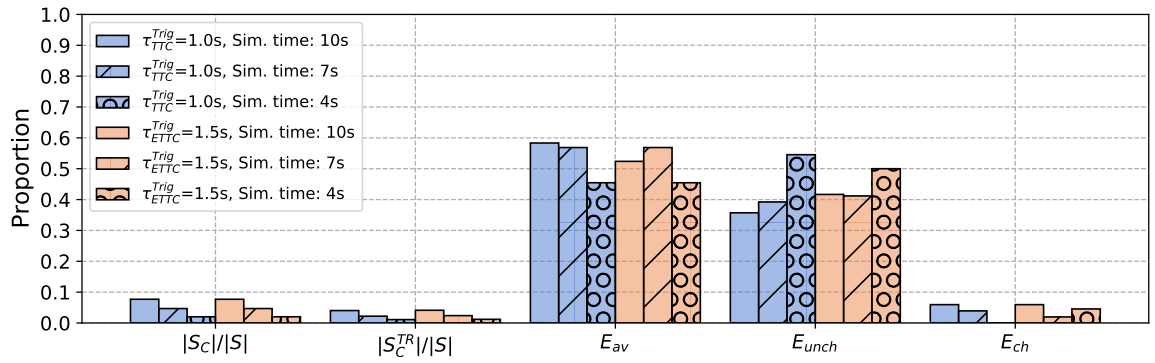

Figure 9.33.: The proportions of baseline ($|S_C|/|S|$) and treatment ($|S_C^{TR}|/|S|$) collisions and metrics related to collision avoidance and the change of collision partner configurations.

collision would lead to an increase in E_{av} of 4.5 %. This means that the metric is likely unstable, as could also be found when considering the convergence in dependence of the number of considered MTFS model runs. Such an analysis was for example done in the exemplary effectiveness study. It is therefore questionable whether the results in the present section for the effectiveness metrics E_{av}, E_{unch} and E_{unch} for the shorter simulation time frame of 4 s length, or possibly also of 7 s length, can be properly interpreted as final results.

9.5.2.4. Changes in minimum TTC and minimum distances

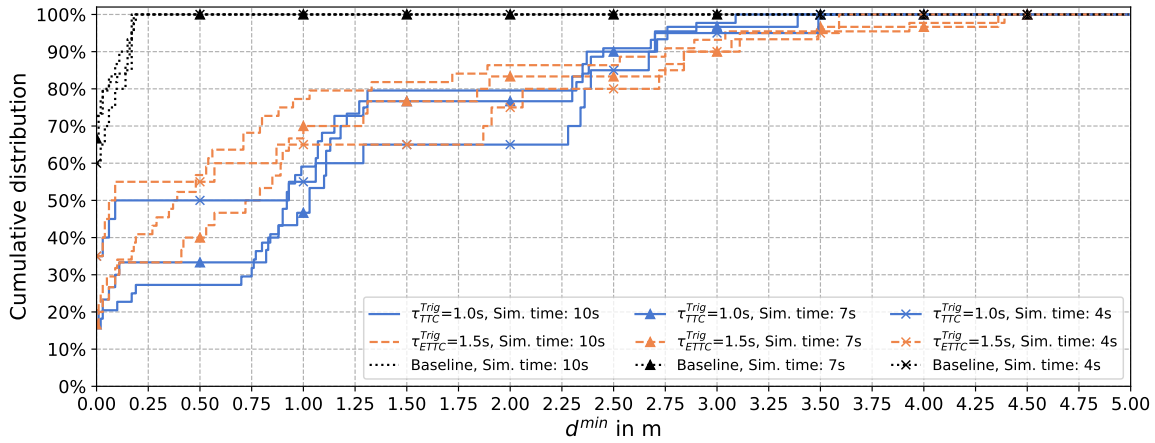

Figure 9.34.: Cumulative distribution of d^{min} in the baseline and the two treatments. The vertical axis represents the quantiles. Collisions are counted as zero values.

As can be seen in Figure 9.34 and Table 9.7, the medians of d^{min} in the treatment, i.e., the metric $E^{\text{dang},TR}_{\text{dist},50\,\%}$, ranged significantly between 0.09 m and 1.03 m for system configuration 1 and between 0.06 m and 0.76 m for system configuration 2. Similar significant changes can be observed for $E^{\text{dang},TR}_{\text{TTC},50\,\%}$ for system configuration 2, see Figure 9.35 or Table 9.7.

For both system configurations and several settings of t_{LA}, several horizontal sections

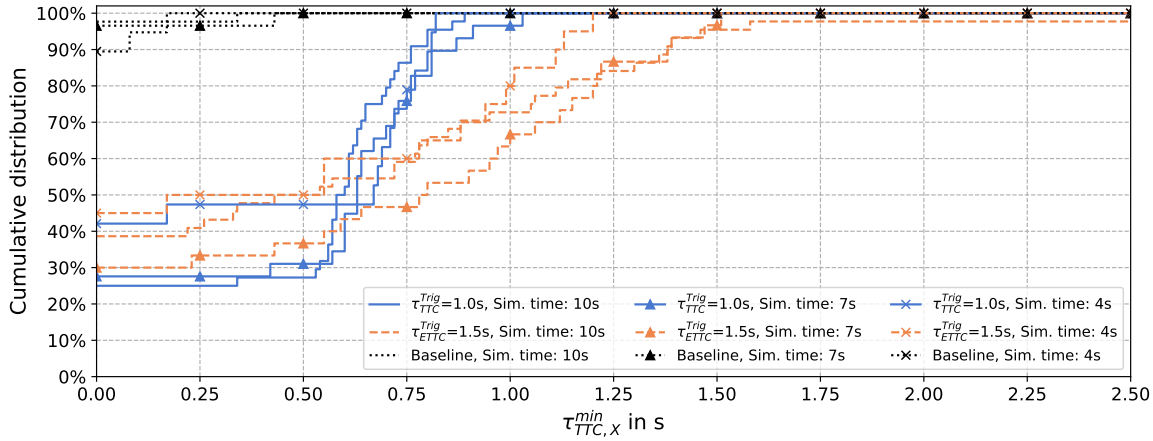

Figure 9.35.: Cumulative distribution of $\tau^{\text{min}}_{\text{TTC,X}}$ in the baseline and the two treatments. Collisions are counted as zero values.

System configuration	Simulation time frame length in s	$E^{\text{dang},TR}_{\text{dist},50\,\%}$ in m	$E^{\text{dang},TR}_{\text{TTC},50\,\%}$ in s
$\tau^{\text{Trig}}_{\text{TTC}} = 1.0\,\text{s}$	10	0.92	0.58
	7	1.03	0.63
	4	0.09	0.67
$\tau^{\text{Trig}}_{\text{ETTC}} = 1.5\,\text{s}$	10	0.37	0.43
	7	0.72	0.78
	4	0.06	0.17

Table 9.7.: The metrics $E^{\text{dang},TR}_{\text{dist},50\,\%}$ and $E^{\text{dang},TR}_{\text{TTC},50\,\%}$ for the investigated system configurations and time frame lengths.

spanning more than 0.5 m can be seen in the graphs in Figure 9.34 (or spanning more than 0.4 s in Figure 9.35), which can indicate instability in the metric $E^{\text{dang},TR}_{\text{dist},50\,\%}$ or $E^{\text{dang},TR}_{\text{TTC},50\,\%}$. Such instabilities can occur when additional observations are included, and if the horizontal section is located around the investigated quantile (e.g., the median). Furthermore, the number of dangerous situations decreased with shorter simulated time frames. Therefore, it can be suspected that convergence was not yet reached with the considered number of conflicts, such that it becomes questionable whether the results for the metrics in Table 9.7 can be interpreted as final results.

In general, it can be suspected that the metrics strongly depended on the characteristics of the collisions that were omitted when the simulation time frame was shortened. For example, if $d^{\text{min}}(TR(s))$ was high for concrete baseline scenarios s with collisions that occurred around 3 s to 4 s after $t_{\tau^{\text{min}}_{\text{TTC}}}$, then the median will likely be affected if those concrete scenarios are omitted from the scenario catalog. The analogous holds true for $\tau^{\text{min}}_{\text{TTC,X}}(TR(s))$ and the related metric $E^{\text{dang},TR}_{\text{TTC},50\,\%}$. For future studies, the consideration of more MTFS model runs would be necessary.

9.5.3. Conclusions

The following conclusions were found in the sensitivity study that investigates the influence of the length of the simulated time frame:

- When shortening the length of the simulated time from 10 s to 7 s or 4 s by 30 % or 60 % respectively, the number of collision events is reduced by at least those percentages.
- Analogously, the proportion $\frac{n^+}{|S|}$ of dangerous situations between the conflict participants decreased from 4.0 % to 2.8 % and 1.8 % when shortening the simulated time to 7 s and 4 s, respectively, corresponding to a respective reduction of 30 % and 65 %.
- The effectiveness metrics $E_{\text{MCC}}^{\text{norm}}$ and E_{sens} were particularly affected by using a shorter simulation time frame.
- For the system configuration that triggers at $\tau_{\text{TTC}}^{\text{Trig}} = 1.0\,\text{s}$, the number of system activations for the other conflict participant decreased by 21 % and 60 % when shortening the simulated time to 7 s, respectively 4 s. For the system configuration that triggers at $\tau_{\text{ETTC}}^{\text{Trig}} = 1.5\,\text{s}$, $\frac{N^{\text{act}}}{|S|}$ decreased from 6.0 % to 3.9 %.
- As the number of dangerous situations and corresponding activations decreased when shortening the simulated time to 7 s and 4 s, also E_{TP} decreased from 3.1 % to 1.1 %. As E_{FN} remained on a very similar level (between 0.6 % and 0.9 %), E_{sens} was reduced from 77.3 % to 60 %. The specificity E_{spec} was less impacted: the values changed by a maximum of 3.2 % for the system configuration that triggers at $\tau_{\text{TTC}}^{\text{Trig}} = 1.0\,\text{s}$.
- Another consequence of the decrease in the number of dangerous situations and corresponding activations is that the number of conflicts used to compute the metrics E_{av}, E_{unch}, E_{ch}, $E_{\text{dist, 50 \%}}^{\text{dang, }TR}$ and $E_{\text{TTC, 50 \%}}^{\text{dang, }TR}$ also decreased, such that their interpretation becomes difficult as their value is likely unstable. To improve stability, consideration of more conflicts is needed in future studies.
- Based on the time of occurrence of collision events and system activations, it is sufficient to start nanoscopic simulation 2.0 s before $t_{\tau_{\text{TTC}}^{\text{min}}}$ without affecting the effectiveness metrics.
- When investigating only safety benefits in regard to the conflict participants (e.g., as is done for metrics related to the system response categories or $E_{\text{dist, 50 \%}}^{\text{dang, }TR}$ and $E_{\text{TTC, 50 \%}}^{\text{dang, }TR}$), the nanoscopic simulation should continue as long as a collision or a dangerous situation between conflict participants or a system activation in response to the other conflict participant is possible, instead of using a fixed maximum simulation time.
- When investigating safety benefits for which interactions with surrounding traffic are considered (e.g., E_{av}, E_{unch}, E_{ch}, E_{new}), it might be necessary to simulate considerably more time than only a few seconds after $t_{\tau_{\text{TTC}}^{\text{min}}}$, as the consequences of the system interventions might propagate through traffic flow, causing more conflicts, collisions or traffic jams. For that purpose, it would be necessary to develop and use appropriate driver models to correctly represent the response of surrounding traffic.

10. Discussion

This chapter draws together the results and conclusions of the previous chapters and aims to put them into perspective in relation to the objective, the resulting research questions and the scope defined in the beginning of this thesis. This is done by discussing the research questions

Q1.1 As a source of stochastically generated concrete scenarios, how can traffic flow simulation be coupled with nanoscopic simulation of driving dynamics and active safety systems?

Q1.2 How can the safety benefit of active safety systems be measured, and which metrics allow the evaluation of the effectiveness in critical scenarios and the system's interactions with the surrounding traffic?

Q1.3 How sensitive are the results of the effectiveness assessment method developed to answer research questions Q1.1 and Q1.2, with regard to changes in the involved components, models and parameters?

in the following three sections, followed by a discussion on the main research question:

Q1 How can the prospective effectiveness assessment of active safety systems be conducted when using concrete traffic scenarios that are generated through microscopic traffic flow simulation, while considering the driving dynamics and including traffic that surrounds the conflicting traffic participants?

10.1. Discussion of Q1.1

To answer Q1.1 ("As a source of stochastically generated concrete scenarios, how can traffic flow simulation be coupled with nanoscopic simulation of driving dynamics and active safety systems?"), an approach was presented that isolates individual relevant concrete scenarios within the MTFS data generated by VISSIM and then recreates the concrete scenario in nanoscopic simulation. Both for the selection process and the representation in nanoscopic simulation, important aspects to consider were discovered.

Since VISSIM as the chosen MTFS tool had currently no way to determine whether a real vehicle can actually follow the proposed trajectory exactly, the resulting trajectories had to be verified in nanoscopic simulation, and deviating trajectories were adapted in MTFS by

trajectory-based safety analysis. However, this is a validation of trajectories in nanoscopic simulation to MTFS. Ideally, a validation of both the trajectories in MTFS and the kinetic path driver model in nanoscopic simulation to a common validation target should be conducted, e.g., traffic observation studies such as the roundD dataset (Krajewski, Moers, et al., n.d.), the highD dataset (Krajewski, J. Bock, et al., 2018) or the TUBS road user dataset (Plachetka et al., 2018). As was found in Section 9.4, this should be done individually for different vehicle models. This validation would likely also lead to a reduction of collision events, which would be desirable, since MTFS is originally not intended to produce collisions.

In the present thesis work, the identification of relevant concrete scenarios, i.e., concrete scenarios that can have an influence on the investigated effectiveness metrics, was conducted based on τ_{TTC}. However, the deviations between trajectories also led to a deviation of the τ_{TTC} detected in MTFS and nanoscopic simulation for the individual conflicts, which led to activations of the safety systems in conflicts where $\tau_{\mathrm{TTC,S}}$ was above the trigger threshold $\tau_{\mathrm{TTC}}^{\mathrm{Trig}}$ of the safety system. A solution to improve the accuracy with which only relevant concrete scenarios are selected, is to improve the validity of trajectories, such that they are more similar in MTFS and nanoscopic simulation and to harmonize the τ_{TTC} calculation algorithms (X-RATE assumes a constant heading angle, while SSAM considers retrospective knowledge on the trajectories that resulted in MTFS). However, this would suffice only if the safety system operates solely based on a τ_{TTC} threshold or another singular SSM. As soon as the trigger mechanisms of the safety system become more complicated or are based on several different trigger conditions at the same time, selection of only the relevant scenarios becomes more difficult. A further problem arises in the case that two different safety systems with different trigger criteria should be compared, based on the same scenario catalog, as was done in the present thesis work. As was seen in Section 9.2.2.1, correlation between $\tau_{\mathrm{ETTC,X}}$ and $\tau_{\mathrm{TTC,X}}$ was low, although the probability for system activation by both systems decreased with higher $\tau_{\mathrm{TTC,S}}^{\mathrm{min}}$, which mitigated the problem of missing predictability of scenario relevance to some extent through a statistical argument.

For the problem of scenario selection, the following solutions would be possible:

- Conducting the scenario selection as inclusive as possible, e.g., by selecting all conflicts in which a collision course existed, regardless of the lowest τ_{TTC} that was reached. In that way, the scenario catalog definition step acts as a coarse pre-filter with the intention to omit those conflicts for nanoscopic simulation, which are definitely irrelevant to the effectiveness metrics. A requirement for this solution is that the effectiveness metrics are defined in such a way that they are as robust as possible to adding an arbitrary number of concrete scenarios to the scenario catalog in which no interaction between vehicles and the investigated safety systems takes place, i.e., concrete scenarios where no collision events, dangerous situations or system activations occur (for more detail how to define such metrics, see discussion on Q1.2).
- Avoiding the selection step altogether, by simulating the traffic in nanoscopic simulation for the full time span covered by MTFS, instead of considering only individual

concrete scenarios which last only for several seconds. This would also improve the presented approach by allowing a more far-reaching investigation of possible consequences of emergency maneuver activations, e.g., by allowing the investigation of traffic jams or the emergence of new conflicts that occurred only due to the emergency maneuver. The question how to correctly define the termination criterion in nanoscopic simulation would also be avoided. An approach that considers the full traffic, instead of individual conflicts, requires a time step based coupling of MTFS and nanoscopic simulation, or the direct integration of one simulation framework into the other, and it would require driver models specifically designed to describe human reactions to emergency maneuvers.

10.2. Discussion of Q1.2

To answer Q1.2 (”How can the safety benefit of active safety systems be measured, and which metrics allow the evaluation of the effectiveness in critical scenarios and the system’s interactions with the surrounding traffic?”), in the following subsections, the investigated effectiveness metrics are discussed, grouped by their category.

10.2.1. Accident avoidance rates and changes in collision partners

The collision avoidance potential E_{av} is a classical metric, which is evaluated in several prospective studies in the literature. In this thesis, E_{av} was computed based on all collisions that occurred, i.e., based on all conflict types that emerged in MTFS (rear-end, lane change and crossing). However, these collisions are considered to be artifacts of the coupling between MTFS and nanoscopic simulation and their number, type or time of occurrence depends on the kinetic path driver model and its parameterization. Therefore, the question arises whether the accidents in real traffic, which occur due to driving errors by humans, exhibit the same or very similar characteristics as the collisions found in this thesis (such characteristics include, for example, relative heading angles, pre-collision trajectories and velocities and the points of first contact). Since no validation was conducted specifically regarding those characteristics, the results for E_{av} cannot be treated as valid results to estimate the effectiveness of the investigated systems in real traffic. This motivates for future research on how to systematically generate concrete scenarios with validated collisions. A potential approach would be to first improve the coupling approach, such that no unintended collision events occur, and then introduce human driving errors in a validated way.

When validation of trajectories to real traffic is conducted, fewer collision events will occur when using the approach presented in this thesis, leading to inferior convergence of E_{av}, since the sample size is decreased. Therefore, the metric E_{av} might be of lower relevance

in general in combination with the presented approach, and in particular, since MTFS is originally designed to not produce collisions.

The metrics E_{ch} or E_{new} present an interesting addition to existing metrics to investigate consequences of safety system interventions. They are only relevant when surrounding traffic is considered, and should be evaluated whenever possible, to better understand the impact of the safety system on the remaining traffic. E_{ch} is defined as the proportion of changed collisions in the number of collisions in the baseline. In future studies, if collision events in the baseline become fewer with additional trajectory validation, it will be necessary to instead define the metric as the number of changed collisions per hour of vehicle operation, or as the proportion in the number of system activations, to ensure the metric's independence from the number of collision events or the number of investigated conflicts. The same can be done with E_{new}, which is the proportion of new collision in the number of concrete treatment scenarios with collisions.

10.2.2. System response categories and related metrics

Many simulative prospective effectiveness studies use accident data as source for concrete scenarios, where critical scenarios (i.e., a collision course exists) that do not lead to a dangerous situation cannot be provided, i.e., scenarios where a collision occurs or the safety zone is intruded. Effectiveness studies with critical scenarios are rare and estimates for the rate of false positives are difficult to find. In studies based on reconstructed real accidents, false-positives do not exist, since every scenario in the baseline is objectively dangerous. Therefore, the possibility to evaluate metrics such as E_{spec} with the presented method represents an important extension of the state of the art.

The advantage of fewer false-positive system responses, due to triggering emergency maneuvers based on $\tau_{\text{ETTC,X}}$, was particularly easy to see through higher values of the metric $E_{\text{spec}} = \frac{TN}{TN+FP}$. In future studies, if effectiveness assessment is based on the simulation of continuous traffic instead of individual conflicts, the definition of true negatives might become difficult, as normal conflict free driving without system activation could be interpreted as an infinite number of true negative responses, rendering the current definition of $E_{\text{spec}} = \frac{TN}{TN+FP}$ useless for studies with continuous traffic. An example for a study where a continuous simulation of traffic flow, driving dynamics and active safety systems is employed is the study Nalic et al., 2019. In this study, VISSIM and IPG CarMaker (*CarMaker* 2020) were coupled in co-simulation.

Furthermore, the effectiveness metrics mentioned in this subsection depended on the conflict selection criterion $\tau_{\text{TTC}}^{\text{Filt}}$. Therefore, an improvement would be to define the metrics as independent as possible from the number of conflicts, e.g., by investigating the number of false-positive responses per hour of vehicle operation.

Since the advantage of triggering based on $\tau_{\mathrm{ETTC,X}}$ was only visible when a filter threshold $0.7\,\mathrm{s} \leq \tau_{\mathrm{TTC}}^{\mathrm{Filt}} \leq 2.0\,\mathrm{s}$ was used (Section 9.2), and since the advantage was not observable when $\tau_{\mathrm{TTC}}^{\mathrm{Filt}} \geq 2.0\,\mathrm{s}$ is chosen, it might be interesting for future studies to adopt the practice to discuss the effectiveness metrics in dependence of the $\tau_{\mathrm{TTC,S}}^{\mathrm{min}}$ reached during the conflict in the baseline, as was done in the sensitivity study in Section 9.2. Alternatively, instead of defining the scenario catalog as the set of all conflicts with $0 < \tau_{\mathrm{TTC,S}}^{\mathrm{min}} \leq \tau_{\mathrm{TTC}}^{\mathrm{Filt}}$ with increasing upper limit $\tau_{\mathrm{TTC}}^{\mathrm{Filt}}$ as the final filter, disjoint scenario catalogs can be investigated such that the differences within the scenario catalogs can be seen more clearly. For example, two scenario catalogs could be defined by $0.5\,\mathrm{s} < \tau_{\mathrm{TTC,S}}^{\mathrm{min}} \leq 1.0\,\mathrm{s}$ and $1.0\,\mathrm{s} < \tau_{\mathrm{TTC,S}}^{\mathrm{min}} \leq 1.5\,\mathrm{s}$.

In addition, it was observed that the metric $E_{\mathrm{MCC}}^{\mathrm{norm}}$ was particularly sensitive (more than E_{corr}) to differences in E_{FN}, E_{FP}, E_{TP} and E_{TN} between individual system configurations or variations in the sensitivity study. Therefore, $E_{\mathrm{MCC}}^{\mathrm{norm}}$ or its transformed variant E_{MCC} can be seen as a valuable metric to measure the capability of the system to decide between dangerous and non-dangerous situations.

10.2.3. Change in minimum TTC and minimum distances

The metrics $E_{\mathrm{dist,50\,\%}}^{\mathrm{dang},\,TR}$ and $E_{\mathrm{TTC,50\,\%}}^{\mathrm{dang},\,TR}$, which describe d^{min} and $\tau_{\mathrm{TTC,X}}^{\mathrm{min}}$ in the treatment, were newly introduced, i.e., no literature comparison was possible. They are computed based on a sub-selection of conflicts (dangerous situations). For the present thesis, in the exemplary effectiveness study, they reached a stable result within 20 MTFS model runs. In those, a sufficient number of dangerous situations occurred. For future studies, where trajectory validation to observations of real traffic is conducted, significantly more MTFS model runs might be required to achieve convergence, as dangerous situations might become fewer. An advantage of the proposed metrics is that instead of simply expressing the avoidance of a collision, they express the safety level in the treatment, which can then be compared to the safety level in the baseline (expressed by $E_{\mathrm{dist,50\,\%}}^{\mathrm{dang},\,BL}$ and $E_{\mathrm{TTC,50\,\%}}^{\mathrm{dang},\,BL}$, which are most likely 0), thereby migrating from a binary variable (collision is avoided or not) to a continuous variable (e.g., d^{min}). These metrics could present an interesting point for comparison in future studies. They can be evaluated not only in combination with the method presented in this thesis, but also in any prospective effectiveness study that analyzes individual concrete scenarios, such as studies that use reconstructed real accidents as data basis.

10.2.4. Collision severity related effectiveness metrics

As mentioned in Section 10.2.1, no validation of the occurring collisions to real accidents was conducted. Therefore, the results for collision related metrics cannot be treated as valid estimates for the effectiveness of the investigated safety system in real traffic.

In addition, with improvements in the validation of the trajectories, fewer collisions in the baseline will occur. Therefore, the collision related metrics will become less relevant in future studies that employ the methodology presented in this thesis. To solve this problem, further research on methods, with which validated collisions can be generated stochastically, is required. However, since it is possible that the activation of a safety system will introduce new collisions or collisions with changed collision partners (e.g., when a vehicle conducts emergency steering to the opposing lane and produces a frontal collision), the related metrics $E_{\Delta v}^{\mathrm{TR},50\,\%}$, $E_{\Delta v}^{\mathrm{new},50\,\%}$ or $E_{\Delta v}^{\mathrm{ch},50\,\%}$ will be of interest. Since such events were rare in the exemplary study among the investigated 2760 conflicts for 50 MTFS model runs (i.e., 50 hours of traffic), significantly more model runs, depending, however, on the MTFS model, will be required for future studies to achieve convergence.

10.3. Discussion of Q1.3

This section contains a general discussion about aspects of the method for which the sensitivity studies in this thesis work, conducted to answer Q1.3 (”How sensitive are the results of the effectiveness assessment method developed to answer research questions Q1.1 and Q1.2, with regard to changes in the involved components, models and parameters?”), provide motivation for further research. Detailed discussions on the conducted sensitivity studies can be found in Chapter 9.

A general limitation to the comparability of the results on the effectiveness metrics that were obtained in this thesis is the ”case study problem”: all considerations were based on the MTFS models WBE and WBE50, which share the exactly same road layout. Although the increase in traffic density by 50 % in WBE50 led to no significant change in the metrics E_{av}, E_{unch}, E_{ch}, $E_{\mathrm{dist},50\,\%}^{\mathrm{dang},TR}$ or $E_{\mathrm{TTC},50\,\%}^{\mathrm{dang},TR}$, it did so in the proportion of false positive system responses, as the systems performed worse in the additional crossing conflicts introduced by exchanging the model WBE by WBE50. While the increase in traffic density is a minor change to the MTFS model, it can be suspected that MTFS models that represent other road sites will produce different types of conflicts, which will have a significant impact on the effectiveness metrics. Therefore, to gain a more holistic understanding of the effectiveness of the investigated safety systems, it would be necessary to simulate further MTFS models which are as diverse as possible but still meet the specification of the investigated safety systems (urban roads, in the case of the City AEB systems investigated in this thesis work).

Furthermore, sight obstructions may have a bigger influence in other MTFS models (e.g., with narrower roads and more static objects close to the road) than they had in the present thesis work, where no change in the effectiveness metrics was found. In the present thesis work, a simple geometrical sensor model was used to determine the visibility status of other traffic participants in nanoscopic simulation, which were represented by simple box-shaped mesh models. Since visibility obstructions by static objects or traffic participants without

collision course were of no influence, it is unlikely that more detailed traffic participant shape models, e.g., vehicle models that represent the tires or side mirrors as individual shapes, would have had an impact on the effectiveness. However, as soon as additional physical effects are represented by the sensor models, such as surface reflectivity for the simulation of RADAR sensors (see Winner, 2015b), more detailed physical properties and geometries of traffic participants and static objects will have to be considered.

Since a significant influence of driver model parameters in MTFS on the number of conflicts and their severity was found in Medicus, 2019, it is likely that those parameters have an influence on the effectiveness metrics as well. Such an investigation should be subject of future studies. The validation of the driver models is directly related to the validation of the trajectories to studies with observations of real traffic. The distribution of the type and severity of conflicts should match the traffic conditions of the investigated real traffic sites.

Two components involved in the simulation of the driving process that particularly require further validation are the sensors and safety systems, since the results of prospective effectiveness assessment studies using simulation are known to be sensitive on certain parameters that describe those components. In this thesis work, due to the lack of data in the literature for real vehicles, sensors and safety systems, several parameters had to be assumed with the same value as was used in other prospective effectiveness studies, even though the authors of the literature studies themselves did not conduct validation to real systems. For example, for the system response time (the time from when a trigger condition is fulfilled to the start of acceleration decrease due to the triggered maneuver), $t_{\mathrm{srt}} = 0.2\,\mathrm{s}$ was chosen in accordance to Wimmer, Düring, et al., 2019. To put that in perspective: J. M. Scanlon et al., 2017 showed that the avoidance potential of an Intersection AEB that triggers with $\tau_{\mathrm{TTC}}^{\mathrm{Trig}} = 1.0\,\mathrm{s}$ can range from 26 % to 36 % with $t_{\mathrm{srt}} = 0$ to $0.5\,\mathrm{s}$. Therefore, for future studies, additional validation of sensor and safety system models is needed.

10.4. Dicussion of the main research question Q1

To answer the main research question Q1 (”How can the prospective effectiveness assessment of active safety systems be conducted when using concrete traffic scenarios that are generated through microscopic traffic flow simulation, while considering the driving dynamics and including traffic that surrounds the conflicting traffic participants?”), a solution approach was presented in Chapter 4 which fulfills the solution requirements in Section 1.2.3. This solution approach was demonstrated in an exemplary effectiveness study and represents an interesting new possibility to conduct prospective effectiveness assessment. Through the introduction of surrounding traffic, the change in collision partner configurations became more complex. The necessity to include the surrounding traffic became clear through the occurrence of new and changed collisions, i.e., collisions that would not have occurred if no safety systems were activated. This is not only of interest for longitudinally acting

braking systems, but also when emergency steering systems are investigated that search for possible evasion paths. When several other traffic participants are present as surrounding traffic, the task of finding an appropriate evasion path becomes increasingly complex. Furthermore, the consideration of arbitrary driving maneuvers only becomes possible through the inclusion of driving dynamics in nanoscopic simulation, since in MTFS, traffic participants are constrained to their defined routes.

However, within the exemplary study and the sensitivity studies, several challenges that arise when using the presented solution approach were identified. The most influential ones are listed in the following:

- In the baseline, collision events can occur (collisions that occur in nanoscopic simulation but not in MTFS), which affect several aspects of the method. The number of collision events and the collision types depend on the chosen kinetic path driver model and its parameterization. The kinetic path driver model applied in this thesis work in nanoscopic simulation uses one parameter configuration for all simulated traffic participants. This is a starting point, but might be an oversimplification. In reality, individual traffic participants exhibit high variability in their steering behavior regarding lane changes or curved driving. Furthermore, different types of traffic participants (e.g., passenger cars, buses) might require different parameterizations of their kinetic path driver model.
- The stop criterion applied in nanoscopic simulation (occurrence of a collision or reaching a fixed maximum simulation time) led to a dependence of the effectiveness metrics on the maximum simulation time, as collision events were omitted when the maximum simulation time was shortened. It remains to be seen whether that dependence still exists when collision events are reduced by validating trajectories and the kinetic path driver model to real traffic.

While those challenges still need to be overcome, the approach presented in this thesis represents a further step toward more accurately reflecting the complexities of real traffic in prospective effectiveness studies. Those who take this approach can consider aspects of active safety effectiveness assessments which were previously not possible. The findings presented in this thesis will motivate other researchers to develop methods that can efficiently and directly incorporate driving dynamics and active safety system simulation in traffic flow simulations.

11. Conclusions

General conclusions on the methodology:

- The combination of MTFS and nanoscopic simulation represents a suitable method for the effectiveness assessment of ADAS. It offers the possibility to investigate the effects of ADAS in complex situations, under the consideration of surrounding traffic, and without the risk of injuries to human test subjects or damage to test equipment.
- Several methods exist to conduct appropriate validation of the investigated MTFS model regarding traffic related aspects, while methods to validate the models regarding safety related aspects are in their infancy. Furthermore, complex ADAS functionalities, such as systems that can conduct arbitrary evasion maneuvers, cannot be implemented directly in VISSIM. Therefore, potentially relevant traffic scenes have to be identified in the MTFS results to be recreated in nanoscopic simulation.
- An appropriate criterion for the identification of potentially relevant scenarios is the existence of a collision course, i.e., the existence of the TTC. The scenario selection rule should be designed to be as inclusive as possible to get the most comprehensive estimate of the effectiveness, e.g., by including scenarios with a TTC up to 2.5 s.
- The driver models implemented in VISSIM do not cause collisions. However, due to differences in the models to represent driving in MTFS (kinematic driving) and nanoscopic simulation (kinetic driving), differences in the trajectories and velocity profiles can occur. This can lead to collisions in nanoscopic simulation that did not occur in MTFS. The differences in the trajectories depend on the kinetic path driver model and its parameterization, the vehicle model (i.e., geometric parameters such as the wheelbase) and other vehicle related parameters that influence the driving dynamics.
- For the investigated safety systems, starting nanoscopic simulation 2 s before the minimum TTC was reached was sufficient to include possible interactions (collisions or system activations) between conflict vehicles. The simulation should only be stopped when no further interactions between the conflict vehicles are possible.
- The presented methodology makes it possible to investigate the capability of the safety systems to correctly distinguish dangerous from non-dangerous situations and react appropriately. In particular, the frequency with which false positive system responses occur can be determined.
- The method allows the quantification of the number of new collisions which occur due to the introduction of the investigated safety systems. However, validation of collisions

to real accidents and validation of trajectories to real traffic is required. Without such validation, the computed number of new collisions and other collision or avoidance related metrics cannot be treated as final estimates for the number of real accidents.

- In several cases, when a collision occurred in the baseline, another traffic participant became involved in the treatment due to activation of the emergency maneuver. This finding, next ot the occurrence of new collisions, represents an incentive to reduce false positive system activations.
- Existing effectiveness metrics to evaluate safety systems should be further harmonized and extended. The metrics $E_{\text{dist},50\,\%}^{\text{dang},TR}$ and $E_{\text{TTC},50\,\%}^{\text{dang},TR}$, which express the remaining safety level after the safety system has responded to a dangerous situation, represent an interesting addition to the collision avoidance metric E_{av}. They can be applied in any type of scenario based effectiveness assessment. Instead of considering only the median of the minimum distance and the minimum TTC, as is done in $E_{\text{dist},50\,\%}^{\text{dang},TR}$ and $E_{\text{TTC},50\,\%}^{\text{dang},TR}$, also an investigation of further quantiles (e.g., the 25 %- or 75 %-quantiles) could be of interest.
- At least 20 MTFS model runs, each representing one hour of the morning peak traffic, were needed to achieve stable results for the effectiveness metrics related to the change of collision partner configurations, the increase in the minimum TTC and distance and the metrics related to the system responses (e.g., the false positive rate).
- The effectiveness metrics should be defined in such a way that they are not affected by adding an arbitrary number of concrete scenarios where no system intervention takes place. In particular, this concerns the metrics E_{new}, E_{ch}, E_{FP}, E_{FN}, E_{TN}, E_{TP} which should be defined, for example, as the ratio of a count per hour of vehicle operation, e.g., the number of new collisions per hour of vehicle operation.
- Since collision events occur, the accident avoidance potential can be investigated, but only under the condition that an additional validation of such collision events to reconstructed real accidents is conducted by comparing accident characteristics such as the impact locations on the vehicle geometries, collision severities and pre-crash trajectories. While the presented method offers considerable other advantages, such as the possibility to investigate the false positive rate by simulation, directly using reconstructed real accidents as scenario source would be the more appropriate method for prospective effectiveness assessment of the classical accident avoidance potential E_{av} through simulation.
- Using only the deceleration that is required to avoid a collision, as with the system configured with the threshold $\tau_{\text{ETTC}}^{\text{Trig}} = 1.5\,\text{s}$, instead of the full available brake deceleration, led to goal braking behavior. As a consequence, the safety margin in dangerous situations in terms of minimum distance or TTC was increased to a smaller degree.
- Sight obstructions such as buildings, parking cars or traffic participants that were not on a collision course with the conflicting vehicles did not influence the effectiveness metrics with any of the investigated system configurations.

Conclusions on the effectiveness, in particular in comparison of the two investigated safety

systems:

- In the exemplary effectiveness study, where conflicts with a minimum TTC up to 1.7 s were considered, the system configured with the threshold $\tau_{\mathrm{TTC}}^{\mathrm{Trig}} = 1.0\,\mathrm{s}$ triggered in around twice as many situations where it was not necessary (i.e., twice as many false positive responses) as the system configured with the threshold $\tau_{\mathrm{ETTC}}^{\mathrm{Trig}} = 1.5\,\mathrm{s}$. The advantage in terms of fewer false positive activations, by triggering based on the ETTC, was most dominant in conflicts with a TTC from 0.7 s to 2.0 s.

12. Outlook

The following promising directions for further research were identified:

- To reduce the number of collision events, i.e., artifacts of the coupling of MTFS and nanoscopic simulation, kinetic path driver models and methods for the validation of those models to real traffic observations need to be researched further. Such models and validation methods should also aim to minimize deviations between MTFS and nanoscopic simulation. In the next step, to investigate metrics related to the collision severity or the collision avoidance potential, driving errors by human drivers need to be modeled appropriately. This could be a step towards a method that stochastically generates collisions that exhibit the same characteristics as real accidents.
- To avoid the necessity of distinguishing individual conflicts, a continuous coupling of MTFS and nanoscopic simulation can be applied, such that the problem which conflicts to choose for nanoscopic simulation is avoided. Furthermore, effects that emergency maneuvers or automated driving can have on the whole traffic can be investigated with a continuous coupling, where a feedback loop integrates results from nanoscopic simulation in traffic flow simulation. Trajectory planning can then also be conducted by a singular module in the simulation framework.
- The method presented in this thesis, including the investigated effectiveness metrics, is applicable when individual scenarios are considered. When continuous traffic simulation is used, new effectiveness metrics are required to investigate the system benefits. For example, the metrics can be defined as the number of occurrences of a certain event per hour of vehicle operation or per driven kilometer. To increase the comparability of such metrics, a description of the traffic conditions through traffic indicators, such as the vehicles per hour in the investigated region, should be provided.

13. References

Abendroth, B. and R. Bruder (2015). "Die Leistungsfähigkeit des Menschen für die Fahrzeugführung." In: *Handbuch Fahrerassistenzsysteme*. Ed. by H. Winner et al. ATZ / MTZ-Fachbuch. Wiesbaden: Springer Vieweg, pp. 3–16. ISBN: 3658057343 (cit. on p. 3).

Aga, M. and A. Okada (2003). "Analysis of vehicle stability control (VSC)'s effectiveness from accident data." In: *Proceedings of 18th International Technical Conference on the Enhanced Safety of Vehicles* (cit. on p. 195).

Allen, B. C. et al. (1978). "Analysis of traffic conflicts and collisions." In: *Transportation Research Record* 667.667, pp 67–74. ISSN: 0361-1981 (cit. on p. 23).

Almqvist, S. et al. (1991). "Use of speed limiters in cars for increased safety and a better environment." In: *Transportation Research Record* (cit. on p. 23).

Alvarez, S. et al. (2017). "Prospective Effectiveness Assessment of ADAS and Active Safety Systems via Virtual Simulation: A Review of the Current Practices." In: *The 25th ESV Conference Proceedings*. Ed. by NHTSA. ESV Conference Proceedings. NHTSA (cit. on pp. 10, 17, 19, 35, 37).

Archer, J. (2005). "Indicators for traffic safety assessment and prediction and their application in micro-simulation modelling: A study of urban and suburban intersections." Doctoral Thesis. Stockholm, Sweden: Kungliga Tekniska Högskolan (cit. on pp. 56, 61).

Arinaldi, A. et al. (2018). "Detection and classification of vehicles for traffic video analytics." In: *Procedia Computer Science* 144, pp. 259–268. ISSN: 18770509. DOI: 10.1016/j.procs.2018.10.527 (cit. on p. 14).

Association for the Advancement of Automotive Medicine (2008). *Abbreviated Injury Scale 2005 Update 2008*. Ed. by Association for the Advancement of Automotive Medicine. Barrington, IL, US (cit. on p. 39).

Astarita, V. and V. P. Giofré (2019). "From traffic conflict simulation to traffic crash simulation: Introducing traffic safety indicators based on the explicit simulation of potential driver errors." In: *Simulation modelling practice and theory* 94, pp. 215–236. ISSN: 1569-190X. DOI: 10.1016/j.simpat.2019.03.003 (cit. on p. 51).

Augenstein, J. et al. (2003). "Characteristics of Crashes that Increase the Risk of Serious Injuries." In: *Annual Proceedings / Association for the Advancement of Automotive Medicine* 47, pp. 561–576. ISSN: 1540-0360 (cit. on pp. 38, 39).

Bahouth, G. et al. (2012). "Influence of Injury Risk Thresholds on the Performance of an Algorithm to Predict Crashes with Serious Injuries." In: *Annals of Advances in Automotive Medicine / Annual Scientific Conference* 56, pp. 223–230. ISSN: 1943-2461 (cit. on p. 39).

Bareiss, M. (2019). "Effectiveness of Intersection Advanced Driver Assistance Systems in Preventing Crashes and Injuries in Left Turn Across Path / Opposite Direction Crashes in the United States." Diploma thesis. Blacksburg, Virginia (cit. on pp. 39, 118, 119).

Bareiss, M. et al. (2019). "Crash and injury prevention estimates for intersection driver assistance systems in left turn across path/opposite direction crashes in the United States." In: *Traffic Injury Prevention* 20.sup1, S133–S138. ISSN: 1538-957X. DOI: 10.1080/15389588.2019.1610945 (cit. on pp. 7, 118).

Bärgman, J. (2016). "Methods for analysis of naturalistic driving data in driver behavior research: From crash-causation analysis using expert assessment to quantitative assessment of the effect of driver behavior on safety using counterfactual simulation." Doctoral thesis. Gothenburg, Sweden: Chalmers University of Technology (cit. on p. 13).

Barnard, Y. et al. (2016). "Methodology for Field Operational Tests of Automated Vehicles." In: *Transportation Research Procedia* 14, pp. 2188–2196. ISSN: 23521465. DOI: 10.1016/j.trpro.2016.05.234 (cit. on p. 197).

Bastien, C. (2013). "Safety Assessment Of Autonomous Emergency Braking Systems On Unbelted Occupants Using A Fully Active Human Model." In: *The 23rd ESV Conference Proceedings*. Ed. by NHTSA. ESV Conference Proceedings. NHTSA (cit. on p. 40).

Berg, G. and B. Färber (2015). "Vehicle in the Loop." In: *Handbuch Fahrerassistenzsysteme*. Ed. by H. Winner et al. ATZ/MTZ-Fachbuch. Wiesbaden: Springer Vieweg, pp. 155–163. ISBN: 978-3-658-05734-3 (cit. on p. 32).

Billicsich, S., E. Tomasch, G. Markovic, et al. (2016). "Evaluation of the impact of C2X systems to the accident severity in motorcycle accidents." In: *6th Transport Research Arena 2016 (TRA)*. Ed. by TRA. ISBN: 978-92-79-10039-0 (cit. on pp. 12, 29).

Billicsich, S., E. Tomasch, W. Sinz, et al. (2015). "Potentieller Einfluss von C2X auf die Vermeidung von Motorradunfällen bzw. Reduktion der Verletzungsschwere." In: *10. VDI-Tagung Fahrzeugsicherheit - Sicherheit 2.0*. Vol. 2265. VDI-Berichte. Düsseldorf: VDI-Verlag, pp. 383–392. ISBN: 978-3-18-092265-2 (cit. on pp. 12, 29).

Björklund, F. and E. Karlström (2017). "Enabling Testing of Lateral Active Safety Functions in a Multi-Rate Hardware in the Loop Environment." Diploma thesis. Linköping University (cit. on p. 31).

Bock, T. (2008). "Vehicle in the loop: Test- und Simulationsumgebung für Fahrerassistenzsysteme." Doctoral thesis. München: Technische Universität München (cit. on pp. 31–33, 35).

Bostrom, O. (2014). *Balancing active and passive safety: FFI Report, Vehicle and Traffic Safety*. URL: https://www.saferresearch.com/projects/balancing-active-and-passive-safety (cit. on p. 14).

Bourier, G. (2013). *Wahrscheinlichkeitsrechnung und schließende Statistik: Praxisorientierte Einführung Mit Aufgaben und Lösungen*. 8., aktualisierte Auflage. Wiesbaden: Springer Gabler. ISBN: 978-3-658-01447-6. DOI: 10.1007/978-3-658-01447-6 (cit. on pp. 21, 111).

Bours, R. and M. Tideman (2010). "Simulation tools for integrated safety design." In: *Proceedings of Airbag* (cit. on p. 8).

Boyle, L. N. et al. (2012). *Integration of analysis methods and development of analysis plan*. Vol. S2-S02-RW-1. SHRP 2 report. Washington, D.C.: Transportation Research Board. ISBN: 978-0-309-12910-7 (cit. on p. 197).

Braess, H.-H. (1996). "Aktive und passive Sicherheit im Straßenverkehr." In: *Zeitschrift für Verkehrssicherheit* 42, pp. 50–52 (cit. on pp. 1, 2).

Brannstrom, M. et al. (2008). "A situation and threat assessment algorithm for a rear-end collision avoidance system." In: *2008 IEEE Intelligent Vehicles Symposium*, pp. 102–107. DOI: 10.1109/IVS.2008.4621250 (cit. on p. 89).

Breuer, J. (1998). "Analysis of driver-vehicle-interaction in an evasive manoeuvre: Results of "Moose test" studies." In: *The 16th ESV Conference Proceedings*. Ed. by NHTSA. Vol. DOTHS808759. ESV Conference Proceedings. NHTSA, pp. 620–627 (cit. on p. 95).

— (2009). "Bewertungsverfahren von Fahrerassistenzsystemen." In: *Handbuch Fahrerassistenzsysteme: Grundlagen, Komponenten und Systeme für aktive Sicherheit und Komfort*. Ed. by H. Winner et al. Wiesbaden: Vieweg+Teubner, pp. 55–68. ISBN: 978-3834802873 (cit. on p. 33).

Burg, H. and A. Moser (2017). *Handbuch Verkehrsunfallrekonstruktion: Unfallaufnahme, Fahrdynamik, Simulation*. 3. Aufl. 2017. ATZ/MTZ-Fachbuch. ISBN: 978-3-658-16143-9 (cit. on pp. 42, 83, 91, 210).

Busch, S. (2005). *Entwicklung einer Bewertungsmethodik zur Prognose des Sicherheitsgewinns ausgewählter Fahrerassistenzsysteme*. Fortschritt-Berichte VDI.: Verkehrstechnik/Fahrzeugtechnik. VDI-Verlag. ISBN: 9783183588121 (cit. on p. 12).

Campbell, K. et al. (2013). *Analyzing Driver Behavior Using Data from the SHRP 2 Naturalistic Driving Study: A SHRP 2 Safety Project Brief*. Ed. by Transportation Research Board (cit. on p. 19).

Cannon, J. W. (2001). "Dependence of a Coefficient of Restitution on Geometry for High Speed Vehicle Collisions." In: *SAE Technical Paper Series*. SAE Technical Paper Series. SAE International400 Commonwealth Drive, Warrendale, PA, United States. DOI: 10.4271/2001-01-0892 (cit. on p. 94).

CarMaker (2020). URL: https://ipg-automotive.com/products-services/simulation-software/carmaker/ (cit. on pp. 29, 165).

CarSim (2020). URL: https://www.carsim.com/products/carsim/ (cit. on p. 29).

Chelbi, N. E. et al. (2018). "Proposal of a new virtual evaluation approach of preventive safety applications and advanced driver assistance functions – application: AEB system." In: *IET Intelligent Transport Systems* 12.9, pp. 1148–1156. DOI: 10.1049/iet-its.2018.5269 (cit. on pp. 25, 26).

Chen, R. et al. (2016). "Comparison of Time to Collision and Enhanced Time to Collision at Brake Application during Normal Driving." In: *SAE Technical Paper Series*. SAE Technical Paper Series. SAE International400 Commonwealth Drive, Warrendale, PA, United States. DOI: 10.4271/2016-01-1448 (cit. on p. 89).

Chicco, D. and G. Jurman (2020). "The advantages of the Matthews correlation coefficient (MCC) over F1 score and accuracy in binary classification evaluation." In: *BMC genomics* 21.1, p. 6. DOI: 10.1186/s12864-019-6413-7 (cit. on pp. 107, 108).

China Automotive Technology and Research, ed. (2013). *CIDAS: China In-Depth Accident Study*.

Cicchino, J. B. (2017). "Effectiveness of forward collision warning and autonomous emergency braking systems in reducing front-to-rear crash rates." In: *Accident Analysis & Prevention* 99.Pt A, pp. 142–152. ISSN: 00014575. DOI: 10.1016/j.aap.2016.11.009 (cit. on pp. 117, 118).

Cichos, D. et al. (2015). *Crash-Analyse: Beschreibung der Kriterien: Version 2.4*. Ed. by Arbeitskreis Messdatenverarbeitung Fahrzeugsicherheit. URL: www.mdvfs.de (cit. on p. 39).

Combest, J. C. (2016). "Current status and future plans of the GHBMC (Global Human Body Models Consortium)." In: *6th International Symposium: Human Modeling and Simulation in Automotive Engineering*. Ed. by CARHS, pp. 1–40 (cit. on p. 39).

Daganzo, C. F. (1995). "The cell transmission model, part II: Network traffic." In: *Transportation Research Part B: Methodological* 29.2, pp. 79–93. ISSN: 01912615. DOI: 10.1016/0191-2615(94)00022-R (cit. on p. 15).

Decker, W. et al. (2017). "Modular use of human body models of varying levels of complexity: Validation of head kinematics." In: *Traffic Injury Prevention* 18.sup1, S155–S160. ISSN: 1538-957X. DOI: 10.1080/15389588.2017.1315637 (cit. on p. 42).

Detering, S. (2011). "Kalibrierung und Validierung von Verkehrssimulationsmodellen zur Untersuchung von Verkehrsassistenzsystemen." Doctoral thesis. Braunschweig: Technische Universität Carolo-Wilhelmina zu Braunschweig (cit. on pp. 15, 16, 19, 20, 28, 57).

Diebel, J. (2006). "Representing Attitude: Euler Angles, Unit Quaternions, and Rotation Vectors." In: *Matrix* 58 (cit. on pp. 199, 202).

Dijkstra, A. et al. (2010). "Do Calculated Conflicts in Microsimulation Model Predict Number of Crashes?" In: *Transportation Research Record* 2147.1, pp. 105–112. ISSN: 0361-1981. DOI: 10.3141/2147-13 (cit. on p. 67).

Dingus, T. (2018). *Naturalistic Driving: Need, History and Some Early Results*. URL: http://www.apps.vtti.vt.edu/PDFs/ndmas_ppt_PDFs/dingusVTTI.pdf (visited on 02/27/2018) (cit. on p. 197).

Dingus, T. A. et al. (2006). *The 100 Car Naturalistic Driving Study: Phase II - Results of the 100-Car Field Experiment* (cit. on p. 197).

Döring, S. et al. (2012). *Effektivitätsbewertung mit rateEFFECT am Beispiel des vorausschauenden Fußgängerschutzes*. Graz, Austria (cit. on pp. 12, 29).

DSD, ed. (2020). *PC-CRASH: A Simulation Program for Vehicle Accidents: Operating and Technical Manual, Version 11.0* (cit. on p. 28).

Ebner, A. et al. (2011). "Identifying and Analyzing Reference Scenarios for the Development and Evaluation of Active Safety: Application to Preventive Pedestrian Safety." In: *International Journal of Intelligent Transportation Systems Research* 9.3, pp. 128–138. ISSN: 1348-8503. DOI: 10.1007/s13177-011-0035-z (cit. on p. 17).

Eichberger, A., R. Rohm, et al. (2011). "RCS-TUG Study: Benefit Potential Investigation of Traffic Safety Systems with Respect to Different Vehicle Categories." In: *Proceedings of the 22th International Conference on the Enhanced Safety of Vehicles (ESV)*, pp. 1–13 (cit. on p. 29).

Eichberger, A., E. Tomasch, R. Rohm, and W. Hirschberg (2009). "Methodik zur Bewertung der Schutzpotentiale von Fahrerassistenzsystemen im realen Unfallgeschehen." In: *Mechatronik mobil* 1.1, pp. 24–29. ISSN: 1867-7371 (cit. on pp. 12, 29).

Eichberger, A., E. Tomasch, R. Rohm, W. Hirschberg, and H. Steffan (2011). "Potenziale von Systemen der aktiven Sicherheit und Fahrerassistenz." In: *Automobiltechnische Zeitschrift* 07-08 2011, pp. 594–601. ISSN: 0001-2785 (cit. on pp. 12, 29, 37, 104).

Eichberger, A., E. Tomasch, R. Rohm, H. Steffan, et al. (2010). "Detailed analysis of the benefit of different traffic safety systems in fatal accidents." In: *Proceedings of the annual EVU meeting*. Ed. by Europäische Vereinigung für Unfallforschung und Unfallanalyse e.V., pp. 301–315 (cit. on p. 29).

Erbsmehl, C. T. (2009). "Simulation of Real Crashes as a Method for Estimating the Potential Benefits of Advanced Safety Technologies." In: *21st International Technical Conference on the Enhanced Safety of Vehicles (ESV 2009)*. Vol. 09-0162 (cit. on p. 29).

— (2014). "Ein neues 3-dimensionales Energy Equivalent Speed (EES)-Modell für Fahrzeuge basierend auf Unfalldaten." Doctoral thesis. Dresden: Technische Universität Dresden (cit. on p. 213).

Erbsmehl, C. et al. (2016). "Analysis and Investigation Method for All Traffic Scenarios (AIMATS)." In: *7th International Conference on ESAR "Expert Symposium on Accident Research"*. Ed. by ESAR (cit. on p. 14).

Euro NCAP (2019). *Test Protocol - AEB VRU systems*. URL: https://cdn.euroncap.com/media/53153/euro-ncap-aeb-vru-test-protocol-v302.pdf (cit. on p. 20).

European Commission, ed. (2008). *ETAC: European Truck Accident Causation* (cit. on p. 12).

Faber, F. et al. (2011). *Analysis methods for user related aspects and impact assessment on traffic safety, traffic efficiency and environment*. Ed. by TNO (cit. on pp. 13, 24, 33, 41).

Fach, M. and D. Ockel (2009). "Evaluation Methods for the Effectiveness of Active Safety Systems with respect to Real World Accident Analysis." In: *The 21st ESV Conference Proceedings*. Ed. by NHTSA. ESV Conference Proceedings. NHTSA (cit. on p. 33).

Fecher, N. et al. (2015). "EVITA – Das Prüfverfahren zur Beurteilung von Antikollisionssystemen." In: *Handbuch Fahrerassistenzsysteme*. Ed. by H. Winner et al. Vol. 2. ATZ/MTZ-Fachbuch. Wiesbaden:

Springer Vieweg, pp. 197–206. ISBN: 978-3-658-05734-3. DOI: 10.1007/978-3-658-05734-3_13 (cit. on p. 32).

Fellendorf, M. and P. Vortisch (2010). "Microscopic Traffic Flow Simulator VISSIM." In: *Fundamentals of Traffic Simulation*. Ed. by J. Barceló. Vol. 145. International Series in Operations Research & Management Science. New York, NY: Springer Science+Business Media LLC, pp. 63–93. ISBN: 978-1-4419-6141-9. DOI: 10.1007/978-1-4419-6142-6_2 (cit. on pp. 15, 45, 50, 54, 55).

FESTA - Field operational teSt supporT Action (n.d.). URL: http://www.its.leeds.ac.uk/festa/index.php (cit. on p. 197).

FESTA Project - Field operational teSt supporT Action: FESTA Handbook Version 2 (2008) (cit. on p. 197).

Feynman, R. P. et al. (1963). *The Feynman Lectures on Physics*. The Feynman lectures on physics. Addison-Wesley. ISBN: 9780201021165 (cit. on p. 210).

FFG, Ö. F., ed. (2020). *IMPROVE: Holistische Methodik zur Erhöhung der Verkehrssicherheit und Unfallprävention durch dreidimensionale Verkehrssimulation*. URL: https://projekte.ffg.at/projekt/1713178 (visited on 12/09/2020) (cit. on p. 46).

FGSV (2006). *Hinweise zur mikroskopischen Verkehrsflusssimulation: Grundlagen und Anwendung*. FGSV (Series). FGSV Verlag. ISBN: 9783939715115 (cit. on p. 51).

Fildes, B. et al. (2015). "Effectiveness of low speed autonomous emergency braking in real-world rear-end crashes." In: *Accident Analysis & Prevention* 81, pp. 24–29. ISSN: 00014575. DOI: 10.1016/j.aap.2015.03.029 (cit. on pp. 3, 118).

Fitch, G. M. and R. J. Hanowski (2012). "Using Naturalistic Driving Research to Design, Test and Evaluate Driver Assistance Systems." In: *Handbook of Intelligent Vehicles*. Ed. by A. Eskandarian. London: Springer London, pp. 559–580. ISBN: 978-0-85729-085-4. DOI: 10.1007/978-0-85729-085-4_21 (cit. on p. 13).

FOT Net, ed. (2018). *FOT-NET Wiki*. URL: http://wiki.fot-net.eu (cit. on pp. 197, 198).

FOT-Net (2020). URL: http://www.fot-net.eu/ (cit. on p. 197).

Fressmann, D. (2016). *The THUMS Human Models: Overview: Infotag Human Modeling*. Ed. by DYNAmore GmbH. Stuttgart. (Visited on 02/02/2019) (cit. on p. 39).

Fuchs, H. et al. (2015). "Car-2-X." In: *Handbuch Fahrerassistenzsysteme*. Ed. by H. Winner et al. ATZ / MTZ-Fachbuch. Wiesbaden: Springer Vieweg, pp. 525–540. ISBN: 3658057343. DOI: 10.1007/978-3-658-05734-3_28 (cit. on p. 2).

Funk, J. R. et al. (2004). "Analytical Model for Investigating Low-Speed Sideswipe Collisions." In: *SAE Technical Paper Series*. SAE Technical Paper Series. SAE International400 Commonwealth Drive, Warrendale, PA, United States. DOI: 10.4271/2004-01-1185 (cit. on p. 94).

Gasser, T. M. et al. (2015). "Rahmenbedingungen für die Fahrerassistenzentwicklung." In: *Handbuch Fahrerassistenzsysteme*. Ed. by H. Winner et al. ATZ / MTZ-Fachbuch. Wiesbaden: Springer Vieweg, pp. 27–54. ISBN: 3658057343. DOI: 10.1007/978-3-658-05734-3_3 (cit. on pp. 2, 3).

Gettman, D. and L. Head (2003). "Surrogate Safety Measures from Traffic Simulation Models." In: *Transportation Research Record* 1840.1, pp. 104–115. ISSN: 0361-1981. DOI: 10.3141/1840-12 (cit. on pp. xix, 5).

Gettman, D., L. Pu, et al. (2008). *Surrogate Safety Assessment Model and validation: Final report*. McLean, Va. (cit. on pp. 23, 46, 57, 58, 63, 64, 66–69, 82).

Gietelink, O. et al. (2007). "Development of advanced driver assistance systems with vehicle hardware-in-the-loop simulations." In: *Vehicle system dynamics* 44.7, pp. 569–590. ISSN: 0042-3114. DOI: 10.1080/00423110600563338 (cit. on pp. 31, 32).

Gilardi, G. and I. Sharf (2002). "Literature survey of contact dynamics modelling." In: *Mechanism and Machine Theory* 37.10, pp. 1213–1239. ISSN: 0094-114X. DOI: 10.1016/S0094-114X(02)00045-9 (cit. on p. 210).

Gipps, P. G. (1986). "A model for the structure of lane-changing decisions." In: *Transportation Research Part B: Methodological* 20.5, pp. 403–414. ISSN: 01912615. DOI: 10.1016/0191-2615(86)90012-3 (cit. on p. 54).

Global Market Insights, I., ed. (2019). *Autonomous Emergency Braking Market worth £20bn by 2024*. URL: https://www.globenewswire.com/news-release/2019/01/03/1679925/0/en/Autonomous-Emergency-Braking-Market-worth-20bn-by-2024-Global-Market-Insights-Inc.html (cit. on p. 2).

Gruber, M., H. Kolk, et al. (2019). "The effect of P-AEB system parameters on the effectiveness for real world pedestrian accidents." In: *The 26th ESV Conference Proceedings*. Ed. by NHTSA. ESV Conference Proceedings. NHTSA (cit. on pp. xiv, 38, 46).

Gruber, M., C. Matt, et al. (2018). "Effectiveness assessment of a generic collision mitigation system for motorcycles at junctions." In: *8th International Conference on ESAR* (cit. on p. xiv).

Gwehenberger, J. and M. Borrack (2015). "Influence of Driver Assistance Systems on Insurance Claims." In: *Automob. Zeitschrift*. Vol. 2015 (cit. on p. 12).

Haberl, M. et al. (2018). "Simulation Assisted Safety Impact Analyses for Signalized Urban Intersections." In: *Transport Research Arena* (cit. on p. xiv).

Hakuli, S. and M. Krug (2015). "Virtuelle Integration." In: *Handbuch Fahrerassistenzsysteme*. Ed. by H. Winner et al. ATZ / MTZ-Fachbuch. Wiesbaden: Springer Vieweg, pp. 125–138. ISBN: 3658057343. DOI: 10.1007/978-3-658-05734-3_8 (cit. on pp. 26, 27, 29, 31).

Hannawald, L. (2008). *Multivariate Bewertung zukünftiger Fahrzeugsicherheit: Entwicklung eines Modells zur Bewertung zukünftiger Fahrzeugsicherheit unter Berücksichtigung der Wechselwirkungen von Sicherheitssystemen: Zugl.: Dresden, Techn. Univ., Fak. Maschinenwesen, Diss., 2008*. Als Ms. gedr. Vol. 682. Fortschritt-Berichte VDI Reihe 12, Verkehrstechnik, Fahrzeugtechnik. Düsseldorf: VDI-Verl. ISBN: 9783183682126 (cit. on p. 4).

Hautzinger, H. et al. (2006). *Hochrechnung von Daten aus Erhebungen am Unfallort: [Bericht zum Forschungsprojekt 82.221/2002]*. Vol. H. 59. Berichte der Bundesanstalt für Strassenwesen / F. Bremerhaven: Wirtschaftsverl. NW, Verl. für neue Wiss. ISBN: 3865095054 (cit. on p. 13).

Helmer, T. (2014). "Development of a methodology for the evaluation of active safety using the example of preventive pedestrian protection." Doctoral thesis. Technische Universität Berlin. DOI: 10.14279/depositonce-3973 (cit. on pp. 2, 4, 10, 106, 107, 115).

Hillenbrand, M. (2011). "Funktionale Sicherheit nach ISO 26262 in der Konzeptphase der Entwicklung von Elektrik/Elektronik Architekturen von Fahrzeugen." Doctoral thesis. Hannover and Karlsruhe. DOI: 10.5445/KSP/1000025616 (cit. on pp. 23, 24).

Hoffmann, S. (2013). "Mikroskopische Modellierung und Bewertung von verkehrssicherheitskritischen Situationen: Am Beispiel kommunikationsbasierter Fahrerwarnungen auf Autobahnen." Doctoral thesis. München: Technische Universität München (cit. on p. 54).

Hu, Y. (2005). "A guided simulation methodology for dynamic probabilistic risk assessment of complex systems." Doctoral thesis. University of Maryland (cit. on p. 26).

Huang, F. et al. (2013). "Identifying if VISSIM simulation model and SSAM provide reasonable estimates for field measured traffic conflicts at signalized intersections." In: *Accident Analysis & Prevention* 50, pp. 1014–1024. ISSN: 00014575. DOI: 10.1016/j.aap.2012.08.018 (cit. on pp. 50, 51, 67).

Hydén, C. et al. (1987). "The development of method for traffic safety evaluation: The Swedish traffic conflic technique." Doctoral thesis. Lund: Lund Institute of Technology (cit. on p. 5).

Isaksson-Hellman, I. and M. Lindman (2015a). "Evaluation of rear-end collision avoidance technologies based on real world crash data." In: *FAST-zero'15: 3rd International Symposium on Future Active Safety Technology Toward zero traffic accidents* (cit. on p. 118).

Isaksson-Hellman, I. and M. Lindman (2015b). "Real-World Performance of City Safety Based on Swedish Insurance Data." In: *The 24th ESV Conference Proceedings*. Ed. by NHTSA. ESV Conference Proceedings. NHTSA (cit. on p. 118).

ITARDA, ed. (1994). *J-TAD*. URL: http://www.itarda.or.jp/english/ (cit. on p. 12).

Jeong, E. and C. Oh (2017). "Evaluating the effectiveness of active vehicle safety systems." In: *Accident Analysis & Prevention* 100, pp. 85–96. ISSN: 00014575. DOI: 10.1016/j.aap.2017.01.015 (cit. on pp. 16, 40).

Junietz, P. M. (2019). "Microscopic and Macroscopic Risk Metrics for the Safety Validation of Automated Driving." Doctoral thesis. Darmstadt: Technische Universität Darmstadt (cit. on pp. 88, 89).

Kafka, P. (2012). "The Automotive Standard ISO 26262, the Innovative Driver for Enhanced Safety Assessment & Technology for Motor Cars." In: *Procedia Engineering* 45, pp. 2–10. ISSN: 18777058. DOI: 10.1016/j.proeng.2012.08.112 (cit. on p. 24).

Kahane, C. J. (2000). *Fatality reduction by safety belts for front-set occpuants of cars and light trucks: Updated and expanded estimates based on 1986-99 FARS data*. Ed. by NHTSA (cit. on p. 2).

Karlsson, R. et al. (2004). "Model-based statistical tracking and decision making for collision avoidance application." In: *Proceedings of the 2004 American Control Conference*. IEEE, 3435–3440 vol.4. ISBN: 0-7803-8335-4. DOI: 10.23919/ACC.2004.1384441 (cit. on p. 89).

Kim, K.-J. and J. Sul (2009). "Development of Intersection Traffic Accident Risk Assessment Model: Application of Micro-simulation Model with SSAM to Sungnam City." In: *4th IRTAD Conference*. Ed. by IRTAD (cit. on p. 67).

Kleinbaum, D. G. et al. (2010). *Logistic Regression: A Self-Learning Text*. 3. ed. Statistics for Biology and Health. New York, NY: Springer Science+Business Media LLC. ISBN: 978-1441917416. DOI: 10.1007/978-1-4419-1742-3 (cit. on p. 107).

Klug, C. et al. (2015). "Testing of bicycle helmets for preadolescents." In: *2015 IRCOBI Conference Proceedings*. Ed. by International Research Council on the Biomechanics of Injury. IRCOBI Conference Proceedings. IRCOBI, pp. 136–155 (cit. on p. 39).

Kodaka, K. et al. (2003). "Rear-End Collision Velocity Reduction System." In: *SAE Technical Paper Series*. SAE Technical Paper Series. SAE International400 Commonwealth Drive, Warrendale, PA, United States. DOI: 10.4271/2003-01-0503 (cit. on pp. 88, 89).

Kolk, H. (2018). *X-RATE: Extended Effectiveness Rating of Advanced Driver Assistance Systems* (cit. on p. 46).

Kolk, H., S. K. Kirschbichler, et al. (2016). "Prospective evaluation of the collision severity of L7e vehicles considering a Collision Mitigation System." In: *Transportation Research Procedia*. Elsevier (cit. on pp. xiii, 4, 10, 12, 14, 22, 29, 37, 46, 66, 105).

Kolk, H., W. Sinz, et al. (2016). "Evaluation of a momentum based impact model and application in an effectivity study considering junction accidents." In: *7th International Conference on ESAR "Expert Symposium on Accident Research"*. Ed. by ESAR (cit. on pp. xiii, 37, 38, 46, 93, 98, 210, 213).

Kolk, H., E. Tomasch, et al. (2018). "Active safety effectiveness assessment by combination of traffic flow simulation and crash-simulation." In: *8th International Conference on ESAR "Expert Symposium on Accident Research"*. Ed. by ESAR (cit. on pp. xiii, 15, 24, 46).

Kondo, M. (1953). "Directional stability (when steering is added)." In: *Journal of the Society of Automotive Engineers of Japan (JSAE)*. Vol. 7, pp. 5–6 (cit. on p. 95).

Kondo, M. and A. Ajimine (1968). "Driver's Sight Point and Dynamics of the Driver-Vehicle-System Related to It." In: *SAE Technical Paper Series*. SAE Technical Paper Series. SAE International400 Commonwealth Drive, Warrendale, PA, United States. DOI: 10.4271/680104 (cit. on p. 95).

Krajewski, R., J. Bock, et al. (2018). "The highD Dataset: A Drone Dataset of Naturalistic Vehicle Trajectories on German Highways for Validation of Highly Automated Driving Systems." In: *2018 21st International Conference on Intelligent Transportation Systems (ITSC)*, pp. 2118–2125. DOI: 10.1109/ITSC.2018.8569552 (cit. on pp. 148, 163).

Krajewski, R., T. Moers, et al. (n.d.). "The rounD Dataset: A Drone Dataset of Road User Trajectories at Roundabouts in Germany." submitted (cit. on pp. 148, 163).

Krapp, M. and J. Nebel (2011). "Deskriptive Statistik." In: *Methoden der Statistik*. Ed. by M. Krapp and J. Nebel. Wiesbaden: Vieweg+Teubner, pp. 19–46. ISBN: 978-3-8351-0154-8. DOI: 10.1007/978-3-8348-9917-0_2 (cit. on pp. 21, 109).

Kreiss, J.-P. et al. (2011). "On the use of real-world accident data for assessing the effectiveness of automotive safety features: Methodology, timeline and reliability." In: *The 22nd ESV Conference Proceedings*. Ed. by NHTSA. Vol. 22. ESV Conference Proceedings. NHTSA (cit. on p. 195).

Kroese, D. P. et al. (2011). *Handbook of monte carlo methods*. Wiley series in probability and statistics. Hoboken, New Jersey: John Wiley & Sons. ISBN: 9780470177938. DOI: 10.1002/9781118014967 (cit. on p. 26).

Kudlich, H. (1966). "Beitrag zur Mechanik des Kraftfahrzeug-Verkehrsunfalls." Doctoral thesis. Technische Hochschule Wien (cit. on pp. 93, 210).

Kühn, M. and L. Hannawald (2015). "Verkehrssicherheit und Potenziale von Fahrerassistenzsystemen." In: *Handbuch Fahrerassistenzsysteme*. Ed. by H. Winner et al. ATZ/MTZ-Fachbuch. Wiesbaden: Springer Vieweg, pp. 55–70. ISBN: 978-3-658-05734-3. DOI: 10.1007/978-3-658-05734-3_4 (cit. on pp. 4, 5).

Kusano, K. D. and H. C. Gabler (2011). "Potential effectiveness of integrated forward collision warning, per-collision brake assist, and automated pre-collision braking systems in real-world, rear-end collisions." In: *The 22nd ESV Conference Proceedings*. Ed. by NHTSA. Vol. 11-0364. ESV Conference Proceedings. NHTSA (cit. on p. 105).

Kusano, K. D. and H. C. Gabler (2012). "Safety Benefits of Forward Collision Warning, Brake Assist, and Autonomous Braking Systems in Rear-End Collisions." In: *IEEE Transactions on Intelligent Transportation Systems* 13.4, pp. 1546–1555. ISSN: 1524-9050. DOI: 10.1109/TITS.2012.2191542 (cit. on pp. 122, 123).

Lagares, P. and J. Puerto (2001). *Grundgesamtheitsanalysen und Stichproben: Betrachtungen zur Stichprobenfindung*. Ed. by Management Mathematics for European Schools (cit. on p. 21).

Langenberg, J. (2015). "Auslegung, Simulation und Bewertung von Verkehrsassistenzsystemen durch die Kopplfung mit Verkehrsflussmodellen." Doctoral thesis. Braunschweig: Technische Universität Carolo-Wilhelmina zu Braunschweig (cit. on p. 15).

Langwieder, K. et al. (2003). *Benefit potential of ESP in real accident situations involving cars and trucks*. Munich, Germany (cit. on p. 195).

Lengyel, E. (2012). *Mathematics for 3D game programming and computer graphics*. 3rd ed. Boston, Mass: Cengage Learning. ISBN: 978-1435458864 (cit. on pp. 84, 205, 207).

Lietz, H. et al. (2011). "Methodische und technische Aspekte einer Naturalistic Driving Study." In: *FAT-Schriftenreihe*. Ed. by Verband der Automobilindustrie eV (cit. on pp. 32, 197).

Lindman, M. et al. (2017). "Basic numbers needed to understand the traffic safety of Automated Cars." In: *2017 IRCOBI Conference Proceedings*. Ed. by International Research Council on the Biomechanics of Injury. IRCOBI Conference Proceedings. IRCOBI (cit. on p. 195).

Mahmud, S. et al. (2017). "Application of proximal surrogate indicators for safety evaluation: A review of recent developments and research needs." In: *IATSS Research* 41.4, pp. 153–163. ISSN: 03861112. DOI: 10.1016/j.iatssr.2017.02.001 (cit. on p. 23).

Mansfield, H. et al. (2008). *Analysis of the On the Spot (OTS) Road Accident Database*. Ed. by Department for Transport (cit. on p. 12).

Marine, M. C. (2007). "On the Concept of Inter-Vehicle Friction and Its Application in Automobile Accident Reconstruction." In: *SAE Technical Paper Series*. SAE Technical Paper Series. SAE International400 Commonwealth Drive, Warrendale, PA, United States. DOI: 10.4271/2007-01-0744 (cit. on p. 93).

Martinus, M. et al. (2013). "Virtual test driving: Hardware independant integration of series software." In: *ATZ Elektronik*. Vol. 8, pp. 16–21 (cit. on p. 29).

MATLAB (2020). URL: https://de.mathworks.com/products/matlab.html (cit. on pp. 29, 80).

McLaughlin, S. B. et al. (2008). "A method for evaluating collision avoidance systems using naturalistic driving data." In: *Accident Analysis & Prevention* 40.1, pp. 8–16. ISSN: 00014575. DOI: 10.1016/j.aap.2007.03.016 (cit. on pp. 37, 42).

Medicus, E. (2019). "Kalibrierung einer Verkehrsflusssimulation mit dem Ziel einer verkehrssicherheitsrelevanten Trajektorienanalyse." Diploma thesis. Graz: Graz University of Technology (cit. on pp. 50–52, 54, 55, 61–63, 72, 148, 168).

Menzel, T. et al. (2018). "Scenarios for Development, Test and Validation of Automated Vehicles." In: *IEEE Intelligent Vehicles Symposium*. Piscataway, NJ: IEEE, pp. 1821–1827. ISBN: 978-1-5386-4452-2. DOI: 10.1109/IVS.2018.8500406 (cit. on pp. xviii–xx, 4, 16).

Mikschofsky, N. (2017). "Methode für die Absicherung der Effektivität der aktiven Sicherheitssysteme für den Fußgängerschutz." Diploma thesis. Graz: Technical University of Graz (cit. on p. 25).

Minderhoud, M. M. and P. H. Bovy (2001). "Extended time-to-collision measures for road traffic safety assessment." In: *Accident Analysis & Prevention* 33, pp. 89–97. ISSN: 00014575 (cit. on pp. 23, 40, 66).

Möller, T. and B. Trumbore (1997). "Fast, Minimum Storage Ray-Triangle Intersection." In: *Journal of Graphics Tools* 2.1, pp. 21–28. ISSN: 1086-7651. DOI: 10.1080/10867651.1997.10487468 (cit. on pp. 47, 202).

Moser, A. (2020). *PC-Crash: Accident-Simulation Program* (cit. on pp. 12, 28, 46, 79, 83, 87, 94, 95).

Müller, G. and S. Müller (2015). "Messung von Reibwerten unter Realbedingungen zur Erhöhung der Fahrzeugsicherheit." In: *10. VDI-Tagung Fahrzeugsicherheit - Sicherheit 2.0*. ISBN: 978-3-18-092265-2 (cit. on p. 91).

Nalic, D. et al. (2019). "Development of a Co-Simulation Framework for Systematic Generation of Scenarios for Testing and Validation of Automated Driving Systems*." In: *2019 IEEE Intelligent Transportation Systems Conference (ITSC)*. IEEE, pp. 1895–1901. ISBN: 978-1-5386-7024-8. DOI: 10.1109/ITSC.2019.8916839 (cit. on pp. 151, 165).

Neale, V. L. et al. (2002). *The 100 Car Naturalistic Driving Study: Phase 1 - Experimental Design* (cit. on p. 197).

Neale, V. et al. (2005). "An Overview of the 100-Car Naturalistic Study and Findings." In: *The 19th ESV Conference Proceedings*. Ed. by NHTSA. ESV Conference Proceedings. NHTSA (cit. on p. 197).

NHTSA, ed. (2013). *National Automotive Sampling System (NASS) General Estimates System (GES) - Analytical User's Manual 1988-2012* (cit. on p. 12).

Ockel, D. et al. (2012). "An initiative towards a simplified international in-depth accident database." In: *5th International Conference on ESAR "Expert Symposium on Accident Research"*. Ed. by ESAR (cit. on p. 12).

OECD (2009). *Society at a glance: OECD social indicators*. Ed. by OECD (cit. on p. 83).

— (2019). *IRTAD Road Safety Database*. Ed. by International Transport Forum. URL: https://www.itf-oecd.org/irtad-road-safety-database (cit. on p. 11).

Östmann, M. and L. Jakobsson (2016). "An Examination of Pre–crash Braking Influence on Occupant Crash Response using an Active Human Body Model." In: *2016 IRCOBI Conference Proceedings*. Ed. by International Research Council on the Biomechanics of Injury. IRCOBI Conference Proceedings. IRCOBI, pp. 275–283 (cit. on p. 40).

P.E.A.R.S. initiative, ed. (2016). *Unpublished internal report of the P.E.A.R.S. initiative*. URL: https://pearsinitiative.com (cit. on pp. 12, 16, 198).

Page, Y. et al. (2015). "A Comprehensive and Harmonized Method for Assessing the Effectiveness of Advanced Driver Assistance Systems by Virtual Simulation: The P.E.A.R.S. Initiative." In: *The 24th ESV Conference Proceedings*. Ed. by NHTSA. ESV Conference Proceedings. NHTSA (cit. on pp. 5, 6, 75, 76).

Parasuraman, R. and V. Riley (1997). "Humans and Automation: Use, Misuse, Disuse, Abuse." In: *Human factors* 39.2, pp. 230–253. ISSN: 0018-7208. DOI: 10.1518/001872097778543886 (cit. on p. 115).

Passos, L. S. et al. (2011). "Towards the next-generation traffic simulation tools: A first appraisal." In: *6th Iberian Conference on Information Systems and Technologies (CISTI 2011)*, pp. 1–6 (cit. on p. 15).

Pirzadeh, H. (1999). *Computational geometry with the rotating calipers*. Montreal, Canada (cit. on p. 109).

Plachetka, C. et al. (2018). "The TUBS Road User Dataset: A New LiDAR Dataset and its Application to CNN-based Road User Classification for Automated Vehicles." In: *21st International Conference on Intelligent Transportation Systems (ITSC)*, pp. 2623–2630. DOI: 10.1109/ITSC.2018.8569765 (cit. on pp. 148, 163).

Plöchl, M. and J. Edelmann (2007). "Driver models in automobile dynamics application." In: *Vehicle system dynamics* 45.7-8, pp. 699–741. ISSN: 0042-3114. DOI: 10.1080/00423110701432482 (cit. on p. 95).

Prüggler, A. (2015). "Pre-collision Applications of Human Body Models - An Approach for Incorporating Reactive Occupant Kinematics when Modeling Critical Driving Situations." Doctoral thesis. Graz: Graz University of Technology (cit. on p. 40).

PTV Planung Transport Verkehr AG, ed. (2017). *PTV VISSIM: Traffic flow simulation – Technical Description*. Karlsruhe (cit. on pp. 46, 54).

Puch, S. et al. (2013). "Evaluation of Drivers Interaction with Assistant Systems Using Criticality Driven Guided Simulation." In: *Digital Human Modeling and Applications in Health, Safety, Ergonomics, and Risk Management. Healthcare and Safety of the Environment and Transport*. Ed. by V. G. Duffy. Berlin, Heidelberg: Springer Berlin Heidelberg, pp. 108–117. ISBN: 978-3-642-39173-6 (cit. on p. 26).

RASSI, ed. (2014). *RASSI Database*. URL: http://rassi.org.in/database.html (cit. on p. 12).

Roesener, C., F. Fahrenkrog, et al. (2016). "A scenario-based assessment approach for automated driving by using time series classification of human-driving behaviour." In: *2016 IEEE 19th International Conference on Intelligent Transportation Systems (ITSC)*. IEEE, pp. 1360–1365. ISBN: 978-1-5090-1889-5. DOI: 10.1109/ITSC.2016.7795734 (cit. on p. 17).

Roesener, C., J. Sauerbier, et al. (2017). "A Comprehensive Evaluation Approach for Highly Automated Driving." In: *The 25th ESV Conference Proceedings*. Ed. by NHTSA. Vol. Paper Number 17-0259. ESV Conference Proceedings. NHTSA (cit. on p. 17).

Rosén, E. and U. Sander (2009). "Pedestrian fatality risk as a function of car impact speed." In: *Accident Analysis & Prevention* 41.3, pp. 536–542. ISSN: 00014575. DOI: 10.1016/j.aap.2009.02.002 (cit. on p. 39).

Rosenblatt, M. (1956). "Remarks on Some Nonparametric Estimates of a Density Function." In: *The Annals of Mathematical Statistics* 27.3, pp. 832–837. ISSN: 0003-4851. DOI: 10.1214/aoms/1177728190 (cit. on pp. 26, 100, 146, 155, 157).

Russell, S. M. et al. (2018). *Naturalistic study of Level 2 driving automation functions*. Ed. by NHTSA (cit. on pp. 13, 19).

Sagberg, F. et al. (2012). *Recommendations for a large-scale European naturalistic driving observation study* (cit. on p. 197).

Saito, H. et al. (2016). "Evaluation of Frontal Impact Restraint System in Integrated Safety Scenario Using Human Body Model with PID Controlled Active Muscles." In: *2016 IRCOBI Conference Proceedings*. Ed. by International Research Council on the Biomechanics of Injury. IRCOBI Conference Proceedings. IRCOBI (cit. on p. 40).

Sander, U. (2017). "Opportunities and limitations for intersection collision intervention-A study of real world 'left turn across path' accidents." In: *Accident Analysis & Prevention* 99.Pt A, pp. 342–355. ISSN: 00014575. DOI: 10.1016/j.aap.2016.12.011 (cit. on pp. 76, 87, 105, 107).

Sander, U. and N. Lubbe (2018). "Market penetration of intersection AEB: Characterizing avoided and residual straight crossing path accidents." In: *Accident Analysis & Prevention* 115, pp. 178–188. ISSN: 00014575. DOI: 10.1016/j.aap.2018.03.025 (cit. on pp. 7, 22, 34, 85, 87, 110, 118, 122, 123).

Sayed, T. et al. (1994). "Simulation of traffic conflicts at unsignalized intersections with TSC-Sim." In: *Accident Analysis & Prevention* 26.5, pp. 593–607. ISSN: 00014575. DOI: 10.1016/0001-4575(94)90021-3 (cit. on p. 58).

Scanlon, J. M. et al. (2017). "Injury mitigation estimates for an intersection driver assistance system in straight crossing path crashes in the United States." In: *Traffic Injury Prevention* 18.sup1, S9–S17. ISSN: 1538-957X. DOI: 10.1080/15389588.2017.1300257 (cit. on pp. 4, 7, 96, 118, 119, 168).

Scanlon, J. et al. (2017). "Preliminary Effectiveness Estimates for Intersection Driver Assistance Systems in LTAP/OD Crashes." In: *FAST-zero'17* (cit. on p. 37).

Schäuffele, J. (2010). *Automotive Software Engineering*. ATZ / MTZ-Fachbuch. Wiesbaden: Springer Fachmedien. ISBN: 978-3-8348-9368-0 (cit. on p. 27).

Schmidt, D. et al. (2018). "KAUSAL – a virtual tool chain to estimate the impact of automated driving on occupant restraint systems." In: *8th International Conference on ESAR "Expert Symposium on Accident Research"*. Ed. by ESAR (cit. on p. 17).

Schöner, H.-P., W. Hurich, et al. (2011). "Koordiniertes automatisiertes Fahren für die Erprobung von Assistenzsystemen." In: *ATZ - Automobiltechnische Zeitschrift*, pp. 40–45 (cit. on p. 32).

Schöner, H.-P. and B. Morys (2015). "Dynamische Fahrsimulatoren." In: *Handbuch Fahrerassistenzsysteme*. Ed. by H. Winner et al. ATZ / MTZ-Fachbuch. Wiesbaden: Springer Vieweg. ISBN: 3658057343 (cit. on pp. 27, 30).

Schramm, S. and F. Roth (2009). "Method to assess the effectiveness of active pedestrian protection safety systems." In: *The 21st ESV Conference Proceedings*. Ed. by NHTSA. Vol. 09-0398. ESV Conference Proceedings. NHTSA (cit. on p. 14).

Schubert, A. et al. (2012). "Standardized pre-crash-scenarios in digital format on the basis of the VUFO simulation." In: *5th International Conference on ESAR "Expert Symposium on Accident Research"*. Ed. by ESAR (cit. on p. 12).

Schwartz, D. et al. (2015). "Development of a computationally efficient full human body finite element model." In: *Traffic Injury Prevention* 16 Suppl 1, S49–56. ISSN: 1538-957X. DOI: 10.1080/15389588.2015.1021418 (cit. on p. 42).

Seeck, A. et al. (2009). "Development of the accident investigation and data handling methodology in the GIDAS project." In: *The 21st ESV Conference Proceedings*. Ed. by NHTSA. ESV Conference Proceedings. NHTSA (cit. on pp. 11, 12, 213).

Seiniger, P. and A. Weitzel (2015). "Testverfahren für Verbraucherschutz und Gesetzgebung." In: *Handbuch Fahrerassistenzsysteme*. Ed. by H. Winner et al. ATZ / MTZ-Fachbuch. Wiesbaden:

Springer Vieweg, pp. 167–182. ISBN: 3658057343. DOI: 10.1007/978-3-658-05734-3_11 (cit. on pp. 17, 32, 33).

Sferco, R. et al. (2001). "Potential Effectiveness Of Electronic Stability Programs (ESP) - What European Field Studies Tell Us." In: *17 th International Technical Conference on the Enhanced Safety of Vehicles* Paper Number 2001-S2-O-327, pp. 4–7 (cit. on p. 195).

Slibar, A. (1966). "Die mechanischen Grundsätze des Stoßvorganges freier und geführter Körper und ihre Anwendung auf den Stoßvorgang von Fahrzeugen." In: *Archiv für Unfallforschung*. Vol. 2. Jg., H. 1, S. 31 ff (cit. on pp. 93, 210).

Slob, J. (2008). *State-of-the-Art Driving Simulators, a Literature Survey*. Ed. by Eindhoven University of Technology (cit. on p. 30).

Al-Smadi, M. et al. (2016). "Traffic surveillance: A review of vision based vehicle detection, recognition and tracking." In: 11, pp. 713–726 (cit. on p. 14).

Smit, S. et al. (2019). "Evaluation of a momentum based impact model in frontal car collisions for the prospective assessment of ADAS." In: *European Transport Research Review* 11.1, p. 75. ISSN: 1867-0717. DOI: 10.1186/s12544-018-0343-3 (cit. on pp. xiv, 12, 46, 213).

Sparmann, U. (1978). "Spurwechselvorgänge auf zweispurigen BAB-Richtungsfahrbahnen." Doctoral thesis. Karlsruhe: Universität Karlsruhe (cit. on p. 54).

Statistik Austria (2000). *Unfalltypenkatalog*. Wien (cit. on p. 22).

— (2020). *Statistik Austria*. www.statistik.at. URL: https://www.statistik.at/web_de/statistiken/menschen_und_gesellschaft/gesundheit/unfaelle/strassenverkehrsunfaelle/index.html (cit. on pp. 11, 19, 58).

Stefan Schramm (2011). "Methode zur Berechnung der Feldeffektivität integraler Fußgängerschutzsysteme." Doctoral thesis. Technische Universität München (cit. on pp. 4, 12, 28).

Steffan, H. and A. Moser (1996). "The Collision and Trajectory Models of PC-CRASH." In: *International Congress & Exposition*. SAE Technical Papers. SAE International. DOI: 10.4271/960886 (cit. on pp. 47, 210).

Stehman, S. V. (1997). "Selecting and interpreting measures of thematic classification accuracy." In: *Remote Sensing of Environment* 62.1, pp. 77–89. ISSN: 00344257. DOI: 10.1016/S0034-4257(97)00083-7 (cit. on p. 107).

Stellet, J. E. et al. (2015). "Testing of Advanced Driver Assistance Towards Automated Driving: A Survey and Taxonomy on Existing Approaches and Open Questions." In: *2015 IEEE 18th International Conference on Intelligent Transportation Systems*, pp. 1455–1462. DOI: 10.1109/ITSC.2015.236 (cit. on p. 4).

Stiller, C. et al. (2015). "Maschinelles Sehen." In: *Handbuch Fahrerassistenzsysteme*. Ed. by H. Winner et al. ATZ / MTZ-Fachbuch. Wiesbaden: Springer Vieweg, pp. 369–393. ISBN: 3658057343. DOI: 10.1007/978-3-658-05734-3_21 (cit. on p. 2).

Sutherland, I. E. and G. W. Hodgman (1974). "Reentrant Polygon Clipping." In: *Commun. ACM* 17.1, pp. 32–42. ISSN: 0001-0782. DOI: 10.1145/360767.360802 (cit. on p. 92).

The Virtual CRASH Team (2017). *On the depth of penetration*. URL: https://www.vcrashusa.com/blog/2017/10/26/depth-of-penetration (cit. on pp. 92, 93).

Thomas, P. et al. (2003). "Real-world Accident Data Coordinated Methodologies for Data Collection to Improve Vehicle and Road Safety." In: *The 18th ESV Conference Proceedings*. Ed. by NHTSA. Vol. 260. ESV Conference Proceedings (cit. on p. 11).

Tomasch, E., H. Kolk, et al. (2015). "Prospektive Bewertung der Kollisionsschwere von L6e Fahrzeugen unter Berücksichtigung eines Kollisionsminderungssystems." In: *10. VDI-Tagung Fahrzeugsicherheit - Sicherheit 2.0*. Vol. 2265. VDI-Berichte. Düsseldorf: VDI-Verlag, pp. 407–418. ISBN: 978-3-18-092265-2 (cit. on pp. xiv, 39, 46).

Tomasch, E., W. Sinz, et al. (2015). "Bewertungsmethodik von integralen Sicherheitssystemen durch Kombination von Test und Simulation am Beispiel von Fußgängerunfällen." In: *10. VDI-Tagung Fahrzeugsicherheit - Sicherheit 2.0*. Vol. 2265. VDI-Berichte. Düsseldorf: VDI-Verlag, pp. 157–169. ISBN: 978-3-18-092265-2 (cit. on pp. xiv, 46).

Tomasch, E. and H. Steffan (2006). "ZEDATU - Zentrale Datenbank tödlicher Unfälle in Österreich - A Central Database of Fatalities in Austria." In: *2nd International Conference on ESAR "Expert Symposium on Accident Research"*. Ed. by ESAR. ESAR (cit. on pp. 11, 12).

Tomasch, E., H. Steffan, and M. Darok (2008). "Retrospective accident investigation using information from court." In: *Transport Research Arena Europe 2008 (TRA)*. Ed. by TRA. ISBN: 978-92-79-10039-0 (cit. on p. 11).

Tumasov, A. V. et al. (2019). "The Application of Hardware-in-the-Loop (HIL) Simulation for Evaluation of Active Safety of Vehicles Equipped with Electronic Stability Control (ESC) Systems." In: *Procedia Computer Science* 150, pp. 309–315. ISSN: 18770509. DOI: 10.1016/j.procs.2019.02.057 (cit. on p. 31).

Ulbrich, S. et al. (2015). "Defining and Substantiating the Terms Scene, Situation, and Scenario for Automated Driving." In: *2015 IEEE 18th International Conference on Intelligent Transportation Systems (ITSC 2015)*. Piscataway, NJ: IEEE, pp. 982–988. ISBN: 978-1-4673-6596-3. DOI: 10.1109/ITSC.2015.164 (cit. on pp. xviii–xxi, 4).

Unfallforschung der Versicherer (2016). *Unfalltypenkatalog: Leitfaden zur Bestimmung des Unfalltyps*. URL: https://udv.de/sites/default/files/tx_udvpublications/unfalltypen-katalog_udv_web_2.pdf (cit. on p. 22).

Unselt, T. et al. (2004). "Fußgängerschutz durch Bremsassistenz." In: *1. Tagung Aktive Sicherheit durch Fahrerassistenzsysteme*. München (cit. on p. 30).

van Schagen, I. et al. (2011). *Towards a large-scale European Naturalistic Driving study: Min findings of PROLOGUE*. Ed. by SWOV Institute for Road Safety Research. Leidschendam, The Netherlands (cit. on p. 197).

Vasconcelos, L. et al. (2014). "Validation of the Surrogate Safety Assessment Model for Assessment of Intersection Safety." In: *Transportation Research Record* 2432.1, pp. 1–9. ISSN: 0361-1981. DOI: 10.3141/2432-01 (cit. on p. 67).

Verburg, D. J. et al. (2003). "VEHIL: Developing and testing intelligent vehicles." In: *Intelligent Vehicle Symposium, 2002. IEEE*. IEEE, pp. 537–544. ISBN: 0-7803-7346-4. DOI: 10.1109/IVS.2002.1188006 (cit. on p. 31).

Wang, L. et al. (2017). "Prospective Safety Assessment of Highly Automated Driving Functions Using Stochastic Traffic Simulation." In: *The 25th ESV Conference Proceedings*. Ed. by NHTSA. ESV Conference Proceedings. NHTSA (cit. on p. 4).

Warner, C. Y. et al. (1983). "Friction Applications in Accident Reconstruction." In: *SAE Technical Paper Series*. SAE Technical Paper Series. SAE International. DOI: 10.4271/830612 (cit. on p. 91).

Weitzel, D. A. (2013). "Objektive Bewertung der Kontrollierbarkeit nicht situationsgerechter Reaktionen umfeldsensorbasierter Fahrerassistenzsysteme." Doctoral thesis. Technischen Universität Darmstadt (cit. on p. 25).

Wiedemann, R. (1974). "Simulation des Straßenverkehrsflusses." Doctoral thesis. Karlsruhe: Universität Karlsruhe (cit. on p. 53).

Wilhelm, U. et al. (2015). "Funktionale Sicherheit und ISO 26262." In: *Handbuch Fahrerassistenzsysteme*. Ed. by H. Winner et al. ATZ / MTZ-Fachbuch. Wiesbaden: Springer Vieweg, pp. 85–103. ISBN: 3658057343. DOI: 10.1007/978-3-658-05734-3_6 (cit. on p. 24).

Wimmer, P., M. Benedikt, et al. (2015). "Fast calculating surrogate models for leg and head impact in vehicle-pedestrian collision simulations." In: *Traffic Injury Prevention* 16 Suppl 1, S84–90. ISSN: 1538-957X. DOI: 10.1080/15389588.2015.1014902 (cit. on p. 39).

Wimmer, P., M. Düring, et al. (2019). "Toward harmonizing prospective effectiveness assessment for road safety: Comparing tools in standard test case simulations." In: *Traffic Injury Prevention* 20.sup1, S139–S145. ISSN: 1538-957X. DOI: 10.1080/15389588.2019.1616086 (cit. on pp. xiii, 38, 46, 86–88, 91, 168).

Wimmer, P., A. Rieser, et al. (2012). "Effectiveness Assessment of Vulnerable Road User Protection Systems via Numeric Simulation." In: *International Crashworthiness Conference* (cit. on p. 3).

Winner, H. (2015a). "Grundlagen von Frontkollisionsschutzsystemen." In: *Handbuch Fahrerassistenzsysteme*. Ed. by H. Winner et al. Vol. 99. ATZ/MTZ-Fachbuch. Wiesbaden: Springer Vieweg, pp. 893–912. ISBN: 978-3-658-05734-3. DOI: 10.1007/978-3-658-05734-3{\textunderscore}47 (cit. on pp. 88, 89, 206).

— (2015b). "Radarsensorik." In: *Handbuch Fahrerassistenzsysteme*. Ed. by H. Winner et al. ATZ/MTZ-Fachbuch. Wiesbaden: Springer Vieweg. ISBN: 978-3-658-05734-3 (cit. on p. 168).

Winner, H. et al., eds. (2015). *Handbuch Fahrerassistenzsysteme: Grundlagen, Komponenten und Systeme für aktive Sicherheit und Komfort*. 3., überarbeitete und ergänzte Auflage. ATZ / MTZ-Fachbuch. Wiesbaden: Springer Vieweg. ISBN: 3658057343 (cit. on p. 2).

Winter, J. de et al. (2012). "Advantages and Disadvantages of Driving Simulators: A Discussion." In: *Measuring Behavior Conference* (cit. on p. 30).

World Health Organization (2018). *Global status report on road safety 2018*. Ed. by World Health Organization. Geneva. URL: https://apps.who.int/iris/bitstream/handle/10665/276462/9789241565684-eng.pdf (cit. on p. 1).

Yamada, K. et al. (2016). "Simulation of Occupant Posture Change during Autonomous Emergency Braking and Occupant Kinematics in Frontal Collision." In: *2016 IRCOBI Conference Proceedings*. Ed. by International Research Council on the Biomechanics of Injury. IRCOBI Conference Proceedings. IRCOBI, pp. 261–274 (cit. on p. 40).

Yerushalmy, J. (1947). "Statistical Problems in Assessing Methods of Medical Diagnosis, with Special Reference to X-Ray Techniques." In: *Public Health Reports (1896-1970)* 62.40, p. 1432. ISSN: 00946214. DOI: 10.2307/4586294 (cit. on p. 108).

Zauner, C. et al. (2014). "Assessment of the effectiveness of Intersection Assistance Systems at urban and rural accident sites." In: *ESAR - Expert Symposium on Accident Research* (cit. on pp. 10, 12, 29).

Zeeb, E. (2010). "Daimler's New Full–Scale, High–dynamic Driving Simulator – A Technical Overview." In: *Conference Proceedings Driving Simulation Conference*. Paris (cit. on p. 30).

List of Figures

List of Tables

A. Retrospective effectiveness assessment

Retrospective effectiveness assessment methods can be used once a safety system has been developed and has already been in the market for a certain span of time. Such methods use data that is recorded from real traffic, e.g., accident reconstructions stored in in-depth databases, data from statistics on the base level such as national statistics (less detailed compared to in-depth data) or from traffic observation studies such as NDSs. The general approach with this type of assessment is to search for effects that the market introduction of specific systems had. This is done by defining and comparing two groups in the accident data: one with the safety system in question (treatment) and the other without (baseline) and to search for changes in characteristic values of the statistic. For example, retrospective analysis was used to assess the safety effect of Electronic Stability Control (ESC): Langwieder et al., 2003 found that 20 % to 25 % of accidents involve skidding, where ESP can provide a stabilizing effect. Sferco et al., 2001 found that ESP can become active in 34 % of all accidents with fatalities. Aga and Okada, 2003 found a 35 % reduction of casualties in single car accidents and head-on collisions for vehicles that have ESP installed.

Kreiss et al., 2011 analyzed retrospective effectiveness assessment methods regarding reliability. According to their research, the method underlies certain constraints, of which some are (Kreiss et al., 2011):

- A sufficiently high market penetration rate of the system must be reached.
- It must be possible to distinguish between scenarios in the investigated data where the system was available and where not.
- Cross-effects with other safety systems must be considered.
- Baseline (control group without system) and treatment group (group with system) must differ only in the presence of the system.
- Driver behavior may change over time due to the presence of a safety system.
- Only accidents are reported in accident databases, not the avoided accidents.
- It is often not possible to distinguish between correlation and causation when a certain effect is observed in the data.

Furthermore, retrospective effectiveness assessment of active safety or autonomous driving functions may require extreme mileages to show significant results. Lindman et al., 2017 concluded, that around 7 000 million kilometers in passenger cars are needed in order to statistically significantly prove with 95 % confidence a 50 % lower crash rate of autonomous vehicles compared to manual driving. The above mentioned constraints represent limitations

that are often too strict, driving the development of prospective effectiveness assessment methods.

B. Naturalistic Driving Studies and Field Operational Tests

In Naturalistic Driving Studies (NDSs) and Field Operational Tests (FOTs), vehicles are equipped with specific safety systems under investigation and with recording equipment to collect data on driving behaviour and the scenery (some examples of FOTs and NDS are listed in Table B.1). FOTs employ a higher degree of experimental control than NDSs (Lietz et al., 2011). A FOT may be defined as "a study undertaken to evaluate a function, or functions, under normal operating conditions in environments typically encountered by the host vehicle(s) using quasi-experimental methods" (*FESTA Project - Field operational teSt supporT Action: FESTA Handbook Version 2* 2008). FOTs have experimental character. This may include the presence of a test engineer to ensure the correct conduction of the test. Barnard et al., 2016 summarized methods used for FOTs. Such studies typically extend over the course of at least a few weeks, during which drivers are instructed to simply follow their daily routines of vehicle usage. The importance of performing FOTs as valuable data source of further evaluations was recognized by the European Commission and is supported through initiatives such as *FESTA - Field operational teSt supporT Action* n.d. or FOT Net, 2018; *FOT-Net* 2020.

NDS use the ideas behind FOTs and extend them by the requirement to conduct the observation of the driver, scenery and vehicle in an unobtrusive way, thus decreasing the driver's awareness of being observed to reduce the possibility that this awareness influences the driver's reactions. A scientifically sound methodology to conduct NDS was for example explored in the PROLOGUE project (van Schagen et al., 2011). Historically, driving studies already started in the mid-eighties (T. Dingus, 2018) but became more relevant since the 100-car-study (V. L. Neale et al., 2002) was carried out by the end of the nineties and the development of accident avoidance systems, i.e., ADAS (Advanced Driver Assistance Systems). In NDS, participants are not involved in experiments, i.e., there is no observer present as may be the case in a FOTs, meaning there is no intervention during the driving process (Sagberg et al., 2012, Boyle et al., 2012 and T. A. Dingus et al., 2006). They are often conducted over the course of months or years, an example being the 100-car study by V. Neale et al., 2005, which is an NDS that recorded 43 000 hours of data for 2 million miles driven on real roads.

Name	Type of study	Region	Number of vehicles	Number of test persons	Duration
100 Car naturalistic driving study	NDS	USA	100	ca. 240	2001-2002
Drive Recorder Database for accident/incident study and its potential for Active Safety Development	NDS	Japan	198	N. A.	2006-open
euroFOT	FOT	Europe (4 countries)	ca. 1000	ca. 1200	2008-2011
TeleFOT	FOT	Europe (8 countries)	N. A.	ca. 3000	2008-2012
SHRP2	NDS	USA	3102	ca. 3000	2010-2012
Sim TD	FOT	Germany	1	1993	ca. 300 each year
U-Drive	NDS	Europe (7 countries)	210	320	2012-2016

Table B.1.: Examples of NDS and FOT studies, based on a report by the P.E.A.R.S. initiative, 2016 and FOT Net, 2018.

C. Ray-tracing for sensor vision

The task of the ray-tracing algorithm is to generate a list of points that are visible to a sensor and, using that information, to compile a list of references to the objects that were detected. Instead of considering a continuous field of view, the algorithm computes the visibility of objects ("tracing") along discrete *vision rays* that resemble the field of view. The field of view has the shape of a planar circle sector (see Figure C.1), and it is oriented in three dimensions, depending on the orientation of the sensor and the vehicle. The higher the density of vision rays, the more reliable the algorithm is in seeing an object at the first possible moment, i.e., the probability that objects that are visible are actually detected by the algorithm increases. The sensor is characterized by a handful of parameters which were already introduced in Section 7.1.3.1, but are recited here:

Sensor position ($\vec{X}_S^V$): The position of the sensor S installed on vehicle is denoted by $\vec{X}_S^V$ and is specified in the vehicle coordinate system. It is the origin of the sensor coordinate system.

Sensor orientation ($\vec{\omega}_S^V$): The angles that represent the rotation of the central sensor ray relative to the vehicle coordinate system. They are given in Euler angles in the zyx-convention (see Diebel, 2006). These angles correspond to the azimuth and polar angle of spherical coordinate representation.

Horizontal opening angle ($\theta^{\max}$): The sensor field of view extends by $\theta_{\max}/2$ to the left and right of the central ray, see Figure C.1. Since each vision ray in the sensor's field of view, resembling a circle sector, is located in the same plane, no vertical opening angle is required for a full description of the field of view.

Horizontal resolution (N_{rays}^h): The number of rays that cover the horizontal opening angle $\theta^{\max}$ is denoted by N_{rays}^h. A uniform spacing of vision rays in angular coordinates is assumed.

Range (R): Describes how far each "vision ray" extends at maximum from the sensor origin. In spherical coordinates, this corresponds to the radius.

The ray-tracing Algorithm 1 first iterates over all 3D objects (static objects and traffic participants), which are not the detecting vehicle itself. Then it iterates over each vision ray, then over the faces (which are triangles) that define the geometry of the 3D objects and checks whether a ray can "see" the face. This is done in the local sensor coordinate system. For that purpose, all 3D objects are transformed to the sensor coordinate system by the coordinate transformations in Section C.1, before applying the algorithm. If the ray

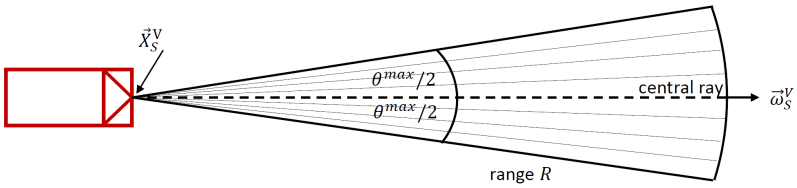

Figure C.1.: Top view of the sensor field of view with a forward facing sensor. The opening angle θ^{max} extends by $\theta^{max}/2$ in spherical coordinates to the left and right of the central vision ray, of which the direction is given by the sensor orientation $\vec{\omega}^S$.

intersects the triangle (see Section C.2), i.e., sees the face, the algorithm checks whether an intersection of this ray with another face has already been detected, but with a closer distance. In that case, it considers the previously detected face as a visibility obstruction and stores only the closest intersection and a unique object ID of the detected 3D object. In Figure C.2, for example, some rays would intersect the faces of the wall. When the algorithm then traces the faces of V1, intersections with the wall will have a shorter distance, i.e., V1 is not detected.

After the execution of Algorithm 1, the arrays *traced* and *objid* are available, where *objid* stores the unique ID of the closest 3D object that was hit by the ray with index k and *traced* stores the distance from the sensor to the closest intersection point that was detected for that ray. By substituting the values in *traced* as values for d in Equation C.2, with the corresponding ray directions $\vec{D}$ that were used in Algorithm 1, and $\vec{O} = (0, 0, 0)$, the detected intersection points for each ray are calculated in the sensor coordinate system. Using the inverse transformations described in Section C.1, the intersection points $\vec{R}_k^S$ are transformed from the sensor coordinate system to the global coordinate system to form the intersection points $\vec{R}_k^G$.

In theory, the algorithm requires a runtime of approximately $C_{TR}\, N_{\text{rays}}^h\, N_{3D}\, N_F$, while C_{TR} is the time needed for a ray-triangle intersection, N_{3D} the number of 3D objects and N_F the average number of faces per object. In practice, however, various optimizations in the implementation are possible and allow skipping of a high percentage of ray-triangle intersections.

Algorithm 1 The sensor algorithm

procedure RAYTRACING
  initialize arrays *traced* and *objid* with the dimensions N^h_{rays}
  for all *obj* **in** the list of 3D-objects **do**
    get global node coordinates *coords* of *obj* and transform to the sensor
    coordinate system $\rightarrow coords_S$
    if *obj* is outside of sensor field of view **then**
      continue to next *obj*
    for all k **in** $\left\{1, 2, \ldots, N^h_{\text{rays}}\right\}$ **do**
      $\theta_k = \theta^{max}\left(\frac{1}{2} + \frac{1-k}{N^h_{\text{rays}}}\right)$
      compute ray direction vector: $\vec{D}_k = [\cos(\theta_k), \sin(\theta_k), 0]$
      for all faces F of *obj* **do**
        compute the *Ray-triangle intersection* with face F, direction $\vec{D}_k$
        and sensor location $\vec{X}^S_S = (0,0,0)$ as origin $\vec{O} \rightarrow d, hitflag$
        if $hitflag$ is *True* **and** $t < traced(k)$ **then**
          $traced(k) \leftarrow d$
          $objid(k) \leftarrow$ unique ID of *obj*
  return *traced* and *objid*

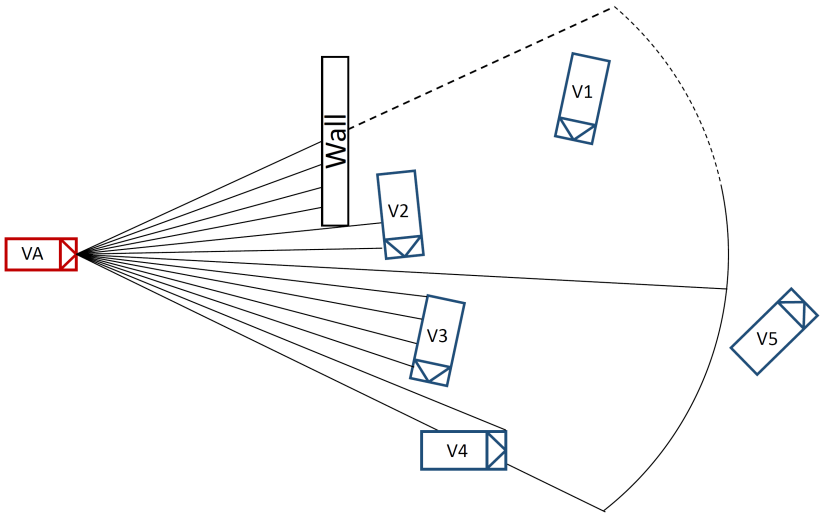

Figure C.2.: Different degrees of visibility. VA cannot see V1, because the view is blocked. V2 is partially hidden. V3 is fully visible. V4 is partially inside the field of view. V5 is outside the field of view.

C.1. Coordinate transformations

For each object which is considered in the sensor vision algorithm, a coordinate transformation is required from the global system to the coordinate system of the sensor. This is done by a chained transformation from the global system G to the vehicle system V and then from V to the sensor coordinate system S. The first transformation from G to V is given by $\vec{X}^V = R^V \cdot (\vec{X}^G - \vec{X}^G_{COG})$, where $\vec{X}^G$ is an arbitrary point to be transformed from G to V, $\vec{X}^G_{COG}$ the origin of the vehicle coordinate system in G (in this implementation, it is the center of gravity), and R^V the rotation matrix

$$R^V = \begin{pmatrix} c_y c_z & c_y s_z & -s_y \\ s_x s_y c_z - c_x s_z & s_x s_y s_z + c_x c_z & s_x c_y \\ c_x s_y c_z + s_x s_z & c_x s_y s_z - s_x c_z & c_x c_y \end{pmatrix}, \tag{C.1}$$

with the abbreviations

$$c_i = \cos\left(\omega_S^{V,i}\right)$$
$$s_i = \sin\left(\omega_S^{V,i}\right)$$

for $i \in \{x, y, z\}$ and $\omega_S^{V,x}$, $\omega_S^{V,y}$ and $\omega_S^{V,z}$ being the pitch, roll and yaw angle, respectively, of the detecting vehicle, given in the Euler xyz-convention (see Diebel, 2006). Analogously, the second transformation from V to S is defined for a point $\vec{X}^V$ in the vehicle coordinate system as $\vec{X}^S = R^S \cdot (\vec{X}^V - \vec{X}^V_S)$, where R^S is the transformation matrix based on the sensor orientation $\vec{\omega}^V_S$ in the vehicle coordinate system (given in the Euler xyz-convention).

The inverse transformations from S to V are given by $\vec{X}^V = \left(R^S\right)^{-1} \vec{X}^S + \vec{X}^V_S$ and from V to G by $\vec{X}^G = \left(R^V\right)^{-1} \vec{X}^V + \vec{X}^G_{\mathrm{COG}}$, with $\left(R^V\right)^{-1}$ and $\left(R^S\right)^{-1}$ denoting the inverse of the matrices R^V and R^S, respectively.

C.2. Ray-triangle intersection

Möller and Trumbore, 1997 presented a method to compute intersections of a ray $\vec{R}$ given by its origin $\vec{O}$, a direction $\vec{D}$ and a distance parameter $d \leq 0$:

$$\vec{R}(t) = \vec{O} + d\vec{D}. \tag{C.2}$$

The method makes use of barycentric coordinates (u, w), which provide a simple way to check whether the ray intersects the triangle or not. A point $\vec{T}(u, w)$ on a triangle is given by

$$\vec{T}(u, w) = (1 - u - w)\vec{V}_0 + u\vec{V}_1 + w\vec{V}_2, \tag{C.3}$$

where $\vec{V}_i$, $i = 1, 2, 3$ are the vertices spanning the triangle and (u, w) must fulfill $u \geq 0$, $w \geq 0$ and $u + w \leq 1$, such that the point T lies on the triangle. Computing the intersection of the triangle and the ray is equivalent to solving the equation

$$\vec{O} + d\vec{D} = (1 - u - w)\vec{V}_0 + u\vec{V}_1 + w\vec{V}_2.$$

Rearranging gives the following linear system:

$$\left(-\vec{D}, \vec{V}_1 - \vec{V}_0, \vec{V}_2 - \vec{V}_0\right) \begin{pmatrix} u \\ w \\ d \end{pmatrix} = \vec{O} - \vec{V}_0.$$

The result vector (u, w, d) contains the barycentric coordinates (u, w) which allow computation of the intersection point $\vec{P}$ using Equation C.2. Alternatively, the distance d from the origin $\vec{O}$ to the intersection point $\vec{P}$ can be used to compute $\vec{P}$ through Equation C.2.

D. Calculation of the TTC, the ETTC and the acceleration required for collision avoidance

D.1. Determination of the Time-to-Collision

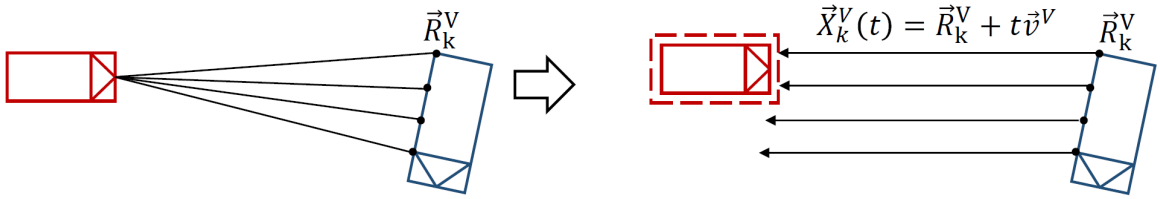

Figure D.1.: Calculation of TTC. For each intersection point $\vec{R}_k^V$ with ray-index k (in the detecting vehicle's coordinate system) that is detected on the geometry of the other vehicle (blue vehicle, left), the possibility of a collision of the intersection point with the detecting vehicle's geometry including the safety zone (dashed red box) is checked (right).

For the $\tau_{\mathrm{TTC,X}}$ calculation algorithm, it is assumed that the detecting vehicle as well as the detected traffic participant continue to move in the same direction, with the same velocity. Under that assumption, the algorithm determines whether a collision of each point $\vec{R}_k^V$ with ray-index k detected by the ray-tracing algorithm (in the detecting vehicle's coordinate system) with the detecting vehicle's geometry including the safety zone is possible. If that is the case, the algorithm determines how long it would take until a collision would occur. The lowest detected time is used to define $\tau_{\mathrm{TTC,X}}$.

Each intersection point $\vec{R}_k^V$ on the geometry of the other traffic participant (blue vehicle in Figure D.1) together with the relative velocity vector $\vec{v}^V$ defines a straight line $\vec{X}_{\vec{R}_k^V}^V(t) = \vec{R}_k^V + t\vec{v}^V$, where t is a scalar that represents the time. The relative velocity vector $\vec{v}^V$ is computed through $\vec{v}^V = R^V\vec{v}^G - (v,0,0)$, where R^V is the transformation matrix from global coordinates to the coordinate system of the detecting vehicle (see Appendix C.1), $\vec{v}^G$ the global velocity vector of the detected traffic participant and v the absolute value of the velocity of the detecting vehicle. Intersections of these lines with the detecting vehicle including the safety zone (dashed red box in Figure D.1), which is defined through a triangular mesh, are calculated using a method analogous to the one that is used by the ray-tracing approach in Appendix C.2. This method leads to the following linear system

with the solution vector $\left(u_R^F, w_R^F, t_R^F\right)$ for each individual triangular face F of the triangulated mesh that represents the detected traffic participant :

$$\left(-\vec{v}^V, \vec{V}_1^F - \vec{V}_0^F, \vec{V}_2^F - \vec{V}_0^F\right) \begin{pmatrix} u_k^F \\ w_k^F \\ t_k^F \end{pmatrix} = \vec{R}^V - \vec{V}_0^F,$$

where $\vec{V}_i^F$ with $i \in 0,1,2$ denote coordinate vectors of the vertices of the face F in vehicle coordinates. The results are times t_k^F for each intersection point $\vec{R}_k^V$ and face F of the traffic participant's mesh model. Furthermore, u_k^F and v_k^F are the barycentric coordinates of the triangular face F, i.e., the conditions $u_k^F \geq 0$, $w_k^F \geq 0$ and $u_k^F + w_k^F \leq 1$ must be fulfilled such that a valid intersection with the face F is detected (see Lengyel, 2012). The value of $\tau_{\mathrm{TTC,X}}$ at the investigated time step is defined as the minimum of times t_k^F where a valid intersection was detected, i.e., where the line $\vec{X}_{\vec{R}_k^V}^V(t)$ intersects the vehicle mesh, $\tau_{\mathrm{TTC,X}} := \min t_k^F$. In no valid intersection is found, $\tau_{\mathrm{TTC,X}}$ does not exist for that time step. That way, the algorithm computes $\tau_{\mathrm{TTC,X}}$ based only on the information that is available, i.e., visible, to the sensor. Furthermore, with this method, it is possible to calculate $\tau_{\mathrm{TTC,X}}$ in relation to objects of arbitrary three dimensional geometry (approximated by triangular meshes), positions and orientations in space as well as arbitrary shapes of sensor fields of view.

To compute the coordinates of the detected traffic participant's geometry under consideration of the safety zone (dashed red box in Figure D.1), the value chosen for the safety zone is added in the vehicle coordinate system to all positive values of the mesh node coordinates in x- and y-direction, and subtracted from all negative values.

D.2. Determination of the Enhanced Time-to-Collision

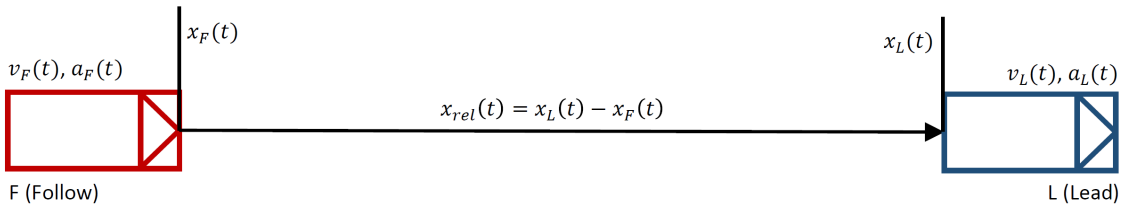

Figure D.2.: Exemplary rear-end conflict, where vehicle F follows vehicle L. The position $x_F(t)$ of F is measured at the vehicle's front, and the position $x_L(t)$ at the rear of L.

For the derivation of ETTC, in this case first presented for an exemplary rear-end conflict with vehicles moving in one dimension, see Figure D.2, constant relative acceleration $a_{\mathrm{rel}}(t_0) = a_L(t_0) - a_F(t_0)$ (where t_0 is the current moment in time and the subscript F and L refer to the accelerations of the vehicles F and L, respectively) is assumed, instead of constant relative velocity $v_{\mathrm{rel}}(t_0) = v_L(t_0) - v_F(t_0)$, as is the case for the TTC. By integrating

$$a_{\mathrm{rel}}(t) = \frac{d\, v_{\mathrm{rel}}(t)}{d\, t} = \frac{d^2\, x_{\mathrm{rel}}(t)}{d^2\, t} = a_{\mathrm{rel}}(t_0) = constant \tag{D.1}$$

once and twice from t_0 to t (with $t > t_0$), expressions for the relative velocity $v_{\text{rel}}(t) = v_L(t) - v_F(t)$ and distance $x_{\text{rel}}(t) = x_L(t) - x_F(t)$ follow:

$$v_{\text{rel}}(t) = a_{\text{rel}}(t_0)t + v_{\text{rel}}(t_0) \tag{D.2}$$

and

$$x_{\text{rel}}(t) = a_{\text{rel}}(t_0)\frac{t^2}{2} + v_{\text{rel}}(t_0)t + x_{\text{rel}}(t_0). \tag{D.3}$$

When a collision between L and F occurs, the relative distance is zero, i.e., $x_{\text{rel}}(t) = 0$ must hold. Solving the quadratic Equation D.3 for t with $x_{\text{rel}}(t) = 0$ leads to two possible solutions:

$$t_{1,2} = \frac{-v_{\text{rel}}(t_0) \pm \sqrt{v_{\text{rel}}^2(t_0) - 2a_{\text{rel}}(t_0)x_{\text{rel}}(t_0)}}{a_{\text{rel}}(t_0)}. \tag{D.4}$$

For a solution of Equation D.4 to be a valid value for the ETTC, it must be positive. Furthermore, if two positive solutions exist, the smaller one is used, as this is the first moment when a collision can occur. If both solutions are negative, no valid value for ETTC exists. If the determinant (the expression inside the square root) is negative, i.e., $v_{\text{rel}}^2(t_0) - 2a_{\text{rel}}(t_0)x_{\text{rel}}(t_0) < 0$, then there is no real-valued solution and the ETTC does not exist. If the relative acceleration $a_{\text{rel}}(t_0)$ approaches 0, the ETTC (denoted by τ_{ETTC}) approaches the TTC asymptotically and is simply expressed by $\tau_{\text{ETTC}} = -d_{\text{rel}}(t_0)/v_{\text{rel}}(t_0)$ (Winner, 2015a).

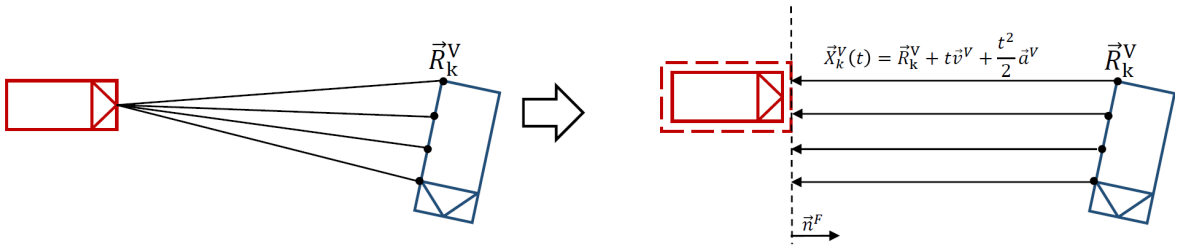

Figure D.3.: Calculation of ETTC. Analogous to the TTC calculation, the possibility of collision of detected points $\vec{R}_k^V$ is checked, but under additional consideration of an acceleration term $\vec{a}^V t^2/2$. The vertical dashed line (right) depicts the plane spanned by the triangular faces representing the vehicle front, with normal vectors $\vec{n}^F$. The red dashed rectangle represents the vehicle geometry including the safety zone d_{SZ}.

To calculate the ETTC for use in nanoscopic simulation, the previously described principle must be generalized to three dimensions. Analogous to the calculation of the TTC described in Appendix D.1, the ETTC algorithm checks whether any of the detected points $\vec{R}_k^V$ can collide with the planes that are spanned by the faces of the extended vehicle geometry (extended by the safety zone d_{SZ}) of the detector vehicle, see Figure D.3. For that purpose, the movement of the points $\vec{R}_k^V$ in the relative coordinate system of the detector vehicle is expressed by the following vector version of Equation D.3:

$$\vec{X}_k^V(t) = \vec{R}_k^V + t\vec{v}^V + \frac{t^2}{2}\vec{a}^V, \tag{D.5}$$

with $\vec{a}^V = R^V \vec{a}^G - (a, 0, 0)$, a being the longitudinal acceleration of the detector vehicle, R^V being the transformation matrix from G to V and $\vec{a}^G$ being the global acceleration vector of the detected vehicle ($\vec{v}^V$ is defined analogously, see previous subsection). Then, the lines $\vec{X}_k^V(t)$ need to be intersected with the planes lying on the triangular faces F that define the detector vehicle's geometry, by defining planes that lie on those faces F. Since the scalar product of two orthogonal vectors must be equal to zero (Lengyel, 2012), the equation

$$(\vec{V}_0^F - \vec{X}) \cdot \vec{n}^F = 0 \tag{D.6}$$

must hold, where $\vec{V}_0^F$ is the first vertex of the triangular face F, $\vec{X}$ an arbitrary point on the plane lying on F that is unequal to $\vec{V}_0^F$ and $\vec{n}^F$ is the normal vector of F, given by $\vec{n}^F = (\vec{V}_1^F - \vec{V}_0^F) \times (\vec{V}_2^F - \vec{V}_0^F)$ (with $\vec{V}_1^F$ and $\vec{V}_2^F$ denoting the second and third vertex of the triangular face F, see Figure D.4). Substituting $\vec{X}_k^V(t)$ (Equation D.5) for $\vec{X}$ in Equation D.6 and solving for t yields the following solutions as potential values for ETTC:

$$t_{1,2}^{F,k} = \frac{-\vec{v}^V \cdot \vec{n}^F \pm \sqrt{(\vec{v}^V \cdot \vec{n}^F)^2 - 2(\vec{a}^V \cdot \vec{n}^F)(\vec{R}_k^V - \vec{V}_0^F) \cdot \vec{n}^F}}{\vec{a}^V \cdot \vec{n}^F}. \tag{D.7}$$

For each face F and point $\vec{R}_k^V$, the algorithm then determines, analogously as in the one dimensional example described at the beginning of this subsection, which of the two solutions are valid candidates for the ETTC. The result is a set $C_{\tau_{\text{ETTC}}}$ of potential values $t_{F,k}^{\text{valid}}$ for the ETTC. If $\vec{a}^V \cdot \vec{n}^F$ equals zero, then the acceleration term $\frac{t^2}{2}\vec{a}^V$ in Equation D.5 can be omitted, leading to

$$t_{F,k}^{\text{valid}} = -\frac{(\vec{R}_k^V - \vec{V}_0^F) \cdot \vec{n}^F}{\vec{v}^V \cdot \vec{n}^F} \tag{D.8}$$

as potential candidates for ETTC. Since the planes spanned by the faces expand indefinitely,

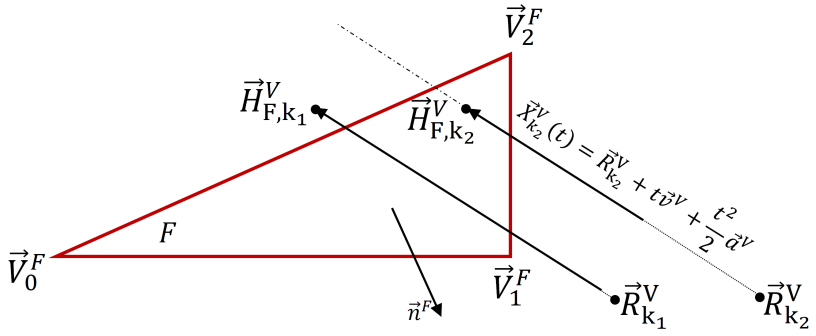

Figure D.4.: Intersection of the lines for the points $\vec{R}_{k_1}^V$ and $\vec{R}_{k_2}^V$ with the plane spanned by the triangular face F, resulting in the hit points $\vec{H}_{F,k_1}^V$ and $\vec{H}_{F,k_2}^V$. The hit point $\vec{H}_{F,k_2}^V$ lies on F, while $\vec{H}_{F,k_1}^V$ does not.

a check must be conducted to verify whether the points $\vec{R}_k^V$ hit the planes inside the triangles that define the faces F, see Figure D.4. Therefore, the values $t_{F,k}^{\text{valid}}$ are substituted for t in Equation D.5, leading to hit points $\vec{H}_{F,k}^V$. The hit points are then transformed to the two dimensional barycentric coordinate systems (see Lengyel, 2012) of the respective faces F:

$$u_k^F = -\left(\left(\vec{H}_{F,k}^V - \vec{V}_2^F\right) \times \left(\vec{V}_2^F - \vec{V}_0^F\right)\right) \cdot \frac{\vec{n}^F}{|\vec{n}^F|^2} \tag{D.9}$$

$$w_k^F = \left(\left(\vec{H}_{F,k}^V - \vec{V}_0^F\right) \times \left(\vec{V}_1^F - \vec{V}_0^F\right)\right) \cdot \frac{\vec{n}^F}{|\vec{n}^F|^2}, \tag{D.10}$$

where $|\cdot|$ denotes the Euclidean norm. If $0 \leq u_k^F$, $0 \leq w_k^F$ and $u_k^F + w_k^F \leq 1$, then the hit point $\vec{H}_{F,k}^V$ lies within the face F, i.e., $\vec{H}_{F,k}^V \in F$. The ETTC can finally be defined as follows:

$$\tau_{\text{ETTC}} = \min_{\substack{t_{F,k}^{\text{valid}} \in C_{\tau_{\text{ETTC}}} \\ \vec{H}_{F,k}^V \in F}} t_{F,k}^{\text{valid}}. \tag{D.11}$$

D.3. Determination of the acceleration required for collision avoidance

The derivation of the acceleration which is required to avoid a potential collision, a_{required}, is based on the one dimensional example mentioned at the beginning of the previous subsection. The derivation starts by solving Equation D.2 for t, which leads to:

$$t = \frac{v_{\text{rel}}(t) - v_{\text{rel}}(t_0)}{a_{\text{rel}}(t_0)}. \tag{D.12}$$

Substituting this solution for t in Equation D.3 yields an alternative representation for the relative distance between the vehicles F and L:

$$x_{\text{rel}}(t) = \frac{1}{2a_{\text{rel}}(t_0)}(v_{\text{rel}}^2(t) - v_{\text{rel}}^2(t_0)) + x_{\text{rel}}(t_0). \tag{D.13}$$

To compute the acceleration required to execute an exact goal braking maneuver (i.e., the front of the follower vehicle almost touches the rear of the lead vehicle), the conditions $v_{\text{rel}}(t) = 0$ and $x_{\text{rel}}(t) = 0$ must be imposed. If the relative velocity were not reduced to 0, then the vehicles would still be traveling further and could potentially collide at a later point. If $x_{\text{rel}}(t) = 0$ holds, then the collision is avoided exactly. However, the follower vehicle F can always brake with a lower acceleration value, such that $v_{\text{rel}}(t) = 0$ while $x_{\text{rel}}(t) > 0$. Applying both conditions in Equation D.13, splitting $a_{\text{rel}}(t_0) = a_L(t_0) - a_F(t_0)$ and rearranging the terms leads to:

$$a_F(t_0) = a_L(t_0) - \frac{v_{\text{rel}}(t_0)^2}{2x_{\text{rel}}(t_0)} =: a_{\text{required}}, \tag{D.14}$$

which is used to define a_{required} in the one dimensional case.

If it were possible to immediately apply a_{required} as the current acceleration for the follower vehicle, a potential collision can be avoided. However, since the active safety systems simulated in this thesis do not apply the brake force immediately, but rather after t_{str} has passed, and since the current acceleration decreases with the brake gradient ∇a, the scenario will become more critical and a lower brake acceleration becomes necessary to avoid the collision. Therefore, a_{required} is adjusted to account for the delay time t_{delay}, by using Equation D.2 and Equation D.3 to predict the relative velocity and distance after t_{delay} has passed, and substitute those values in Equation D.14:

$$a_{\text{required}}^{\text{adj}} = a_L(t_0) - \frac{(a_{\text{rel}}(t_0)t_{\text{delay}} + v_{\text{rel}}(t_0))^2}{a_{\text{rel}}(t_0)t_{\text{delay}}^2 + 2v_{\text{rel}}(t_0)t_{\text{delay}} + 2x_{\text{rel}}(t_0)}. \tag{D.15}$$

The delay time is composed of t_{srt} and the time t_{lag}, which is the time needed to decrease the current longitudinal acceleration a of the detector vehicle down to a_{required}, i.e., $t_{\text{delay}} = t_{\text{srt}} + t_{\text{lag}}$ with $t_{\text{lag}} = \frac{max(a_{\text{required}}, a^{\min}) - min(0, a)}{\nabla a}$. The maximum of a_{required} and $a^{\min}$ is used in this case, since the lowest achievable acceleration is bounded by $a^{\min}$. The minimum of 0 and a is used, since it is assumed that no time is required to reduce positive accelerations to 0.

The generalization of the calculation of $a^{\text{adj}}_{\text{required}}$ to three dimensions is conducted only in longitudinal direction of the detector vehicle, since braking only influences the acceleration longitudinally. This is done by replacing a_{rel} in Equation D.15 by the longitudinal coordinate of $\vec{a}^V$, i.e., a^V_x, and a_L is substituted by $a^V_x + a$, where a is the current longitudinal acceleration of the detector vehicle. Furthermore, v_{rel} is replaced by v^V_x. Finally, to achieve a worst-case approximation, the relative distance $x_{\text{rel}}(t_0)$ is replaced by the longitudinal distance from the most frontal point of the vehicle geometry, extended by the safety zone, to the detected points $\vec{R}^V_k$:

$$a^{adj,F,k}_{\text{required}} = a^V_x + a - \frac{(a^V_x t_{\text{delay}} + v^V_x)^2}{a^V_x t^2_{\text{delay}} + 2v^V_x t_{\text{delay}} + 2(R^V_{k,x} - (d_{\text{SZ}} + max_F\ max_{i\in\{0,1,2\}} V^F_{i,x}))}. \quad \text{(D.16)}$$

To compute the final value of $a^{\text{adj}}_{\text{required}}$ for the use in nanoscopic simulation, the minimum is taken over all $a^{adj,F,k}_{\text{required}}$ for faces F and detected points $\vec{R}^V_k$, such that a valid solution for ETTC and a valid hit point $\vec{H}^V_{F,k} \in F$ is found by the ETTC calculation algorithm:

$$a^{\text{adj}}_{\text{required}} = \min_{\substack{t^{\text{valid}}_{F,k} \in C_{\tau_{\text{ETTC}}} \\ \vec{H}^V_{F,k} \in F}} a^{adj,F,k}_{\text{required}}. \quad \text{(D.17)}$$

E. Momentum-based impact model

For the purpose of having a possibility to approximate the course of events of a collision by a fast computation, a model based on momentum conservation equations is used. This model balances the total momentum before and after the crash and is described in Burg and Moser, 2017, Gilardi and Sharf, 2002, Steffan and Moser, 1996 or Kolk, Sinz, et al., 2016. The underlying equations are based on work by Kudlich, 1966; Slibar, 1966.

E.1. Basic principles of momentum exchange

The presented impact model relies on conservation equations, stating that the total angular L and linear momentum p in a system of n bodies remains constant (see e.g., Feynman et al., 1963):

$$\vec{p} = \vec{p_1} + \cdots + \vec{p_n}$$
$$\vec{L} = \vec{L_1} + \cdots + \vec{L_n}.$$

The model is established under the following limitations:

- No tire forces are considered.
- The crash phase is infinitely short, i.e., no positional changes, deformation or accelerations during the crash phase are resolved.
- The described equations in the following subsections apply to two dimensions, although they can be extended to three dimension.

The collision phase is separated into the compression and restitution phase. In the compression phase, the kinetic energy deforms the vehicles, until the relative movement between the vehicles at their contact area amounts to zero. In the restitution phase, a portion of the kinetic energy is retained. This portion is described by the coefficient ϵ (the restitution coefficient):

$$\epsilon = \frac{\vec{S}_{rest}}{\vec{S}_{comp}},$$

where $\vec{S}_{comp}$ and $\vec{S}_{rest}$ denote the exchanged momentum during the compression and restitution phases, respectively. The total exchanged momentum then amounts to:

$$\vec{S} = \vec{S}_{rest} + \vec{S}_{comp} = (1 + \epsilon) \cdot \vec{S}_{comp}. \tag{E.1}$$

The calculation of $\vec{S}_{comp}$ is explained in the following section.

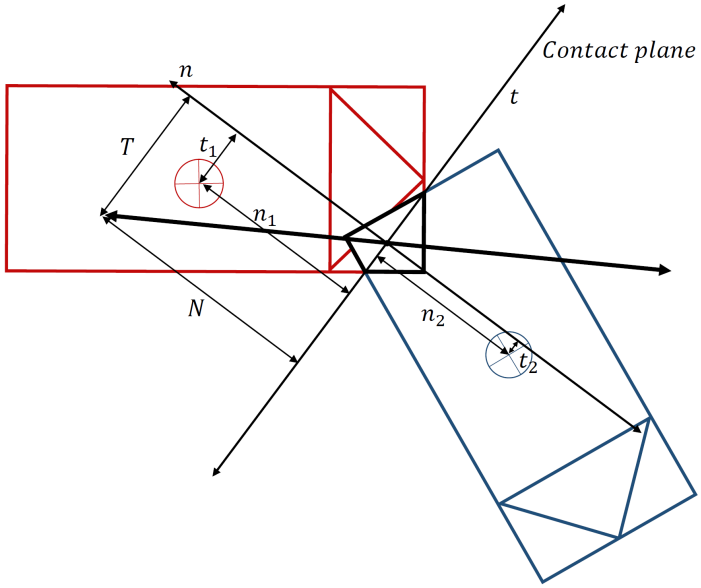

Figure E.1.: Introducing a coordinate system for the momentum-based collision model: the point of impact is chosen as the origin and t and n as the axes.

E.2. Derivation of the impact model

When two vehicles collide, they are in contact with each other along a surface over which the momentum is exchanged. Equivalent to the surface, it is assumed that the momentum is instead exchanged over a single point, the point of impact (POI). If the two vehicles slide along this surface, it is regarded a sliding collision. This sliding motion is simplified as motion tangential to a contact plane. The contact plane and point of impact together span a new coordinate system, shown in Figure E.1, with axis n and t as the axes and POI as the origin (the next subsection explains how to choose those model parameters). The contact plane is parallel to t and n is normal to t.

The projection of the centers of gravity of the two vehicles to the axes n and t lead to the coordinates n_i and t_i with $i \in \{1,2\}$ as indices for the two vehicles. Analogously, projection of the velocity vectors $\vec{v}_{\mathrm{COG},i}$ of the center of gravity of vehicle i leads to the components $v^N_{\mathrm{COG},i}$ and $v^T_{\mathrm{COG},i}$. With the yaw-rate γ^z_i (rotation around the z-axis), the velocity in the center of gravity is transformed to the POI:

$$v^T_i = v^T_{\mathrm{COG},i} + \gamma_i n_i$$
$$v^N_i = v^N_{\mathrm{COG},i} - \gamma_i t_i.$$

With these velocities, the linear momentum conservation equations are established (valid in the center of gravity):

$$m_i(v^{T,p}_{\mathrm{COG},i} - v^T_{\mathrm{COG},i}) = T \cdot (-1)^{i-1}, \tag{E.2}$$
$$m_i(v^{N,p}_{\mathrm{COG},i} - v^N_{\mathrm{COG},i}) = N \cdot (-1)^{i-1}, \tag{E.3}$$

for both vehicles with $i \in \{1,2\}$, where $v_{\mathrm{COG},i}^{T,p}$ and $v_{\mathrm{COG},i}^{N,p}$ are defined as the post crash velocities of vehicle i in tangential and normal direction. Angular momentum balance leads to the equations

$$I_{zz,i}(\gamma_i^p - \gamma_i) = (-1)^{i-1} \cdot (T \cdot n_i - N \cdot t_i), \tag{E.4}$$

where $I_{zz,i}$ denotes the moment of inertia around the z-axis of collision partner i. Through definition of the relative pre-crash velocities $v_T = v_{T,1} - v_{T,2}$ and $v_N = v_{N,1} - v_{N,2}$, Equations E.2 to E.4 can be rewritten to form an expression for the relative post-crash velocities:

$$v_T^p = v_T + c_1 T - c_3 N, \tag{E.5}$$

$$v_N^p = v_N - c_3 T + c_2 N, \tag{E.6}$$

with

$$c_1 = \frac{1}{m_1} + \frac{1}{m_2} + \frac{n_1^2}{I_{zz,1}} + \frac{n_2^2}{I_{zz,2}},$$
$$c_2 = \frac{1}{m_1} + \frac{1}{m_2} + \frac{t_1^2}{I_{zz,1}} + \frac{t_2^2}{I_{zz,2}},$$
$$c_3 = \frac{t_1 n_1}{I_{zz,1}} + \frac{t_2 n_2}{I_{zz,2}}.$$

For non-sliding impacts, the relative velocities at the end of the compression phase are zero, i.e., $v_T^p = v_N^p = 0$. That leads to the following crash pulse in the compression phase:

$$T_c = \frac{v_N c_3 + v_T c_2}{c_3^2 - c_1 c_2},$$
$$N_c = \frac{v_N c_1 + v_T c_3}{c_3^2 - c_1 c_2}$$

and consequently with $\vec{S}_{comp} = (T_c, N_c)$ to the total exchanged momentum $\vec{S} = \vec{S}_{comp} \cdot (1+\epsilon)$ (see Equation E.1). Substituting back into Equation E.2 leads to the post-crash velocities. The crash-induced velocity change experienced by vehicle i is defined as the Euclidean norm of the difference between pre-crash and post-crash velocity vectors:

$$\Delta v_i = \sqrt{(v_i^T - v_i^{T,p})^2 + (v_i^N - v_i^{N,p})^2}. \tag{E.7}$$

In sliding collisions, the amount of momentum that can be exchanged over the surface is limited by inter-vehicle friction μ_{IV}, i.e., the relative tangential post-crash velocity is no longer zero, $v_T^p \neq 0$. Therefore, Equation E.5 must be replaced by $T_c = \mu N_c$, leading to

$$N_c = \frac{v_N}{c_2 - c_3 \mu_{\mathrm{IV}}}.$$

E.3. Model parameters: point of impact and contact plane

In principle, the parameters point of impact and contact plane can be chosen freely. For automated calculation of collisions however, a rule to define these parameters is needed.

Kolk, Sinz, et al., 2016 and Smit et al., 2019 analyzed the sensitivity of the model output Δv to the input parameters point of impact and contact plane. As soon as the tangential force between vehicles approaches and exceeds the limits of the friction between the vehicles (sliding collision), the model becomes sensitive to small changes in the input parameters. For other cases, a simple geometrical rule is sufficient. This geometrical rule uses the center of gravity of the overlap region, discretized as polygon with x_i and y_i as the coordinates of the i-th vertex of the polygon, as the point of impact:

$$POI_x = \frac{1}{6A} \sum_{i=0}^{n-1} (x_i + x_{i+1})(x_i y_{i+1} - x_{i+1} y_i),$$
$$POI_y = \frac{1}{6A} \sum_{i=0}^{n-1} (y_i + y_{i+1})(x_i y_{i+1} - x_{i+1} y_i),$$
$$A = \frac{1}{2} \sum_{i=0}^{n-1} (x_i y_{i+1} - x_{i+1} y_i),$$

where POI_x and POI_y denote the coordinates of the centroid. To define the contact plane, Kolk, Sinz, et al., 2016 propose to interpolate a line through the intersection points between the polygonal lines that represent the vehicles' exterior and to translate this line in parallel such that it goes through the point of impact. An alternative method for the definition of the point of impact and contact plane is presented by C. T. Erbsmehl, 2014, which uses a statistical approach considering vehicle deformations based on real accidents in the GIDAS database (Seeck et al., 2009).

F. Convergence depending on the number of MTFS model runs

F.1. System response categories and related metrics

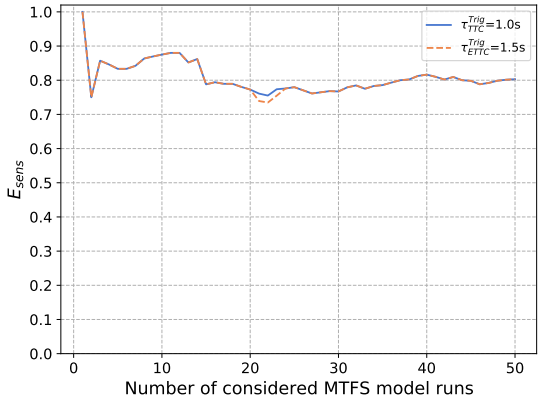

(a) Sensitivity

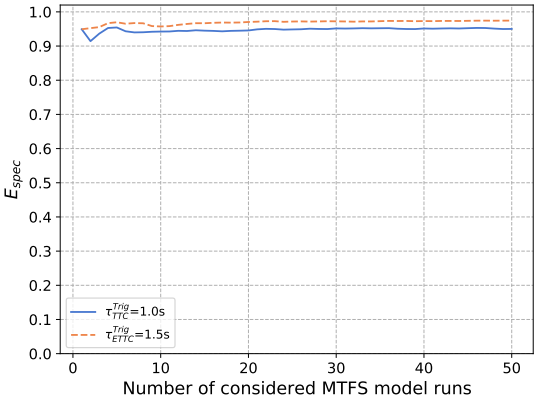

(b) Specificity

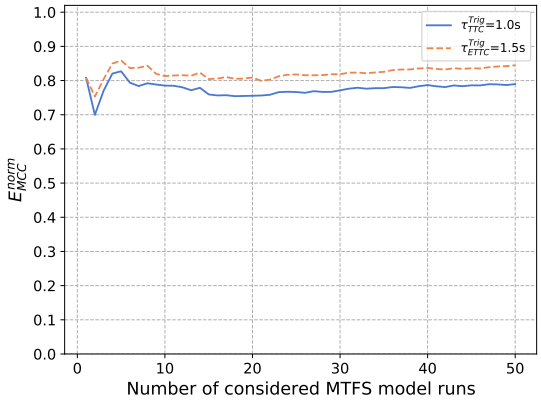

(c) Normed Matthew's correlation coefficient

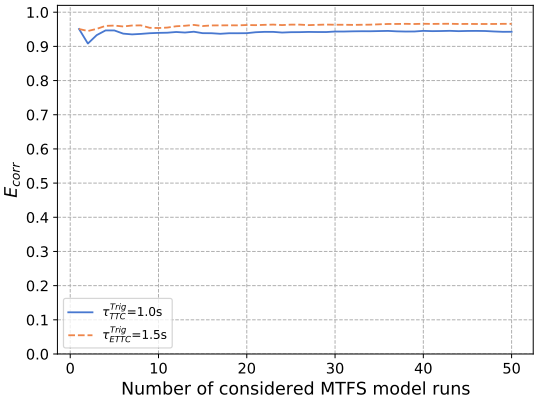

(d) Proportion of correct decisions

Figure F.1.: Effectiveness metrics related to the system response categories.

F.2. Accident avoidance and changes in collision partners

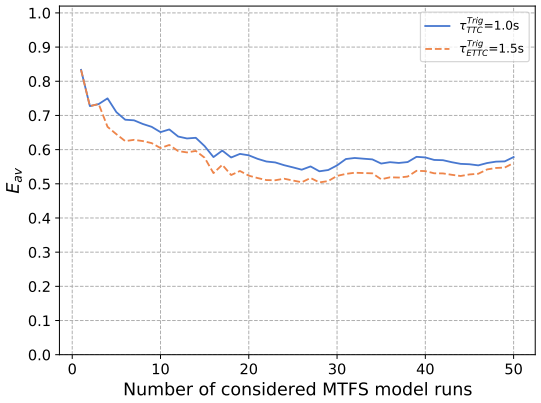

(a) Proportion of avoided baseline collisions

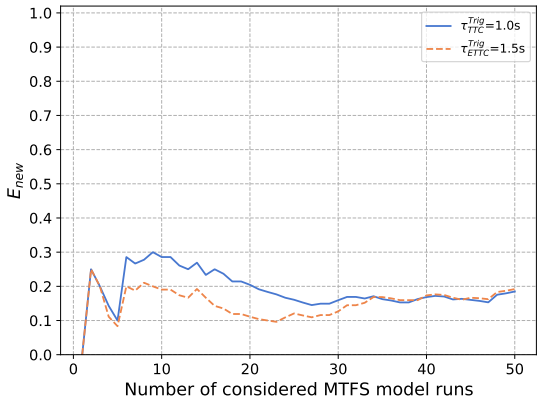

(b) Proportion of new collisions in the number of treatment collisions

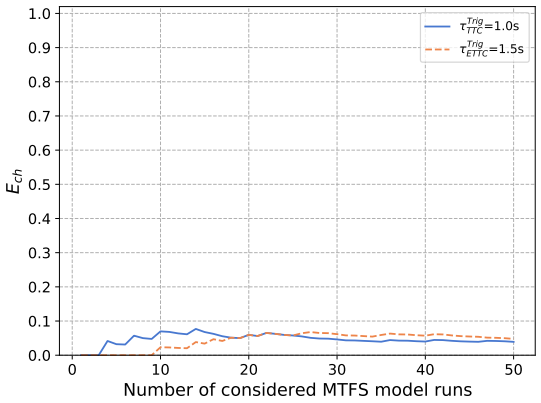

(c) Proportion of changed collisions in the baseline collisions

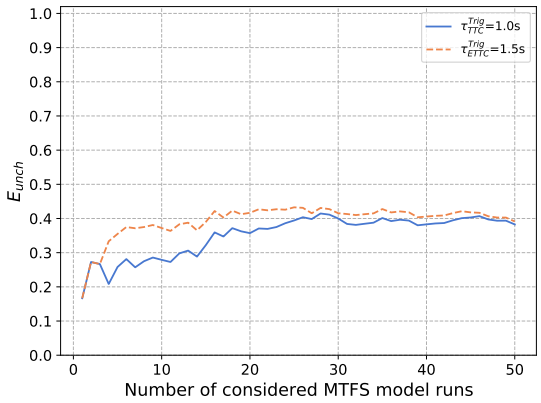

(d) Proportion of unchanged collisions in the baseline collisions

Figure F.2.: Effectiveness metrics related to the change in collision partner configurations.

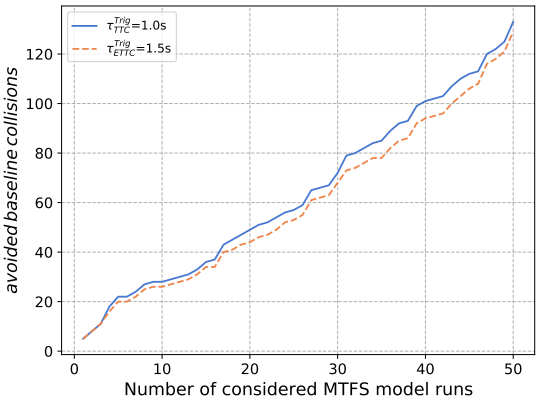

(a) Number of avoided collisions

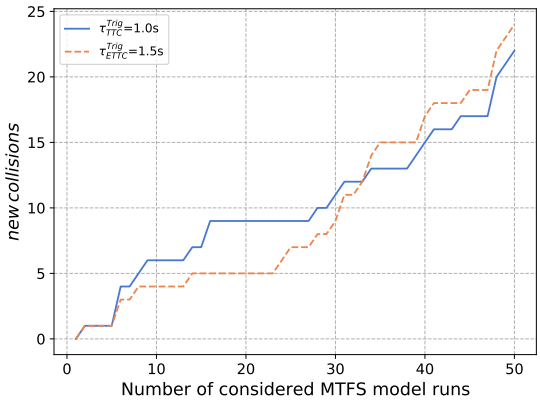

(b) Number of new collisions

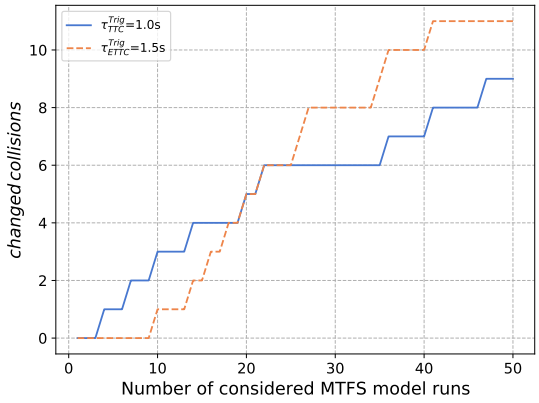

(c) Number of changed collisions

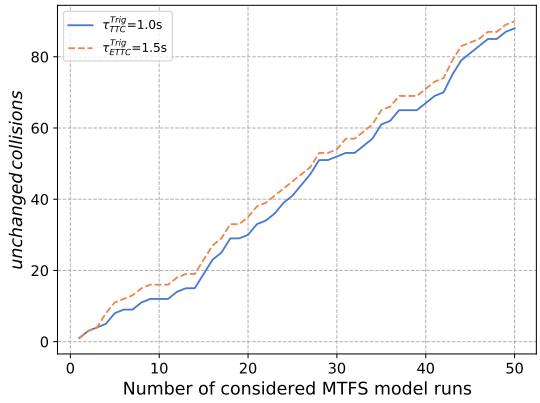

(d) Number of unchanged collisions

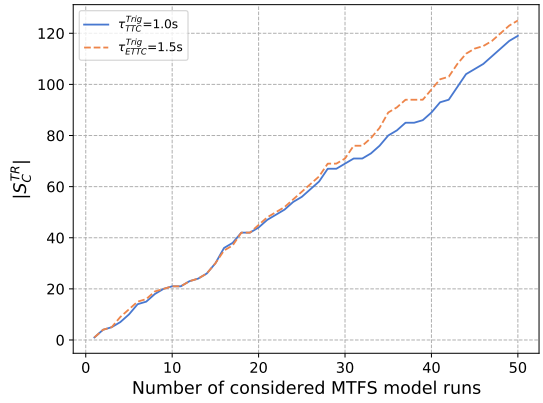

(e) Number of collisions in the treatment

Figure F.3.: Number of collisions in the collision partner configuration categories introduced in Section 8.1.1.

F.3. Changes in minimum TTC and minimum distance

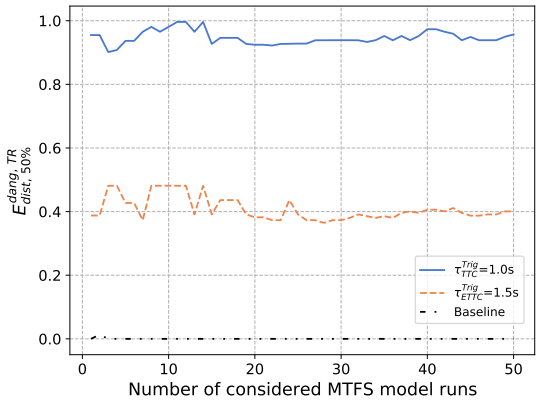

(a) Median $d^{\min}$ in conflicts with objective danger

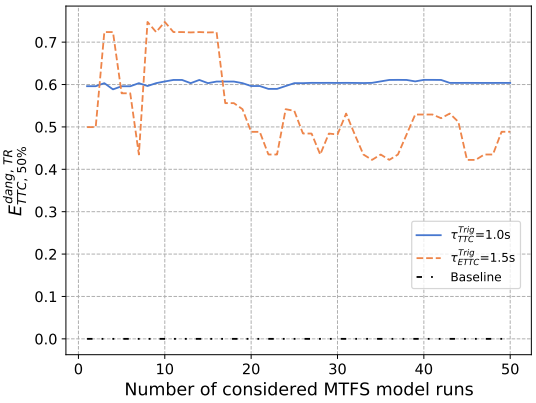

(b) Median $\tau^{\min}_{\mathrm{TTC}}$ in conflicts with objective danger

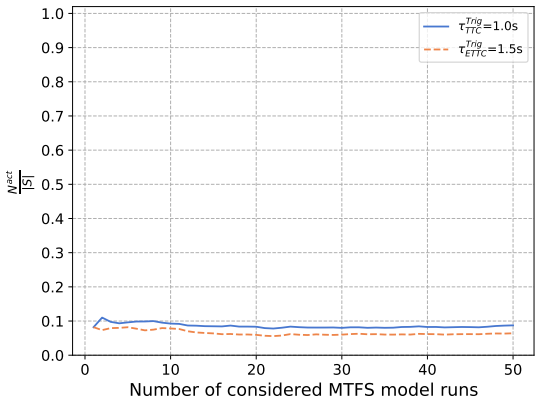

(c) Number of conflicts where the safety system activated

Figure F.4.: Effectiveness metrics related to $d^{\min}$ and $\tau^{\min}_{\mathrm{TTC},X}$ between the conflict participants.

F.4. Effectiveness metrics related to the collision severity

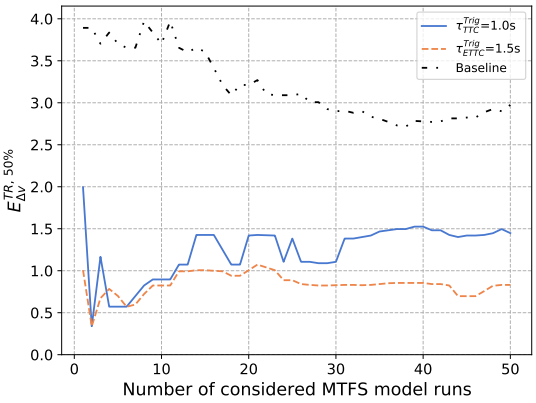

(a) Median Δv in the treatment and baseline

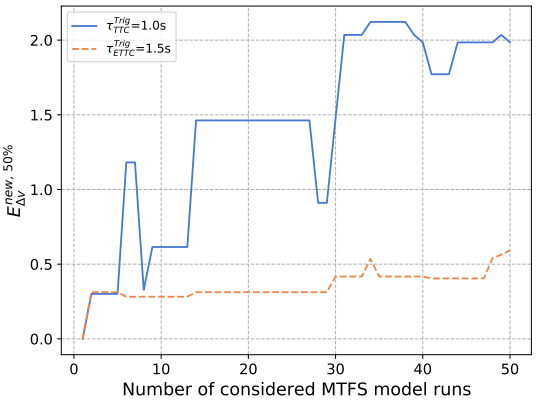

(b) Median Δv in new collisions

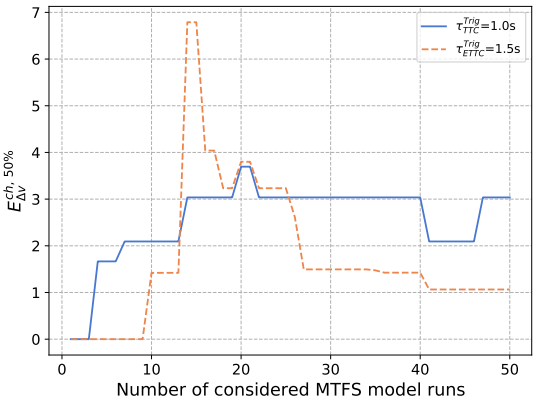

(c) Median Δv for changed collisions in the treatment

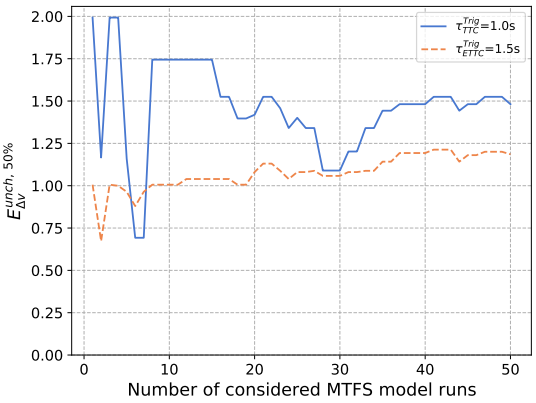

(d) Median Δv for unchanged collisions in the treatment

Figure F.5.: Median Δv values for various collision partner configuration categories.

G. Convergence of effectiveness metrics depending on the conflict filter threshold

G.1. System response categories and related metrics

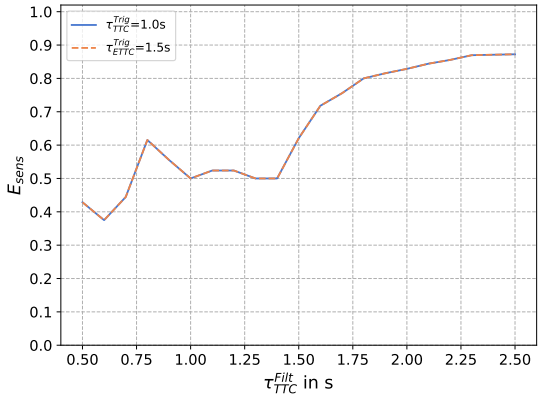

(a) Sensitivity

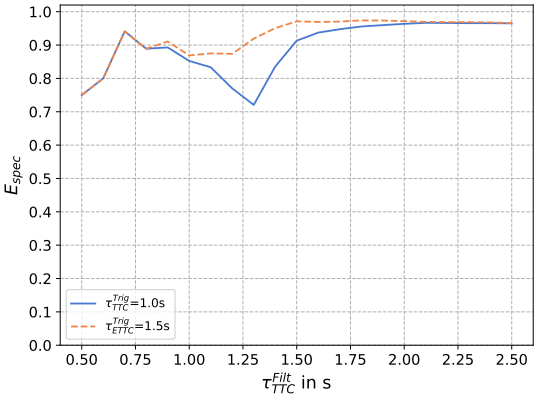

(b) Specificity

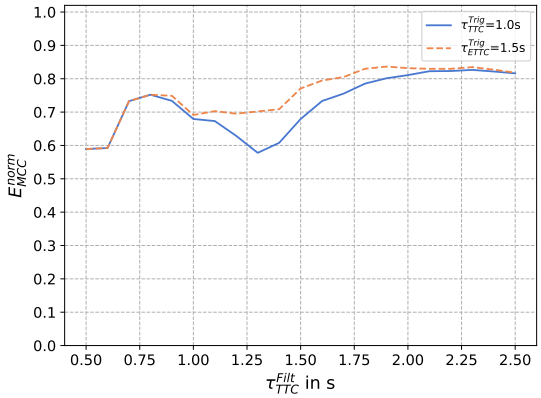

(c) Normed Matthew's correlation coefficient

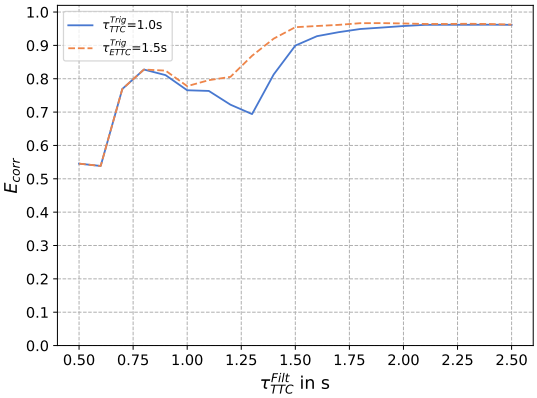

(d) Number of correct decisions

Figure G.1.: Rate of correct decisions E_{corr}, for two investigated systems with different activation thresholds $\tau^{\text{Trig}}_{\text{TTC}}$.

G.2. Accident avoidance and changes in collision partners

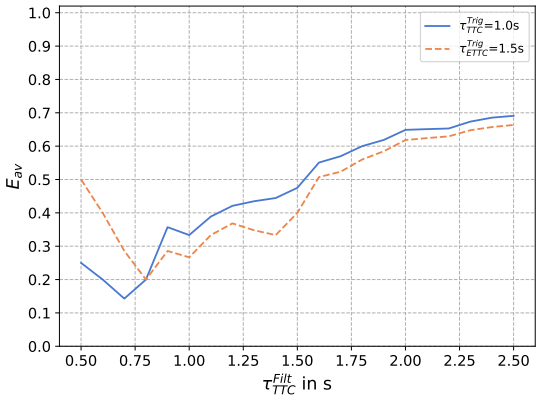

(a) Proportion of avoided baseline collisions

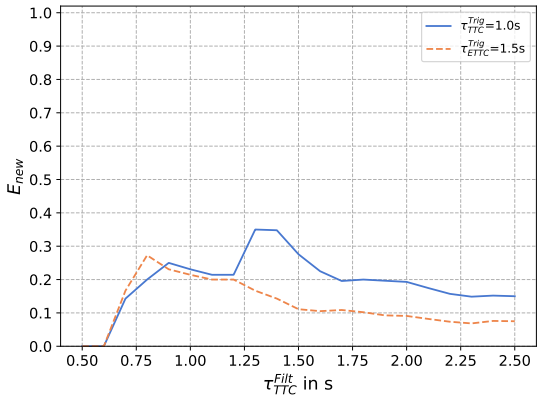

(b) Proportion of new collisions in the number of treatment collisions

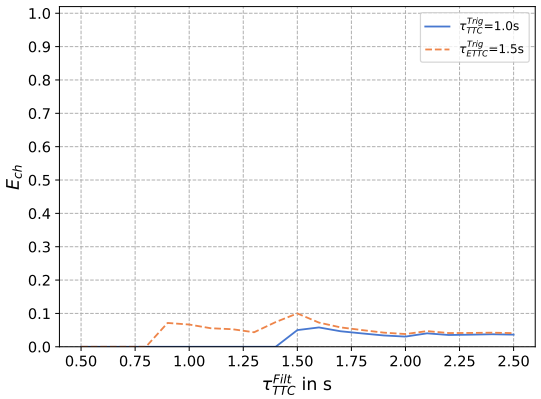

(c) Proportion of changed collisions in the baseline collisions

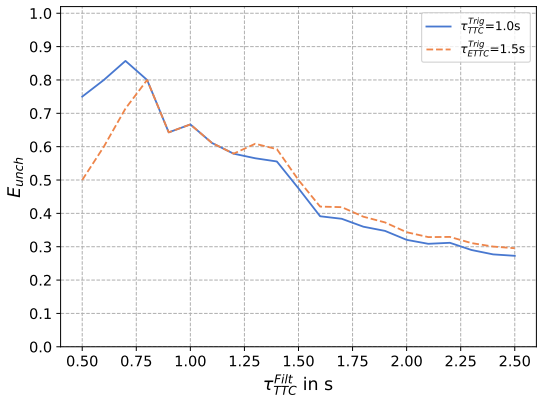

(d) Proportion of unchanged collisions in the baseline collisions

Figure G.2.: Effectiveness metrics related to the change in collision partner configurations, for two investigated systems with different activation thresholds $\tau_{\mathrm{TTC}}^{\mathrm{Trig}}$.

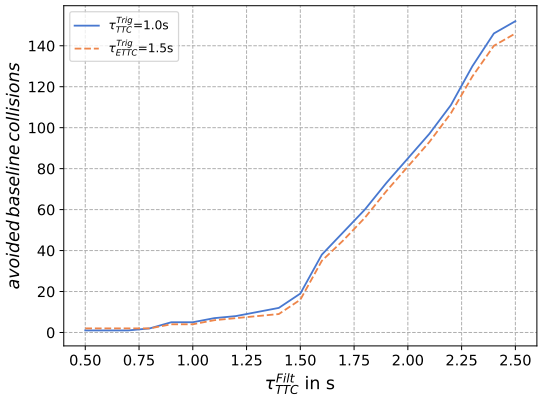

(a) Number of avoided collisions in the baseline

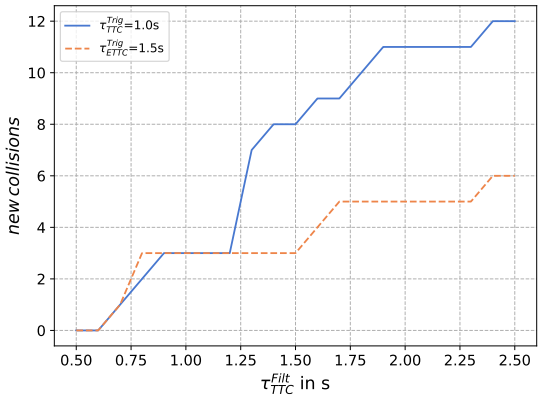

(b) Number of new collisions

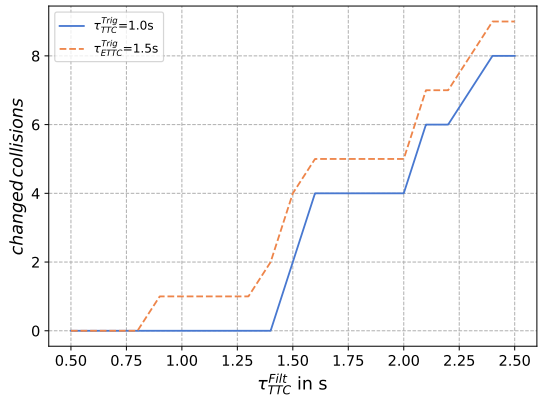

(c) Number of changed collisions

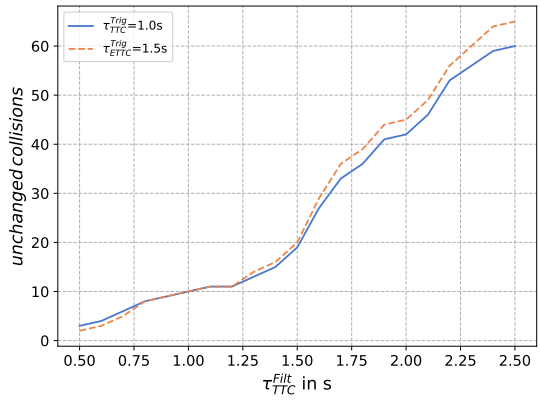

(d) Number of unchanged collisions

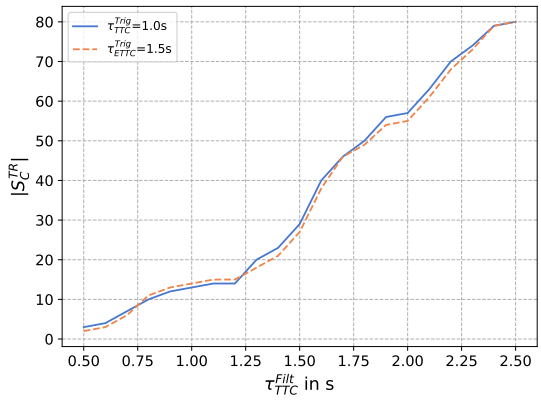

(e) Number of collisions in the treatment

Figure G.3.: Number of collisions in the collision partner configuration categories introduced in Section 8.1.1, for two investigated systems with different activation thresholds $\tau_{\text{TTC}}^{\text{Trig}}$.

G.3. Changes in minimum TTC and minimum distance

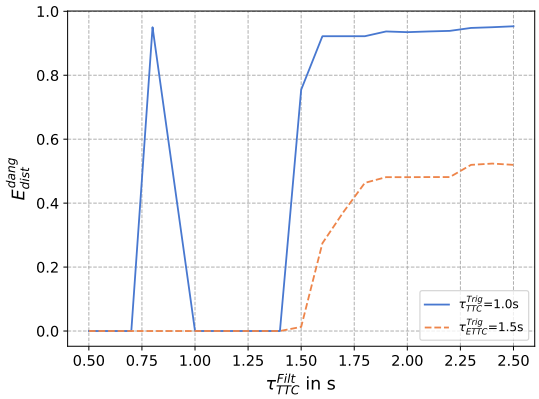

(a) Median $d^{\min}$ in conflicts with objective danger

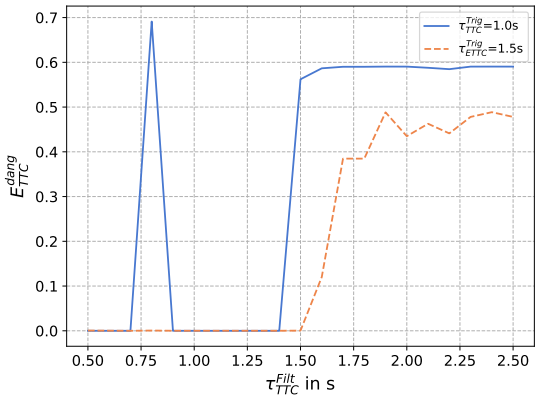

(b) Median $\tau_{\mathrm{TTC}}^{\min}$ in conflicts with objective danger

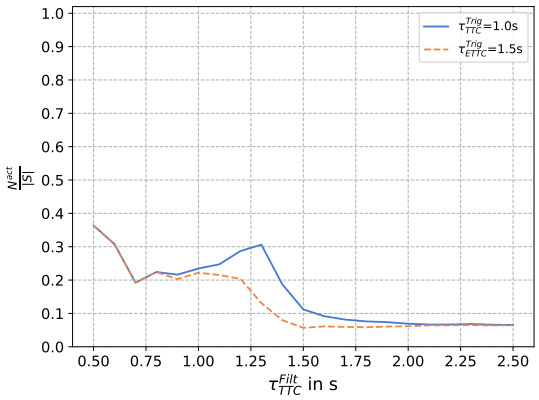

(c) Number of conflicts where the safety system activated

Figure G.4.: Effectiveness metrics related to the change in $d^{\min}$ and $\tau_{\mathrm{TTC},X}^{\min}$ between the conflict participants.

H. Required computational resources

The involved computational resources should not be neglected when planning to apply the presented method. The generation of traffic through MTFS requires few minutes for a single model run on a modern standard computer, amounting to a total of approximately one to three hours to produce 50 model runs. Each of the model runs requires, when storing the output in binary format, around 400 to 500 MB, which results in approximately $50 \cdot 500\ \text{MB} = 25\ \text{GB}$ for the WBE model.

For nanoscopic simulation, on average, 3.5 minutes are required on a virtual machine (one Intel Xeon CPU core at 2.5 Ghz) for the simulation of one individual conflict and one individual simulation configuration. On a desktop computer with an Intel i7 core at 2.67 Ghz, each conflict takes 1.5 minutes to simulate. Neglecting the sight obstructions, i.e., kinematic vehicles in the surrounding traffic and static objects, cuts the computation times down to 60 %. For a simulation that includes the sight obstructions, on a virtual machine, almost 7 days are therefore required to simulate all 2 760 conflicts that were identified for the 50 model runs of WBE.

A run-time analysis of nanoscopic simulation with the full scenery revealed the following approximations: 5 % of the simulation time is required for I/O operations (reading MTFS data as input and writing output in the form of time series data for each conflict), 45 % is required for the ray-tracing approach used for sensor vision and 5 % for other calculations in X-RATE, 10 % is required for simulation in PC-Crash and 35 % is required for the communication over the programming interface between X-RATE and PC-Crash. For one treatment, i.e., one configuration of model and system parameters, around 650 MB are required to store the time series data of the simulation of all 2 760 conflicts in the 50 model runs in WBE.

Several optimizations are possible by reducing the accuracy of the sensor vision algorithm, by parallelization of the ray-tracing calculations or by employing the GPU for ray-tracing calculations.